Design and encapsulation of complex lipid based dispersions for oral delivery of active (macro)molecules

Inauguraldissertation

zur
Erlangung der Würde eines Doktors der Philosophie
vorgelegt der
Philosophisch-Naturwissenschaftlichen Fakultät
der Universität Basel

von
JAN KENDALL DE KRUIF
aus den Niederlanden

Basel, 2016

Genehmigt von der Philosophisch-Naturwissenschaftlichen Fakultät auf Antrag von:

Prof. Dr. Georgios Imanidis, Dissertationsleiter

Prof. Dr. Gerrit Borchard, Korreferent

Basel, 23.06.2015

The Dean of Faculty

Prof. Dr. Jörg Schibler

La science, mon garçon, est faite d'erreurs, mais d'erreurs qu'il est bon de commettre, car elles mènent peu à peu à la vérité.[*]

— Jules Verne

[*] Science, my lad, is made upon many errors, but they are errors that it is good to make, for they lead little by little to the truth.

Abstract

Lipid-based (LB) formulations are versatile systems that can solubilise poorly water-soluble drugs, but also work as dispersing medium for hydrophilic formulation components. Dispersed particles can consist of more complex structures. Interesting is the dispersion of water-based microgels in LB systems to create hydrophilic compartments within a non-aqueous medium, suitable for direct capsule filling. Such systems represent a suitable milieu for protein microencapsulation to ensure protection from degradation of these macromolecules. In fact, while oral macromolecule delivery is a thriving topic in modern pharmaceutics, the first challenge is to achieve a stable drug product throughout manufacturing. Owing to the structured and complex nature of such system, a thorough characterisation is needed to gain adequate understanding of the system. Identification of critical material attributes and process parameters is key in the framework of the Quality-by-Design (QbD) initiative. The purpose of this thesis is to formulate novel LB systems suitable for capsule filling that allow oral delivery of proteins and small molecules.

The present thesis consists of four studies. The first two introduce new manufacturing approaches for protein microencapsulation using LB systems as carrying medium for oral delivery. The third and fourth studies address manufacturing criticalities of LB systems using macromolecules and small molecules as active ingredients, respectively. A special focus is kept on the development aspects of these systems by using statistical methods to design quality into the novel drugs delivery formulations.

The first study focused on the feasibility of protein microencapsulation by prilling into a LB hardening bath. Here, prilling was applied by dropping a protein-containing polymeric solution into a LB hardening bath where cross-linking occurred. Bovine serum albumin (BSA) and a chitosan derivate were used as a model protein and a polyfunctional gel-forming polymer, respectively. The hardening bath was loaded with calcium ions to allow ionotropic gelling of the polymer. Particle morphology and size were dependent on the LB hardening bath used. The microgels had high protein encapsulation efficiency and were able to rapidly release their content during *in vitro* dissolution testing. Additionally, the model protein remained unscathed throughout the entire manufacturing process and during preliminary stability studies in the LB hardening baths. Overall this approach demonstrated the technical viability of LB systems to act as hardening bath for the prilling process and simultaneously as dispersing medium for the thereby formed microgels to achieve liquid capsule filling.

The second study focused on improving the previously introduced LB drug delivery systems (DDS). The aim was to achieve a multi-compartmental system composed of protein-containing nanotubes embedded into the microgels obtained by prilling. To increase protein loading by better fitting the large model protein, *i.e.*, BSA, the nanotubes' lumen was chemically enlarged. The obtained Nanoparticles-in-Microsphere Oral System (NiMOS) showed hardening bath-dependent morphology and good protein entrapment efficiency. Protein stability during the process was confirmed. Furthermore, the proposed NiMOS demonstrated protection from enzymatic degradation after preliminary *in vitro* testing. Also, the multi-compartmental structure extended the protein release profile. This study showed the feasibility of this flexible multi-compartment system for oral protein delivery.

The third study investigated systematically LB formulations as hardening baths for prilling using Design of Experiments (DoE). Over 880 formulations were screened with respect to miscibility, counter-ion solubility, and droplet gelling by using 60 ternary phase diagrams comprising two co-solvents, ten different glycerides, and three so-called complementary excipients. Soft and hard capsules were filled with 245 selected hardening bath formulations for a preliminary compatibility assessment. The ternary phase diagrams' centre points were statistically evaluated to understand the formulation effect on microgel

morphology, protein encapsulation efficiency, and protein stability. The large datasets were analysed by means of partial least squares (PLS) regression to correlate the formulation and experimental factors with the chosen response variables. This work generated an improved understanding for this type of LB systems.

Finally, a fourth study introduced novel tools within the QbD initiative to evaluate complex LB dispersions such as highly concentrated suspensions. The surface energy of the particles intended for suspension was profiled using inverse gas chromatography to understand the heterogeneity in energy distribution. This was correlated to different inter-batch rheological properties at higher solid fractions after LB suspension manufacturing. A mathematical model was then used to predict experimental viscosity values as a function of suspended solid fraction. The agglomeration patterns of the manufactured suspensions were interpreted using the fractal concept of flocculation. This concept as well as the surface energy profiling showed great potential for designing quality into concentrated pharmaceutical suspensions.

This thesis introduced new complex LB systems suitable for oral delivery of proteins and small molecules. Novel formulations approaches have been investigated and developed within a QbD framework. A particular emphasis was on microgel dispersions in lipids for oral (local) protein delivery. The technical viability of this delivery approach was demonstrated on the level of manufacturing and *in vitro* release testing. Future research may include *in vivo* studies to understand and improve the biopharmaceutical performance of the proposed LB DDS, as well as a thorough mechanistic investigation for these complex LB formulations.

Contents

Abstract ..... **i**

Contents ..... **iv**

Acknowledgements ..... **ix**

Introduction **1**
1.1 Background 1
1.2 Objectives 2

Theoretical section **4**
2.1 Lipid-based (LB) dispersions 4
2.1.1 Introduction to LB dispersions 4
2.1.2 Theoretical aspects of dispersions for formulation and manufacturing 5
2.1.3 Advantages and limitations of LB dispersions 8
2.2 Encapsulation of LB dispersions 8
2.2.1 Recent advancements in capsules as dosage forms 9
2.2.2 Liquid capsule-filling technology 9
2.3 Oral delivery of proteins 10
2.3.1 Gastrointestinal (GI) barriers and formulation strategies 11
2.3.1.1 Enzymatic degradation 11
2.3.1.2 Mucus layer 12
2.3.1.3 Epithelial absorption 13
2.3.2 Protein formulation 14
2.3.2.1 Protein stability 14
2.3.2.2 Protein formulation for oral delivery 14
2.3.2.2.1 Microencapsulation for oral protein delivery 14
2.3.3 Protein characterisation 15
2.4 Microencapsulation by prilling 15
2.4.1 Prilling and vibrating nozzle technique 15
2.4.2 Polymers for prilling 19
2.5 Multi-compartmental drug delivery systems (DDS) 20
2.5.1 Nanoparticle-in-Microsphere Oral System (NiMOS) as dosage forms 21
2.5.1.1. Clay nanotubes – halloysite (HNT) 22
2.6 Quality aspects of drug formulation 23
2.6.1 Quality-by-Design (QbD) initiative and LB suspensions 23
2.6.2 Design of Experiments (DoE) and statistical analysis 24

Design and manufacturing of novel LB systems for oral protein delivery **28**

3.1 On prilling of hydrophilic microgels in lipid dispersions using mono-N-carboxymethyl chitosan for oral biologicals delivery 28
3.1.1 Summary 28
3.1.2 Introduction 28
3.1.3 Materials and methods 30
3.1.3.1 Materials 30
3.1.3.2 Preparation of polymeric solution and hardening baths 30
3.1.3.3 Hardening bath characterisation 31
3.1.3.4 Stability of capsules filled with hardening baths 32
3.1.3.5 Manufacturing of microgels 32
3.1.3.6 Microgel morphological characterisation 32
3.1.3.7 Encapsulation efficiency of bovine serum albumin (BSA) in microgels 32
3.1.3.8 Degradation of BSA 33
3.1.3.9 In vitro release of BSA from microgels 33
3.1.3.10 Data analysis 33
3.1.4 Results 33
3.1.4.1 Hardening bath characterisation 33
3.1.4.2 Microgel characterisation 34
3.1.4.2.1 Morphological characterisation 34
3.1.4.2.2 Encapsulation efficiency and leakage 36
3.1.4.3 Degradation of BSA 38
3.1.4.3.1 Circular dichroism 38
3.1.4.3.2 Sodium dodecyl sulphate polyacrylamide gel electrophoresis (SDS-PAGE) 38
3.1.4.3.3 Fluorescence profile 38
3.1.4.4 In vitro release of BSA from microgels 39
3.1.5 Discussion 39
3.1.5.1 Hardening bath properties and microgel morphology 39
3.1.5.2 BSA encapsulation efficiency, leakage, and release from microgels 40
3.1.5.3 Protein denaturation 41
3.1.6 Conclusions 42
3.2 On prilled Nanotubes-in-Microgel Oral Systems for protein delivery 42
3.2.1 Summary 42
3.2.2 Introduction 42
3.2.3 Materials and methods 44
3.2.3.1 Materials 44
3.2.3.2 Halloysite nanotubes (HNT) activation by luminal etching 45
3.2.3.3 HNT characterisation 45
3.2.3.3.1 Particle size and ζ-potential 45
3.2.3.3.2 Specific surface area, pore volume, and pore diameter 45
3.2.3.4 Loading of HNT with bovine serum albumin (BSA) 45
3.2.3.5 HNT imaging 45
3.2.3.5.1 Transmission electron microscopy (TEM) 45
3.2.3.5.2 Scanning electron microscopy (SEM) 46
3.2.3.6 Formation of NiMOS by prilling 46
3.2.3.6 NiMOS and microgel characterisation 46
3.2.3.6.1 Particle size by laser diffraction 46
3.2.3.6.2 Particle shape by dynamic image analysis 46
3.2.3.6.3 Particle imaging by optical microscopy 46
3.2.3.7 Protein content 46
3.2.3.7.1 Loading efficiency of BSA onto HNT 46
3.2.3.7.2 Encapsulation efficiency of BSA in microgels 47
3.2.3.8 Release test 47
3.2.3.8 Protein stability after prilling process 47
3.2.3.8.1 Circular dichroism 47
3.2.3.8.2 Fluorescence profile 47

3.2.3.9 Protein stability after enzymatic digestion ... 48
3.2.3.9.1 Enzymatic digestion ... 48
3.2.3.9.2 SDS-PAGE ... 48
3.2.4 Results ... 48
3.2.4.1 HNT characterisation ... 48
3.2.4.2 HNT imaging ... 49
3.2.4.3 Microgel and NiMOS size and morphology ... 49
3.2.4.4 Protein content ... 51
3.2.4.5 Release test ... 51
3.2.4.6 Protein stability after prilling ... 53
3.2.4.7 Protein stability after enzymatic digestion ... 54
3.2.5 Discussion ... 54
3.2.5.1 HNT characterisation ... 54
3.2.5.2 Prilled NiMOS characterisation ... 55
3.2.5.3 Protein stability ... 57
3.2.6 Conclusion ... 57

Manufacturing and formulation quality aspects of LB pharmaceutical dispersions as drug delivery systems ... 58
4.1 A systematic study on manufacturing of prilled microgels into lipids for oral protein delivery ... 58
4.1.1 Summary ... 58
4.1.2 Introduction ... 58
4.1.3 Materials and methods ... 59
4.1.3.1 Materials ... 59
4.1.3.2 Polymeric solution preparation ... 60
4.1.3.3 Ternary phase diagrams ... 60
4.1.3.4 Capsule compatibility with hardening bath excipients ... 60
4.1.3.5 Prilling of the polymeric solution ... 61
4.1.3.6 Morphological characterisation of the microgels ... 61
4.1.3.7 BSA encapsulation efficiency in microgels ... 62
4.1.3.8 Protein stability ... 62
4.1.3.8.1 Circular dichroism of BSA ... 62
4.1.3.8.2 Microfluidic capillary electrophoresis ... 62
4.1.3.9 Data handling and partial least square (PLS) regression analyses ... 62
4.1.4 Results ... 63
4.1.4.1 Ternary phase diagrams ... 63
4.1.4.1.1 Excipient miscibility ... 64
4.1.4.1.2 Calcium chloride solubility ... 64
4.1.4.1.3 Mono-N-carboxymethyl chitosan (MCC) gelling ... 65
4.1.4.1.4 Overall score ... 65
4.1.4.1.5 Capsule compatibility ... 65
4.1.4.2 Prilling of the microgels ... 66
4.1.4.2.1 Morphological characterisation of the microgels ... 66
4.1.4.2.2 BSA encapsulation efficiency in microgels ... 69
4.1.4.3 Protein stability ... 69
4.1.4.3.1 Circular dichroism ... 69
4.1.4.3.2 Microfluidic capillary electrophoresis ... 70
4.1.5. Discussion ... 71
4.1.5.1 Ternary phase diagrams and capsule compatibility ... 71
4.1.5.2 Microgel characteristics ... 72
4.1.5.3 Protein stability ... 72
4.1.6 Conclusions ... 73
4.2 Novel Quality-by-Design tools for concentrated drug suspensions: surface energy profiling and the fractal concept of flocculation ... 73
4.2.1 Summary ... 73
4.2.2 Introduction ... 74

4.2.3 Materials and methods ... 75
4.2.3.1 Materials ... 75
4.2.3.2 Methods ... 75
4.2.3.2.1 Active pharmaceutical ingredient (API) characterisation ... 75
4.2.3.2.2 Surface energy profiling ... 76
4.2.3.2.3 Suspension manufacture ... 77
4.2.3.2.4 Suspension analysis ... 78
4.2.3.2.5 Data analysis ... 78
4.2.4 Results ... 78
4.2.4.1 Initial API characterisation ... 78
4.2.4.2 Specific surface area measurement ... 80
4.2.4.3 Surface energy profiling ... 80
4.2.4.4 Rheological suspension analysis ... 81
4.2.5 Discussion ... 82
4.2.5.1 Surface energy profiling ... 82
4.2.5.2 Rheology and the fractal concept of flocculation ... 84
4.2.6 Conclusion ... 86

Final remarks and outlook ... 87

Bibliography ... 90

List of abbreviations ... 113

List of symbols ... 117

List of equations ... 121

List of figures ... 124

List of tables ... 127

Acknowledgements

Firstly, I'd like to thank Prof. Georgios Imanidis and Prof. Martin Kuentz for their support and guidance throughout the long and winding road that led me to this thesis. The quality of our academic talk, the high level of their scientific knowledge, and their passion for the "pharma-world" propelled me often out of troubled waters. Again and pleonastically, thank you.

My gratitude also goes to Tillotts Pharma AG, who kindly funded my entire doctoral studies. Needless to say, my thanks go to the many people who form this company, especially Dr Roberto Bravo and Dr Felipe Varum, for their invaluable help and for the chance they gave me to work in collaboration with an industrial reality in Switzerland.

The efforts of Prof. Gerrit Borchard are kindly acknowledged in reviewing the present manuscript and providing a stimulating scientific conversation. Similarly, I'd like to thank Prof. Matthias Hamburger for taking the time to chair the dissertation committee.

I would like to express my gratitude to the School of Life Sciences of the University of Applied Sciences and Arts Northwestern Switzerland (FHNW) and the University of Basel for the possibility of growing and learning, for the chance to wear a lab coat and do what I love, and for exploring an academic reality so unique and challenging. My thanks must be extended to the entire staff and personnel of these institutions for their collaboration. Among these people, I would like to express my gratitude to Dr Elizaveta Fasler-Kan, who collaborated closely on most of this study.

It is important to acknowledge the competence and skill of all my colleagues from the Institute of Pharma Technology, with whom I shared several years of work. A special mention goes to my lab mates during these years, Dr Zdravka Misic and Ms Wiebke Kirchmeyer, who were always helpful and were able to endure the peevish days which at times accompany research. Furthermore, I'm glad that I had the chance to also call some of these people friends and got to know them also outside of the scientific field.

My thanks also go to my students and interns, Ms Eman Darwish, Ms Carla Garofalo, Mr Nicolas Gautschi, and Ms Gisela Ledergeber. Each of these remarkable fellows shared with me the scientific work hereby presented, allowed me to review and discuss their work, and braved my sense of humour.

My gratitude goes to all those who supported my work in these years unconditionally, although did not actively do research with me. I want to thank my sister, my mother, my stepfather, and my grandmother for the kind-hearted and encouraging attitude they've always maintained throughout my academic career, regardless of distance and hardships. I thank each and every friend, near and far, new and old, who remained close to me during these years for the support, the solace, and the merry laughter. Last but not least, I would like to thank Katerina for her loving support and her selflessness, who praised, scolded, cheered and motivated me at home and at work through the entirety of this scientific journey.

Chapter 1

Introduction

1.1 Background

Lipid-based (LB) systems have shown great potential in terms of drug delivery. While not a recent invention, LB formulations have become especially important in recent years because of a rising number of biopharmaceutically challenging drug candidates that are emerging from high throughput screenings [1]. For example, different LB products are available on the market, such as Juvela®, Duspatalin®, Sandimmune Neoral®, and Norvir®. The functionality of LB systems, however, is not limited to solubilise lipophilic compounds. LB formulations can also work as dispersing medium for simple drug powder, as well as for active pharmaceutical ingredients (API) loaded into more complex particulate systems. A solid dispersion or suspension has the advantage, compared to a solution, that the drug dosage per unit can be dramatically increased. When compared to a purely solid system, a dispersion has the particular advantage of exposing the active ingredient to the gastrointestinal milieu with a higher surface area, thus improving its dissolution in the biological fluids [2]. While LB dispersions find limited application as final dosage forms, these systems can be easily filled into capsules for oral administration. Lipids have also shown great potential for protein delivery [3]. In addition, the dispersed particulate systems could comprise a protein-loaded complex system. LB dispersions may constitute platforms to form a stable drug product suitable for oral (local) protein delivery. A further biopharmaceutical rationale to employ LB systems is that many lipids are known to increase the oral bioavailability of API, *e.g.*, by forming drug-loaded micellar dispersions during digestion in case of poorly water-soluble drugs [4,5]. The design of such complex LB systems for oral protein delivery is a particular focus of this thesis.

Many therapeutically active macromolecular compounds, such as peptide, enzymes, and monoclonal antibodies, are nowadays either commercially available or taking part of clinical development programmes [6–10]. These large molecules generally possess complex three-dimensional structures. In proteins, for example, the overall structure is divided in four structural hierarchies that are named primary (amino acid sequence), secondary (localised three-dimensional structures), tertiary (overall protein spatial configuration), and quaternary (arrangement of different protein monomers). The therapeutic activity of a protein is closely related to the integrity of each structure [11] Furthermore, proteins are strongly influenced by the surrounding medium and chemical, physical, and structural instabilities may occur even under relatively mild physicochemical or mechanical stress [12,13]. Instability during manufacturing is therefore a key hurdle in formulating oral protein delivery systems and mild conditions must be applied to the production process. Hence, the manufacturing of a stable drug product is a first formulation challenge.

Protein formulation for oral delivery must also face a biopharmaceutical challenge to achieve adequate oral bioavailability [14]. Oral administration would be a desired way to achieve either systemic action or to treat local gastrointestinal diseases, which both may lead to increased patient compliance and reduced cost. However, proteins undergo extensive and thorough digestion in the gastrointestinal (GI) tract [15]. This begins in the stomach, where the proteins are cleaved and degraded by hydrolytic enzymes and by the acidic environment. Further digestion occurs in the small intestine through the action of pancreatic proteases and brush border enzymes, whereas enzymatic activity decreases only in the large intestine [15]. Furthermore, relevant enzymatic degradation may occur because of colonic bacteria for the macromolecules which escape digestion in the upper gut [16]. Another obstacle is given by the mucus layer, which can hinder protein absorption or action, according to the required site of action [17].

Much effort has been invested in modern pharmaceutics to overcome the aforementioned issues [14]. Many approaches have been proposed to deliver proteins to the GI tract [18,19]. Protection of the macromolecular API from the GI milieu has been addressed with microencapsulation [20,21]. This formulation approach has shown potential to overcome especially enzymatic degradation. However, most research has been limited to designing the microencapsulation system and direct *in vitro* or *in vivo* testing. Many of these drug delivery systems (DDS) do not represent final dosage forms which can be directly administered orally. As earlier mentioned, further processing steps required to obtain a final dosage form may cause protein instabilities and foil the carefully designed systems. Hence, mild conditions must be applied during formulation.

Microencapsulation is considered one of the most effective methods to formulate proteins with regards to protection from enzymatic degradation [20]. Several other formulation techniques are available in this sense, but not all can combine mild manufacturing conditions with effective encapsulation [22]. Prilling is a technique that uses the Plateau-Rayleigh instabilities to form equally sized droplets from a liquid stream extruded through a nozzle [23]. An external vibration is applied to induce and control this instability, thus the technique is also named vibrating nozzle method. To achieve drug encapsulation, the API and a polymer can be loaded in the prilled liquid. The droplets are collected in a hardening bath where ionotropic cross-linking of the polymer occurs, which entraps an API into the forming microgel. By using concentric nozzles, this method can also produce microcapsules with separate core and shell compartments [24]. While this technique is devoid of potentially harmful conditions for protein microencapsulation, its application in macromolecule encapsulation has received only preliminary investigation [25,26]. Furthermore, the state-of-the-art application of this technique uses alginates as polymers and an aqueous hardening bath [27]. Polyfunctional polymers, such as chitosan derivates, have found only preliminary applications with this technique [23]. Moreover, aqueous hardening baths require removal to further process the formed microgels into a final dosage form, such as liquid capsule filling. The prilled microgels can be used as suitable containers for protein API [28].

In recent years, with the widespread use of nanotechnologies also in pharmaceutical development, DDS have attained new levels of sophistication. The research on multi-compartmental DDS is gaining momentum due to high flexibility and versatility ensured, and it is mostly focused on macromolecular delivery. These DDS exploit the different properties of each compartment to modify the API release or to increase its oral bioavailability. Several architectures and production technologies are available, for instance Nanoparticles-in-Microsphere Oral System (NiMOS) or Janus nanoparticles [29,30]. However, not all processes are suitable for scale-up, and some biopharmaceutically promising DDS may encounter issues in later pharmaceutical development if the complexity is excessive [31]. Such complex drug delivery systems can become a challenge for pharmaceutical development, particularly when a robust process quality is targeted in manufacturing.

In recent years a great effort has been put by regulatory authorities to embed quality in all steps of the design and production of a drug product [32–34]. The Quality-by-Design (QbD) initiative has been proposed by the Food and Drug Administration (FDA), where a thorough understanding of formulation and production processes with the different sources of variability is targeted [32]. Design of Experiments (DoE) has been typically employed in the framework of QbD to assess the critical properties of design, development, and manufacturing, as well as to optimise these steps [35]. Owing to their high complexity, structured dosage forms, such as highly concentrated LB suspensions and multi-compartmental DDS, require a systematic investigation to comply with modern pharmaceutical quality standards.

1.2 Objectives

The present thesis aims to formulate novel LB systems suitable for capsule filling that allow oral (local) delivery of proteins and small molecules. A QbD framework is applied to identify critical attributes and parameters of the proposed formulations and processes. A novel manufacturing approach is introduced to formulate proteins into LB dispersion medium, while ensuring adequate pharmaceutical quality. To achieve this goal, an innovative microencapsulation approach has been adapted for LB formulations to avoid stressful manufacturing conditions that are potentially harmful for an active protein. Such DDS are then further developed to improve protein stability after oral administration. The relevant quality aspects of these formulations are analysed using experimental design and statistically evaluated by partial least squares (PLS) regression. Furthermore, new tools for LB system characterisation are introduced for mechanistic process understanding and modelling. This thesis presents individual chapters that study the design of LB formulations and systematically investigate their properties for manufacturing.

The second chapter aims to provide adequate theoretical background to the underlying the research conducted. The state-of-the-art pharmaceutical technology employed for complex LB dispersion design and development is described, as well as the background necessary to

understand the fundamentals of protein oral delivery. Focus is put on formulation and manufacturing of these structured systems, including relevant quality aspects for their implementation.

The objective of the third chapter is to develop lipid-based systems for oral delivery of macromolecules. The chapter is divided in two sections. The purpose of the first section is to introduce prilling, a microencapsulation technique, as a suitable manufacturing approach to prepare protein-loaded microgels into lipid medium for direct capsule filling. The microencapsulated system is evaluated in terms of particle morphology, encapsulation efficiency, and protein stability after manufacturing.

The second part of the third chapter aims to form NiMOS-based multi-compartmental DDS using the previously outlined prilling approach. A model protein is here loaded into natural nanotubes, which are then microencapsulated, to ensure further protection from enzymatic degradation after oral administration. The NiMOS system is characterised and protein stability is assessed after prilling and after preliminary enzymatic digestion.

The fourth chapter's objective is to investigate understand the quality aspects in the design and manufacturing of complex lipid-based pharmaceutical dispersions. Two studies are presented in the fourth chapter. The first part's purpose is to find suitable excipient combinations for the previously introduced prilling process and to investigate systematically diverse material and process factors. An experimental design is employed to identify correlate process parameters and LB formulation properties to microgel characteristics and protein stability.

Finally, the second study of the fourth chapter aims to introduce new QbD tools to understand and predict the behaviour of complex lipid-based dispersions, such as highly concentrated suspension. Novel concepts with potential for designing quality into concentrated pharmaceutical suspensions are proposed to obtain mechanistic understanding of these LB systems' instabilities.

Chapter 2

Theoretical section

2.1 Lipid-based (LB) dispersions

2.1.1 Introduction to LB dispersions

Lipids are a group of molecules which comprises several water insoluble organic compounds, such as acylglycerols, oils, waxes, sterols, and vitamins [36]. They have been used over centuries in pharmaceutical applications for their therapeutic action and as excipients. In fact, several lipids are well-known to exhibit an activity in the organism, for example vitamins, sterols, or polyunsaturated fats. The application of lipids in pharmaceutics is focusses on their use as carrying, dispersing, or dissolving medium mostly for poorly water-soluble drugs. Up to 70% new chemical entities (NCE) discovered and developed by pharmaceutical companies are poorly water-soluble [37]. According to the biopharmaceutics classification system (BCS), these compounds belong to class II (low solubility and high permeability) and IV (low solubility and low permeability) [38].

Several techniques are known to increase solubilisation and hence oral bioavailability of poorly soluble compounds, such as particle size reduction or salt formation. However, most techniques have practical limitations, such as the lack of ionisable groups on the molecule for salt formation. Other options to increase the bioavailability of these compounds are available, for instance solubilising the molecule in the formulation. A key formulation approach is to employ lipid-based (LB) formulations. Different mechanisms have been proposed to understand how such delivery systems are capable of increasing oral drug absorption of biopharmaceutically challenging drugs [39,40]. However, drug solubilisation is limited in the medium

especially for compounds that are rather hydrophobic. LB formulations can also be biopharmaceutically meaningful as particulate dispersions of active pharmaceutical ingredients (API) [1], which is especially the case for compounds that are labile or that require permeation enhancement for an effective oral delivery.

Pharmaceutical dispersions consist of a dispersing medium and a dispersed solid fraction [41]. This solid fraction is usually the API alone, but it may also be formulated in larger carrier particles to ensure proper dispersability. The typical particle size of dispersions may vary greatly, between 100 nm and 100 µm, thus ranging from colloidal dispersions to coarse suspensions. In the present thesis, the words “suspension” and “dispersion” are used synonymously. When differentiation is needed, the wording “colloidal dispersion” and “coarse suspension” are employed. Generally, the increase in surface area of dispersed systems represents an advantage, especially compared to solid dosage forms. Thus, dispersed drugs exhibit typically increased dissolution rates in gastrointestinal fluids and absorption compared to classical solid dosage forms [2]. It has also been shown that pharmaceutical suspensions provide an edge in paediatric and geriatric populations who cannot easily swallow tablets or capsules [42]. Compared to other liquid systems, namely solutions or syrups, suspensions allow higher API content to meet the required therapeutic need.

Dispersed systems often require the presence of surfactants to provide adequate dispersion of the solid fraction, avoid particle agglomeration, and prevent settling. Surfactants are amphiphilic molecules, *i.e.*, they possess both a hydrophilic and a hydrophobic part, which migrate to the interface between two phases or adsorb according to affinity onto the surface of a particle. Different surfactant types exist, namely non-ionic, cationic, anionic, and zwitterionic. Non-ionic compounds act through steric interaction, whereas ionic surfactants interact predominantly by means of electrostatic forces.

Suitable lipid media for suspensions are usually medium- (from 6 to 12 carbon atoms) and long chain (more than 12

carbon atoms) mono-, di-, and triglycerides as well as to some extent their corresponding free fatty acids (FFA) [43]. Longer chain FFAs and glycerides, however, tend to have high melting points, thus being solid at room temperature. Nevertheless, the presence of unsaturated bonds in the fatty acid chain decreases the melting point, and therefore these lipids can be liquid at room temperature. Most vegetable oils are employed as dispersing media. Many of these lipids are available as excipients on the market with various trade names in pure form, as well as in mixtures. Some lipids may be also modified by adding polymers, such as polyethylene glycol (PEG), or other moieties, such as propylene glycol to the glyceride structure. Similar modifications may also give surfactant properties to the excipients. Finally, phospholipids like phosphatidyl choline may also be formulated in the dispersing medium due to the specific zwitterionic nature and their functionality as suitable wetting agents. A list of the lipids commonly employed in pharmaceutical oral delivery is shown in Table 2.1.

A specific type of LB dispersions is solid dispersions. In these systems, the API is dispersed in a solid excipient or matrix. This system may protect the API from the external environment, allows high drug loading, and typically enables rapid drug dissolution. The advantages of these systems and their limitations have been well reviewed, *e.g.*, by Serajuddin [44]. Apart from lipid-based solid dispersions, there are other solid systems that make use of lipid excipients. Solid lipid nanoparticles (SLN) and nanostructured lipid carriers (NLC) have been proposed as formulation principles for poorly soluble drugs [45,46]. The differences and properties of these formulation approaches have been adequately reviewed by Saupe and co-workers [47].

The different LB systems span from solutions to semisolids and solids, which all require further processing to achieve suitable patient compliance in a final dosage form. A common dosage form containing LB formulations is a capsule. Different encapsulation processes exist for LB systems that are further described in Section 2.2. Lipid-based suspensions are available on the market, for instance Lamprene® capsules (clofazimine, from Alliance Pharmaceuticals), Juvela® N Soft capsules (tocopherol, from Eisai Co), and Duspatalin® capsules (mebeverine hydrochloride, from Abbot Laboratories). Lipid-based suspensions are typically filled into soft capsules and more recently also into two-piece hard capsules [48].

2.1.2 Theoretical aspects of dispersions for formulation and manufacturing

Pharmaceutical suspensions are typically complex systems that are kinetically stabilised while they are still unstable from a thermodynamic viewpoint. Dispersions and suspensions are defined as lyophilic when the dispersed particles display affinity for the dispersing media, or lyophobic in the opposite case. Lyophilicity is useful to understand wetting of the particles' surface by the suspending medium. A lyophilic dispersion can be easily wetted by the surrounding milieu, whereas a lyophobic system will require the use of surfactants to ensure stability.

Several types of interactions and forces need to be taken into account to evaluate suspension instability. The first and foremost factor is the sedimentation of the suspended particles. Sedimentation is typical for suspension (or flotation depending on the density gradient) and the velocity is described by the well-known Stokes equation (Equation 2.1):

TABLE 2.1 – Lipids commonly employed in oral pharmaceutical formulations.

Glycerides	Natural compounds	Modified compounds
Caprylic/capric triglyceride (Labrafac™ Lipophile)	Olive oil	Propylene glycol monocaprylate (Capryol™ 90)
Glyceryl monolinoleate (Maisine™ 35-1)	D-α-tocopherol	PEG-8 caprylic/capric glycerides (Acconon® MC8-2)
Glycerol monooleate (Peceol™)	Apricot kernel oil	PEG-80 sorbitan monooleate (Tween 80)
Glyceryl monocaprylate (Capmul® MCM-C10)	Peppermint oil	D-α-tocopheryl PEG-1000 succinate (TPGS)
Glyceryl tricaprylate (Captex® 1000)	Peanut oil	PEG-35 castor oil (Kolliphor® EL)
Glyceryl trioleate (Captex® GTO)	Sesame oil	PEG-6 oleic glycerides (Labrafil® M1944CS)
	Beeswax	
	Corn oil	
	Canola oil	
	Linseed oil	
	Coconut oil	

$$v_s = \frac{(\rho_p - \rho_f)}{18\,\eta} \cdot g \cdot {d_p}^2 \qquad 2.1$$

Where v_s is the settling velocity, ρ_p is the particle density, ρ_f is the fluid density, η is the fluid viscosity, g is the gravitational acceleration, and d_p is the particle diameter. Sedimentation alone can be considered only in dilute suspensions, whereas in concentrated suspensions other factors need to be taken into consideration [49]. Dilute suspension are intended as dispersed system where the particles' Brownian motion is predominant over hydrodynamic interaction between particles [50]. Usually a solid volume fraction (Φ) of 0.01 is assumed as an upper threshold to define these diluted systems. An increase in solid fraction requires considering also interparticle interaction. Four different types of particle interactions can be distinguished and are described in Table 2.2.

The combination of the electrostatic repulsion energy (G_r) and the van der Waals attraction energy (G_a) are the base for the Derjaguin, Landau, Verwey, Overbeek (DLVO) theory [51,52]. The simplified equations that describe G_r and G_a are shown in Equations 2.2 and 2.3, respectively [50].

$$G_r = \frac{4\pi \cdot \varepsilon_0 \cdot \varepsilon_r \cdot r^2 \cdot {\psi_0}^2}{2r + h} \cdot e^{-\kappa h} \qquad 2.2$$

$$G_a = -\frac{A \cdot r}{12h} \qquad 2.3$$

Where ε_0 is the permittivity in vacuum, ε_r is the relative permittivity, r is the particle radius, ψ_0 is the surface potential, κ is the reciprocal Debye length, h is the shortest distance between two particles, and A is the Hamaker constant. The negative sign in Equation 2.3 represents the attractive nature of this type of interaction, provided that A of the particles is higher than A of the medium.

The sum of interaction energies (G_t) of G_a and G_r creates two distinct regions of attraction. The first one occurs at very close distance between the particles and causes strong and irreversible particle agglomeration, defined as primary G_t minimum. A second attraction region is present at higher interparticle distance, called secondary G_t minimum. This allows a reversible particle agglomeration, defined as flocculation. An accurate understanding of this instability is useful to define the final characteristics of a dispersion.

Formulation scientists often use polymers or macromolecular surfactants as excipients for dispersions and therefore further stabilising factors must be considered. The theory underlying surfactant repulsion forces is defined by the steric hindrance of the surfactant chains. When two particles are close, the non-ionic surfactant (or polymeric) layers adsorbed on their surfaces begin to mix. The interpenetration of the two layers causes a localised increase in osmotic pressure, which creates an osmotic repulsion force [53]. Especially when two macromolecular surfactants are used, the free energy of mixing can be used to calculate this repulsion [54–56], as described in Equation 2.4 [50,57].

TABLE 2.2 – Interparticle interactions.

Interaction	**Description**
Hard-sphere	Particles behave as rigid spheres. When very small interparticle distance occurs (*i.e.*, when centre-to-centre distance is smaller than twice the particle radius), suspension behaviour changes from liquid- to solid-like.
Electrostatic	Particles possess here surface charges or have ionic surfactants adsorbed, on which a counter-ion layer from the surrounding medium is formed. A further layer of co-ions covers this layer. Particles interact according to the overlaying of their respective double layers.
Steric	Particles have adsorbed non-ionic surfactants or polymers on their surface. When the adsorbed layers of different particles encounter and overlap and slightly compress. Repulsion occurs due to local increase of osmotic pressure and volume restriction.
van der Waals	Particles are attracted at short distances due to dipole-dipole interactions, dipole-induced dipole interaction, and dispersion forces.

$$\frac{G_{mix}}{k_B \cdot T} = \left(\frac{2{V_{m,2}}^2}{V_{m,1}}\right) \cdot {n_2}^2 \cdot \left(\frac{1}{2} - \chi\right) \cdot \left(\delta - \frac{h}{2}\right)^2 \cdot \left(3r + 2\delta + \frac{h}{2}\right) \quad 2.4$$

Where G_{mix} is the polymer free mixing energy, k_B is the Boltzmann constant, T is the absolute temperature, $V_{m,2}$ is the molar volume of the polymer or surfactant chain, $V_{m,1}$ is the molar volume of the dispersing medium, n_2 is the number of polymer or surfactant chains per unit area, χ is the Flory-Huggins interaction parameter, and δ is the surfactant or polymer layer thickness. The sign of G_{mix} is positive (*i.e.*, repulsion occurs) when a good solvent is employed as dispersing medium. Furthermore, the layer interpenetration causes a loss of configurational entropy of the surfactant chains, especially on larger molecules, as explained by the Hesselink, Vrij, Overbeek (HVO) theory [54]. This causes further repulsion (G_{con}) between two surfactant-stabilised particles, according to Equation 2.5:

$$\frac{G_{con}}{k_B \cdot T} = 2n_2 \cdot \ln\frac{\Omega_h}{\Omega_\infty} \quad 2.5$$

Where Ω_h represents the number of configurations the surfactant or polymeric chain can assume when another particle hinders it sterically; Ω_∞ represents the configuration number when the surfactant or polymeric chains are free to rotate. The combination of G_{mix} and G_{con} with the van der Waals attraction G_a form the G_t for surfactant-stabilised suspensions. While allowing reversible flocculation (G_{min}), steric hindrance may prevent stronger instabilities by creating strong repulsion forces at close distances. LB dispersions are rarely administered as final dosage form and usually go through a further manufacturing step, namely encapsulation into soft and hard shell capsules. Here, poor dispersion stability could lead to poor content uniformity in an administered volume and therefore incorrect dosing may result.

The aforementioned models are limited to the interaction between two spheres in the suspending medium. On a larger scale, these effects reflect on the bulk properties of the suspensions. In terms of manufacturing, the most important suspension bulk property is viscosity. This property exhibits often a strong influence on overall manufacturability of a suspension. Einstein first proposed a correlation between solid fraction and viscosity for diluted dispersions described in Equation 2.6 [58]:

$$\eta_r = 1 + 2.5\Phi \quad 2.6$$

Where η_r is the relative viscosity. This equation is valid only for systems with $\Phi < 0.1$ and for hard-sphere interactions. Batchelor later proposed a modification to Einstein's equation to consider the hydrodynamic contribution due to interparticle interaction. The modified version, which is valid for $0.1 < \Phi < 0.2$, is shown in Equation 2.7 [59]:

$$\eta_r = 1 + 2.5\Phi + 6.2\Phi^2 + \vartheta \quad 2.7$$

Where the second order term accounts for the hydrodynamic interactions and the term ϑ for higher order interactions. To describe the behaviour of highly concentrated systems, different semi-empirical equations have been proposed. For example, Dougherty and Krieger developed the following equation (Equation 2.8) [60,61]:

$$\eta_r = \left(1 - \frac{\Phi}{\Phi_{max}}\right)^{-[\eta]\Phi_{max}} \quad 2.8$$

Where $[\eta]$ is the intrinsic viscosity, and Φ_{max} is the maximum packing fraction. Another semi-empirical model was proposed by Mooney, as described in Equation 2.9 [62]:

$$\eta_r = exp\left(\frac{2.5 \cdot \Phi}{1 - \frac{\Phi}{\Phi_{max}}}\right) \quad 2.9$$

This equation was found to be especially useful for predicting viscosity at highly elevated volume fractions. Recently, Brady and co-workers have proposed a mechanistic understanding of suspension bulk viscosity starting from the particles' microscale interactions [63]. However, when surfactant-stabilised suspensions are used the volume fraction is usually substituted with the effective volume fraction (Φ_{eff}) that accounts for the adsorbed surfactant layer thickness (δ) on the particles surfaces, as defined in Equation 2.10 [50]:

$$\Phi_{eff} = \Phi \cdot \left[1 + \left(\frac{\delta}{r}\right)\right]^3 \quad 2.10$$

Rheological properties become even more complex at high Φ, since shear thinning and shear thickening effects become more prominent [64,65]. The presence of a surfactant may decrease these phaenomena, although the addition of

surfactants increases the Φ_{eff}, thus increasing viscosity. Other viscosity prediction models have been proposed for the other different types of interparticle interaction, as well as for agglomerated and flocculated suspensions. For further information, the reader is referred to the works from Tadros [66] and Nutan [67]. Also, for flocculation in non-aqueous media and in LB dispersing systems, the scientific contributions by van Mil *et al.* and Lyklema *et al.* should be mentioned here [68–71].

Particle size and morphology are known to influence suspension properties such as stability and rheological properties. Intuitively, smaller particles have higher surface area and have decreased stability [72]. Ellipticity, for example, has been shown to augment viscosity in suspensions [73,74]. The decrease of particle sphericity also decreases Φ_{max}, which in turn increases viscosity. However, effects such as shear thinning and thickening may be positively or negatively influenced by irregular particle shapes [67]. This brief summary of dispersion rheology indicates that, although over a century of research has been conducted, open research questions remain. Therefore, especially the fields of concentrated dispersions and mechanistic modelling give rise to much contemporary research in basic as well as applied rheology.

2.1.3 Advantages and limitations of LB dispersions

LB suspensions are promising yet challenging formulations. When considering oral administration, formulation of a LB system has a number of advantages, which are hereby summarised:

- *Versatility*. LB suspensions are suitable for both hydrophilic and lipophilic compounds, and generally for all insoluble compounds. Low drug solubility in the dispersing medium is advised to avoid recrystallization that could alter the biopharmaceutical API behaviour.
- *High dosage*. Compared to LB formulations with dissolved drug, suspensions have the advantage that higher drug loading is enabled. Thus, suspensions are suitable also for rather low potent drugs.
- *Dissolution*. Reduction in particle size enhances dissolution rate by increasing the surface area of the suspended particles. There is no disintegration step need as compared to tablets and fast dissolution is often associated with higher availability of the drug at the site of action or absorption.
- *Absorption*. According to the site of action, absorption through the intestinal epithelium may be required. The lipids presented in the LB dispersing medium are known to enhance permeation through the gut wall by acting on the tight junctions between the cells of the epithelial lining [75]. In addition, LB formulations increase permeability by improving enterocyte membrane fluidity [76,77] Moreover, lipid dispersions can have further biopharmaceutical advantages regarding expected intestinal solubilisation during lipolysis [78].
- *Drug stability*. An API may be prone to degradation in aqueous media, and the absence thereof increases dramatically the compound's stability. Similarly, aqueous environments are a favourable milieu for microorganism proliferation, which may degrade the drug thus impairing its therapeutic activity. Furthermore, simple dispersion or suspension can avoid manufacturing processes stressful for the molecule, like compression forces in tabletting, shear forces in homogenisation, or temperature in spray-drying or hot melt extrusion.

Still, LB suspensions possess some disadvantages that must be duly considered upon considering this formulation type. Hereby are listed some of the most challenging aspects of LB suspensions formulation for oral administration:

- *Biopharmaceutical limitations*. Drug suspensions in lipids are often beneficial regarding dissolution and absorption compared to other standard dosage forms using crystalline drug, but there are typically clear biopharmaceutical limitation in comparison to LB formulations with dissolved drug.
- *Formulation instability*. Most suspensions are thermodynamically unstable while retaining kinetic stability for different time spans. Different mechanisms of physical instability can occur ranging from aggregation to sedimentation (or flotation) as well as dissolution/recrystallization.
- *Final dosing*. LB suspensions are often not suitable as final dosage forms regarding especially palatability. The dispersions are generally filled into soft or hard shell capsules.
- *Viscosity*. While an increase in drug loading is positive for low potency drugs, it can harm the formulation's machinability. Especially highly concentrated dispersions exhibit a rather too high viscosity, which is often accompanied with high variability.

2.2 Encapsulation of LB dispersions

While LB suspensions show interesting pharmaceutical properties for oral administration as earlier described, they have to be generally filled into capsules that constitute a

final dosage form. Different capsule materials exist and they come in several sizes and shell compositions [79]. Capsules may have benefits compared to other solid dosage forms in terms of patient compliance [80]. While capsules are suitable for liquid filling mostly of lipid systems, their shell material – usually gelatine – is incompatible with fillings containing water or high organic co-solvent percentage [81].

Capsules are classified as soft and hard depending on the shell type [82]. Hard capsules have a two-piece shell that is interlocked, and the shell production and capsule filling are two separate processes. This type of capsule offers great possibilities and flexibility in terms of formulation design, since powders, beads, granules, tablets, semi-solids, and liquids may be easily filled into these dosage forms. This versatility may be further exploited by loading modified release drug delivery systems into the capsule. Furthermore, hard capsules may be used not only for oral administration, but find application also in pulmonary delivery for loading of dry powders for inhalation [83,84]. A certain disadvantage on the side of machinability is a lower output of the filling machines in terms of capsules per hour compared to tableting equipment. Moreover, gelatine, the material usually employed to form the shell, can cause compatibility issues due to chemical cross-linking, as well as raise ethical and religious concerns due to its animal origin.

Soft capsules are a single piece shells produced and filled in a single process. Soft shell capsules are usually composed of gelatine which has been further plasticised by addition of glycerol or sorbitol [79]. The shell water content is comparatively higher in soft capsules and they are practically exclusively used for filling of liquid formulations, which makes a difference to the more versatile hard capsules.

2.2.1 Recent advancements in capsules as dosage forms

The history of soft capsules starts with Mothes and DuBlanc's first patent in 1834 [85], whereas that of hard capsules begins with Lehuby in 1846 [86]. Since these pioneer days of the prototype capsules, much has been achieved in terms of novel shell materials and production techniques for both types.

While gelatine represents the state-of-the-art in terms of capsule shell material, the need for valid alternatives has increased due to multiple factors. Gelatine is an animal-derived product, which entails an adequate quality screening to avoid microbiological contamination. Moreover, gelatine has shown several compatibility issues with hydrophilic fillings, *e.g.* low molecular weight PEGs, as well as cross-linking phaenomena in presence of aldehydes or at pH > 7.5 [79].

Several novel materials have been proposed, developed, and commercialised to overcome the technical issues of gelatine, as well as to circumvent religious or dietary concerns that are linked to the animal source of the shell material [79,87,88]. For hard capsules, the most widespread alternative shell material is hydroxypropyl methylcellulose (HPMC). This semisynthetic polymer is widely used in pharmaceutics for coating, granulation, and tableting. HPMC can be used as capsule shell material using the same dipping technology as two-piece hard gelatine capsules, although a gelling agent is needed in the composition to allow suitable manufacturing properties [89]. Among the commercially available products based on HPMC, Qualicaps® SA (Alcobendas, Spain) introduced Quali-V®, formed with carrageenan as gelling agent. Similarly, Capsugel® NV (Bornem, Belgium) has developed several HPMC capsules, such as VCaps® and DRcaps™, which both contain gellan gum as gelling agent. Recently, Capsugel® also introduced VCaps® Plus, which do not contain any gelling agent in the shell formulation. These novel shell materials have been found to closely mimic the behaviour of standard hard gelatine capsules, and their performance has been elsewhere reviewed [90–96]. Shell materials have been proposed for example by Capsugel, such as starch (Capill®) and pullulan (Plantcaps®) [97–99]. These materials may become possible alternatives to gelatine, but further research and development is still needed to create competitive products compared to gelatine capsules. Other materials have been tested for suitable capsule shell formation [100,101], but a significant amount of research is still needed to bring such novel materials to the pharmaceutical market. As for non-gelatine soft capsules, several new products have already entered the market using starch as an alternative capsule material. For instance, Catalent Pharma Solutions (Somerset, NJ) has proposed Vegicaps® Soft Capsules, Aenova GmbH (Starnberg, Germany) has introduced VegaGels®, and Acsana AG (Cham, Switzerland) has developed Soft SANA Caps™. Although starch appeared to be the most investigated and commercially successful alternative to gelatine for soft capsules, synthetic polymer polyvinyl alcohol display also potential as a substitute capsule shell material [88,102].

2.2.2 Liquid capsule-filling technology

Soft and hard capsules have different liquid filling technologies due to their diverse type of production. Soft capsules are produced, filled, and sealed within the same manufacturing process. While several techniques are known to form this kind of liquid-filled capsules, the two most widespread processes are the rotary die method (Scherer) and the bubble method (Globex). The rotary die method (Figure 2.1a), which was first invented by R. P. Scherer in 1931 [103,104], is the most known continuous

industrial process for soft capsule manufacturing. Briefly, after melting the capsule shell material, two films thereof are formed and casted on two separate die rolls. These rolls are set in parallel at close distance and are separated by an injection wedge, which will pump the liquid fill between the two casted films. The rolls have small symmetrical pockets that allow the shell material to swell during the forceful injection of the liquid filling. The convergent die roll rotation leads to the sealing of the die pockets, and subsequently to the cut out of the formed soft capsules. The bubble method (Figure 2.1b), which was first industrially applied on the Globex Mk II Encapsulator, forms seamless one-piece soft capsules. A concentric tube extrudes molten

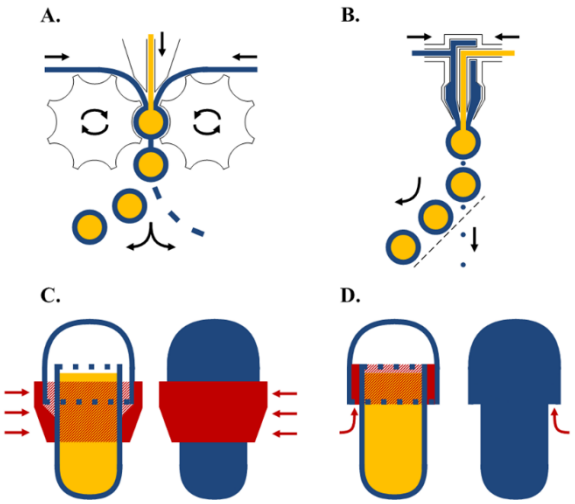

FIGURE 2.1 - Schematics of the rotary die method (a) and bubble method (b) for liquid capsule filling process, and of the capsule sealing techniques using banding (c) and LEMS™ (d).

shell material from the outer annulus and the liquid fill from the internal tube. The droplets assume a spherical shape due to surface tension, and the molten shell material solidifies into a cooled oil column. The thereby formed capsules undergo a final drying step. Schematics of the rotary die method (a) and bubble method (b) for liquid capsule filling process, and of the capsule sealing techniques using banding (c) and LEMS™ (d).

Unlike soft capsules, the filling of hard capsules is separated from the production step. The shell formation of the hard capsules is usually achieved by dipping metal pins into molten shell material or a solution thereof. Different pins are used for the two components of hard shells, namely cap and body, to ensure later the adequate interlocking of the two pieces. The pins are subsequently extracted to allow deposition of the material thereon and dried to form the shell [79]. The filling step of hard shell capsules follows general operations that are common to most equipment, namely rectification, capsule body and cap separation, dosing, rejoining, sealing, and ejection. In the first step, the empty capsules are automatically oriented in the same direction, *i.e.* cap upwards and body downwards. Afterwards, the cap and body are separated in order to allow the filling of the body compartment. The dosing or filling step is the most critical, and a variety of different instruments, both laboratory and industrial scale, are available on the market [105]. Since the liquid or semi-solid fill is dispensed in the capsule volumetrically, its physicochemical and especially its rheological properties are of critical importance. For example, apparent viscosity at the given shear rate in the nozzle plays a major role during the dosing into capsules [106,107]. Once the fill has been loaded, cap and body are rejoined and subsequently sealed to prevent liquid leakage from the capsules. Two industrial sealing methods are commonly used for this last step, *i.e.* banding and LEMS™ sealing (Figure 2.1c and 2.1d, respectively). Banding is the most known technique, in which band of shell material is applied on the overlap between capsule cap and body [108]. Instead, in the LEMS™ sealing process from Capsugel, a hydroalcoholic solution is sprayed on the gap between capsule cap and body [109,110]. This mixture is drawn further in the overlap between the two capsule halves by capillary forces and there the presence of moisture lowers the melting point of the shell material. The sealing is then finalised by the application of gentle heat in a machine drying tunnel. The most common liquid-filling and sealing techniques together with their equipment have been thoroughly reviewed by Cole [111].

2.3 Oral delivery of proteins

Several different peptide and protein drugs are available for different therapeutic applications. Many pharmaceutical companies have also refocused their research and development from small molecules to therapeutically active macromolecules. Proteins and peptides, such as insulin, calcitonin, octreotide, glucagon-like peptide-1, and interferon α, are currently being developed by major pharmaceutical companies for oral administration [14]. Currently, however, nearly all macromolecular compounds are administered parenterally. Stepping towards oral administration could increase patient compliance. Furthermore, for local gastrointestinal (GI) delivery there may be the additional advantage of targeting directly the pharmacological site of action. However, the low oral bioavailability due to the characteristics of the GI tract itself poses several challenges to this administration route. Proteins and peptides are naturally metabolised as part of

the digestion process, which is certainly a hurdle to macromolecular oral delivery. In order to have a systemic action, the macromolecular APIs must cross a mucus layer, which covers most of the GI tract's epithelium, and has to permeate the epithelium itself. However, if systemic action is not intended and only local GI activity is required, mainly intestinal degradation is targeted. Consequently, mucus or enterocyte permeation is optional given the specific mode of pharmacological action [112]. Therefore, oral peptide and protein administration appears to be a much more realistic goal to reach for local action as compared to an intended systemic therapy. This enables many novel therapeutic options for the treatment of intestinal ailments [113]. Regardless of the GI tract barriers, an adequate drug delivery system must also allow a technically feasible and competitive manufacturing process. To deliver its therapeutic effect, the macromolecular API must retain its structure and activity throughout compounding and processing to a final dosage form. The oral delivery of proteins, either systemic or local, represents a significant challenge for modern pharmaceutics. Many systems have been devised and preliminary tests have shown some potential to achieve the goals, but these efforts have so far not provided suitable drug delivery systems that are viable for the pharmaceutical market [114].

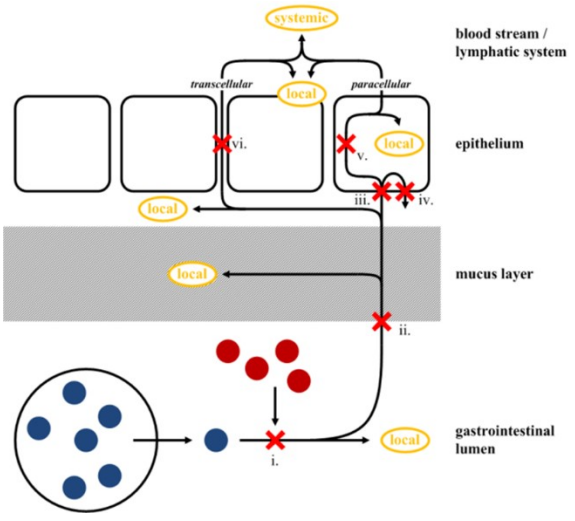

FIGURE 2.2 - Gastrointestinal barriers to drug action and absorption. The drug is represented by blue circles and digestion enzymes are shown as red circles. Enzymatic degradation (i), mucus layer penetration (ii), enterocyte absorption (iii) and efflux pumps (iv), cellular metabolism (v), tight junction closure (vi).

2.3.1 Gastrointestinal (GI) barriers and formulation strategies

The stomach constitutes a particular hurdle to oral peptide and protein delivery because of the acidic environment and the enzymatic activity. Therefore, enteric coating is probably needed for any suitable oral drug delivery system using this type of active principles. The lower intestine may represent a better site of release for peptides and proteins and the formulation technique would have to address the barriers for this kind of APIs. Beside the acidic environment in the stomach, the GI tract possesses three major hurdles to be overcome for successful API action, namely enzymatic degradation (i), mucus penetration (ii), and absorption (Figure 2.2). The last step can be further divided into overcoming permeation into the enterocytes (iii) and avoiding efflux pumps (iv), surviving cellular metabolism (v), and, if paracellular absorption occurs, pass the tight junctions (vi). For systemic delivery of macromolecules all three barriers must be overcome, whereas according to the type of local action, only some of the hurdles may truly represent limiting steps to the therapeutic efficacy of the API.

2.3.1.1 Enzymatic degradation

The most relevant enzymes which could degrade a protein drug in the GI tract are listed in Table 2.3 (modified from Woodley [15]). While the stomach and the small intestine show high enzymatic activity, this is reduced in the large intestine. However, the enzymatic activity is here still comparatively high due to surviving enzymes from the small intestine. Additionally, the colonic bacteria also contribute to the metabolism of nutrients which escape digestion in the upper gut, including proteins [115,116]. The epithelial cells of the lumen also have a relatively high turnover (3-6 days), and after being sloughed off they may release further digestive enzymes in the GI tract, such as lysosomal cathepsins [15].

One of the most widespread formulation techniques to prevent enzymatic digestion is encasing or embedding the API within a nano- or microparticle. this creates a physical separation between the digestive enzymes and the loaded API. The method to obtain such drug loaded microparticles is commonly defined as microencapsulation and is discussed in depth in Paragraph 2.3.2.2.1. Enzymatic inhibitors have been extensively studied to overcome the enzymatic barrier step. These molecules can be added in the formulation to reduce enzymatic degradation. Several compounds are available and have shown different selectivity for digestive enzymes. In the formulation step, the addition of an enzymatic inhibitor requires the knowledge of the exact degradation mechanism of the intended protein API. Many enzymatic inhibitors demonstrated potential toxicity. Different classes of inhibitors are available, such as polypeptidic [117], peptidic

TABLE 2.3 – Relevant enzymes of the gastrointestinal tract (GI) tract (modified from Woodley [15]).

Stomach	**Small intestine**	
	Pancreatic juices [a]	***Brush border***
Endopeptidase	*Endopeptidase*	*Endopeptidase*
Pepsin	Trypsin	Endopeptidase 24.11
	Chymotrypsin	Endopeptidase 24.18
	Elastase	Enteropeptidase [b]
	Exopeptidase	*Exopeptidase*
	Carboxypeptidase A	Aminopeptidase N
	Carboxypeptidase B	Aminopeptidase A
		Aminopeptidase P
		Aminopeptidase W
		γ-glutamyl transpeptidase
		Dipeptidyl peptidase IV
		Carboxypeptidase P
		Carboxypeptidase M
		Peptidyl dipeptidase A
		γ-glutamyl carboxypeptidase

[a] *the proteolytic enzymes secreted by the pancreas are in their zymogen form*
[b] *enteropeptidase is a highly specific protease that activates trypsinogen, the zymogen of trypsin. After activation, trypsin activates the other pancreatic enzymes.*

[118], amino acidic [119], non-amino acidic [120]. Especially polypeptidic compounds have shown comparatively lower toxicity and high potency. Polypeptidic enzymatic inhibitors are divided into Bowman-Birk inhibitor and Kunitz trypsin inhibitor families. Size and sequence differences occur between these two families, but both are known to inhibit trypsin, chymotrypsin, and elastase [121]. Due to the molecular weight of these compounds, which is comparable to therapeutically active proteins, these inhibitors could be formulated directly with the macromolecular API and have similar release profiles if controlled release is required. For example, Kimura *et al.* showed that insulin formulated in gel spheres with aprotinin, a well-known Kunitz-type enzymatic inhibitor, could increase oral drug bioavailability *in vivo* and these compounds had a similar release rate [122]. However, all enzymatic inhibitors hinder negative feedback to further digestive enzyme secretion. This has been linked to pancreatic hypersecretion and potential pancreatic hyperplasia [123].

An effective approach is to chemically modify the desired macromolecular API to prevent its enzymatic digestion. This can be achieved by modifying the N and C terminus of the therapeutic protein [124], by PEGylating the protein [125], or by replacing labile amino acid bonds with more stable ones [126]. Several chemical residues have been covalently conjugated to proteins, for example PEG [127], D-amino acids [128], vitamin B12 [129], and fatty acids [130]. Such modifications, however, alter the chemical structure of the protein, thus requiring substantial safety and quality understanding due to their status of new biological entities (NBE). Non-covalent protein modifications, which would not require a NBE profiling, have been proposed and have proven successful in initial *in vivo* screening [131].

2.3.1.2 Mucus layer

A valuable technique to increase oral bioavailability of APIs is to increase their residence time in the GI tract in proximity of the epithelial cells. Developing mucoadhesive

systems is a valuable approach to achieve this purpose. Mucus is mainly composed of water (95%) and mucin, a high molecular weight glycoprotein. Other components include electrolytes, lipids, lysozyme, IgA, and sloughed cells [132]. The mucus layer has different thicknesses in the GI tract, starting between 50-500 μm in the stomach and decreasing to 15-150 μm in the colon [133]. This glycoproteic layer also has a very short turnover time, entailing that although high adhesion may be achieved, the mucus is frequently sloughed off, thus removing the attached delivery system. The underlying mechanisms of the mucoadhesion process have been excellently reviewed by Smart [134] and by Khutoryanskiy [135], and are summarised in Table 2.4.

Lamprecht and co-workers also showed the influence of particle size on the interaction with mucus [142]. Furthermore, particle size appeared to be critical not only to interact with the mucus, but also to penetrate and cross it [143]. Many polymers have suitable mucoadhesive properties, for example polylactic acid [144], polylactic-*co*-glycolic acid [145], chitosan [146], and alginate [147]. The target protein API may then be embedded in a polymeric matrix, or a polymeric coating may be applied to the formulation. Mucoadhesion is especially useful for multiparticulate systems, whereas for single dosage units it could lead to localised dose dumping and differences in therapeutic response [148]. In addition, single dosage units have shorter transit time that could lead to lack of effectiveness [149].

TABLE 2.4 – Mucoadhesion theory.

Mechanism	Type of interaction
Electronic theory	Mucus and polymer have opposite charges and electrostatic interactions occur [136].
Adsorption theory	Hydrogen bonds are formed and van der Waals forces act between mucus and polymer [137].
Wetting theory	Correlated to the surface tension of polymers and mucus. Polymers with better ability to spread over the mucus layer have increased mucoadhesive properties [138].
Diffusion theory	Mucin chains enter and diffuse slightly in the polymeric network, thus forming an interpenetration layer [139].
Fracture theory	Concerns the strength needed to separate polymer and mucus after adhesion [140].
Mechanical theory	Mucoadhesion is correlated to the roughness and the porosity of the polymeric structure [141].

2.3.1.3 Epithelial absorption

The final step to overcome, especially when systemic action is required, is the absorption. The intestinal epithelium typically allows two types of transportation, namely transcellular and paracellular [150]. Extensive literature exists on the mechanistic aspects of each transportation type [151–155] also in regards of peptides and proteins [14,150,156,157]. Many *in silico, in vitro*, and *ex vivo* models have been proposed to adequately predict *in vivo* absorption of drugs, but much research is still needed [158,159].

Transcellular absorption may occur by passive diffusion, by transporter systems, or by pinocytosis. Preliminary reports have shown that bile salts potentially increase *in vivo* transcellular permeation of peptides and proteins by solubilising the membrane phospholipids [118,160]. Several transport systems take care of both influx and efflux through the cell membranes. Most of the influx pumps work with small molecules, whereas some others work selectively with oligopeptides [161]. Efflux pumps like the P-glycoprotein, however, may be inhibited to improve bioavailability with small molecules [162], PEGs and PEGylated compounds [163], and ionic polymers [164,165]. However, similarly to affecting influx pumps, this approach is useful mostly for smaller molecules such as peptides. A more protein-specific type of transcellular absorption is pinocytosis. This is a type of endocytosis, often mediated by clathrins, where the luminal cell membrane invaginates to sample some luminal fluid, and an apical early endosome is formed. The compound may then be recycled back into the lumen, undergo degradation in the cellular lysosomes, or cross the cell through the common endosome and be released on the basolateral side of the epithelium.

Paracellular absorption occurs through the tight junction complexes, which interconnect epithelial cells. These structures comprise several types of proteins, which provide scaffolding and maintain the junction integrity [150]. Tight junctions, however, are dynamic structures that can be easily modulated. For instance, medium chain fatty acid salts, *i.e.*, caprylates, caprates, and laureates, have shown to loosen the tight junctions and lead to increased paracellular absorption of peptides [5,166]. A similar effect on peptide paracellular absorption was also demonstrated for medium chain mono- and diglycerides [4]. Furthermore, other small molecular compounds can be used, for example nitric oxide donors [167]. Polymers have been proposed as permeation enhancers, and especially chitosan has shown encouraging results from the start [168]. Furthermore, two chitosan derivates, namely N,N,N-trimethyl chitosan (TMC) and mono-N-carboxymethyl chitosan (MCC), exhibit even

more potential for enhancement of peptide paracellular permeation enhancement [169]. The reader is referred to other excellent reviews on the topic of protein permeation and absorption enhancers [170–172], and for the use of LB DDS in these regards [3].

2.3.2 Protein formulation

2.3.2.1 Protein stability

Biotechnological products such as therapeutic proteins displayed a significant development in recent years. However, formulation for these compounds is still problematic due to their stability profile. Owing to their large size (> 5 kDa) [173] and highly complex polymeric nature, protein structure is usually divided into a primary, secondary, tertiary, and quaternary type of formation. The characteristics of each type of structure are listed in Table 2.5.

In order to maintain therapeutic effect, the protein structure must be preserved throughout the manufacturing steps of the drug products, during storage, and following administration. A major challenge for correct manufacturing is to prevent unwanted degradation. Two typical issues in protein physical stability are denaturation and aggregation. Denaturation is a spatial alteration of the protein's three-dimensional structure. This structural unfolding can cause loss of activity, or alter the physical properties of the protein such as solubility, although it is not always an irreversible process [11].

The denaturation occurs according to a three state model, where the protein is in a native state, moves to an intermediate state, and finally the denatured species is formed [174]. The intermediate, which does not always occur, usually retains some secondary structure, and it can also lead to protein aggregation. Formulation and manufacturing can cause stress to the protein and lead to denaturation, although each protein behaves differently. Denaturation is triggered by several factors, such as pH, pressure, shear forces, temperature, and chemical denaturants [13]. During manufacturing, any shear stress involved may harm the protein structure [12]. Even formulation techniques that are usually employed with proteins may lead to denaturation [175]. Aggregation is caused by unfolded proteins' response to external stimuli, *e.g.*, variations in protein concentration or ionic strength. The interactions that take place between proteins may be covalent, such as disulphide bond formation, or non-covalent, for instance by hydrophobic forces. Further interactions may occur that lead to precipitation of protein aggregates and formation of protein fibrils.

TABLE 2.5 – Structures of protein.

Structure	Characteristics
Primary	L-α-amino acid sequence.
Secondary	Local three-dimensional arrangement due to hydrogen bond formation. Typical structures are α-helices and β-sheets.
Tertiary	Global three-dimensional arrangement of secondary structure and side chains. Structure maintained by hydrophobic and steric interactions, as well as disulphide bridges between cysteine residues.
Quaternary	Non-covalent assembly of protein monomers to form larger complexes.

Chemical instability must be taken in consideration when peptides and proteins are formulated. Each composing amino acid may respond to chemical stimuli which could lead to an overall conformational change and finally to protein degradation [176]. The pH certainly plays a major role with respect to chemical instability [177]. For instance, high pH may entail hydrolysis of aspartate-proline and aspartate-tyrosine peptidic bonds. Furthermore, at low pH, tryptophan, methionine, cysteine, tyrosine, and histidine groups may undergo oxidation. Photooxidation may also occur in presence of light, for example on phenylalanine groups. Reduction and oxidation of cysteine groups also can lead to denaturation [178].

2.3.2.2 Protein formulation for oral delivery

To ensure adequate protein stability, different formulation approaches have been proposed. Due to protein instability and limited bioavailability by oral administration, most techniques are tailored for parenteral delivery. Direct protein solubilisation or lyophilisation are the most widespread methods and have been adequately reviewed [173,179,180]. As for oral delivery strategies, Hwang and Byun [181] have recently reviewed the currently available approaches. To increase oral bioavailability of macromolecules, the authors suggested the use of absorption enhancers (which were earlier outlined in this chapter), microencapsulation (which is discussed in Paragraph 2.3.2.2.1.) and chemical modifications (covalent and non-covalent) of the protein API (Paragraph 2.3.1.1). Further suggested reading on peptide and protein delivery is available from several different research groups [181–185].

2.3.2.2.1 Microencapsulation for oral protein delivery

Microencapsulation allows API loading into typically micron-sized particles, thus enabling protection from

digestive enzymes, and adhesion to the mucus layer. The nomenclature of the obtained drug delivery systems, however, is not entirely consistent within the scientific literature [186]. The terminology used is closely related to the particle's size and architecture. Generally, "microparticle" represents an umbrella term which comprises all particles with a diameter between 1 and 1000 µm. Microparticles are furthermore divided into "microcapsules" and "microspheres", which are represented in Figure 2.3. Microcapsules are spherical microparticles where two different domains are present. The classical example of a microcapsule is a microparticle with an external shell and an internal core (Figure 2.3a), but the core structures may hold for a dispersion within the particle (Figure 2.3b). To ensure protection from the external environment, the API is usually loaded in the core compartments, whilst other adjuvants such as enzymatic inhibitors may be present in both domains. Microspheres, instead, are made of a matrix-like single compartment in which the API is finely and homogenously dispersed or dissolved (Figure 2.3c). A specific type of microspheres is microgels, defined by Bysell *et al.* as cross-linked gel particles whose structure responds to environmental stimuli [187]. Microgels exhibit the advantage of the specific characteristics of the polymeric type that composes the network, and form a suitable environment for a macromolecular API, while protecting it from the GI milieu [187]. Furthermore, some polymers such as alginates and chitosans have shown mucoadhesive and permeation enhancing properties [188–190].

Chitosan and its derivates have especially shown feasibility for oral delivery of proteins and peptides [191–196]. Several different methods are known for microencapsulation, such as solvent evaporation [197], spontaneous emulsification and solvent diffusion [198], supercritical fluids [199], and ionic gelling, and have elsewhere been reviewed [20,21,200–202]. Microencapsulation methods, however, must take into consideration the protein structure, which can be easily harmed in presence of elevated temperatures, denaturing agents, or high shear forces [12,173]. There are preliminary findings of successful protein encapsulation and delivery. For instance, Sarmento and co-workers demonstrated *in vivo* that insulin alginate/chitosan microparticles could be successfully delivered to rats' intestine and thereby absorbed without substantial loss due to enzymatic degradation [203]. Rekha and Sharma showed the *in vivo* efficacy of lauryl succinyl chitosan nano- and microparticles as drug delivery systems for insulin, which could protect the peptide from enzymatic degradation and increased its bioavailability in diabetic rats [204].

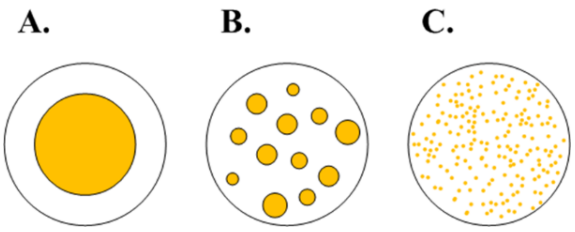

FIGURE 2.3 - Microparticle types. Microcapsules with single core (a) and with dispersed cores (b), and microspheres (c).

2.3.3 Protein characterisation

Protein structure and its stability are a major concern during its formulation. As earlier described, proteins have different structures that affect overall protein properties, such as solubility or therapeutic effect. An adequate characterisation of these structures during the formulation step and during *in vitro* or *in vivo* experiments is required as proof of protein stability for the proposed drug delivery system. If the chosen macromolecular API is a NBE, a thorough characterisation of the protein is part of pharmaceutical profiling before the formulation development. Several techniques are available to assess protein structure, its degradation, and potential aggregation phaenomena. A non-exhaustive list of suitable techniques for protein characterisation alone or in formulation can be found in Table 2.6 (modified from Jorgensen[13]). It is clear that many techniques describe similar protein characteristics, so only a limited selection of these approaches is necessary to evaluate the stability of a protein after formulation or administration. However, after the protein formulation, the composition of the dosage form must be carefully considered to avoid possible interferences in the protein analytical evaluation.

2.4 Microencapsulation by prilling

2.4.1 Prilling and vibrating nozzle technique

Microencapsulation as formulation technique for macromolecules appears to be promising in terms of enzymatic protection and mucoadhesion. Many technologies for protein microencapsulation are available but not all may be suitable for protein formulation due to the mild condition needed [22,187,227]. Prilling is based on high speed extrusion of a polymeric solution through a small nozzle. Historically, the technique was first patented in Germany to form ammonium nitrate pellets [228]. The approach has then found further applications for example in the fertilising industry and, more recently, in cell biology and in pharmaceutics [229]. Prilling can be obtained by

TABLE 2.6 – Protein characterisation techniques.

Technique	Information	References
Chromatography		
Size exclusion c. (SEC)	Molecular weight	[205]
Ion-exchange c. (IEC)	Degradation, molecular charge	[206]
Electrophoresis		
Sodium dodecyl sulphate polyacrylamide gel e. (SDS-PAGE)	Aggregates, impurities, molecular weight	[207,208]
Capillary e. (CE)	Aggregates, impurities, molecular weight	[209]
Isoelectric focussing (IEF)	Isoelectric point	[210,211]
Mass spectrometry (MS)	Molecular weight, amino acid sequencing	[212]
Spectroscopy		[213]
Fourier transform infrared s. (FTIR)	Secondary structure, crystallinity	[214]
Raman s.	Secondary structure, three-dimensional structure [c], crystallinity	[215,216]
Ultraviolet absorption s. (UV)	Protein content	[82,217]
Fluorescence s.	Three-dimensional structure [c]	[218]
Circular dichroism (CD)	Secondary structure of protein	[219]
Thermal techniques		
Differential scanning calorimetry (DSC)	Protein stability, crystallinity, glass transition	[220,221]
Thermogravimetric analysis (TGA)	Water content	[220,221]
Scattering		
Dynamic light s. (DLS)	Aggregates, molecular weight	[222]
Static light s. (SLS)	Aggregates, molecular weight	[222]
Small angle X-ray s. (SAXS)	Three-dimensional structure	[223]
Small angle neutron s. (SANS)	Three-dimensional structure	[223]
X-ray crystallography	Three-dimensional structure	[224]
Nuclear magnetic resonance (NMR)	Three-dimensional structure	[225]
Enzyme-linked immunosorbent assay (ELISA)	Protein content, binding site integrity	[226]
Chemical assays	Protein content	[82]
Lowry a.		
Bradford a.		
Bicinchoninic acid (BCA) a.		
Biuret a.		
O-phthalaldehyde conjugation		
Nitrogen content		
Activity [d]	Enzymatic activity	

[c] *localised to specific amino acids*
[d] *if analysed protein is an enzyme*

different methods and technologies, namely by simple dripping, dripping with concentric air jet, dripping and spraying with electrostatic forces, rotating disk and jet cutting, and vibrating nozzle (Figure 2.4). These techniques have been outlined by Heinzen *et al.* [229]. The vibrating nozzle method has found wide application in modern pharmaceutics. This technique has its physical explanation in the Plateau-Rayleigh instability [230].

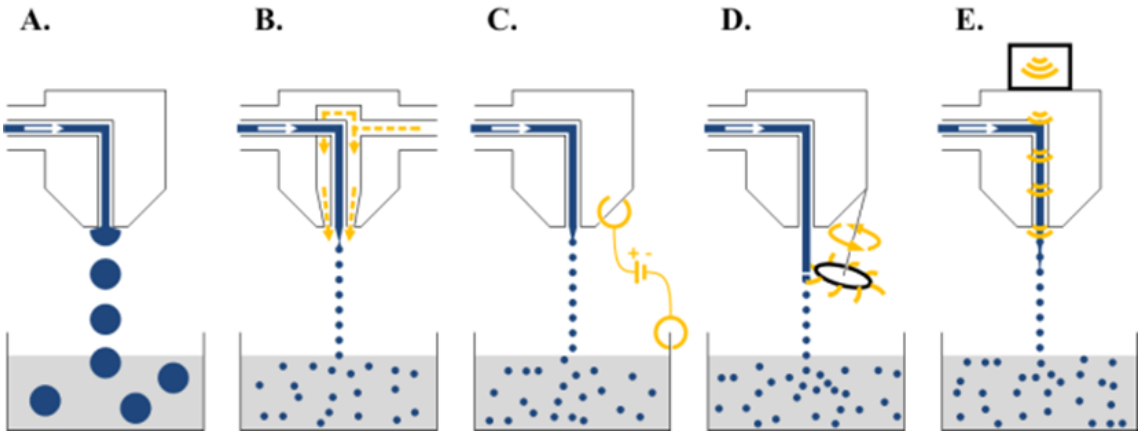

FIGURE 2.4 - Different types of prilling. Dripping (a), concentric air jet (b), electrostatic force-driven dripping (c), jet cutting (d), and vibrating nozzle (e).

After a liquid is forced through a nozzle or orifice due to pressure or simple gravity, a liquid stream is formed. Small perturbations affect the stream's regularity, and once a threshold vibration frequency is reached, the stream is broken into droplets (Figure 2.5). The frequency (f) of such perturbations is related to wavelength according to Equation 2.11:

$$f = \frac{v_j}{\lambda} \qquad 2.11$$

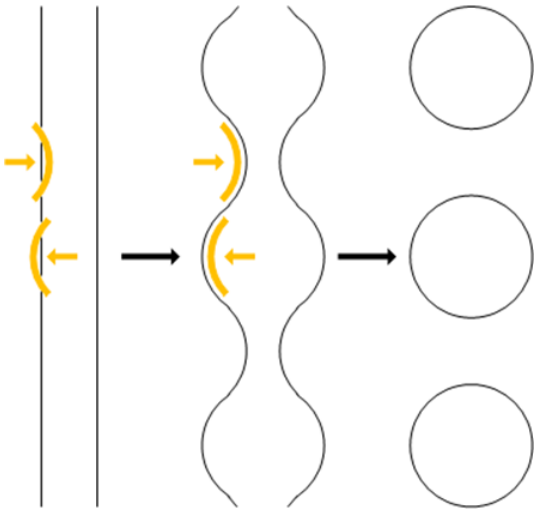

FIGURE 2.5 – Development of the Plateau-Rayleigh instability on a liquid stream (black lines) due to perturbations in water (yellow lines).

Where v_j is the jet velocity and λ is the wavelength. The optimal wavelength of these vibrations to allow the jet breakup is calculated according to Equation 2.12:

$$\lambda_{opt} = \pi \cdot \sqrt{2} \cdot d_j \qquad 2.12$$

Where λ_{opt} is the optimal wavelength, and d_j is the jet diameter. Constantin Weber included the properties of the falling liquid and modified the equation as follows [231]:

$$\lambda_{opt} = \pi \cdot \sqrt{2} \cdot d_j \cdot \sqrt{1 + \frac{3 \cdot \eta}{\sqrt{\rho_f \cdot \varsigma \cdot d_j}}} \qquad 2.13$$

Where η represents viscosity, ρ_f is fluid density, and ς is the surface tension. Serp *et al.* first calculated the drop diameter d_d according to Equation 2.14 [232]:

$$d_d = \sqrt[3]{6 \cdot \frac{F}{\pi \cdot f}} \qquad 2.14$$

Where F represents liquid flow in terms of volume. Flow can be further expressed by Equation 2.15:

$$F = \frac{\pi \cdot {d_n}^2}{4} \cdot v_j \qquad 2.15$$

Where d_n is the nozzle diameter. By merging Equation 2.14, 2.15 and 2.11, Equation 2.16 is obtained:

$$d_d = \sqrt[3]{\frac{3}{2} \cdot {d_j}^2 \cdot \lambda_{opt}} \qquad 2.16$$

Clearly, liquid jet velocity and vibration frequency are paramount for the successful droplet formation [229,233].

The Plateau-Rayleigh instability can thus be used to form equally sized droplets from a liquid jet by applying vibration and this method is generally called the vibrating nozzle technique. An API can be loaded into the prilled liquid, which may be composed of a polymeric solution or of a non-aqueous carrier, such as fatty acids and waxes [234,235]. Suitable polymers for prilling are discussed in Paragraph 2.4.2. The droplets formed from the broken up liquid stream can solidify mid-air or can be collected in a hardening bath. In the latter case, the microencapsulation step takes place according to the properties of the microsphere-forming compound. In fact, the hardening may occur due to several physicochemical triggers, for instance temperature change, ionic cross-linking, pH variation, or a mixture thereof. Prilling has been confused with spray congealing (also known as spray chilling and spray cooling) if the microparticle solidification occurs mid-air rather than in a hardening bath [236,237]. The major difference between these techniques is that prilling does not require a nebulisation or atomisation step, which is instead fundamental for spray congealing.

Many modifications have been proposed to the basic vibrating nozzle system. For example, Brandenberger *et al.* introduced an electrostatic ring to reduce drop coalescence mid-air and after entrance into the hardening bath [238]. Herein, the liquid stream falls through the electrostatic ring that charges each droplet mid-air to promote repulsion. The hardening bath is grounded to allow entrance of the falling droplets. Additionally, the nozzle employed can be single or concentric. The former system allows direct entrapment of the API within a matrix, whereas the latter forms a microcapsule with distinct core and shell compartments. With the concentric nozzle system, air can be flowed through the external annulus to reduce the particle size without causing atomisation. High viscosity is a known limitation for this system, but Rodríguez-Rivero and co-workers proposed a modified pressurised system to allow prilling of systems with unfavourable rheological properties [239]. Brandenberger and Widmer, and Vilesov *et al.* separately proposed two systems to increase the yield of the prilling systems by using different geometries on a multi-nozzle apparatus [233,240]. This is an interesting technical approach as it demonstrates a possible modular scale-up for microparticles production. For example, Brandau introduced an industrially viable process which applies the vibrating nozzle principle to produce microspheres [241,242]. Prilling devices based on vibrating technology are already commercially available from different companies, *e.g.* the Encapsulator B-390 from Büchi Labortechnik AG (Flawil, Switzerland), the Spherisator S from BRACE GmbH (Karlstein am Main, Germany), and the Variation D from Nisco Engineering AG (Zürich, Switzerland).

Many different products and compounds can be microencapsulated by using prilling or, in particular, the vibrating nozzle method. For instance, Chandramouli *et al.* formed alginate microspheres containing *Lactobacillus acidophilus* with the vibrating nozzle method in order to prevent gastric instability [243]. Much literature has been generated on this topic and this scientific field has been excellently reviewed [23,229,244]. Del Gaudio and co-workers analysed the effects of the initial solution properties on the prilling process [27]. Working on a Variation D from Nisco Engineering AG, they differentiated between simple vibration-assisted dripping and laminar jet break-up, *i.e.* vibrating nozzle method. Recently, Auriemma *et al.* produced by prilling piroxicam-loaded pectin blend microspheres, which were further coated for colonic delivery [245]. Homar *et al.* showed how microencapsulation by prilling could be useful to formulate poorly soluble drugs [24]. In their study, they were able to form core/shell microcapsules with an Inotech IE-50 R encapsulator using a concentric nozzle apparatus. A ketoprofene-loaded self-microemulsifying system (SMES) provided the core compartment, whereas the outer shell was formed by employing an alginate solution. Several aqueous hardening baths were used, employing $CaCl_2$, $ZnCl_2$, $AlCl_3$, or chitosan as cross-linking agents. More recently, Dorati and co-workers compared microcapsules formed using an Encapsulator B-395 Pro with microcapsules prepared by emulsion phase inversion [246]. The particles produced using the vibrating nozzle method demonstrated better entrapment, worked at mild conditions, avoided organic solvents, had high reproducibility, and could be prepared rapidly. Finally, a notable example of non-aqueous media for prilling was suggested by Zhang and Rochefort, who prepared polyethyleneimine microspheres loaded with enzymes using the vibrating nozzle [26]. This approach employed polymer interfacial reticulation with sebacoyl chloride that was dissolved in the cyclohexane hardening bath. The use of non-aqueous hardening baths has been pioneered by Buthe *et al.* [247], and it was proposed for protein microencapsulation by Zhou *et al.* [248]. However, it entails the complete removal of the toxic organic solvents of the hardening bath to be considered for pharmaceutical use.

2.4.2 Polymers for prilling

Different compounds can be used for the prilling medium according to the characteristics required from the formed microparticles. Hydrophobic prilling media have been suggested, such as fatty acids [234,235,249] and poly(lactic-*co*-glycolic acid) (PLGA) in acetone [250]. However, these systems may not be suitable for macromolecule microencapsulation, for which an aqueous milieu is preferred. If hydrophilic media are selected, the use of a polymer is necessary to allow microparticle formation. Hydrogels, *i.e.*, gels where the main liquid component is water, proved to be of critical importance in biomedical and pharmaceutical sciences, due to their favourable properties in terms of tissue engineering and drug carrying [251–253]. Furthermore, hydrogel properties can be tailored to meet the therapeutic needs and API characteristics. For example, many hydrogels respond to specific physiological triggers, which allow modified release, or have mucoadhesive properties [254]. The transition from polymeric solution to a gel requires cross-linking in the hardening bath. Several types of cross-linking are known, both of chemical and physical nature, which have been thoroughly reviewed by Hennink and van Nostrum [255]. Most chemical cross-linkers have relevant toxicity, requiring potential health hazards and lengthy removal steps. Physical approaches, such as temperature, pH, ionic strength, non-covalent bonds, and hydro- and lipophilicity, are inherently less toxic and the gelling step can be easily controlled. Therefore, physical cross-linking is generally the preferred method for microcapsule production.

Among the different hydrophilic polymers available (Figure 2.6), alginates currently represent the state of the art for prilling [232,256,257]. This water-soluble anionic polysaccharide is composed of 1-4 linked β-D-mannuronate and α-L-guluronate, and it is found naturally in the cell walls of brown algae. The carboxylic groups allow cross-linking with divalent ions such as barium and zinc [258,259], but calcium is the most used for microencapsulation [260,261]. In terms of oral delivery, alginates have shown some mucoadhesive properties [262], especially in combination with other polymers [263], and are also suitable for protein entrapment [264]. Chemical modifications have been proposed to improve drug delivery properties [265,266]. Along with alginate, chitosan gels have demonstrated promising drug delivery and microencapsulating properties on *in vitro* and *in vivo* models [188,195,267,268]. Chitosan is a cationic polysaccharide formed by de-acetylation of chitin, a polymer commonly found in crustacean shells, and is composed of 1-4 linked β-D-glucosamine (Figure 2.6). Although this polymer is soluble only at acid pH, chitosan has successfully been used to

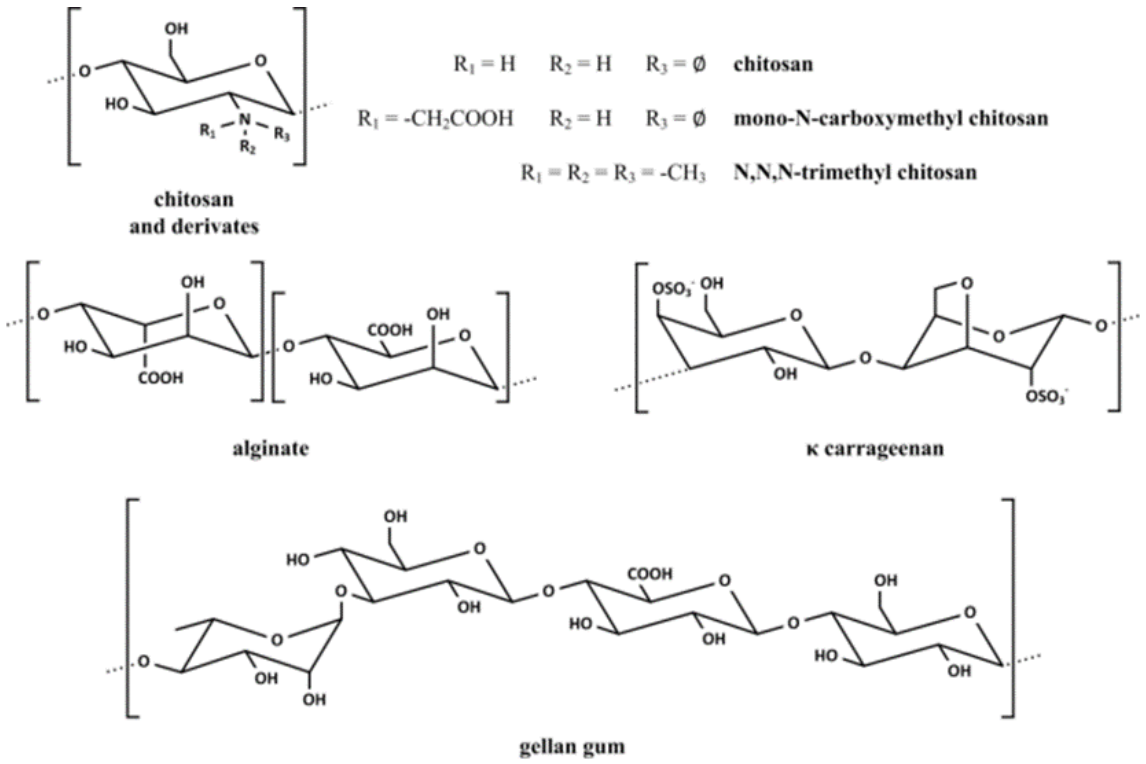

FIGURE 2.6 - Chemical structures of natural and semi-synthetic polymers for prilling.

microencapsulate peptides and polymers [269]. The cationic nature of this polymer, due to the amine group on its glucosamine monomers, allows ionotropic gelling using tripolyphosphate ions [270,271] (Figure 2.6). Furthermore, chitosan microparticles possess mucoadhesive and permeation-enhancing properties useful for oral administration [169,272,273].

Many chitosan derivates have been synthesised to enhance its pharmaceutical properties, such as solubility across a wider pH range [192,274–276]. The most promising chitosan derivates are anionic mono-N-carboxymethyl chitosan (MCC) and cationic trimethyl chitosan (TMC) [277–279], and have been used for entrapment of macromolecules [280,281] and in prilling [28]. Several other polymers have been proposed for prilling. Carrageenan was used by Patil and Speaker to successfully encapsulate horse radish peroxidase via prilling [282]. Auriemma *et al.* compared prilled pectin and alginate-pectin blends after Eudragit® S100 coating for piroxicam microencapsulation [245]. Due to ionotropic cross-linking, as well as thermal hysteresis, gellan gum has promising gelling characteristics suitable for prilling [283].

2.5 Multi-compartmental drug delivery systems (DDS)

Multi-compartmental DDS appear as an attractive and promising formulation approach for advanced dosage forms, which has been gaining momentum in recent years. However, there is still a lack of an exact definition for these systems. A multi-compartmental DDS is a dosage form that has different and distinguishable structural regions, which may be also defined as domains or compartments. Each compartment may present itself in liquid, solid, or gaseous phase. Moreover, in case of liquids, different phases may be present that separate hydrophilic from lipophilic formulation domains. A compartmentalised drug delivery system is desired to exhibit reduced API diffusion or migration between regions. Different approaches can be used to ensure this separation, for example by creating physical boundaries (polymeric coating), by embedding the API in a solid structure (polymeric matrix, solid wax), or simply by chemical affinity (poorly water-soluble drugs in a micelle). Care must be taken not to confuse a multi-compartmental DDS with a multiple unit dosage form. In the former case, a DDS is classified by the number of regions with identical physicochemical properties, whereas the latter definition simply indicates whether the dosage form is divided into smaller fractions. Multi-compartmental DDS are particularly advantageous due to their inherent versatility, which justifies their level of complexity. Each compartment possesses distinct features that allow

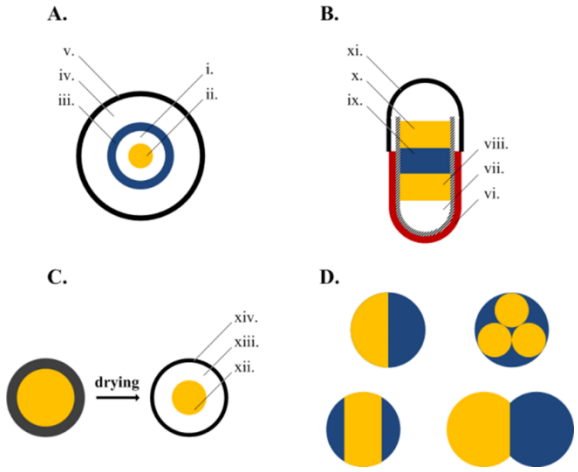

FIGURE 2.7 – Schematics of multi-compartmental drug delivery systems. In (a): multi-layered Chronotopic® system, with insulin-containing core (i), first HPMC layer (ii), protease inhibitor-loaded coat (iii), second HPMC layer (iv), and enteric trigger coating (v). In (b): PORT System® capsule, with semi-permeable capsule body coating (vi), osmotically active compartment (vii), retarded release drug dose (viii), insoluble sliding plug (ix), immediate release drug dose (x), and water soluble capsule cap (xi). In (c): gastroretentive system, with drug-loaded alginate core (xii), air compartment (xiii), and buoyancy shell (xiv). In (d): different geometries of Janus nanoparticles with different drugs or properties.

different delivery possibilities and technical manufacturing solutions. For example, different release kinetics may be applied to each compartment, to ensure pulsatile delivery [284]. Different types of coatings can respond to different stimuli and triggers, ensuring optimal targeting [285]. Furthermore, size hierarchies (micro- and nanoparticles) can be used to exploit dimension and morphology-related properties [286]. One of the most prominent exponents of this last category, namely Nanoparticle-in-Microsphere Oral Systems (NiMOS), will be comprehensively discussed in Paragraph 2.5.1.

Several types, geometries, and combinations of multi-compartmental DDS have been proposed over the last decades. A typical approach to form these structured DDS is by applying multiple coatings over a central core. This creates a series of concentric layers with different properties (Figure 2.7a). For example, the group of Del Curto further developed the Chronotopic® system [285,287]. Herein, a fast-dissolving insulin-containing core (i) is coated with an HPMC layer (ii) to delay protein release and separate the API from the protease inhibitor-loaded

layer (iii). This is in turn coated with a further HPMC coating (iv), which has defined swelling and erosion time to account for transit duration in the small intestine. Finally, an enteric coating (v) is applied, which acts as a trigger for the swelling of the most external HPMC layer (iv).

Capsules can also be used to create multi-compartment systems. For example, the PORT System® first patented by Amidon in 1995 can be modified to have three compartments to achieve pulsatile release (Figure 2.7b) [288,289]. Briefly, a capsule body covered in semi-permeable coat (vi) is filled with osmotically active excipient (vii) and a mixture of API (viii). This compartment is covered by an insoluble wax-based sliding separator (ix). On top of this separator, another compartment contains a separate dose of API (x), and finally the non-coated cap head is locked on the body (xi). After ingestion, the cap (xi) is readily dissolved and the first dose of API (x) is released. Meanwhile, water steadily penetrates through the body (vi) into the lower compartment (vii) and creates an osmotic pressure that pushes the separator layer (ix). At a given time, the separator exits the body and the second API dose (viii) can be released. Similar technologies, which are also available on the market, have been described in edited books by Rathbone and co-workers [290–292].

Another notable example of multi-compartment system is a gastroretentive formulation (Figure 2.7c), introduced by Iannuccelli *et al.* [293,294]. This system is formed by an API-containing alginate bead (xii) located in an empty cavity (xiii) formed within an alginate/polyvinyl alcohol (PVA) outer shell (xiv). The presence of the outer membrane (xiv) traps the air in the system (xiii), which allows buoyancy. Upon release, the alginate core (xii) may allow some mucoadhesion and prolong the release. Recently, multi-compartment anisotropic particles have been proposed as DDS. These systems are usually defined as Janus particles, but several geometries are available (Figure 2.7d). Janus particles are formed with different polymers using different techniques such as microfluidics [295] or electrohydrodynamic co-jetting [296]. In terms of drug administration, they have been used for API co-administration [295], modified release kinetics [297,298], targeting [299,300], and theranostics [301]. Excellent reviews on manufacturing and on applications of these particles are available [30,302]. Further other pioneering multi-compartment DDS exist, for example vesosomes and dendrosomes [303–305], and this field of pharmaceutical sciences is rapidly moving towards highly structured systems and closely approaching that of biomimicry [306–308].

2.5.1 Nanoparticle-in-Microsphere Oral System (NiMOS) as dosage forms

NiMOS are multi-compartmental systems which have a hierarchical organisation. Kriegel defines NiMOS as solid-in-solid multi-compartmental systems, differentiating them from solid-in-liquid systems (also known as nanoparticles-in-emulsions, NiE) [309] and from liquid-in-liquid systems (such as W/O/W multiple emulsions) [310]. Specifically, NiMOS are API-loaded polymeric nanoparticles that are located in polymeric microspheres. The definition of NiMOS was first proposed by Bhavsar *et al.*, who formed fluorescently labelled gelatine nanoparticles and embedded them in poly(ε-caprolactone) (PCL) microspheres [311]. Briefly, the nanoparticles were prepared by adding ethanol-aided gelatine precipitation. The nanoparticle aqueous suspension was emulsified with PCL and dichloromethane. After addition of PVA, the dichloromethane was removed by evaporation and the microspheres were lyophilised. NiMOS demonstrated suitability for macromolecule delivery in subsequent experiments. Accordingly, these multi-compartment systems were loaded with plasmid DNA vectors to test for local intestinal transfection and with small interfering RNA (siRNA) to treat inflammatory bowel disease [29,312–314]. A similar nano-in-micro approach was introduced by Kaye and his team for pulmonary delivery of a model antibody using a spray drying process [315].

NiMOS have shown a synergic combination of nanoparticles and microspheres [316]. Nanoparticles alone have shown great potential for oral delivery of proteins and other macromolecules [31,317,318]. The main characteristic of these particles is certainly their size. Nanoparticle sizes around 100 nm have proven especially effective in mucus penetration, and can eventually be taken up by local immune cells and macrophages [142,319]. Furthermore, the polymer used for this compartment may also be useful to optimise delivery and ensure uptake from the luminal lining. Polymer properties are also highly relevant for the microsphere compartment in which the nanoparticles are embedded. As earlier described, polymers can possess biopharmaceutically promising properties, such as mucoadhesion or permeation enhancement, or even a combination thereof. When a macromolecular drug is present and oral delivery is required, the polymer must allow the microsphere to protect the API from enzymatic degradation. To ensure macromolecular stability, protease inhibitors may be loaded in the microsphere compartment. NiMOS, thus, should possess the aforementioned properties whether local or systemic action is intended.

2.5.1.1. Clay nanotubes – halloysite (HNT)

Currently, the geometry of NiMOS compartments is limited to spherical nanoparticles and microspheres. Among other nano-geometries suitable for this system, nanotubes have shown great potential in terms of drug delivery, but their toxicity and cost remain strong concerns for development [320,321]. In recent years, however, a new type of natural and non-toxic nanotubes called halloysite (HNT) has been proposed for biomedical applications [322,323]. Halloysite is an aluminium silicate clay mineral extracted from quarries worldwide. Its structure is formed by repeated $Al_2Si_2O_5(OH)_4{\cdot}nH_2O$ units that are distributed in layers [324]. These layers are overlapped and folded as a scroll to form a nanotubular structure (Figure 2.8a). The silicate groups SiO_4 form tetrahedron-like structures placed on the external surface of the layer, whereas the aluminium groups AlO_6 have an octahedral geometry and are located on the inner surface [325]. This diverse distribution of silicate and aluminate groups creates a specific charge distribution. The external nanotube surface is negatively charged, whereas the luminal surface has positive charge. Furthermore, the aluminium luminal groups are hydrated as $Al(OH)_2$ aluminol groups. Generally, HNT display a length from 200 nm to 2 µm, inner diameter from 5 to 20 nm, and external diameter 40 to 100 nm [321]. The specific surface can vary greatly, between 50 and 150 $m^2\ g^{-1}$. The great variability is to some extent due to the mining site of the halloysite clay [326,327]. HNT have been introduced as drug delivery systems by Price and co-workers [328].

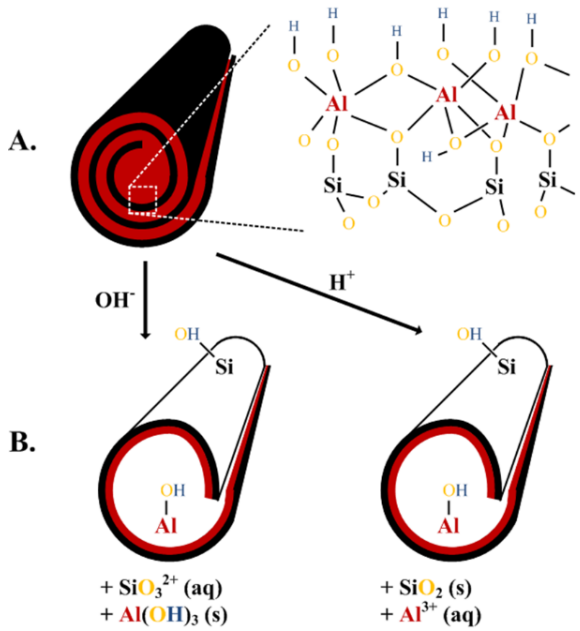

FIGURE 2.8 – Chemical structure of halloysite nanotube before (a) and after chemical etching (b).

Herein, two small molecules and a dinucleotide were loaded in HNT and were subsequently released, obtaining prolonged releases over several hours, which was depending on the given compound. The HNT use for pharmaceutical purpose has since increased, for example using doxycycline for periodontitis treatment [329], diltiazem and benzalkonium chloride [330], and different poorly water-soluble drugs [331]. The purpose of HNT-based DDS is to have the API within the HNT lumen and adsorbed on the surface. To achieve HNT loading, the concentrated API solution is mixed with the suspended halloysite. Vacuum is applied to remove air from the lumen, as it hinders the capillary force-driven penetration of the API-containing solution due to surface tension [332–334]. While electrostatic interactions (due to HNT charge distribution) would lead to preferential attraction of the drugs molecules, these may still be adsorbed on either side of the nanotubes [321]. Furthermore, Cornejo-Garrido *et al.* showed promising anti-inflammatory properties of HNT *per se* [335]. In most recent applications, HNT have been used to form biocomposite nanomaterials and mesoporous drug carriers [334,336–338].

Halloysite is also interesting regarding its great versatility in terms of chemical modifications [322], and some examples are hereby listed. To increase loading capacity, the HNT lumen has been chemically etched both in acid and in alkaline conditions [339,340] as shown in Figure 2.8b [325]. In both cases, the chemical etching acts selectively in the inner lumen acting on the aluminium groups. Another chemical modification was proposed by Yuan *et al.*, who functionalised the internal aluminol groups with γ-aminopropyltriethoxysilane (APTES) to increase dye loading [333]. Not only the dye loading was increased by interaction with the chemical groups introduced, but also the release kinetic was successfully modified. Guo and co-workers modified HNT with respect to an application in cancer treatment [341]. Briefly, the external silica groups were activated and grafted with Fe_3O_4 and folic acid. The particles were finally loaded with doxorubicin, and selective cancer cell toxicity was demonstrated *in vitro*. In terms of polymer wrapping of HNT, Zhai *et al.* used chitosan to anchor horseradish peroxidase (HRP) to HNT for phenol removal from wastewater [342]. Chitosan, owing to its cationic nature, adhered to the negatively charged external HNT surface. Glutaraldehyde was used to activate the N-termini of chitosan, and then the polymer-HNT was incubated with HRP. This system showed increased loading and HRP survived the grafting while maintaining its activity. Shamsi and co-workers proposed a technically advantageous polymeric wrapping of HNT by adhering DNA on its external surface, and were able to completely solubilise the nanodispersion, further increasing its stability [343].

It is finally interesting to mention an analogue clay mineral, imogolite, which has inverted disposition of alumina and silica, and consequently opposite charge distribution [344]. It further displays longer length (1-5 μm), smaller diameter (2-10 nm external, 1-5 internal), and higher surface area (300-400 $m^2 g^{-1}$) [321]. Another major difference from HNT, is that imogolite is single-walled and available only in very small quantities, whereas halloysite is multi-layered and can be supplied on a scale of industrial quantities.

2.6 Quality aspects of drug formulation

2.6.1 Quality-by-Design (QbD) initiative and LB suspensions

Quality in drug formulation is pivotal throughout the product's life cycle, starting from the raw materials, going through manufacturing process and shelf-life, up to administration and *in vivo* performance. The definition of quality in pharmaceutical development comes from two viewpoints, one focusing on the compliance to specifications, the other on the respect of the expected therapeutic benefit [32,34,345]. In terms of pharmaceutical quality, the objective is to create a product capable of carrying out a therapeutic action, comply with regulatory aspects, be reproducible and thoroughly documented. Furthermore, it should be obtained according to a defined process where variables are accounted for and all potential issues are known and understood. According to the "Guidance for Industry, Q8(R2) Pharmaceutical Development" issued by the Food and Drug Administration (FDA) [34]:

> "*The aim of pharmaceutical development is to design a quality product and its manufacturing process to consistently deliver the intended performance of the product. The information and knowledge gained from pharmaceutical development studies and manufacturing experience provide scientific understanding to support the establishment of the design space, specifications, and manufacturing controls*"

These guidelines are aimed to surpass a previously established concept of quality, namely Quality-by-Testing (QbT) [32,346]. QbT is based on the idea that drug product quality comes from raw material quality and the respect of FDA-approved specifications according to a static manufacturing process. Whenever the drug product does not meet specifications, the entire production batch is discarded. The manufacturer may submit supplements to the controlling authority to revise acceptance criteria. This process is usually time consuming and expensive, since each in-process variation needs to be adequately documented at the regulatory authority. Pharmaceutical Quality-by-Design (QbD) proposes a different approach to similar issues. According to Yu, pharmaceutical QbD represents an approach to develop a drug product by thoroughly understanding and controlling product and process by identifying a series of critical quality attributes, process parameters, and sources of variability [32,346]. Thus, the idea is that pharmaceutical quality should be designed into the drug product. The QbD approach was first proposed by Juran [347], and it has been eventually accepted for the pharmaceutical industry by the FDA in 2004 [33]. The most important terms of QbD are listed in Table 2.7, as defined by the FDA [34].

Different tools are suggested to evaluate the criticalities of a pharmaceutical development process or of a given factor. Risk assessment tools can help identifying the critical variables in process and formulation, *e.g.*, Ishikawa diagrams, and ranking said criticalities, *e.g.*, by a failure mode and effect analysis (FMEA). The impact of each risk can be then evaluated through statistical analysis after conducting thorough and systematic experimental work. Gaining such extensive understanding of both process and formulation factors on CQAs is an important goal to define a design space. The most used approach that may be used here is the Design of Experiments (DoE), and this topic is described in Paragraph 2.6.2. QbD and DoE are so often jointly applied in formulation development that the definition of Formulation-by-Design (FbD) is used in these cases [348]. While FDA guidelines generally use the word critical material attributes (CMA) for raw material variables affecting CQAs of the final product, Singh used the more specific (but non-official) term critical formulation attributes (CFA).

QbD, or rather FbD, has found application for different types of drug formulation processes, for example tabletting [349–351], suspension [352], or co-precipitation [353], as well as for biotechnological products [354]. As for LB systems, formulation development according to QbD has been employed for different types of DDS. Dhawan and co-workers developed a SLN formulation for quercetin to improve the permeation across the blood-brain barrier to better reach the central nervous system [355]. After defining CFAs and CPPs, Dhawan's team could identify a formulation with a known design space that could meet the *in vivo* therapeutic specifications. After a preliminary QbD-based evaluation of hydrophilic API in liposomes [356,357], Xu and co-workers recently analysed formulation and processing of enzyme-loaded liposomes within the QbD framework [358]. Not only they conducted a typical DoE-modelled set of experiments, but they also proposed a risk assessment charts for each of the liposome's CQA. This work

TABLE 2.7 – Brief glossary of Quality by Design terms.

Term	Definition
Quality by Design (QbD)	Systematic approach to development that begins with predefined objectives and emphasises product and process understanding and process control, based on sound science and quality risk management.
Quality Target Product Profile (QTPP)	Prospective summary of the quality characteristics of a drug product that ideally will be achieved to ensure the desired quality, taking into account safety and efficacy of the drug product.
Critical Quality Attribute (CQA)	A physical, chemical, biological, or microbiological property or characteristic that should be within an appropriate limit, range, or distribution to ensure the desired product quality.
Critical Process Parameter (CPP)	A process parameter whose variability has an impact on a critical quality attribute and therefore should be monitored or controlled to ensure the process produces the desired quality.
Design Space	The multidimensional combination and interaction of input variables (*e.g.*, material attributes) and process parameters that have been demonstrated to provide assurance of quality. Working within the design space is not considered as a change. Movement out of the design space is considered to be a change and would normally initiate a regulatory post-approval change process. Design space is proposed by the applicant and is subject to regulatory assessment and approval.

allowed the identification of a suitable design space for this formulation. A final example of successful implementation of QbD on a LB system was performed by the group of Pund during the formulation of cilostazol, a platelet aggregation inhibitor, as self-nanoemulsifying drug delivery system (SNEDDS) [359]. In this work, the QbD strategy was applied by using DoE to understand the effect of the formulation components on final LB system's CQA. Multivariate analysis was employed as a complementary tool for DoE to correctly model the effect on the selected response variables, namely droplet size and its distribution, equilibrium solubility, ζ-potential, and dissolution efficiency, in order to chart an optimal design space for the SNEDDS.

2.6.2 Design of Experiments (DoE) and statistical analysis

A DoE, also called formal experimental design, is "a structured, organised method for determining the relationship between factors affecting a process and the output of that process" [34]. The main areas of application for DoE are comparing, screening, characterising, modelling, and optimising. Thus, in agreement with what was previously explained (Paragraph 2.6.1.), the DoE systematic approach can be viewed as integrated in the QbD initiative. Some DoE studies have not a particular focus on process understanding but rather emphasise how formulation factors impact CQA of the product. For example, Pawar *et al.* screened, developed, and optimised an oil formulation to increase curcumin oral bioavailability using DoE [360]. Many other studies employed DoE under the QbD initiative, including designs of LB DDS [355,358,359,361–363]. DoE represents an evolution of previously employed techniques to optimise process or formulations [35,364]. This traditional approach is defined as changing one single (or separate) variable or factor at a Time (COST). Other known definitions are one variable at a time (OVAT), or one factor at a time (OFAT) [365–367]. This approach is extremely specific and is unsuitable to evaluate multiple factors at the same time, because it ignores interactions among variables. Furthermore, the COST approach is extremely time consuming and expensive. DoE obviates these drawbacks of the COST approach [368,369]. Although DoE appears in the official FDA guidelines only at the beginning of the 21st century, DoE was first developed in 1925 by Fisher [370]. A main limitation to DoE implementation was the calculation of the mathematical equations underlying optimisation. With the advent of modern computers and dedicated software, however, this drawback was easily overcome.

The core component of DoE is the layout of the experimental runs to be carried out, *i.e.*, the experimental design. Several types of experimental designs are available, *e.g.*, factorial [371], Placket-Burman [372], central composite design [373], Box-Behnken [374], or d-optimal [375], and have been reviewed, for example, by Singh [35]. The choice of the best experimental design is taken according to the study's aim, the number of factors to be

analysed, and the type of model desired [376]. As earlier mentioned, a design model can be chosen according to the type of factor to be analysed, *i.e.*, formulation, process, or both. The number of factors represents the number of independent variables to be considered during the DoE. Since DoE proposes an equation to fit and predict the relationship between experimental factors and response variables, the choice of the model basically defines the order and the complexity of this equation. Linear models result in a first approximation of the experimental main effects and interaction models are essentially a key advantage of DoE compared to the COST approach. Quadratic models are used especially in formulation optimisation, and higher order models are usually avoided in pharmaceutical DoE because the efficiency in terms of the number of experiments and gained information is comparatively low. The desired DoE output reflects the study's objectives. Screening designs are employed to identify the effects deemed relevant for the formulation or process properties. Screenings can be carried out with a small number of experimental runs while investigating several factors. This approach avoids the use of large DoE study plans that would be excessively time consuming. The main drawback of using screening design is that the employed models are usually not suitable to identify factor interactions. Subsequently, a factor influence study can be carried out on significant factors, to assess the extent of the interactions between independent variables. Care must be taken in a critical analysis of the proposed interactions. In fact, the scientist must take in consideration the acceptability and the sense of the interaction which have been found statistically relevant. Finally, to define an optimal formulation or processing area, a response surface design may be used on the relevant factors. Herein, the DoE allows plotting a surface which includes factor interactions as well as non-linear terms. The factor effects (and interactions thereof) are plotted to better understand for example optima and minima of the response variables. Interesting is often also the region around a local extreme as it indicates how robust a "sweet spot" is.

To obtain equations capable of fitting and predicting the effect relation between factors and responses, different mathematical and statistical tools can be applied:

- Ordinary least square (OLS) regression [377]. Also defined as linear regression, is a method to correlate the explanatory factors (defined as independent variable X) with the response variables (defined as dependent variable Y) according to Equation 2.17:

$$Y = \beta_0 + \beta_1 \cdot X_1 \qquad 2.17$$

The values of coefficients β are found by minimising the error of prediction. OLS can be used also for higher orders of the same independent variable, as shown in Equation 2.18:

$$Y = \beta_0 + \beta_1 \cdot X_1 + \beta_{11} \cdot {X_1}^2 \qquad 2.18$$

OLS is widely used but it cannot fit factor interactions.

- Multiple linear regression (MLR) [378]. This technique uses the same principle as OLS, but it can be applied to different independent variables, as shown in Equation 2.19:

$$Y = \beta_0 + \beta_1 \cdot X_1 + \beta_2 \cdot X_2 + \beta_1 \cdot \beta_2 \cdot X_1 \cdot X_2 \qquad 2.19$$

Like OLS, MLR can be used for higher order interactions and terms. MLR, however, is not suited to fit more than one Y, and the data may be misinterpreted in case of co-linearity between X variables.

- Principal component analysis (PCA) and principal component regression (PCR) [379]. PCA identifies the sources of highest data variation among the X variables. PCA is carried out by identifying eigenvectors and eigenvalues. When the data is represented in set of Cartesian axes, an eigenvector is a line that crosses the dataset to ensure the greatest variance among the data (Figure 2.9a). The eigenvalue represents the extent of this variation. The eigenvector with the highest eigenvalue is the principal component. The number of eigenvectors, and consequently eigenvalues, is the same as the number of the analysis's dimensions. Furthermore, each eigenvector must be orthogonal to the other (Figure 2.9b). Eigenvectors with low eigenvalues can be discarded, thus creating systems with fewer dimensions but still accounting for most experimental variability. Thus, the data can be plotted using the discovered principal components as Cartesian axes, and used as classification tool to identify data clusters and outliers (Figure 2.9c). The PCR is then operated similarly to OLS or MLR, using the principal components as X variables versus the selected response variable (Figure 2.9d). PCR can be carried out with a very high number of X variables without having a higher sample number, and is not altered by X variable co-linearity.

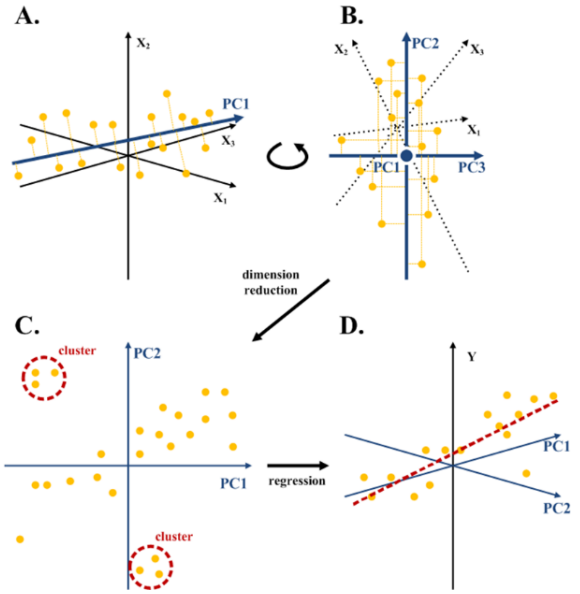

FIGURE 2.9 – Graphical explanation of principal component analysis (PCA) and principal component regression (PCR). Identification of first principal component (*PC*; a), identification of orthogonal *PC* (b), dimension reduction and Cartesian system change (c), and regression (d).

- Partial least squares (PLS) regression [380]. This regression technique allows fitting and predicting several *X* variables with different *Y* variables. In PLS, a vector explaining the most variation in *Y* is plotted, similarly to a principal component (Figure 2.10a). Then, a vector that best explains the *Y* vector is plotted among the *X* variables (Figure 2.10c). The second vector, however, is not necessarily a principal component for *X* variables. The scores of these factors can be plotted on a Cartesian system and a model equation can be fitted (Figure 2.10b). More vectors can be fitted to account for additional variation among *Y* and *X* variables. PLS regression can evaluate on different *X* and *Y* variables at the same time and it copes with data multiple co-linearity. Furthermore, categorical *X* variables can be analysed with partial least square discriminant analysis (PLS-DA).

While different models can be plotted with the aforementioned tools, the fitting and the predictivity of these systems is usually evaluated with R^2 and Q^2, respectively. The R^2 is calculated according to Equation 2.20:

$$R^2 = 1 - \frac{SS_{residual}}{SS_{total}} \qquad 2.20$$

Where $SS_{residual}$ is the residual sum of squares and SS_{total} the total sum of square, which are calculated according to Equation 2.21 and 2.22, respectively.

$$SS_{residual} = \sum (y_i - f_i)^2 \qquad 2.21$$

$$SS_{total} = \sum (y_i - \bar{y})^2 \qquad 2.22$$

Where y_i represents a given data point, f_i is a predicted data point, and $\bar{y}$ is the mean of observed data. In case of the Q^2, instead, the calculation follows Equation 2.23:

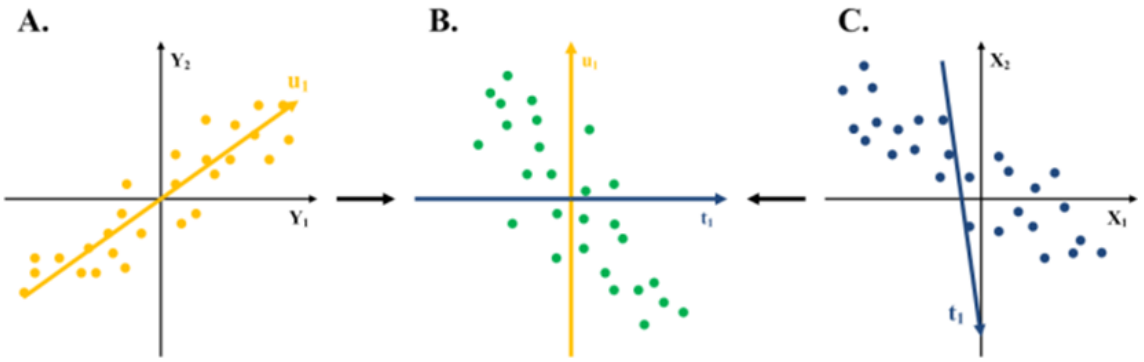

FIGURE 2.10 – Graphical explanation of partial least square (PLS) regression. Plotting of vector u_1 that explains most *Y* variability (a), plotting in *X* of vector t_1 that explains *Y* variability (c), and plotting of data scores using u_1 vs. t_1 as Cartesian system (b).

$$Q^2 = 1 - \frac{PRESS}{SS_{total}} \quad 2.23$$

$$PRESS = \sum \left(y_i - f_{i,-i}\right)^2 \quad 2.24$$

Where PRESS is the predicted residual sum of squares. PRESS is a form of cross-validation that is obtained from the observed values y_i and the predicted values ($f_{i,-i}$). The value $f_{i,-i}$ is obtained by omitting the relative observed value from its calculation, one at a time. The PRESS calculation is expressed as Equation 2.24:

Many other mathematical, statistical, and graphical tools are available to evaluate and optimise DoE, as well as to understand large datasets, *e.g.*, artificial neural networks [381,382]. Statistics are strongly entwined in modern pharmaceutics to develop novel formulations, identify relevant effects in all steps of development, and embed quality in a pharmaceutical process.

Chapter 3

Design and manufacturing of novel LB systems for oral protein delivery

3.1 On prilling of hydrophilic microgels in lipid dispersions using mono-N-carboxymethyl chitosan for oral biologicals delivery †

3.1.1 Summary

Oral delivery of biologicals is a thriving field in pharmaceutics and a first challenge is to achieve a stable drug product. Interesting is prilling of an API as microgel into an aqueous hardening bath where cross-linking occurs. However, to deliver a final dosage form, *e.g.*, soft gelatine capsules, the aqueous hardening bath must be removed, thus leading to manufacturing processes that are potentially harmful for the active. The current work introduces a prilling method with a lipid-based hardening bath, which could theoretically be filled directly into capsules. Bovine serum albumin (BSA) and mono-N-carboxymethyl chitosan (MCC) were selected as model biological and encapsulating polymer, respectively. Several non-aqueous formulations of the receiving bath were investigated; calcium chloride was added to these formulations to allow the MCC gelling. The obtained microgels had average diameters of ~300 µm and spherical to toroidal shapes, according to the hardening bath composition. Along with a high encapsulation efficiency (> 85%), the microgels protected the BSA from any denaturing effect of the hardening bath. The release study showed a rather fast BSA release within the first 10 minutes from most microgels. This novel approach demonstrated technical viability for encapsulation of biologicals using lipid formulations regarding oral delivery.

3.1.2 Introduction

Microencapsulation, which is the formulation of an API or cells in a microsphere, microgel, or microcapsule, is a well-established approach for oral delivery of active compounds. Since its introduction, drug inclusion in such microparticles has constantly gained interest, both from academia and industry, in terms of scientific publications and patents [383]. Microencapsulation has also been identified as a very promising platform for the administration of proteins,[187,384,385] because these compounds require specific characteristics from their delivery system, *e.g.*, prevention from gastrointestinal degradation, targeted release, and absorption enhancement, which can potentially be enabled by this method [183]. Several microencapsulation techniques have been introduced in the literature, such as coacervation [386], emulsification [227], spray drying [387], and microfluidics [388], and have been reviewed elsewhere

† de Kruif JK *et al*. On prilling of hydrophilic microgels in lipid dispersions using mono-N-carboxymethyl chitosan for oral biologicals delivery. *Journal of Pharmaceutical Sciences*, **2014**, 103, 3675-3687.

[22,389]. However, these processes require complex handling and several steps to successfully achieve a final dosage form with an acceptable yield and product stability. Particularly critical for macromolecules are processes that use high–shear forces (emulsification), and extreme temperatures, such as drying and lyophilisation [12,175].

The vibrating nozzle technique is based on the extrusion of a laminar jet of a polymeric solution, which is broken up into separate droplets by vibration. This technique is also known as prilling. The API is usually dissolved or suspended in the extruded liquid. The forming droplets are collected in a hardening bath, where the gelling or cross-linking of the polymer takes place (Figure 3.1). This technique, which was first introduced by Hulst *et al*. [390], finds its physical explanation in the Plateau-Rayleigh instability [230]. Herein, the surface tension of the falling liquid stream forms droplets to minimise the surface area. The applications of this technique are wide, embracing fields such as pharmaceutics (*e.g.*, modified release drug delivery systems) and biology (*e.g.*, microbeads for cell entrapment), and are elsewhere well described [23,229]. The vibrating nozzle system has been further developed with a ring electrode that charges electrostatically the droplets and thus prevents their coalescence by electrostatic repulsion (Figure 3.1) [238]. Moreover, Brandenberger and Widmer proposed a scale-up version of the system, although without the ring electrode [233].

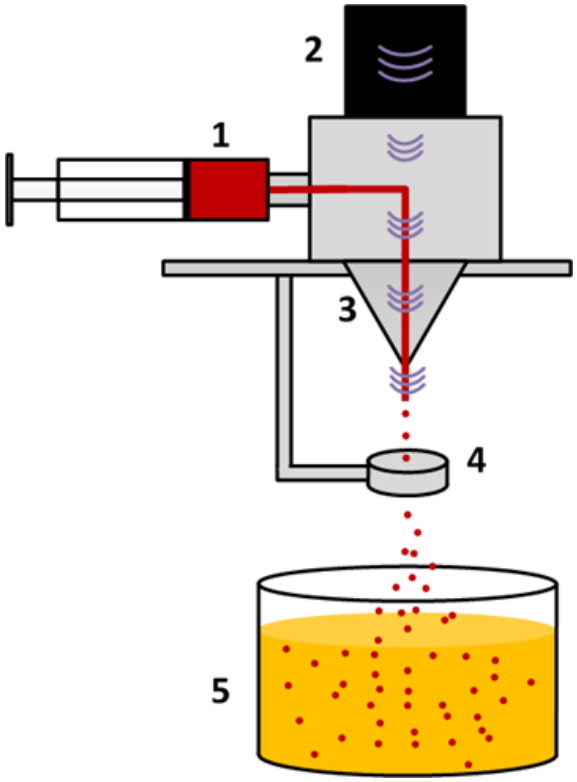

FIGURE 3.1 – Schematics of vibrating nozzle apparatus. 1 pumping system (syringe) containing the API and the polymeric solution; 2 vibrating unit; 3 nozzle; 4 electrode ring; 5 hardening bath.

Many polymers have been used with the prilling technique, such as alginate [391,392], chitosan [267], PLGA [250], or even polymeric mixtures [245]. Especially chitosan, a natural linear polysaccharide composed of D-glucosamine and N-acetyl-D-glucosamine, displays interesting properties for drug delivery [268,269,393]. However, its aqueous solubility profile represents a limitation when neutral to alkaline pH is required, because it only dissolves in acidic conditions. Many modifications have therefore been proposed to optimise its potential as a suitable polymer for oral drug delivery [192]. Among others, the chitosan derivates N,N,N-trimethyl chitosan and mono-N-carboxymethyl chitosan (MCC) , showed promising results for drug delivery, although the former has comparatively higher cell toxicity issues than the latter, due to the cationic interaction of the trimethylated amine with cell membranes [278,394]. Moreover, MCC is also known for its mucoadhesive and permeation enhancing properties, which can contribute to improve oral bioavailability [169,395,396].

For an efficient encapsulation, the polymers used in prilling should display a prompt onset of gelling. The fastest way to allow it is by ionotropic cross-linking. This is achieved by adding a counter-ion (*e.g.*, calcium chloride or pentasodium triphosphate for alginates and for chitosan, respectively) into the receiving bath before dropping the polymeric solution. Calcium ions are suitable to cross-link MCC, as shown by Liu *et al.* [397], due to the ionic interaction between the divalent cation and the carboxylic group attached on the N-terminus of the glucosamine monomers. This approach also avoids the toxicity of chemically cross-linking agents, *e.g.*, glutaraldehyde or polyethyleneimine. Different cross-linking methods were excellently reviewed by Hennink and van Nostrum [255]. Traditionally, only water solutions have been used to dissolve the counter-ions to allow the ionotropic gelling. A notable exception is the work from Buthe *et al.* [247], who used n-hexane and calcium chloride dissolved in n-butanol to form alginate microgels. However, the polymer drops only pass through the non-aqueous layers but are finally gathered again in a water solution. The use of water as a final receiving bath for microgel implies that a direct filling into capsules is not possible, due to the expected shell incompatibility. Thus, a further drying process is needed to obtain a final oral dosage form, and the active macromolecule could therefore be harmed during manufacturing.

Our aim is to introduce prilling of hydrophilic microgels in lipid-based systems that allow the ionotropic gelling of the polymer in media that are suitable for direct filling into

capsules. Accordingly, a viable dosage form for oral delivery of macromolecules would be achieved using this process, which can then be further tailored according to the target region in the human gastrointestinal tract. Bovine serum albumin (BSA) was selected as a model protein and the novel microgel dispersions were fully characterised in terms of loading efficiency, protein stability, and release from the microgels.

3.1.3 Materials and methods

3.1.3.1 Materials

Transcutol® HP (ethoxydiglycol or highly purified diethylene glycol monoethyl ether; DEGEE) and Labrafil® M2125CS (linoleoyl macrogol-6 glycerides) were kindly offered by Gattefossé SAS (Saint-Priest, France). Capmul® MCM EP (glyceryl monocaprylocaprate) and Capmul® MCM C8 EP (glyceryl monocaprylate) were generously supplied by ABITEC Co. (Janesville, US). Mono-N-carboxymethyl chitosan (deacetylation degree 96.1%, carboxymethylation degree 82.1%, loss on drying 20.5%) was purchased from Shanghai Boyle Chemical Co. Ltd (Shanghai, China). Peppermint oil was and Imwitor® 742 (glyceryl caprylocaprate) obtained from Hänseler AG (Herisau, Switzerland), and polyethylene glycol (PEG 600) was bought from AppliChem GmbH (Darmstadt, Germany). Bovine serum albumin 96% (BSA), calcium chloride anhydrous, propylene carbonate, guanidine hydrochloride, sodium chloride, sodium dihydrogen phosphate dihydrate, sodium hydroxide, potassium dihydrogen phosphate, and dipotassium hydrogen phosphate were purchased from Sigma-Aldrich (Saint-Louis, US). Tris(hydroxymethyl)aminomethane (TRIS), sodium dodecyl sulphate, bromophenol blue, dithiothreitol, glycerol, NuPAGE® MOPS SDS Running Buffer, NuPAGE® Bis-Tris-Gel, and SimplyBlue™ SafeStain were purchased from Invitrogen™ Life Technologies Inc. (Grand Island, US). *DC*™ Protein Assay, and Novex® Sharp Protein Standard were purchased from BioRad Laboratories AG (Cressier, Switzerland). The Micro BCA™ Protein Assay Kit was purchased from Thermo Fisher Scientific Inc. (Rockford, US).

3.1.3.2 Preparation of polymeric solution and hardening baths

After screening several possible polymer concentrations, a 4.76% (dry substance; w/v) solution of MCC was prepared by dissolving it in demineralised water, and the complete hydration of the polymer was allowed by mixing overnight. The solution was then vacuum-filtered through glass microfiber filters Whatman™ GF/D, and appropriate amounts of BSA and sodium azide were added therein to obtain a 2.5% and 0.05% (w/v) solution, respectively. The solution was subsequently stored in a glass brown bottle at +4°C, and it was allowed to reach room temperature before each use. The blank solutions were prepared in the same way without adding any BSA to the solution.

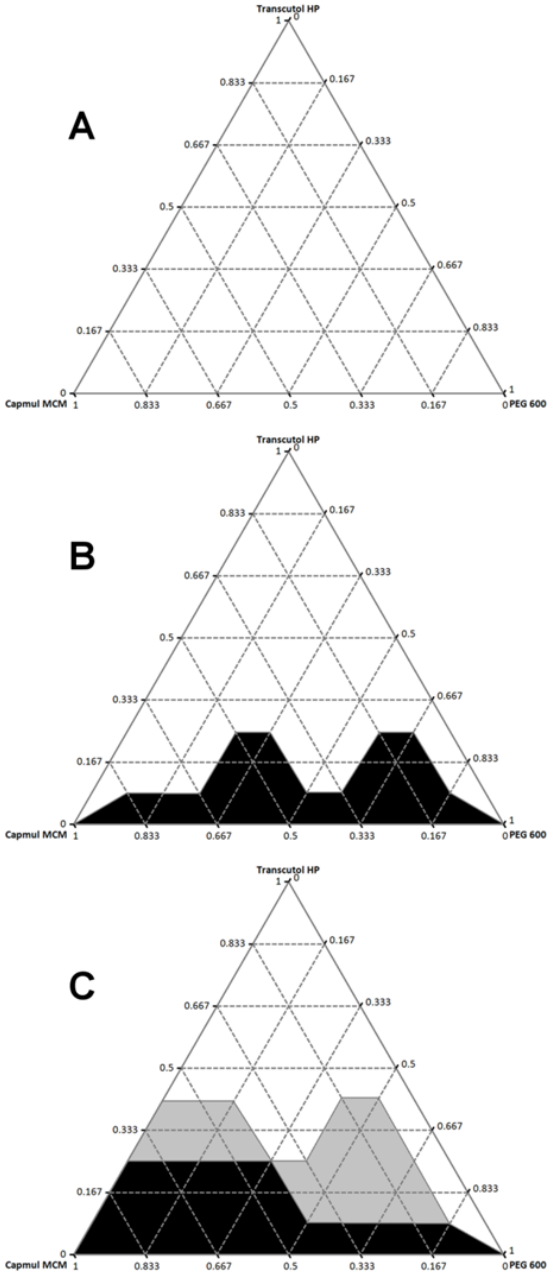

FIGURE 3.2 – Ternary phase diagrams of mixtures for formulation HBE. Evaluation of components' miscibility (A), calcium chloride solubility (B), and MCC gelling (C). White, grey, and black areas indicate good, medium, and poor properties of the formulation, respectively.

TABLE 3.1 – Hardening bath composition.

Hardening bath	Composition	Ratio (w/w)	Quantity [e] (w/w)
HBW	Water	1	95.24%
EtOH	Ethanol	1	95.24%
HBA	Transcutol® HP (ethoxydiglycol)	1	95.24%
HBB	Transcutol® HP (ethoxydiglycol)	1 : 1 : 1	31.74%
	Imwitor® 742 (glyceryl caprylocaprate)		31.74%
	Propylene carbonate		31.74%
HBC	Transcutol® HP	2 : 1 : 1	47.62%
	Capmul® MCM-C8 EP (glyceryl monocaprylate)		23.81%
	Propylene carbonate		23.81%
HBD	Transcutol® HP (ethoxydiglycol)	2 : 1 : 1	47.62%
	Capmul® MCM EP (glyceryl monocaprylocaprate)		23.81%
	PEG 600		23.81%
HBE	Transcutol® HP (ethoxydiglycol)	1 : 1 : 1	31.74%
	Labrafil® M2125CS (macrogol-6 glycerides)		31.74%
	Peppermint oil		31.74%

[e] *after adding calcium chloride to 4.76% of total*

Several ternary phase diagrams were prepared to find a suitable composition for the hardening baths. Each ternary phase diagram comprised of 25 mixtures. An example of these ternary phase diagrams is shown in Figure 3.2. All mixtures comprised one co-solvent (ethanol or ethoxydiglycol), one glyceride (Imwitor® 742, Capmul® MCM, Capmul® MCM-C8, or Labrafil® M2125CS), and one complementary capsule-compatible excipient (propylene carbonate, PEG 600, or peppermint oil). The three components of the mixtures were weighed in a glass vial to the appropriate concentration and then mixed for one hour. First, the miscibility of the components was evaluated by visual inspection after one-hour equilibration at room temperature. After addition of anhydrous calcium chloride (4.76% w/w), the turbidity of the mixture was assessed after mixing thoroughly for 24 hours at room temperature. In the last step, the droplet gelling was evaluated by dropping the polymeric solution from a syringe into the hardening baths. The suspended droplets were then immediately mixed vigorously on an Ika® Vortex Genius 3 (Hüber & Co. AG, Reinach, Switzerland) to confirm their gelling. The ternary phase diagrams are overlaid to select an optimum region where the formulations display the required properties [398]. Four mixtures, and three pure solvents and co-solvents were chosen. The compositions of these seven hardening baths are listed in Table 3.1.

3.1.3.3 Hardening bath characterisation

Since the viscosity range of the proposed hardening bath formulations was low, a chip-based capillary rheometer m-VROC™ (RheoSense Inc., San Ramon, US) was used to assess the rheological properties of the hardening baths. This device measures the viscosity from the pressure drop of a sample while it flows through a microfluidic slit. A constant shear rate of 1000 s^{-1} was applied while maintaining the sample at 25°C ± 0.15°C by means of a ThermoCube 200/300/400 (Solid State Cooling Systems Inc., Wappinger Falls, US).

The surface tension of the samples was measured at 25°C ± 0.5°C with the bubble method using a DynoTester (SITA Messtechnik GmbH, Dresden, Germany).

3.1.3.4 Stability of capsules filled with hardening baths

Different types of two-piece hard capsules and soft capsules were filled with the hardening baths, and stored for two weeks at 40°C / 75% relative humidity and for four weeks at 25°C / 45% relative humidity. The excipient compatibility with the capsule shell materials was assessed visually.

The two-piece hard capsules used were gelatine Licaps® (Capsugel France SAS, Colmar, France; HGC) and hydroxypropyl methylcellulose (HPMC) Quali-V® (Qualicaps® Europe SAU, Alcobendas, Spain). The capsule types were opaque white and of size 0. Moreover, oval soft capsules of size 10 with different shell materials, namely gelatine (SGC), starch (VegaGels®), and starch-based polyvinyl alcohol (S-PVA) [102], were supplied by Swiss Caps AG (now Aenova GmbH, Kirchberg, Switzerland). The two-piece hard capsules were loaded with 500 µL of the hardening bath formulations. The soft capsules were all filled with the same quantity of hardening bath formulation by means of syringes equipped with a 20 gauge needle. The thereby formed opening in the capsule was subsequently sealed on a hot plate.

3.1.3.5 Manufacturing of microgels

Microgels were prepared by means of the vibrating nozzle technique using the Encapsulator Biotech (EncapBioSystems Inc., Greifensee, Switzerland; this product is now commercialised by Büchi Labortechnik AG, Flawil, Switzerland). The solution of BSA and MCC was loaded in 20 mL Omnifix® plastic syringes (B. Braun Melsungen AG, Melsungen, Germany). The polymeric solution was then pumped through a 150 µm stainless steel nozzle, at a nominal flow rate of 3.10 mL min^{-1} (3.79 g min^{-1} of polymeric solution). A total of 5 g of polymeric solution was used for each batch. The droplets were formed by applying a frequency of 1240 Hz and by setting the electrode ring to 1500 V. The hardening bath (100 mL) was stirred at 400 rpm at room temperature, and the droplets' fall distance was approximately 13 cm. The aforementioned conditions were found to be optimal for the microgel manufacturing during preliminary investigations. The microgels were then left in the hardening baths for 20 minutes before further analyses.

3.1.3.6 Microgel morphological characterisation

The microgels collected from the different hardening baths were observed through an Olympus CKX41SF microscope (Olympus Co., Tokyo, Japan) equipped with an Olympus SC30 digital camera. Pictures were taken at different magnifications to visually inspect the shape of the produced microgels.

The particle size and shape of the microgels were assessed by dynamic image analysis with an XPT-C flow-through cell particle analyser (PS-Prozesstechnik GmbH, Basel, Switzerland). The microgels were suspended in their hardening bath, and then flowed (n = 1000) in front of a near-infrared light source. The particle size was expressed as Waddle disk diameter, which is the diameter of a disk with the same area as the detected particle. The particle shape was described by the elongation factor, which is the maximum (max) Feret diameter (the linear segment connecting the two perimeter points that are the furthest apart) divided by the Feret equivalent rectangular short side (the shortest side of the rectangle with the same area as the particle and the longest side equal in length to the max Feret diameter). The particle size distribution was expressed by the 10^{th}, 50^{th}, and 90^{th} percentiles, x_{10}, x_{50}, and x_{90}, respectively.

3.1.3.7 Encapsulation efficiency of bovine serum albumin (BSA) in microgels

For the sample preparation, the complete microgel batch was passed through a 125 µm opening stainless steel sieve, and then washed with water, then ethanol, and again with water to remove the remaining hardening baths. The samples were then dissolved with phosphate buffer saline pH 6.8 and stirred for 24 hours. The samples were subsequently stored at +4°C. Before each analysis, the required amount of solution was centrifuged at 10 000 rpm for 10 minutes in a 5415C centrifuge (Eppendorf GmbH, Leipzig, Germany), and then the supernatant was filtered through Titan3 nylon filters 0.45 µm (SMI-LabHut Ltd, Maisemore, UK). The encapsulation efficiency was measured *via* the total protein content by means of *DC*™ Protein Assay, which is based on the Lowry protein assay [399,400], according to the protocol supplied by the company. The protein content was determined using a Jasco V-630 UV-Vis spectrophotometer (Jasco Inc., Easton, US) at 750 nm in 1 cm optical path Plastibrand® disposable semi-micro PMMA cuvettes (Brand GmbH + CO KG, Wertheim, Germany). The encapsulation efficiency (EE) is expressed in percentage as the ratio between the BSA encapsulated and the amount of BSA present in the polymeric solution used for manufacturing. To evaluate the BSA leakage from the microgels to the receiving bath, the encapsulation efficiency was estimated over a period of 4 weeks. The suspended microgels in the corresponding receiving baths were kept at 25°C over a period of one month in amber bottles; the EE was measured at weeks 1, 2, 3, and 4. The leakage is expressed in percentage as the EE at a given time point compared to the time zero EE.

3.1.3.8 Degradation of BSA

To investigate the degradation of the microgel loaded BSA the following methods were used: circular dichroism, sodium dodecyl sulphate gel electrophoresis (SDS-PAGE), and fluorescence spectroscopy.

To evaluate possible changes in the secondary structure of the protein, the circular dichroism spectra of the BSA after release from the microgels was recorded using a Jasco J-810 spectropolarimeter (Jasco Inc., Easton, US). The sample was loaded in a 1 cm optical path quartz cuvette and the spectra were taken in the range between 200 and 260 nm from the far-UV. The data are expressed as mean residue ellipticity [θm], which is equal to $\theta\ (n\ c\ l)^{-1}$, where θ is the measured ellipticity in mdeg, n is the number of amino acids in BSA, l is the optical path length in cm, and c is the BSA concentration in g mL^{-1}. For comparison, the spectra of a reference BSA solution and of BSA denatured with an 8 M solution of guanidine hydrochloride were also recorded.

The SDS-PAGE was conducted to detect protein aggregation or degradation. All samples were mixed with an equal volume of 2x Laemmli buffer (100 mM tris(hydroxymethyl)aminomethane pH 6.8, 4% SDS, 0.2% bromophenol blue, 3.1% dithiothreitol, and 20% glycerol) and applied to a NuPAGE® Bis-Tris-Gel in a MOPS SDS running buffer. The gels were stained with a SimplyBlue™ SafeStain reagent according to the manufacturer's instructions.

Fluorescence spectroscopy was employed to gain information about potential changes in protein folding. The fluorescence emission profile was obtained from a SpectraMax M2^e (Molecular Devices LLC, Sunnydale, US). The instrument was set to an excitation wavelength (λ_{ex}) of 280 nm and the emission wavelengths (λ_{em}) were recorded in the range from 300 to 500 nm. The samples were prepared by loading 700 µL of buffered solution in 48-well clear plates Falcon® Multiwell™ (Becton Dickinson France SA, Le Point De Claix, France). The emission spectra from a BSA solution and BSA denatured with an 8 M guanidine hydrochloride solution were used as references.

3.1.3.9 In vitro release of BSA from microgels

The *in vitro* release of BSA from the microgels was tested by using an Erweka DT 600 dissolution tester (Erweka GmbH, Hausenstamm, Germany) equipped with paddle, as described in the European Pharmacopoeia [82]. Briefly, each dissolution vessel was filled with 500 mL of phosphate buffer saline pH 6.8, which was heated to 37 ± 0.5°C and stirred at 50 rpm. Then, washed BSA-loaded microgels were added (n = 3) to a nominal total content of 15 mg of BSA per vessel. At different time points (5, 10, 15, 20, 30, 45, 60, 90, and 120 minutes), a 1 mL sample was withdrawn from the release medium and filtered through nylon filters 0.45 µm; the corresponding volume of release medium withdrawn was then compensated with fresh buffer. A final aliquot was taken after 12 hours at 100 rpm, to obtain the BSA release from the microgels at equilibrium. Due to the high dilution of the samples, the BSA content was measured with a protein assay kit. The employed Micro BCA™ Protein Assay Kit (Thermo Fisher Scientific Inc., Rockford, US) had the advantage of accurately detecting BSA at very low levels. This method is based on the bicinchoninic acid protein assay [401–404]. The samples were prepared according to the protocol supplied by the company, loaded in 96-well clear BRANDplates® pureGrade™ (Brand GmbH + CO KG, Wertheim, Germany) and the absorbance was measured in the SpectraMax M2^e at λ = 562 nm. The values obtained are expressed as a percentage of the release at the equilibrium value.

3.1.3.10 Data analysis

All measurements are in triplicate (n = 3) and means are given together with standard deviations as error bars, where not otherwise specified. STATGRAPHICS Centurion XVI version 16.1.18 (StatPoint Technologies Inc., Warrenton, US) was used as statistical software package. The Spearman rank correlation ($p \leq 0.05$) was employed for non-linear correlation analysis. The statistical significance of the difference of means was analysed with Student's t-test ($p \leq 0.05$).

3.1.4 Results

3.1.4.1 Hardening bath characterisation

An initial mixture screening indicated that the presence of a co-solvent, namely ethoxydiglycol and ethanol, typically allowed a better miscibility of the components, higher solubility of calcium chloride, and gelling of the polymeric droplets [398]. However, pure organic co-solvents are not suitable for direct filling into capsules due to well-known shell compatibility issues. Such pure co-solvents were therefore compared to more promising excipient mixtures that were selected from the initial hardening bath screening (Table 3.1).

The data generated from the surface tension and viscosity measurements are shown in Table 3.2. These data indicate that, among the batches containing ethoxydiglycol, an increase in viscosity occurred in presence of glycerides and other excipients (especially PEG 600). Considering surface tension, the highest value was obtained from the aqueous system and noteworthy is the comparatively high value for the hardening bath formulation containing PEG 600. However, all the formulation mixtures showed a surface tension within the same range which was significantly

TABLE 3.2 – Hardening bath characterisation.

Hardening bath	Viscosity (mPa s)	Surface tension (mN m^{-1})
HBW	≈ 1	73.5 ± 0.36
EtOH	≈ 1	22.2 ± 0.06
HBA	9.14 ± 0.03	30.7 ± 0.35
HBB	22.99 ± 0.12	30.4 ± 0.06
HBC	18.29 ± 0.09	31.5 ± 0.76
HBD	56.79 ± 0.20	33.9 ± 0.27
HBE	21.02 ± 0.27	30.6 ± 0.25

different than the surface tension of receiving baths made of water or ethanol.

The next step was to generate first preliminary capsule compatibility data using different shell materials. Table 3.3 summarises the compatibility assessment of the different capsule types with the proposed receiving bath mixtures. After four weeks at 25°C and 45% relative humidity, the HGC containing HBB, HBC, HBD, and HBE were visually intact, despite the relative high amounts of co-solvent. In these conditions, HBD was compatible also in HPMC capsules. All other capsules and formulations caused rupture or softening of the capsule. After two weeks at 40°C and 75% relative humidity, only HPMC hard-shell capsules and S-PVA soft capsules, both filled with formulation HBD, exhibited suitable shell compatibility, while all other capsule samples showed leakage or softening of the shell.

TABLE 3.3 – List of capsule compatible with the proposed hardening baths.

Hardening bath	Compatible capsule shells	
	after 2 weeks, 40°C / 75% RH	after 4 weeks, 25°C / 45% RH [f]
HBB	-	HGC
HBC	-	HGC
HBD	HPMC, S-PVA	HGC, HPMC
HBE	-	HGC

[f] *S-PVA not tested at these conditions*

3.1.4.2 Microgel characterisation

3.1.4.2.1 Morphological characterisation

Microscopic images demonstrated that the microgels' shape was strongly influenced by the selected hardening bath (Figure 3.3). Microgels from HBW (Figure 3.3A) formed very thin, concave particles, which appeared similar to deformed contact lenses. Particles gathered from EtOH hardening bath showed elliptic to almost spherical shapes (Figure 3.3B). The microgels obtained from hardening bath HBA exhibited a toroidal shape (Figure 3.3C and 3.3D), which resembled that of erythrocytes. The microgels from HBB had a spherical to irregularly elongated shape (Figure 3.3E). Interestingly, the microgels collected from HBC and HBD had an irregular, mushroom-like cap (Figure 3.3F and 3.3G, respectively), which was possibly linked to a higher ratio of ethoxydiglycol. Finally, the microgels from hardening bath HBE showed a spherical to irregularly spherical shape (Figure 3.3H). Microscopy also revealed some droplets that may indicate traces of a phase separation. Adhesion of such droplets on the surface of a HBE microgel can result in a bias in the automated shape analysis.

The data from size distribution and particle shape are shown in Table 3.4. The microgels with lowest x_{50} and x_{90} values were those obtained from EtOH, while those formed in HBW demonstrated the largest particle size at all the three percentiles analysed. HBW also showed higher elongation factors for its microgels when compared to all the other systems. Among the formulations containing ethoxydiglycol, HBA exhibited the lowest median value for the microgels formed, whereas the HBD hardening bath yielded microgels with the highest size on x_{10}, x_{50}, and x_{90}. The microgels produced from these two hardening baths, however, shared practically the same mean elongation factor. The dynamic size and shape analysis of the toroidal microgels (using formulation HBA) is illustrated in a scatter plot (Figure 3.4). The shape in terms of the elongation factor was not a constant but depended on the detected size, as it is graphically highlighted in the Figure 3.4.

Since the gelling takes place as soon as the droplet impacts the hardening bath surface, we correlated statistically (Spearman rank test) viscosity and surface tension of the

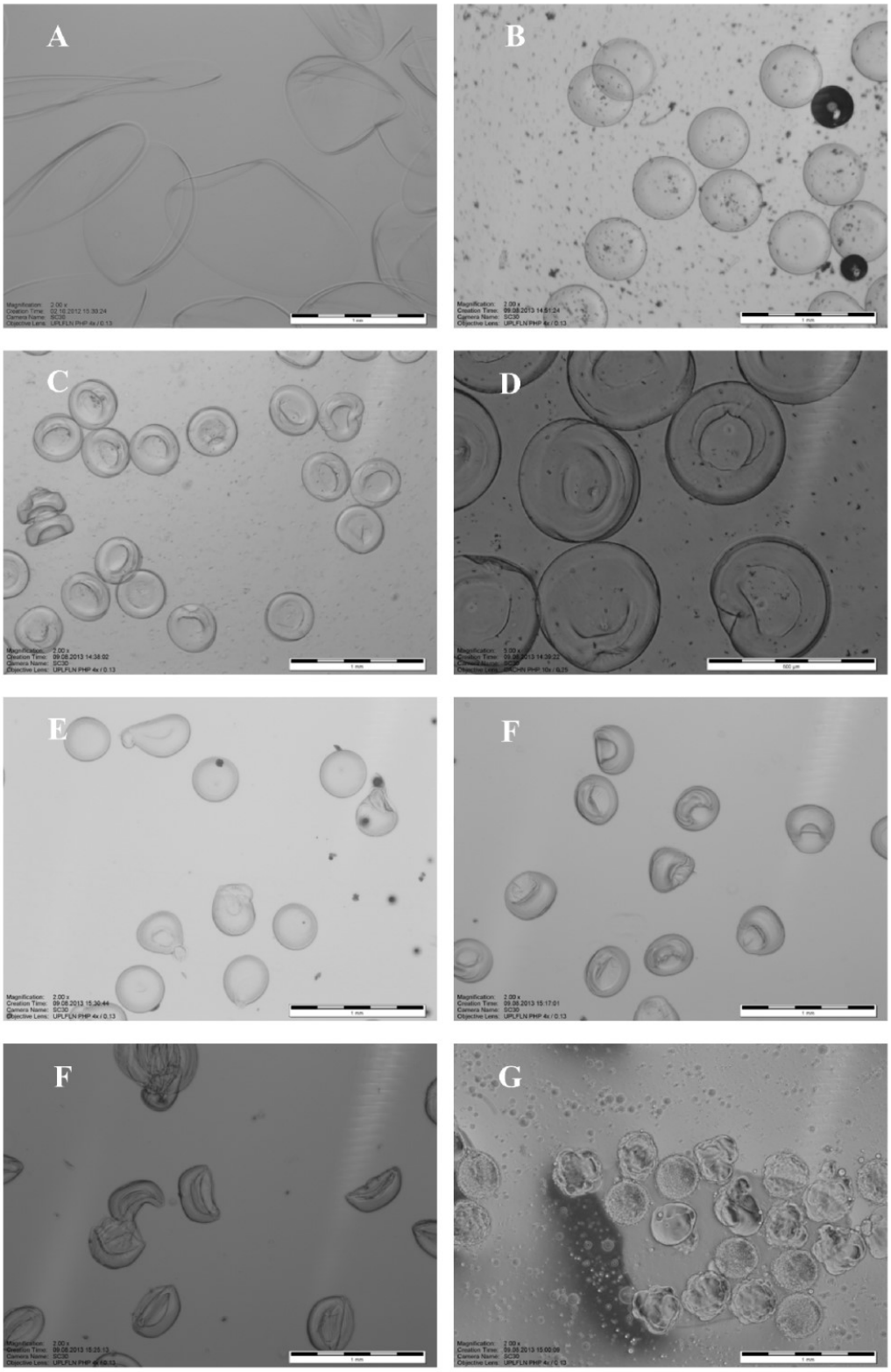

FIGURE 3.3 – Microscope pictures of BSA-loaded microgels from hardening baths HBW (A, at 4x), EtOH (B, at 4x), HBA (C, at 4x; D, at 10x), HBB (E, at 4x), HBC (F, at 4x), HBD (G, at 4x), and HBE (H, at 4x). The scale bar in the bottom right corner of each picture represents 1 mm, except figure D where it is 500 μm.

TABLE 3.4 – Microgel shape and size characterisation.

Hardening bath	Particle size (µm)			Elongation factor
	x_{10}	x_{50}	x_{90}	
HBW	295.4	410.0	473.7	2.9 ± 0.54
EtOH	236.9	292.9	346.4	2.1 ± 0.64
HBA	228.1	300.5	347.8	2.0 ± 0.57
HBB	255.6	320.7	364.1	1.8 ± 0.50
HBC	247.4	319.9	364.1	1.8 ± 0.58
HBD	259.0	332.7	400.3	2.0 ± 0.53
HBE	223.0	316.0	355.6	1.7 ± 0.46

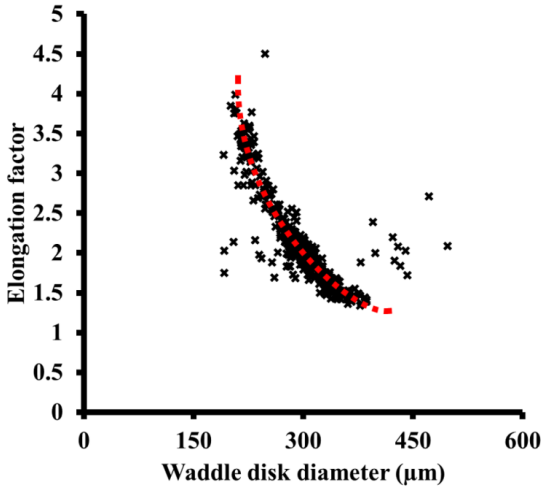

FIGURE 3.4 – Scatter plot of the BSA-loaded microgels obtained in hardening bath HBA (n = 1000). The red dotted line highlights the trend of the microgels due to the toroidal shape.

hardening baths with the resulting particle size and shape. As a result, both particle size and shape of the microgels were significantly correlated (0.5902 and 0.2679, respectively; $p < 0.05$) with the surface tension of the hardening bath. Based on the experimental data, an increase in surface tension could have increased the particle size and decreased the sphericity. On the other hand, the correlation between viscosity and microgel morphology was not statistically significant.

3.1.4.2.2 Encapsulation efficiency and leakage

The fraction of BSA that could be loaded in the microgels is shown in Table 3.5. Interestingly, all microgels formed in non-aqueous hardening baths were able to encapsulate much more BSA than those produced in the aqueous hardening bath (HBW). The microgels from formulation HBE showed a lower mean EE compared to the other lipophilic systems, whilst the microgels formed from HBD and EtOH exhibited highest EE among the prepared formulations. There was no statistical difference ($p > 0.05$) in BSA content between time zero and 4 weeks for all hardening baths containing ethoxydiglycol. On the other hand, the microgels from hardening baths HBW and EtOH revealed a statistically significant protein loss over one month. While the leakage in EtOH was limited (-6.3%), the microgels in HBW resulted in an EE drop below 5% already after the first week. Water as receiving bath was obviously leading to continuous diffusion of BSA out of the microgels.

TABLE 3.5 – Encapsulation efficiency (EE) and leakage of the microgels after 4 weeks. Significance of difference of encapsulation efficiency, [g] $p \leq 0.001$, [h] $p \leq 0.01$, and [i] $p \leq 0.05$.

Hardening bath	**Encapsulation efficiency (%)**		
	time zero	**4 weeks**	**difference**
HBW	19.40 ± 2.17	3.74 ± 0.27	-80.73 **
EtOH	95.04 ± 3.49	89.09 ± 3.02	-6.26 *
HBA	93.69 ± 6.86	95.86 ± 1.03	2.32
HBB	91.99 ± 4.16	85.68 ± 4.14	-6.86
HBC	92.41 ± 2.57	92.91 ± 0.91	0.54
HBD	98.42 ± 5.22	93.82 ± 1.79	-4.68
HBE	86.79 ± 10.62	92.43 ± 7.97	6.50

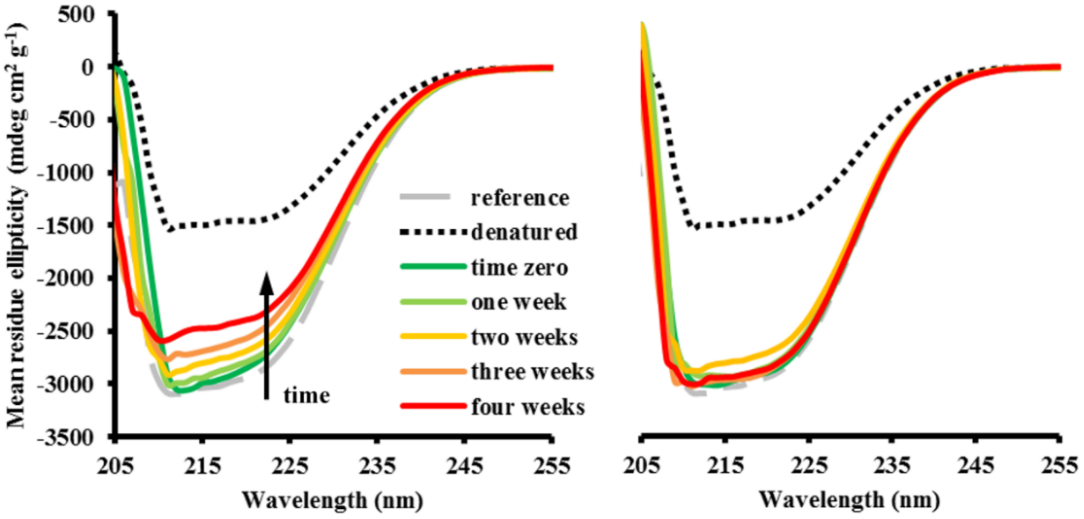

FIGURE 3.5 – Overlaid circular dichroism spectra of BSA-loaded microgels formed in HBE (left) and EtOH (right) according to time. Reference (grey long dashes), denatured BSA solution (black dots), time zero (dark green), one week (light green), two weeks (yellow), three weeks (orange), four weeks (red).

3.1.4.3 Degradation of BSA

3.1.4.3.1 Circular dichroism

Circular dichroism is a spectropolarimetric technique based on the differential absorption of the circularly polarised components of a radiation through an optically active substance [219]. This approach allows, for example, to study the secondary structure of a protein, as well as to detect some specific amino acids and bonds. The recorded circular dichroism profiles generally showed no sign of BSA denaturation over time. However, in the case of the microgels gathered from receiving bath HBE, a clear trend could be identified over the course of 4 weeks' stability, as seen in Figure 3.5.

The major area of interest is between 205 and 255 nm, which best describes the far-UV profile of the protein α-helix [219]. In the case of the BSA encapsulated with hardening bath HBE, the spectrum shifted toward the profile obtained by BSA denatured with an 8 M solution of guanidine hydrochloride in phosphate buffer saline pH 6.8. Such a shift has been also shown by Liu *et al.* [405], when BSA was denatured with increasingly higher quantities of ethanol. However, in the present work, the BSA microencapsulated in the EtOH hardening bath did not exhibit any specific trend over time. This demonstrates that the resulting microgels were able to protect the loaded BSA from any denaturing effect of the ethanol hardening bath. This protection from denaturation was found also in all the other proposed formulations, except HBE.

3.1.4.3.2 Sodium dodecyl sulphate polyacrylamide gel electrophoresis (SDS-PAGE)

The gel electrophoresis of the samples after 4 weeks can be seen in Figure 3.6. A 25 µg BSA sample without any further treatment was used as a positive control to compare with the BSA loaded in microgels (nominal quantity of 37.5 µg BSA).

The BSA sample (lane 1) had several bands on a gel with a major band around 67 kDa (in the red dotted circle) and several high molecular weight bands. All samples (lanes 3-9), as well as a reference sample of MCC+BSA (lane 10), showed patterns similar to a BSA sample and no degradation bands were observed. The sample obtained from HBW showed an extremely reduced band at 67 kDa due to the very poor encapsulation efficiency. We also analysed samples without any BSA (data not shown); these samples did not show any traces of proteins. Thus, after 4 weeks' incubation, the results did not show any degradation of BSA when the microgels are exposed to the hardening baths.

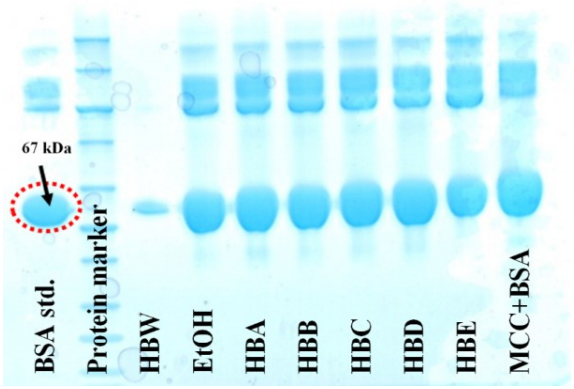

FIGURE 3.6 – SDS-PAGE of BSA loaded in microgels after four weeks in the hardening bath. In the lanes, from left to right, BSA standard, protein marker, HBW, EtOH, HBA, HBB, HBC, HBD, HBE, and MCC+BSA (before gelling). The dotted circle marks the 67 kDa major band of BSA.

3.1.4.3.3 Fluorescence profile

The fluorescence of BSA and of other proteins comes from the presence of specific amino acids, namely tryptophan, tyrosine, and phenylalanine. In BSA, the fluorescence of the Trp-212 has a predominant role given by its position in an internal hydrophobic pocket of the protein [406]. The presence of ethanol or denaturing compounds can alter the three-dimensional structure of the protein, thus exposing the Trp-212 residue to the external environment. This, in turn, modifies its fluorescence emission spectrum, serving as an indicator of protein denaturation [405,407]. Figure 3.7 depicts the spectrofluorimetric profiles of BSA encapsulated from different hardening baths at time zero and after 4 weeks.

The emission spectra recorded from the microgels formed in receiving bath formulations EtOH and HBA were the closest to the reference curve (maximum λ_{em} = 342 nm). In contrast, the emission spectra from BSA encapsulated using the hardening baths HBB, HBC, and HBD underwent a hypsochromic shift (maximum λ_{em} = 332-336 nm), whereas the BSA from hardening bath HBE maintained the maximum λ_{em} as the reference. Hardening baths HBB, HBC, HBD, and HBE caused a drop in the intensity at the maximum λ_{em}, which could be a sign of structural protein change [405]. Interestingly, no difference in the emission profile of BSA was found over time, indicating that the protein changes probably occurred during the manufacturing step.

3.1.4.4 In vitro release of BSA from microgels

The release profiles of the BSA-loaded microgels are shown in Figure 3.8.

The microgels formed in HBW were not analysed due to the poor EE. All proposed microgels appeared to immediately release most of their content (> 75%) within the first 20 minutes. Such fast release probably occurred because BSA was already in solution inside a swollen microgel, and thus could readily diffuse to the outer medium. The microgels that showed comparatively slower release were formed in the EtOH hardening bath. Microgels obtained from hardening baths containing ethoxydiglycol were similar regarding BSA release with the exception of HBB. The latter system demonstrated also a comparatively lower total amount of BSA released by the microgels (90.32% ± 8.56%). After 2 hours testing, the total amount of released protein was in all cases above 90% of the initial content.

3.1.5 Discussion

The current work introduces a novel approach to microencapsulate a model protein by means of prilling directly in a lipid-based system. This technique should enable a subsequent liquid-filling of the microgel dispersions into pharmaceutical capsules, without the need for further steps of microgel collection from the hardening bath and drying prior to filling into capsules. The obtained results are discussed with respect to the gelling in the hardening baths, the encapsulation efficiency, the protein stability, as well as the drug release from the formulations.

3.1.5.1 Hardening bath properties and microgel morphology

A hardening bath for prilling would have to fulfil several requirements to obtain suitable microgels. A composition should certainly not display any phase separation and the bath should further have some polarity or dielectric properties for ions to dissolve and hence allow ionotropic gelling. However, the polarity of the composition should not be similar to aqueous media because otherwise this would likely result in capsule incompatibility. Balanced medium properties were therefore targeted for finding suitable hardening baths. The co-solvent ethoxydiglycol was found to be interesting with respect to facilitating polymer gelling. This excipient may have also contributed to lower the surface tension and viscosity of the mixtures (final hardening baths) compared to glyceride and non-glyceride excipients alone. The surface tension and the viscosity of the hardening bath can theoretically influence the microgel shape, due to their effect on the impacting droplets. However, only the first property could be statistically correlated to the microgels' morphology. HBW had a rather low viscosity but a very high surface tension, whereas HBA showed higher viscosity and lower surface tension. Both systems failed to form spherical microgels. For instance, EtOH exhibited the lowest surface tension among the proposed formulations and also a very low viscosity, which led to the formation of spherical microgels. The presence of

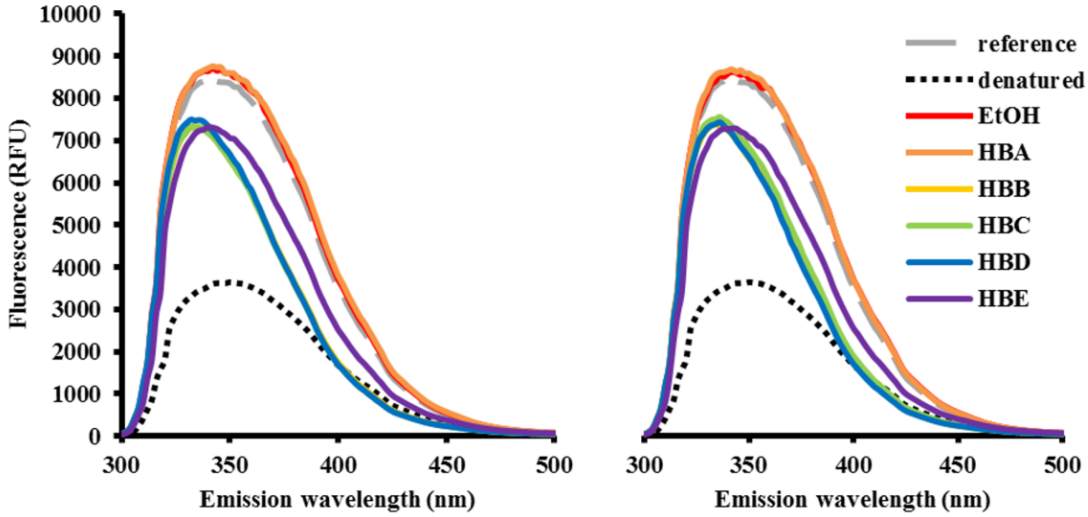

FIGURE 3.7 – Fluorescence spectra of BSA-loaded microgels from different hardening baths at time zero (left) and after four weeks (right). Reference (grey dashes), denatured BSA (black dots), EtOH (red line), HBA (orange line), HBB (yellow line), HBC (green line), HBD (blue line), HBE (purple line).

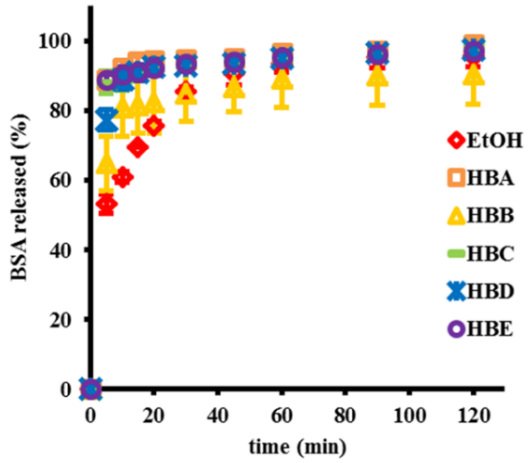

FIGURE 3.8 – BSA release profiles of microgels in PBS pH 6.8, 50 rpm, and 37°C. Microgels were prepared in hardening baths EtOH (red diamonds), HBA (orange squares), HBB (yellow triangles), HBC (green dashes), HBD (blue asterisks), and HBE (purple circles). Error bars represent standard deviation (n = 3).

PEG 600 in receiving baths formulated with ethoxydiglycol seemed to enhance the shape curvature as seen in batch HBD. Interestingly, Lee *et al.* showed in a study regarding calcium alginate beads that the viscosity of the polymer solution played a major role in the microgel size and shape [408]. However, in our case, surface tension was primarily found to be relevant for the microgel morphology, which may point to the importance of the individual system composition. This emphasises the complexity of shape as a response in a micro-gelling process like prilling.

The morphology of colloids or microparticles can be viewed as the result of spontaneous curvature that is based on surface bending energy [409]. The latter energy is influenced by several material factors and additional process factors of prilling contribute to the complexity. We therefore described the morphology primarily on an empirical basis and noted changes of the individual hardening bath composition on the shape of the microgels. However, one aspect that should be discussed regarding microgel shape as well as size is the degree of polymer cross-linking/gelling.

The extent of polymer swelling and the nature of the microgel surface are known to be influenced by the surrounding medium properties, *i.e.*, the affinity between the solvent molecules and the polymer chains [410]. A lower affinity causes the polymer to prefer self-contact over interaction with the solvent [55]. This leads to surface-localised coiling of the polymeric chains. Consequently, the overall surface of the gel shrinks and the gel size decreases. Some hardening baths were therefore "better solvents", in the sense that complete swelling was retained when compared to the other hardening bath compositions. In terms of particle size, ethanol and the ethoxydiglycol-based hardening baths showed least affinity for MCC, which led to lower polymer swelling and a smaller particle size compared to batch HBW.

Other authors have used alginate or chitosan as ionically cross-linking polymers [24,392]. In the present work, the latter could not be used due to the very poor solubility of the chitosan counter-ion, namely pentasodium triphosphate, in the proposed formulations. Alginate is still the most commonly used polymer in prilling and can be easily cross-linked with calcium ions. However, alginate failed our preliminary tests, since it did not form any stable microgel when dropped in lipid media. However, Buthe *et al.* could form microgels in a n-hexane and n-butanol system by dropping the polymer solution with a syringe in the hardening bath [247]. Surprisingly, MCC could gel in water [397], but also in ethanol and other lipophilic media, as shown in the present work.

Another required property is the capsule stability upon filling with the hardening bath. At mild storage conditions, *i.e.*, 25°C / 45% relative humidity, all formulations were compatible with HGC. However, only the filled HPMC and the S-PVA capsules were stable at 40°C, and only with formulation HBD. This preliminarily stability study indicates that these combinations could directly form a final dosage form, since all capsules used in this work, except for S-PVA, are currently commercially available. Further modifications of the receiving bath formulation may be needed to allow an improved stability at stress conditions. However, this represents further development work that is outside of the current research scope and proof of this microencapsulation concept.

3.1.5.2 BSA encapsulation efficiency, leakage, and release from microgels

The surprisingly high EE of the microgels formed in all non-aqueous hardening baths (Table 3.5), could be described by the structure of the microgel itself. As previously mentioned, the gel formed by MCC in the receiving bath is in a relative "swollen" state, which is determined by the polymeric chains' hydration and the formed network. This network is maintained by cross-linking interactions between calcium ions and the carboxylic groups of the modified chitosan. The microgel can therefore be viewed as a leaky mesh, where the water and the dissolved BSA may partition between the microgel and the bulk of the hardening bath. Such partitioning most likely explains why the system proved to be very "leaky"

when left in the aqueous hardening bath (HBW) for several weeks, in contrast to the other lipid-based formulations.

The BSA entrapment in the microgels from the EtOH hardening bath presents similarities with an aqueous receiving bath, but with a comparatively lower polarity of the medium. This polarity is expected to play an important role for a less extensive polymer swelling, and hence for the lower diffusion of the large BSA molecule.

Sano *et al.* demonstrated that the alcohol content strongly influences the gel stability made from chitosan solutions [411]. Since polymer swelling is closely linked to the solvent properties, the MCC microgel may form a rather tight and dense network, which may hinder BSA release, during exposure to the receiving bath medium. Such considerations about medium polarity and the degree of microgel swelling apply not only to the EtOH formulation, but also to all the other systems.

The BSA's EE obtained in our system was higher than the one obtained in the system composed of the same polymer and protein from the work of Liu *et al.* [397]. Herein, the authors reported that the droplets were hardened in a calcium chloride aqueous solution and further hardened by chitosan. The presence of chitosan could increase the EE from 44.4% up to 73.2%. Such increase could be also induced by the electrostatic interaction between the cationic chitosan and the anionic MCC, which form poly-electrolyte complexes. The BSA, whose isoelectric point is 4.7 [412], has prevalently negative charges in the solution used, therefore it can electrostatically interact with both the chitosan and the calcium ions.

Regarding the *in vitro* release test, all the systems could successfully liberate the model biological within 20 minutes. This fast release was explained by the facilitated BSA diffusion through the completely swollen MCC microgel in the aqueous environment. The only remarkable variation occurred with the EtOH system, where BSA released from the microgel was slower than in the other proposed systems. Such difference in the release profile may again be explained by the different solvent properties of the receiving medium and their impact on the network density, when compared to the ethoxydiglycol-based formulation. However, the rather fast release would require development of enteric coated capsules filled with the microgels to bypass possible degradation in gastric fluids. Further biopharmaceutical research would have to prove an adequate protein protection from the intestinal fluids by the microgels.

3.1.5.3 Protein denaturation

The data regarding protein stability showed that the microgels prepared in lipid-based hardening baths could protect BSA from denaturation in most cases. Some of the excipients from the selected hardening baths are known to harm or modify proteins and their structure. For instance, ethanol is regarded as a protein denaturing agent, due to its major role in the disruption of tertiary structure and in the modification of α-helices in the secondary structure [405,413–415]. Propylene carbonate has been described in literature as a potential protein denaturant [416]. According to our findings, the BSA loaded into microgels formed in EtOH was unmodified for the entire study length.

The BSA in the microgel formulation HBA, *i.e.*, containing only ethoxydiglycol and calcium chloride, proved to have no detectable denaturation by means of spectropolarimetry, gel electrophoresis, and spectrofluorimetry. These results were consistent over a four-week stability period at room temperature. To the best of our knowledge, no literature data is available on the influence of ethoxydiglycol on protein stability.

SDS-PAGE has previously been used to study other particle-based drug delivery systems to evaluate the structural integrity of encapsulated macromolecules [319,417]. When using this method, there were no indications that the process or the lipid-based systems harmed the model protein in terms of degradation. However, according to the circular dichroism spectra, the BSA from formulation HBE showed a variation in the α-helix region over time. The signal in this region varied with a constant trend during a four-week period by moving from the reference profile to the denatured profile. A plausible interpretation of this result is based on the known fact that the end-products of lipid peroxidation can lead to protein damage and denaturation due to their interaction with lysine groups in proteins [418,419]. The Labrafil® M2125CS contained in formulation HBE is a mixture of lineoyl macrogol-6 glycerides, which means that the additive contains polyunsaturated fatty acids. If oxidation stress occurs on the unsaturated chains, the subsequent end-products, *e.g.*, malondialdehyde, can interact with the ε-amine of lysine. This amino acid has a very high α-helix propensity [420], and its modification could disrupt this structure, hence altering the circular dichroism spectra in the corresponding range. Similar effects could also be caused by the presence of oxidising impurities in this excipient that are derived by the PEGylation step of the glycerides.

An interesting effect was seen on the fluorescence emission profiles. The maximum λ_{em} from a guanidine hydrochloride-denatured protein undergoes a bathochromic shift, as described by Pajot [421]. In the case of BSA, such as in the present work, this red shift moves the peak to 350 nm. Whilst the spectra emitted from the BSA encapsulated using the receiving bath formulations EtOH and HBA maintained a maximum λ_{em} = 342 nm, the formulations containing glycerides appeared to modify the profiles. The hypsochromic effect shown in BSA by these systems can be due to an increase in lipophilicity due to the

hardening bath, which moves the Trp-212 further into a less polar area in the lipophilic cavity in sub-domain IIA [407]. Overall, the emission intensity undergoes a hypochromic effect, which may be caused by quenching following nearby three-dimensional rearrangement [422]. Such explanation implies a possible modification of the secondary structure of the protein. This was probably a rather subtle effect as it was not shown by the spectropolarimetric data. Moreover, such a change in conformation may not necessarily lead to an activity loss in case of a therapeutic protein.

3.1.6 Conclusions

This work introduced a novel lipid-based dispersion of MCC hydrophilic microgels suitable for macromolecules encapsulation and compatible with hard- or soft-shell capsules by means of prilling. The vibrating nozzle system produced microgels with reproducible particle size by means of Ca^{2+}-mediated gelling, directly in a lipid hardening bath. The lipid-based dispersion can be loaded directly into hard or soft capsules, whereas an alternative water-based system would cause strong incompatibilities with the capsule shell materials. This approach allows a simpler and straightforward manufacture of a final dosage form for oral drug delivery, thus bypassing further time-consuming manufacturing steps, like drying or lyophilisation. The presence of a water compartment within the "swollen" gel may grant a fast release of the macromolecule when exposed to the physiological fluid, as well as optimal stability. The proposed system showed high encapsulation efficiency (> 86%) for all the lipid-based dispersions. Also, the loaded BSA did not show, in most systems, clear signs of denaturation, even in presence of pure ethanol in the hardening bath after a four-week long stability investigation at room temperature.

The findings presented here introduce a novel, viable, and robust approach for macromolecule microencapsulation, to achieve a straightforward production of a dispersion that can be directly filled in commercially available capsules, which can then be further tailored according to the product specification.

3.2 On prilled Nanotubes-in-Microgel Oral Systems for protein delivery ‡

3.2.1 Summary

Newly discovered active macromolecules are highly promising for therapy, but poor bioavailability generally hinders their oral use. Microencapsulation approaches, like protein prilling into microspheres, may enable protection from enzymatic degradation in the gastrointestinal tract, which could increase oral bioavailability mainly for local delivery. This work's purpose was to design a novel architecture, namely a Nanotubes-in-Microgel Oral System, by prilling for protein delivery. Halloysite nanotubes (HNT) were selected as orally acceptable clay particles and their lumen was enlarged by alkaline etching. After loading albumin as model drug, the HNT were entrapped in microgels by prilling. The formed Nanoparticles-in-Microsphere Oral System (NiMOS) was assessed regarding morphology, entrapment efficiency, and release profile. Protein stability was determined throughout the microencapsulation process and after *in vitro* enzymatic degradation. The results showed successful HNT lumen enlargement, which facilitated higher protein loading. Prilled NiMOS had spherical shape and good entrapment efficiency. Release profiles depended largely on the employed system and HNT type. NiMOS prilling did not harm the protein structure, and this novel composite system demonstrated even higher *in vitro* enzymatic protection compared to pure nanotubes or microgels. Therefore, prilled NiMOS were shown to be a promising and flexible multi-compartment system for oral (local) macromolecular delivery.

3.2.2 Introduction

New proteins as active pharmaceutical ingredients (API) have drawn much attention to scientists in modern pharmaceutics [10,18,423]. The oral delivery of these compounds is challenging in terms of bioavailability, which is substantially reduced by the conditions in the gastrointestinal (GI) tract [14,183]. The GI barriers to overcome consist of drug solubility, enzymatic drug digestion, mucus penetration of the API or of the delivery system, and absorption of the API [424]. If primarily luminal activity is required for the therapeutic action of the macromolecule, only enzymatic protection must be achieved, which is a still challenging but realistic pharmaceutical objective. Herein, microencapsulation has

‡ de Kruif JK *et al*. On prilled Nanotubes-in-Microgel Oral System for protein delivery. *European Journal of Pharmaceutics and Biopharmaceutics*, **2016**, submitted

shown potential to overcome this major hurdle by protecting proteins from the GI environment [20–22,425]. Among several other techniques, prilling can be a way to formulate proteins as microparticles [23]. The mild conditions of the process avoid thermally induced protein degradation. Prilling is also known as vibrating nozzle technique. This approach embeds the macromolecular API in a polymeric microgel by dropping a solution of both components in a hardening bath. Herein, the API-containing polymeric solution is extruded through a nozzle. The liquid stream is then broken into droplets by applying vibration. The droplets pass through a ring electrode that charges them electrostatically to avoid mid-air coalescence [238]. Finally, the droplets are collected in a hardening bath where cross-linking occurs and the API is efficiently entrapped. Both polymer and hardening bath may be varied to achieve a suitable formulation for the process. Several polymers have been proposed for prilling, like alginate [391,392], pectin [245], and chitosan [267]. Chitosan is a natural linear polysaccharide formed by D-glucosamine and N-acetyl-D-glucosamine, and this excipient displays interesting drug delivery properties [268,269,393]. Many chemical modifications of this compound were suggested to enhance or modify its physicochemical properties [192]. A most promising chitosan derivate is mono-N-carboxymethyl chitosan (MCC). Mucoadhesive and permeation enhancing properties have been reported for this polymer, as well as improved tolerability compared to chitosan and other of its cationic derivates [169,394–396]. The hardening bath is generally aqueous, but lipid-based pharmaceutical compositions were recently identified as technically feasible for prilling. [28]. The hardening bath can then be optimised for later steps of manufacturing, such as capsule filling of the microgel dispersion [426]. Prilled microgels have therefore shown flexibility and suitability in terms of protein formulation as a final oral dosage form.

Apart from the technology of microgels, nanoparticles have become an important field for oral delivery of macromolecules, such as proteins [319] and nucleotides [427,428]. This formulation approach has been excellently reviewed by several authors [31,194,318]. It seems particularly attractive to embed a nanoparticulate system into microgels or microspheres [314]. Thus, the biopharmaceutical formulation properties may be improved by forming highly versatile Nanoparticles-in-Microsphere Oral Systems (NiMOS). Such systems have been proposed as multi-compartment carriers and were especially applied in RNA and DNA delivery [316]. Bhavsar *et al.* pioneered this field with a multi-compartment system by using gelatine nanoparticles encapsulated in poly(ε-caprolactone) microspheres for intestinal mucosal delivery of proteins, and were reported to be more successful for oral macromolecule administration than nanoparticles alone [311,312,316]. The promising multi-compartment has seen only a preliminary application of solid nanotubes for oral delivery of proteins. A first example of nanotubes that were intended as potential drug delivery system was carbon nanotubes [429]. However, their costs and toxicity may strongly hinder their application in pharmaceutics [320,321]. Halloysite is, by contrast, a natural and inexpensive aluminium silicate clay with a hollow nanotubular structure. It is regarded as non-toxic, and there are preliminary findings of even anti-inflammatory properties [335,430,431]. Hallyosite nanotubes (HNT) are extracted from clay quarries, and their characteristics vary according to the extraction site [326,327]. The use of halloysite in drug delivery was first proposed by Price *et al.* [328], and has since then gained increasing interest [329–331,432]. These clay nanotubes showed the capacity of storing APIs in their lumen or to adsorb compounds on their surface. Both luminal and surface additions and modifications to HNT have been proposed as a strategy to increase the loading efficiency of the tubes or to modify the drug release properties of this system [332,333,343,433,434]. For example, to improve the control over the drug release profiles from HNT, lumen end-stoppers were implemented [321,435]. Many of these modifications were reviewed elsewhere [322]. Most notably, chemical etching of the inner clay surface has been proposed to enlarge the luminal diameter thereby increasing the loading capacity of the tubular structure [325,339,340]. While HNT have been loaded with small molecules, peptides, small proteins, and nucleotides, the addition of larger proteins into the lumen may be hindered by the macromolecule size.

First steps in formation of halloysite-containing gel structures were attempted to achieve nanocomposite films [336] and beads [337]. In both cases, the nanocomposite systems were evaluated only in terms of structure, physicochemical and mechanical properties, as well as biocompatibility. Wang *et al*. recently developed ofloxacin-containing magnetic microspheres obtained by spray-drying [436]. This approach allowed successful loading the model API in HNT-containing magnetic microspheres. Thinking of a macromolecular drug, however, the spray-drying process may cause thermal drug degradation. Chao and co-workers proposed an interesting structural architecture for enzymatic immobilisation outside of the pharmaceutical field by forming a HNT-based mesoporous microgel [338]. There is certainly much biopharmaceutical promise in such multi-compartment systems. However, the risk of the system complexity to become a major hurdle for scale-up and manufacturing still remains. In fact, drug delivery systems are required not only to show biopharmaceutical promise, but also to be viable for later stages of galenical development regarding clinical research and finally the market [31].

The aim of this work is to design and manufacture Nanotubes-in-Microgel for protein (local) oral delivery,

which falls under the umbrella of Nanoparticles-in–Microsphere Oral System (NiMOS). A simple microencapsulation method is introduced to form such complex structures, namely prilling (Figure 3.9).

This mild process has the potential to embed protein-loaded HNTs into a microgel. HNTs were chemically etched in order to increase drug loading capacity and to allow protection from enzymatic protein degradation. The feasibility of the prilling approach was assessed, and the obtained NiMOS were characterised in terms of morphology, protein loading, and release. The protein stability after manufacturing was evaluated. A preliminary biopharmaceutical characterisation was performed by evaluating the enzymatic digestion of the proposed NiMOS compared to HNT and microgels alone.

3.2.3 Materials and methods

3.2.3.1 Materials

Mono-N-carboxymethyl chitosan (MCC; deacetylation degree 96.1%, carboxymethylation degree 82.1%, loss on drying 11.2%, MW = 9000-13000 g mol^{-1}) was purchased from Boylechem Co Ltd (Shanghai, China). Ethanol (brand J.T. Baker® Chemicals) was obtained from Avantor Performance Materials BV (Deventer, The Netherlands) and hydrochloric acid solution 1 M from Scharlau SL (Sentmenat, Spain). Miglyol® 812 (triglyceryl caprylocaprate) was supplied by Hänseler AG (Herisau, Switzerland). Transcutol® HP (diethylene glycol monoethyl ether; DEGEE) was a kind gift of Gattefossé AG (Luzern, Switzerland). Acetic acid, bovine serum albumin 96%, calcium chloride anhydrous, guanidine hydrochloride,

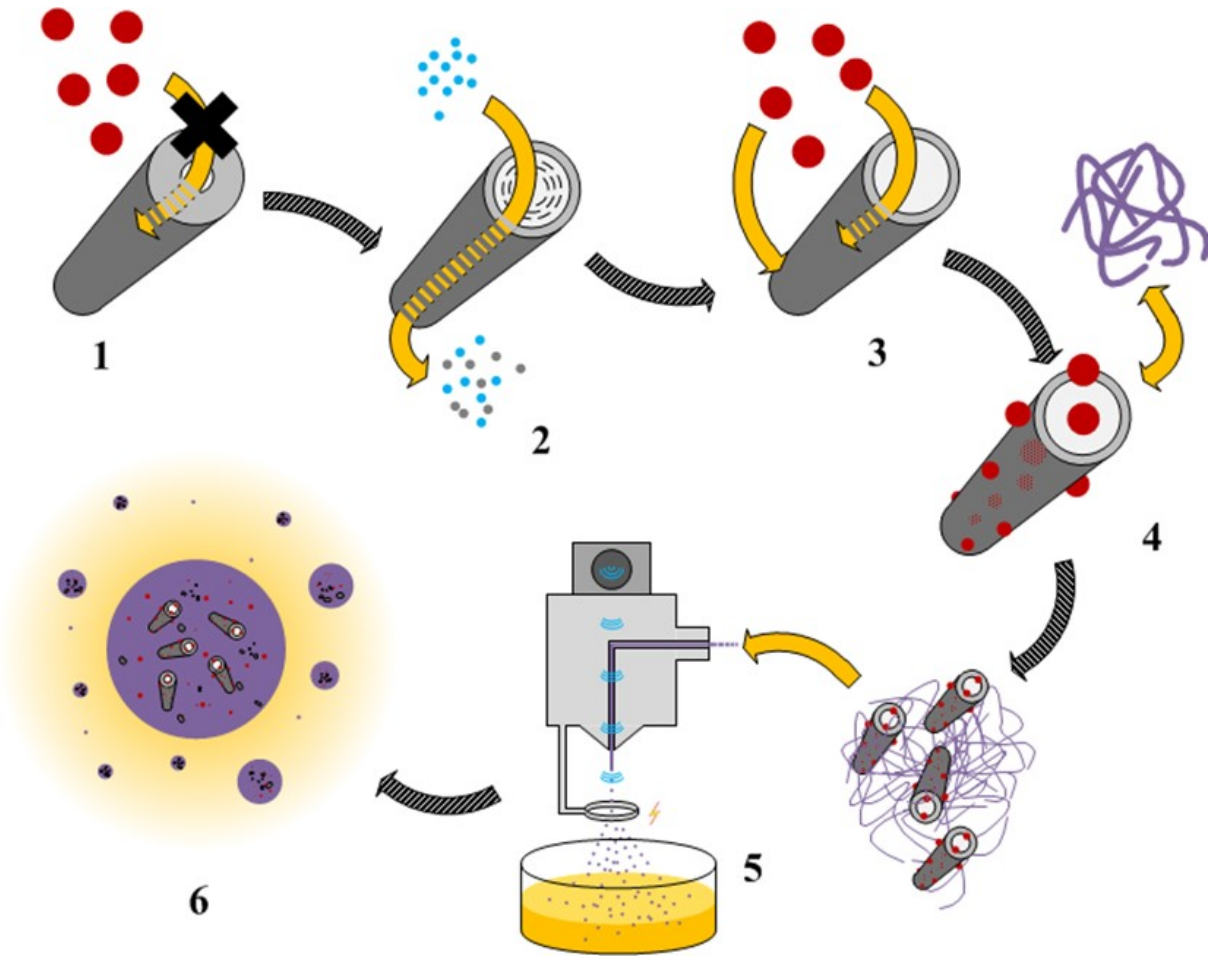

FIGURE 3.9 – Schematic approach of Nanotubes-in-Microgels (as a Nanoparticle in Microparticle Oral System, NiMOS) manufacturing by means of prilling. 1, loading of protein into halloysite nanotubes possibly hindered by lumen diameter; 2, chemical etching enlarges nanotube lumen; 3, loading of protein onto nanotubes; 4, dispersion of protein-loaded nanotubes in polymeric solution; 5, prilling process; 6, prilled NiMOS. Red circles are BSA, azure circles represent sodium hydroxide, and purple lines indicate polymer chains. The schematic figure is not to scale.

halloysite nanotubes (HNT), potassium phosphate dibasic, potassium phosphate monobasic, sodium chloride, sodium hydroxide, sodium phosphate monobasic, sodium phosphate tribasic, trypsin, trypsin inhibitor from *Glycine max*, glycerol and Tween® 80 (polyoxyethylene (20) sorbitan monooleate) were purchased from Sigma-Aldrich Chemie GmbH (Buchs, Switzerland). Acrylamide/Bis 40% solution, ammonium persulfate (APS), Coomassie Brilliant Blue G-250, bromophenol blue, dithiothreitol (DTT), sodium dodecyl sulphate (SDS), tetramethylethylenediamine (TEMED) were purchased from Bio-Rad Laboratories AG (Cressier, Switzerland). Tricine, tris-(hydroxymethyl)-aminomethane (Tris) base and Tris hydrochloride (Tris-HCl) were purchased from Carl Roth GmbH & Co KG (Karlsruhe, Germany). The Micro BCA™ Protein Assay Kit and the molecular weight marker PageRuler™ Plus Prestained Ladder were obtained from Fisher Scientific AG (Reinach, Switzerland).

3.2.3.2 Halloysite nanotubes (HNT) activation by luminal etching

The HNT internal lumen diameter was enlarged by alkaline chemical etching according to a previously reported method [340]. Briefly, HNT were suspended in a 2 M solution of sodium hydroxide in a ratio 1:10 (w/w). The dispersion was sonicated for 50 minutes at 50°C. The HNT samples were centrifuged at 4000 rpm for 15 minutes. Then, the supernatant was removed and 40 mL of demineralised water were added. Subsequently, both centrifugation and washing steps were repeated three times using phosphate buffer saline (PBS) pH 6.8 instead of demineralised water. A final centrifugation and washing steps were repeated with demineralised water. This base-modified HNT (bHNT) was desiccated at 105°C until no weight variation could be detected. The pH of a 1% (w/w) dispersion bHNT and non-treated HNT (nHNT) were 7.3, and 6.8, respectively.

3.2.3.3 HNT characterisation

3.2.3.3.1 Particle size and ζ-potential

A mean HNT size was measured by dynamic light scattering using a Nano-Zetasizer (Malvern Instruments Ltd, Malvern, UK). The same instrument was employed for the ζ-potential determination of the different HNT. One part of HNT was suspended in 500 parts of demineralised water and sonicated for 3 hours. The particle size and the ζ-potential were then measured at room temperature in a 1.5 mL semi-micro disposable cuvette Plastibrand® (Brand GmbH + CO KG, Wertheim, Germany) and in a folded capillary cell (Malvern Instruments Ltd), respectively. The particle size distribution was expressed as the span, as described in Equation 3.1, where d_{90}, d_{10}, and d_{50} represent the 90th percentile, the 10th percentile, and the median particle size, respectively.

$$Span = \frac{d_{90} - d_{10}}{d_{50}} \quad 3.1$$

3.2.3.3.2 Specific surface area, pore volume, and pore diameter

The BET (Brunauer-Emett-Teller) specific surface area was measured on a Gemini™ V (Micromeritics Instrument Inc., Norcross, GA). The test tubes and approximately 500 mg of sample were dried overnight at 105°C under nitrogen. The dry weight was measured and the sample was then transferred into the instrument that analysed the specific surface area, the pore volume, and the pore diameter.

3.2.3.4 Loading of HNT with bovine serum albumin (BSA)

The BSA was loaded by modifying previously proposed methods [332,333]. One gram of dried non-treated (nHNT) or base-modified (bHNT) halloysite was added to one millilitre of BSA solution at different concentrations, namely 2.5, 5.0, 7.5, 10.0, 12.5, and 15.0% (w/v). The 10% (w/v) concentration was found to be optimal and was used for all further testing. The samples were mixed for 5 minutes on an IKA® Vortex Genius 3 (Huber & Co AG, Reinach, Switzerland). Subsequently, they were put in a vacuum chamber at room temperature for 1 minute at 100 mbar. This step was repeated twice to remove air in the suspensions and from the nanotube lumen. The suspension was then centrifuged for 10 minutes at 4000 rpm. After removing the supernatant, a fresh aliquot of BSA solution with identical concentration was added, and the loading process repeated to ensure highest loading efficiency. Once the supernatant was removed again, the sample was dried at 40°C for about 20 hours in an XYTS 11 vacuum oven (Renggli AG, Rotkreuz, Switzerland).

3.2.3.5 HNT imaging

3.2.3.5.1 Transmission electron microscopy (TEM)

Images of the nanoparticles were taken with a Morgagni 268D TEM (FEI Europe BV, Zürich, Switzerland) by using an acceleration voltage of 80 kV. The samples were prepared by suspending HNT in demineralised water in a ratio of 1:500, and subsequently sonicating for 15 minutes. A 5 µL suspension aliquot was loaded on a copper grid and incubated for 60 seconds at room temperature. Finally, the sample was loaded in the microscope and analysed.

3.2.3.5.2 Scanning electron microscopy (SEM)

SEM pictures of the different HNT were gathered with a Supra 40 VP microscope (Carl Zeiss AG, Oberkochen, Germany) using an extra high tension of 5 kV. The nanotubes were suspended in demineralised water in a ratio of 1:500. Then, the suspensions were sonicated for 15 minutes with a PELCO® Mica Sheet Grade V5 (Ted Pella Inc., Redding, CA). The adhesive sheets were then fixed on conductive stickers (Plano GmbH, Wetzlar, Germany).

3.2.3.6 Formation of NiMOS by prilling

Prilling was carried out on an Encapsulator Biotech from EncapBioSystems AG (Greifensee, Switzerland; currently commercialised by Büchi Labortechnik AG, Flawil, Switzerland). A polymeric solution containing 4% (w/v; dry weight) of MCC was prepared in PBS pH 6.8. The solution was stirred overnight to allow complete dissolution and hydration of the MCC polymeric chains. Subsequently, the solution was vacuum filtered through a Whatman™ GF/D glass microfiber filter (GE Healthcare AG, Glattbrugg, Switzerland). The BSA-loaded HNT, both non-treated and alkali-activated, were added to the polymeric solution (ratio 1:20 w/w). This ratio was found to be optimal after screening several possible combinations from 1:1 to 1:50 (w/w). The system was then thoroughly mixed for 30 minutes and sieved through a 125 µm mesh stainless steel sieve to separate HNT clusters. Three different hardening bath compositions were chosen to collect the droplets falling from the prilling device, namely ethanol, DEGEE, and water. Calcium chloride anhydrous was added up to 4% (w/w) concentration in the hardening baths and these were stirred until complete dissolution of the salt. Tween® 80 was also added in the aqueous solution to a 2% (w/w) concentration to reduce its surface tension, according to the Encapsulator Biotech instructions.

An Omnifix® syringe (B. Braun Melsungen AG, Melsungen, Germany) was filled with HNT-loaded polymeric solution and then attached to the prilling device. This solution was pumped through a 300 µm nozzle with a 12.5 mL min^{-1} flow rate. The vibration was set to a 1240 Hz frequency and to an amplitude of 9. The droplet stream passed through the electrode ring charged with 2500 V. The droplets were collected after a ~13 cm fall into a grounded beaker containing 75 mL of hardening bath. A total quantity of 5 g of polymeric solution was prilled for each batch. The HNT-containing microgels were left in the hardening baths for 30 minutes. The microgels loaded with nHNT were named under the term nNiMOS, whereas those containing bHNT were called bNiMOS. "Blank" microgels, *i.e.*, without HNT but still loaded with BSA, were produced using the same settings.

3.2.3.6 NiMOS and microgel characterisation

NiMOS and blank microgels were filtered through a 125 µm mesh stainless steel sieve. All the microgels were then washed with water, ethanol, and water again. The microgel batches were gently dried in a glass oven B-585 (Büchi Labortechnik AG) at 40°C for 3 hours in 20 mbar vacuum, at a rotation speed of 20 rpm. The dried microgels were stored in sealed vials at 4°C.

3.2.3.6.1 Particle size by laser diffraction

The microgel particle size was measured with the laser diffraction sensor Helos/KF equipped with a CUVETTE holder (Sympatec GmbH, Clausthal-Zellerfeld, Germany). A 50 mL optical glass cuvette was used to disperse the microgels. Non-dried microgels were suspended in pure ethanol, whereas the dry microparticles were dispersed in Miglyol® 812.

3.2.3.6.2 Particle shape by dynamic image analysis

An XPT-C particle analyser (PS Prozesstechnik GmbH, Basel, Switzerland) was used for the dynamic image analysis of the microparticles. The non-dried microgels were redispersed in their respective hardening baths, whereas the dry microgels were suspended in ethanol. Subsequently, the dispersions were flowed through the 1.5 mm diameter cell of the XPT-C, where the images were taken. The shape of the microgel is expressed by the elongation factor, which is the maximum Feret diameter (the linear segment linking the two perimeter points that are the furthest apart) divided by the Feret equivalent rectangular short side (the shortest side of the rectangle with the same area as the particle and the longest side equal in length to the maximum Feret diameter). The more elliptical the particle is, the higher its elongation factor. A perfectly spherical particle has an elongation factor of $4/\pi$ (~1.27).

3.2.3.6.3 Particle imaging by optical microscopy

The microgels were observed through an Olympus optical microscope CKX41SF (Olympus Schweiz AG, Volketswil, Switzerland) equipped with an Olympus SC30 digital camera. Pictures of both non-dried and dry microgels were taken to evaluate their morphology.

3.2.3.7 Protein content

3.2.3.7.1 Loading efficiency of BSA onto HNT

An aliquot of 200 mg of BSA-loaded HNT was dispersed in 1 mL of PBS pH 6.8 to allow complete release of the protein 48 hours. Then, the sample was centrifuged for 10 minutes

at 14 000 rpm with a 5415C centrifuge (Eppendorf Instrumente GmbH, Hamburg, Germany). The loading efficiency is given by the quantity of BSA loaded onto one gram of HNT (mg g^{-1}) as described in Equation 3.2.

$$Loading\ efficiency\ (mg \cdot g^{-1}) = \frac{Quantity\ of\ BSA\ on\ HNT\ (mg)}{Quantity\ of\ HNT\ (g)} \quad 3.2$$

The BSA content was measured with a Micro BCA™ Protein Assay Kit, which is based on the bicinchoninic acid method for protein content assessment [401–404]. An aliquot of supernatant from the centrifuged sample was taken and the protein content was measured according to the protocol supplied by the manufacturer. The measurement was carried out on a 96-well plate pureGrade™ (Brand GmbH + CO KG, Wertheim, Germany) in a SpectraMax M2^e microplate reader (Molecular Devices LLC, Sunnyvale, CA).

3.2.3.7.2 Encapsulation efficiency of BSA in microgels

Batches of prilled microgels were suspended in PBS pH 6.8 at a ratio 1:4 (w/w). The suspension was mixed for 12 hours at room temperature to allow complete BSA release. Aliquots of the samples were then centrifuged in a 5415C centrifuge (Eppendorf Instrumente AG) at 14 000 rpm for 10 minutes. The protein content was measured using a Micro BCA™ Protein Assay Kit according to the manufacturer's instructions. The protein content is then expressed as the encapsulation efficiency, as shown in Equation 3.3.

$$Encapsulation\ efficiency\ (\%) = \frac{[BSA]_{in\ microgels}}{[BSA]_{in\ polymeric\ mixture}} \cdot 100 \quad 3.3$$

Where the term at the denominator represents the protein content of the BSA-loaded polymeric solution used for prilling. The microgels and NiMOS formed in the alcoholic hardening bath were chosen for further characterisation.

3.2.3.8 Release test

The BSA release test was carried out on the different HNT, on the blank dried microgels, and on the different NiMOS obtained using the ethanol hardening bath. These samples were transferred into 15 mL CellStar® tubes (Greiner Bio-One GmbH, Frickenhausen, Germany) and 10 mL of PBS pH 6.8 were added as dissolution medium. Each sample was repeated 6 times. The test tubes were laid horizontally in a Multitron Standard shaking incubator (Infors AG, Bottmingen, Switzerland), incubated at 37.0°C and shaken at 200 rpm. Aliquots of 100 µL were drawn at selected time points (5, 10, 15, 30, 45, 60, 75, 90, 105, 120, 150, 180, and 210 minutes). A final aliquot was taken after 24 hours at equilibrium. After each withdrawal, the sample taken was replaced with 100 µL of fresh medium. The samples were centrifuged for 10 minutes at 14 000 rpm and the supernatant was further filtered. The protein content was assessed with the Micro BCA™ Protein Assay Kit as previously described. Where applicable, the release profiles were compared with the f_2 similarity factor [437–439]. If f_2 is below 50, the release profiles were considered different. The comparison was carried out using the freely available add-in programme DDSolver [440].

3.2.3.8 Protein stability after prilling process

3.2.3.8.1 Circular dichroism

The potential denaturation of the protein secondary structure during the process was assessed by spectropolarimetry. The circular dichroism spectra of BSA were recorded on a Jasco J-810 spectropolarimeter (Jasco Inc., Easton, MD) in a range between 200 nm and 260 nm. The samples were prepared by allowing the BSA release from blank microgels, HNT, and NiMOS in PBS pH 6.8. After centrifugation at 14 000 rpm for 10 minutes, the supernatant was filtered through 0.45 µm Titan3 filters (Fisher Scientific AG). The filtered solution was then transferred in 1 cm optical path quartz cuvettes and measured. The circular dichroism data is expressed in terms of mean residue ellipticity (mdeg cm^2 g^{-1}), which is calculated according to Equation 3.4:

$$mean\ residue\ ellipticity\ (mdeg \cdot cm^2 \cdot g^{-1}) = \frac{\theta}{n \cdot c \cdot l} \quad 3.4$$

Where θ is the measured ellipticity (mdeg), n is the number of amino acids in BSA, c is the BSA concentration (g mL^{-1}), and l is the optical path length of the quartz cuvette (cm). The circular dichroism profiles were then deconvoluted to obtain quantitative information regarding the secondary protein structure with the software CDNN [441]. The calculated α-helix fraction of BSA was chosen for the statistical evaluation. A positive control for protein denaturation was also measured by denaturing BSA in presence of an 8 M guanidine hydrochloride solution.

3.2.3.8.2 Fluorescence profile

The emitted fluorescence spectra of BSA were obtained with a SpectraMax M2^e microplate reader. The fixed excitation wavelength (λ_{ex}) was set to 280 nm, whereas the

emission wavelength (λ_{em}) was recorded from 310 nm to 450 nm. The BSA emitted fluorescence in this range is given by a tryptophan residue in position 212 of the protein. A volume of 700 µL of each sample was loaded in 48-well clear plate Falcon® Multiwell™ (Becton Dickinson France SA, Le Point de Claix, France). The emission maximum (λ_{max}) and the area under the curve (AUC) were measured to evaluate bathochromic or hypsochromic shifts, and hyperchromic or hypochromic variations, respectively. Similarly, to the spectropolarimetric measurements, a positive control for protein denaturation was measured on BSA denatured in an 8 M solution of guanidine hydrochloride.

3.2.3.9 Protein stability after enzymatic digestion

3.2.3.9.1 Enzymatic digestion

To simulate the enzymatic digestion, the microgels were incubated in PBS pH 6.8 containing trypsin (5 mg mL^{-1}) at 37°C in a Multitron Standard shaking incubator (Infors AG) with an agitation of 200 rpm. The enzymatic digestion was then halted after one hour by adding trypsin inhibitor (5 mg mL^{-1}). The incubation was allowed for further 3 hours at the same temperature and shaking. After the entire incubation period, the samples were then evaluated by means of sodium dodecyl sulphate gel electrophoresis (SDS-PAGE). To evaluate the extent of BSA digestion by trypsin, we prepared negative controls by adding the trypsin inhibitor at the beginning of the enzymatic digestion and positive controls by allowing digestion of BSA standard.

3.2.3.9.2 SDS-PAGE

The SDS-PAGE was carried out according to the work from Schägger and von Jagow [442]. Briefly, the 13.3% separating gel consisted of 4.0 mL of a 3 M Tris-HCl and 0.3% SDS solution at pH 8.5, 1.3 mL of Milli-Q water, 2.7 mL of glycerine solution 64%, 4.0 mL of 40% Acrylamide/Bis solution, and 0.1 mL of a 10% APS solution. The 6% stacking gel was composed of 1.8 mL of a 3 M Tris-HCl and 0.3% SDS solution at pH 8.5, 4.2 mL of Milli-Q water, 1.0 mL of 40% Acrylamide/Bis solution, and 0.1 mL of 10% APS solution 10%. In both cases, 10 µL of TEMED were added before casting to begin polymerisation. A 10 µL aliquot of loading dye (100 mM Tris-HCl pH 6.8, 8% SDS, 24% glycerine, 4% DTT, 6 M urea, and 0.05% bromophenol blue) was mixed to 10 µL of each sample. These solutions were first incubated for 5 minutes at 95°C in an Eppendorf Thermomixer (Eppendorf Instrumente GmbH), and then loaded into each well at room temperature. The cathode buffer was composed of 10 mM Tris, 10 mM tricine, and 0.01% SDS, whereas the anode buffer was composed by a 20 mM Tris-HCl solution. The electrophoresis apparatus Mini-PROTEAN® Tetra Cell (Bio-Rad Laboratories AG) was set to 100 V and 20 W. The electrophoresis was run for ~1.5 hours. The gels were incubated in an aqueous fixing solution containing 5% aluminium sulphate, 10% ethanol, 0.02% Coomassie Brilliant Blue 250-G, and 2.35% phosphoric acid for one hour. All percentages are intended as w/v, unless otherwise specified. The gels were then dried at 70°C for one hour. The dried gels were then scanned and the bands' intensities were compared semi-quantitatively with the image processing and analysing software ImageJ v1.48v (National Institute of Health, Bethesda, MD). The band intensities were normalised to avoid influence of total protein concentration differences. The digested BSA band intensity was taken at ~60 kDa, whereas the intact BSA band intensity y at ~66.5 kDa. The protection from trypsin digestion is expressed by Equation 3.5 (below).

3.2.4 Results

3.2.4.1 HNT characterisation

The nanotubular structure of halloysite clay, before and after chemical modification, was studied using different analytical methods. Results of this characterisation are listed in Table 3.6. The measured particle size of the nanotubes was in good agreement with literature [323]. The rather high variation in particle size distribution (span ≥ 1) was expected and is due to the anisotropic geometry of the nanotubes. In fact, the measured particle size represents the statistical average of HNT's projections in different orientations, which includes their length and diameter as extreme values. As a result, chemical treatment did not show a significant variation in terms of particle size and span.

The measured ζ-potential values were consistent with literature [323]. These surface charge values were not significantly influenced by the chemical treatment that is expected to act on the luminal surface. While chemical

$$Protection\ from\ trypsin\ digestion\ (\%) = \left[1 - - \frac{\left(\frac{digested\ BSA}{digested\ BSA + intact\ BSA}\right)_{sample}}{\left(\frac{digested\ BSA}{digested\ BSA + intact\ BSA}\right)_{\substack{positive \\ control}}}\right] \cdot 100 \qquad 3.5$$

TABLE 3.6 – Comparison of non-treated and treated nanotubes (nHNT and bHNT, respectively). Statistical significance calculated by Student's t-test (n = 3). Significance expressed as *** ($p < 0.001$), ** ($p < 0.01$), and ($p < 0.05$).

Property	nHNT	bHNT	Significance
Nanoparticle characterisation			
Particle diameter (nm)	202.0 ± 8.5	215.3 ± 2.5	
Span	0.969 ± 0.178	1.190 ± 0.085	
ζ-potential (mV)	-48.7 ± 3.2	-43.6 ± 1.6	
Surface area measurements			
Specific surface area ($m^2\ g^{-1}$)	55.53 ± 0.68	53.41 ± 1.16	
Pore volume ($\mu L\ g^{-1}$)	153.6 ± 10.9	216.3 ± 11.9	**
Pore diameter (nm)	11.00 ± 0.78	16.23 ± 0.60	***
Protein content			
Loading efficiency ($mg\ g^{-1}$)	36.15 ± 2.50	59.60 ± 4.20	**

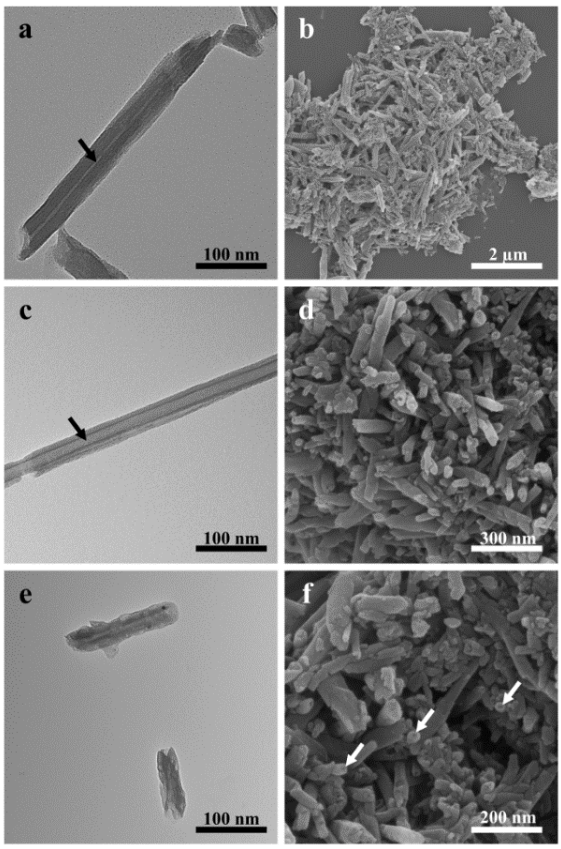

FIGURE 3.10 – TEM (left column) and SEM (right column) pictures of HNTs. nHNT (a, b, d) bHNT (c, f), and bHNT loaded with BSA (e). The nanotubes' lumen is indicated by the arrows.

etching increased the pore volume and the pore size of the nanotubes, the HNT specific surface exhibited only a slight variation. Student's t-test showed statistically significant difference in pore volume and size ($p < 0.05$), whereas such significance could not be confirmed for the specific surface area.

3.2.4.2 HNT imaging

The TEM pictures of the HNT, which are shown in the left column of Figure 3.10, confirmed the hollow nanostructure of the halloysite clay. The analysed nanotubes had a strongly elongated structure, which appeared to be longer than 200-300 nm in most cases. The inner diameter of the nanotubes shown in Figure 3.10a was ~6 nm, whereas the external diameter of the HNT was ~30 nm. The bHNT represented in Figure 3.10c retained the same external diameter as nHNT, but the lumen diameter was increased up to ~20 nm. Figure 3.10e exhibits bHNT after protein loading and their external surface appeared to be comparatively rougher and less defined. This may suggest BSA adsorption on the external HNT surface in addition to a likely penetration into the lumen of the clay nanotubes. In the right column of Figure 3.10 are shown the images gathered from SEM microscopy. The nanoparticle appeared to form large clusters in the micrometre range (Figure 3.10b). Despite the formation of such agglomerates, the tubular and elongated structure of each nanoparticle can still be clearly identified in both nHNT and bHNT (Figures 3.10d and 3.10f, respectively).

3.2.4.3 Microgel and NiMOS size and morphology

The size and the morphology of the microgels were evaluated to understand the HNT influence on the gel

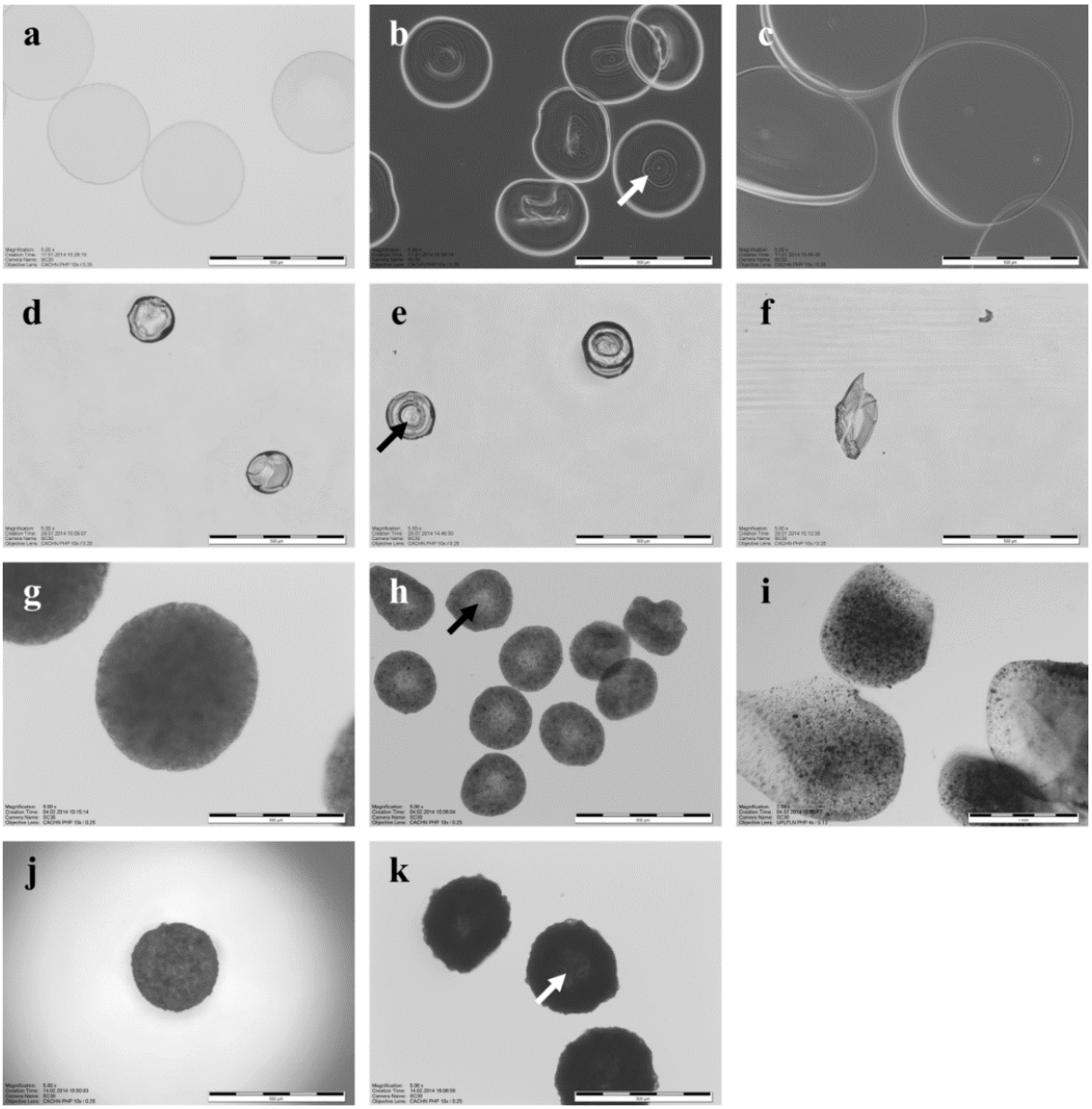

FIGURE 3.11 – Optical microscope images of prilled microgels. Microgels formed in ethanol (left column), in DEGEE (central column), and in water and Tween® 80 (right column). Their composition is non-dried microgels (first row), dried microgels (second row), non-dried NiMOS (third row), and dried NiMOS (fourth row). The scale bar is 500 μm for all images, except (i) where it is 1 mm. The arrows highlight the thinner central structure of the toroidal-like microgels.

structure during prilling. The median particle sizes of the different microgels loaded with HNT are summarised in Table 3.7. Microgels produced in water had the largest particle size, whereas those formed in DEGEE demonstrated smallest particle size. The drying step greatly reduced the median particle size for ethanol (~39%). Instead, the diameter reduction for particle formed in DEGEE after drying was ~23%. The particles formed in water could not be measured after drying because of significant microgel clustering. Results indicated at least for the non-aqueous hardening baths that particle size distribution decreased after drying of the microgels.

TABLE 3.7 – Particle size and shape of nNiMOS formed in different hardening baths

Hardening bath	Median particle size (μm)		Particle size span		Elongation factor	
	wet	*dry*	*wet*	*dry*	*wet*	*dry*
Water and Tween® 80	1193.1	n.a.[g]	0.91	n.a.[g]	n.a.[h]	n.a.[h]
Ethanol	502.9	311.3	0.68	0.38	1.70	1.70
DEGEE	396.7	306.7	0.61	0.49	1.66	1.80

[g] *Dried microgels in water formed large clusters*
[h] *The microgels formed in water, both wet and dry, were too large for the flow-through cell*

The pictures taken by optical microscopy are shown in Figure 3.11. The microgels formed in ethanol showed spherical geometry (Figure 3.11a), which was retained regardless of drying (Figure 3.11d) or of the presence of HNT (Figure 3.11g and 3.11j). However, the microgels prilled into DEGEE (Figure 3.11b, 3.11e, 3.11h, and 3.11k) displayed a rather toroidal shape, which was retained after drying and was further not affected by inclusion of HNT. The microgels obtained in the aqueous hardening bath displayed irregular shapes. The non-dried microgels resembled thin disks (Figure 3.11c), whereas the dried microgels could not maintain structural integrity and cracked (Figure 3.11f). After being loaded with HNT, the microgels had enhanced irregular shape (Figure 3.11i).

3.2.4.4 Protein content

The loading efficiency (Table 3.6) was calculated to understand how much protein was either loaded into the lumen or adsorbed onto the external surface of HNT after loading with the BSA solution. The chemical modification of the nanotubes obviously enabled a significantly higher incorporation of protein compared to the non-treated particles ($p < 0.05$). However, in either case, it was not possible to differentiate how much was adsorbed on the particle surface in comparison to the protein fraction that entered the nanotubes' lumen. The encapsulation efficiency was assessed in blank microgels and in both types of NiMOS dropped in different hardening baths. The data are summarised in Table 3.8. The encapsulation efficiency was found to be higher in non-aqueous media, in accordance to previous reports [28,426]. Both NiMOS showed lower encapsulation efficiency than the blank microgels. The nHNT-containing microgels displayed higher encapsulation efficiency when formed in a DEGEE bath and in aqueous medium. bNiMOS had higher encapsulation efficiency when formed in ethanol. These differences were found to be statistically significant ($p \leq 0.01$) after ANOVA testing.

In light of these findings, further characterisation of the microgels and NiMOS, *i.e.*, release test and protein stability, was conducted only using systems formed in ethanol as hardening bath.

3.2.4.5 Release test

Overall, 5 different samples were tested over 24 hours, and the initial 4 hours of BSA release are depicted in Figure 3.12. Blank microgels were used as a reference. Up to ~95% of their BSA content was released and the microgels displayed initially almost zero order release kinetics after 24 h. Then,

TABLE 3.8 – Encapsulation efficiency of NiMOS and blank microgels (*i.e.*, without clay nanotubes) formed in different hardening baths. Data are expressed as mean value ± standard deviation (n = 3).

Type of microgels	Encapsulation efficiency in different hardening baths (%)		
	Ethanol	***DEGEE***	***Water + 2% Tween® 80***
Blank	75.05 ± 5.18	86.09 ± 6.47	68.33 ± 1.88
nNiMOS	57.27 ± 3.81	52.95 ± 5.55	45.16 ± 4.31
bNiMOS	63.16 ± 4.66	48.07 ± 5.39	39.30 ± 2.19

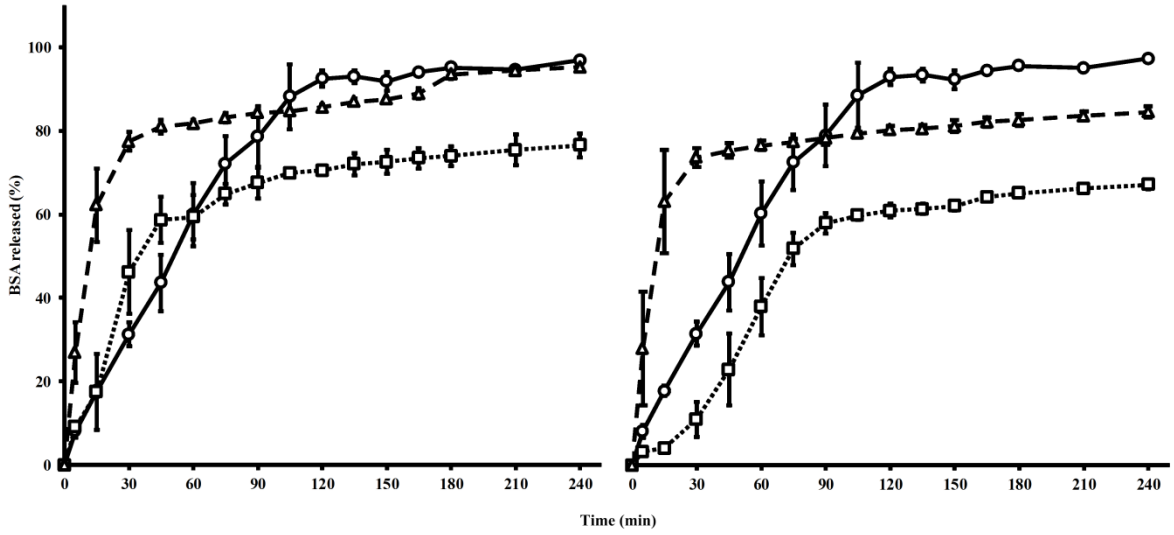

FIGURE 3.12 – BSA release profiles over four hours in PBS pH 6.8. Left graph: dried microgels as a reference (circles and continuous line), nHNT (triangles and long dashes), and nNiMOS (squares and dotted line). Right graph: dried microgels as a reference (circles and continuous line), bHNT (triangles and long dashes), and bNiMOS (squares and dotted line). Error bars represent standard deviations (n = 6).

after about 105 minutes a plateau state was reached and the final fraction released after 4 hours is 96.9% ± 0.7%. As for the BSA-loaded HNT, these samples released their content in a first phase rapidly (> 70% in 30 minutes) and then released continuously at a slow rate. After 4 hours, nHNT and bHNT exhibited a release of 95.3% ± 0.3% and 84.1% ± 1.4%, respectively. In both cases, the 24-hour release was above 95% of the nominal content. An interesting behaviour was observed for the BSA release from nNiMOS. The initial release rate was between that of the reference and of nHNT, while matching the slower release kinetic of the latter after ~90 minutes. nNiMOS eventually released 90.3% ± 1.2% of their nominal content. bNiMOS showed a sigmoidal release profile of BSA. A brief initial lag phase occurred for the first 15 minutes. Subsequently, the BSA was released almost linearly until 60% after 90 minutes. Finally, the profile stabilised to match the release kinetics of the BSA-loaded bHNT and reached 89.2% ± 2.2% release after 24 hours. The f_2 similarity factors are represented in Table 3.9. All release

TABLE 3.9 – f_2 similarity factors calculated from the release profiles. Values expressed between 0 and 100; if $f_2 < 50$, profiles are considered different.

***f*₂ similarity factors**					
	Microgel	*nHNT*	*bHNT*	*nNiMOS*	*bNiMOS*
Microgel	-	33.6	34.9	44.9	31.8
nHNT		-	58.0	33.7	21.1
bHNT			-	38.7	24.1
nNiMOS				-	37.3
bNiMOS					-

TABLE 3.10 – Comparison of protein stability after manufacturing and enzymatic digestion. Significance (Sign.) expressed as *** ($p < 0.001$), ** ($p < 0.01$), and * ($p < 0.05$) after ANOVA testing. Data are expressed as mean value ± standard deviation (n = 3).

Stability	Microgel [i]	nHNT	bHNT	nNiMOS	bNiMOS	Sign.
Circular dichroism						
α-helix fraction (%)	51.4 ± 0.7	51.6 ± 0.5	52.0 ± 0.9	51.3 ± 0.3	51.4 ± 0.6	
Fluorescence						
AUC (RFU nm)	95980 ± 541	105809 ± 1996	105753 ± 2207	96075 ± 258	96339 ± 198	***
λ_{em} (nm)	349.3 ± 1.5	351.0 ± 1.0	351.0 ± 1.0	350.0 ± 1.0	350.3 ± 1.5	
SDS-PAGE						
Protection from digestion (%)	4.85 ± 4.38	45.99 ± 6.99	56.53 ± 6.98	62.22 ± 9.64	81.54 ± 3.76	***

[i] *dried microgel obtained from prilling into the ethanol hardening bath*

profiles appeared different from one another, except the comparison between treated and non-treated HNT.

3.2.4.6 Protein stability after prilling

The protein structure stability after manufacturing was assessed by spectropolarimetry and spectrofluorimetry. The stacked circular dichroism profiles of the samples are shown in Figure 3.13. The observed profiles describe the typical α-helix structure of BSA with a small contribution of its β-sheet fraction [219]. No difference between the BSA reference curve and the other samples can be observed, neither after loading on the HNT, nor after the prilling step. This was further confirmed by the data obtained from the circular dichroism spectra deconvolution (Table 3.10). In fact, differences in the α-helix fraction of the different samples compared to the reference (53.27 ± 1.20%) were minimal and they were found to be statistically non-significant after ANOVA testing. Also, the profiles did not show the decrease in intensity and shape modification seen in the denatured BSA profile, which had also significantly lower α-helix fraction (29.13 ± 3.31%).

The data collected from the spectrofluorimetric analysis confirmed the findings from the circular dichroism profiles (Table 3.10). BSA's three-dimensional structure appeared to remain unscathed throughout the manufacturing process. The emitted fluorescence profile, in fact, could be closely associated to the profile of the BSA standard (λ_{max} = 351 nm), which can be seen in Figure 3.14. However, a modest yet statistically significant hypochromic effect was found for the HNT-loaded BSA according to calculated AUC for the measured range. Similar effects have been previously reported, and could be due to small electrostatic interactions with unbound carboxylic groups of MCC with unusually low pK_a. However, this hypochromic effect cannot be attributed to any structural change [443]. Also, the samples' fluorescence intensity was clearly higher than the denatured BSA profiles.

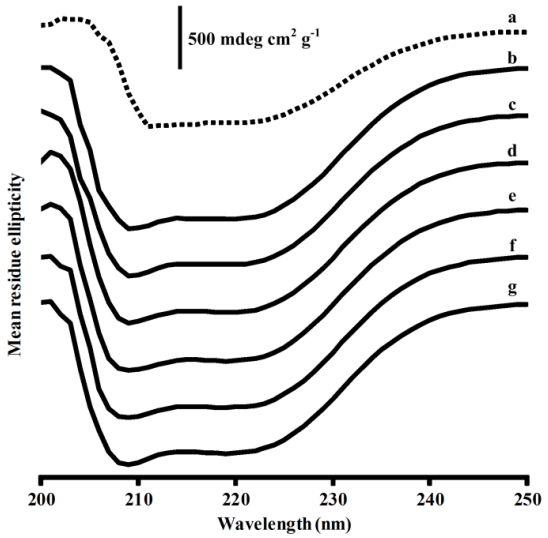

FIGURE 3.13 – Overlaid circular dichroism profiles of denatured BSA with guanidine hydrochloride (a), of BSA standard (b), and of BSA loaded in dried microgels (c), nHNT (d), bHNT (e), nNiMOS (f), and bNiMOS (g).

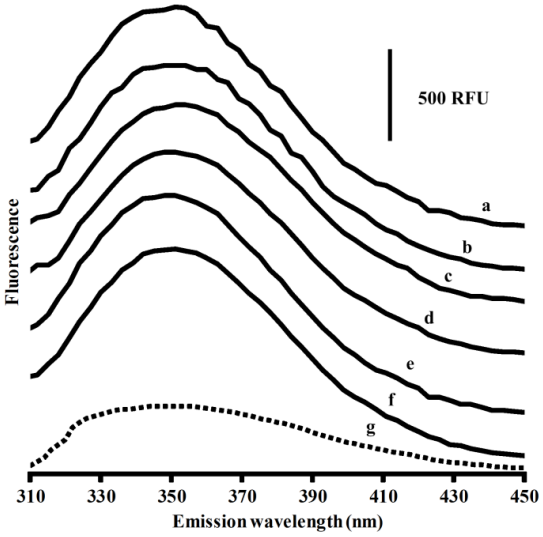

FIGURE 3.14 – Overlaid emitted fluorescence profiles of BSA as standard (a), loaded in dried microgels (b), nHNT (c), bHNT (d), nNiMOS (e), and bNiMOS (f), and denatured with guanidine hydrochloride (g). λ_{ex} = 280 nm.

3.2.4.7 Protein stability after enzymatic digestion

The microgels and the NiMOS were digested with trypsin to evaluate the extent of their protein protection from enzymatic degradation. The results of the SDS-PAGE analysis are shown in Figure 3.15. The BSA standard (lane 2) exhibits a large band between the protein marker bands at ~55 and ~70 kDa, which was in agreement with BSA's molecular weight of 66.5 kDa. Also, a secondary band appeared at higher molecular weight, which was due to impurities and BSA aggregates. A blank sample containing trypsin (~22.3 kDa) and trypsin inhibitor (20.1 kDa) is shown in lane 3. A second band close to the trypsin inhibitor band was present, which was apparently due to the self-digested trypsin enzyme. The positive and the negative controls are in lanes 4 and 5, respectively. The positive control was obtained by directly adding BSA standard in the trypsin digesting medium, and then adding trypsin inhibitor after one hour, similarly to the other samples. The negative control had the inhibitor added from the start of the digestion. The BSA after enzymatic digestion appeared as a shorter band with a molecular weight between that of BSA and ~55 kDa (indicated by the arrow in the figure, in lane 4). The BSA-loaded microgels showed poor protection of the protein, either when non-dried (lane 6) or when dried (lane 7). The protection from trypsin digestion was, in both cases, below 5%. The use of non-treated and treated HNT considerably increased protection to 46.0 ± 7.0% (lane 8) and 56.5 ± 7.0% (lane 9), respectively. However, by forming NiMOS with the nHNT, 62.2 ± 9.6% of BSA remain unscathed, as seen in lane 10. Finally, the luminal etching of halloysite combined with microencapsulation, *i.e.* bNiMOS, demonstrated protection from enzymatic digestion to a highest value of 81.5 ± 3.8% (lane 11). The differences between these means were found to be statistically significant after ANOVA testing (n = 3, $p < 0.001$), as seen in Table 3.10.

3.2.5 Discussion

This work designed and studied a novel multi-compartment system obtained by prilling for potential oral protein delivery. Thus, protein-loaded natural clay nanotubes were dispersed in a polymeric solution followed by prilling into a hardening bath to form microgels. The results are discussed in terms of nanotube characterisation, feasibility and properties of prilled NiMOS, which includes protein stability in this multi-compartmental drug delivery system.

3.2.5.1 HNT characterisation

The used HNT exhibited morphological and physicochemical properties that were consistent with data reported in the literature. Moreover, the alkaline activation step did not alter the external appearance of the HNT and did not change the average particle size. Chemical etching led to larger lumen size by reducing the nanotube wall thickness, which agreed well with previous findings [340]. The alkaline groups in the lumen may have selectively removed aluminium-containing internal layers from the nanotubes. However, the inner layer removal did not result in greatly impaired mechanical wall strength, because no indication of collapsed tubes was detected. A similar nanotubular structure was clearly visible for both the treated and the non-treated HNT by TEM and SEM. While TEM images could only provide an indication of enlarged luminal size, the BET data confirmed an increased lumen diameter and volume thereby demonstrating the success of the chemical etching step.

A key finding from the loading efficiency measurements (Table 3.6) was that the chemical etching improved the BSA loading of HNT. Given the rather large structure of BSA (~14 × 4 × 4 nm [444,445]), the steric hindrance caused by the ~10 nm wide HNT lumen may limit protein access into the nanotubes. This luminal enlargement effect is interesting because previous work often had small molecules loaded into HNT [328,329] and the inner diameter was there less critical for drug loading. Especially for BSA, the inner surface of the nanotubes is important because the protein has an isoelectric point of ~ 4.7 [412] so

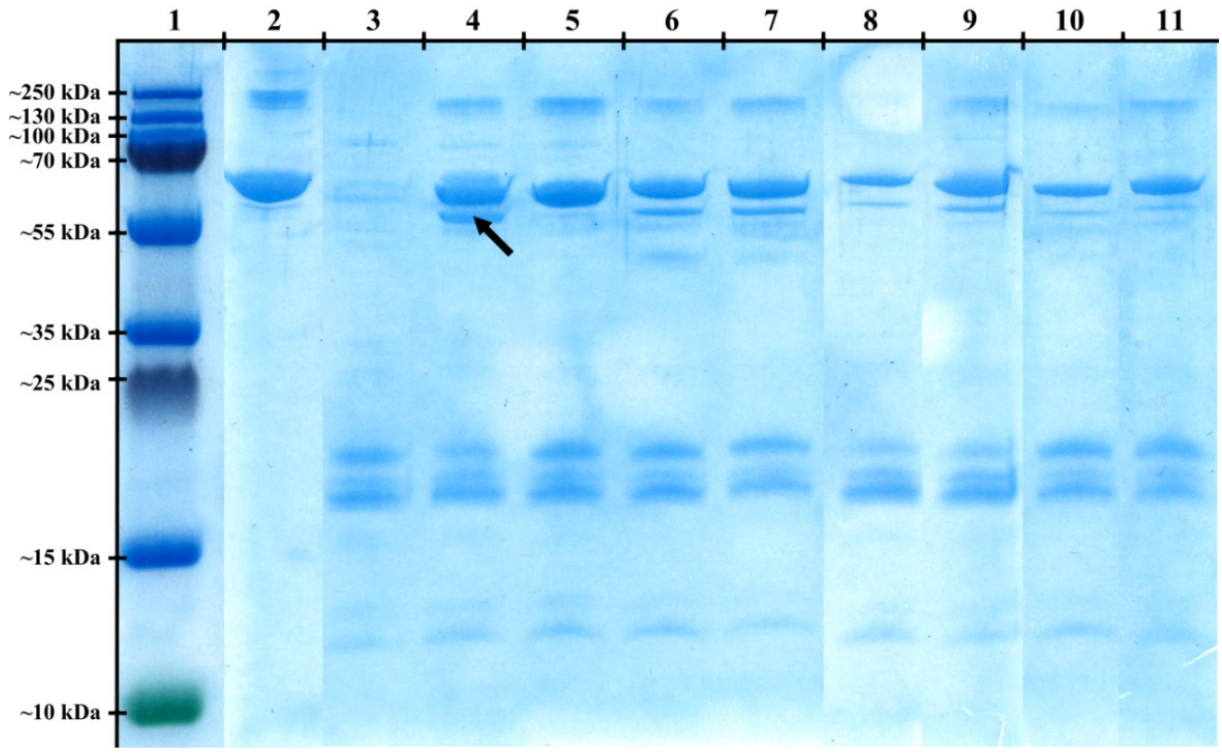

FIGURE 3.15 – SDS-PAGE of BSA loaded into different dried microgels, HNTs, and NiMOS. From left to right, protein marker (lane 1), BSA standard (lane 2), blank with trypsin and trypsin inhibitor (lane 3), positive control (lane 4), negative control (lane 5), non-dried microgels (lane 6), dried microgels (lane 7), nHNT (lane 8), bHNT (lane 9), nNiMOS (lane 10), and bNiMOS (lane 11). Further description of the samples in the different lanes is given in the text. The arrow highlights the trypsin-digested BSA protein.

that a net negative charge is given at neutral conditions. A similar net negative surface charge is expected on the surface of HNT caused by the SiO_2 groups and was confirmed by the measured negative ζ-potential. Different from this outer surface chemistry is the inner layer of the nanotubes, which is dominated by aluminium hydroxide and displays a positive ζ-potential at neutral conditions [321]. This positive surface charge could be beneficial for an interaction with BSA regarding efficient loading into the HNT. Due to the layered structure of HNT, the positively charged inner surface layer may be retained after chemical etching. Our finding of a high protein loading into the treated HNT may confirm that even though the pores were enlarged, the surface charge was likely to remain positive at the luminal surface layer.

Compared to the chemical etching and loading of BSA primarily into the HNT, there are other methods reported for drug loading. Drug was for example adsorbed onto the HNT external surface by using charged polymers [342], or formation of a mesoporous structure [338]. The loading of a therapeutically active protein into the lumen, however, may provide a biopharmaceutical advantage by granting degradation protection. As mentioned earlier, halloysite from different extraction sites exhibited different properties, such as larger luminal diameter [327]. Consequently, a suitable chemical activation may need to be fine-tuned according to the geometry of the employed HNT.

3.2.5.2 Prilled NiMOS characterisation

An important finding was that prilling proved to be a suitable technology for manufacturing Nanotubes-in-Microgel Oral Systems. MCC was employed as microgel-forming polymer to host the HNT that incorporated BSA as model protein. This nanocomposite material seems very interesting regarding the regulatory acceptance of the excipients employed and the rather narrow size distribution of the microparticles. Different ratios of HNT-to-polymer solution were tested. From a manufacturing perspective, a lower solid fraction is preferred to reduce viscosity, while otherwise highly concentrated suspensions

could lead to processing issues. Inadequate rheological properties are a more general issue in pharmaceutical dispersion manufacturing. A high viscosity at a given processing shear rate can for example negatively affect quality attributes, such as the filling adequacy into capsules [446]. Viscosity is also a key factor in the process of prilling when the liquid stream is passing through the narrow prilling nozzle and for liquid jet breakup [23,231,249,391].

From a formulation viewpoint, however, a higher solid fraction is preferred for it would allow a higher macromolecule loading into the microgels. While a HNT-to-polymer solution ratio of 1:10 (w/w) was found to be close to the limit of technical processability, a ratio of 1:20 (w/w) appeared to optimally balance drug-loading and manufacturing aspects.

The NiMOS formation by prilling further revealed lower encapsulation efficiency, compared to blank microgels. As known from previous literature, the presence of nanotubes appears to affect the microgel matrix [447]. This is especially critical during the hardening step as part of the prilling process. The likely mechanism of hardening in a non-aqueous medium has been described earlier by De Kruif *et al*. [28,426]. Briefly, when the droplets enter the hardening bath, the polymers undergo local surface coiling, which is caused by the difference in physicochemical properties between the aqueous microgel medium and the non-aqueous hardening bath environment [55,410]. In parallel, the polymer chains begin cross-linking by the Ca^{2+} ions present in the hardening bath. Both effects may cause a shrinking of the microgel especially close to the surface layer. In presence of HNT, this complex hardening process was evidently disturbed and the strength of the MCC cross-linking affected by the presence of solid material, which was finally leading to poorer encapsulation efficiency due to BSA leakage. When using an aqueous hardening bath, the surface coiling of the polymers due to the different properties of the microgel solution and the hardening bath is barely given. Gel strength is here primarily achieved by the cross-linking via Ca^{2+}-ions.

However, the network formed by the MCC gel may not be tight enough to prevent the BSA leakage from the microgel of HNT. The encapsulation efficiency of the aqueous hardening bath may therefore have been lower than in non-aqueous systems.

The kinetic profiles of nHNT and bHNT showed a comparatively fast initial release, followed by a phase of much slower release rate. Different compounds have shown different release profiles from the nanotubes [328]. Diverse release profiles are mainly determined by electrostatic interactions of given APIs with the outer or inner surface of the nanotubes. As previously mentioned, BSA (pI ~4.7) was to some extent loaded into the HNT at pH 6.8, so that the model drug could interact with the positive charges of the inner HNT surface. However, the external HNT surface still possessed a considerably high surface area, thus allowing here at least some absorption of BSA. These two interactions may explain the bimodal release of the BSA from HNT, namely rapid kinetics from the surface and slower release from the lumen. Previous reports have shown that HNT alone released macromolecules between 50-500 hours [321]. However, such long release times are less relevant for oral delivery, which is limited by GI transit time. We selected 24 hours as observation time to obtain a good overview of the release kinetics, while still being physiologically relevant. Within this time frame, HNT showed initially a faster release that in a second phase stabilised at a lower release rate over time. Such comparatively fast initial release was also previously observed with for example insulin release from HNT within a 24-hour time span [321].

Blank dried microgels had initially a kinetic order close to zero (R^2 = 0.97). The slower release of blank microgels compared to BSA-loaded HNT was linked to the swelling process that is typical for a dried hydrophilic polymer-based microgel. Before releasing the content, the MCC chains need to be hydrated and go through a swelling step. Consequently, water can penetrate the gradually swelling polymer structure and allow BSA diffusion into the surrounding medium.

Both BSA-loaded HNT revealed significantly different profiles compared to the blank microgels alone. However, the presence of HNT obviously influenced the release of BSA from the microgels. In fact, the release behaviour of NiMOS was evidently determined by the combination of both HNT and microgel. As earlier described, HNT interacts with the microgel structure. Cavallaro *et al*. for example showed that, in HNT-filled dried alginate beads, the nanotubes tended to be more concentrated closer to the core than to the surface of the droplet [447]. This effect may explain the initial lag time in the release of the bNiMOS. Already the pure nanotubes demonstrated a complex release behaviour that consisted of more than one kinetic phase. It was assumed that the fractions of albumin in the nanotubes as well as on the external surfaces may have caused such different kinetic phases. The added microgel present in the NiMOS further added complexity in terms of structure and release mechanism. Interesting was that initial release from nNiMOS and bNiMOS exhibited larger differences compared to nHNT and bHNT.

Considering particle morphology, the presence of HNT appeared not to modify the shape of the prilled microgels. Similarly, HNT also helped the NiMOS to retain their shape even after the drying step. The close interaction of the clay nanoparticles with the polymer was probably strengthening the swollen MCC gel structure during drying. Consequently, the particle size reduction after gelling was diminished in presence of HNT compare to blank microgels.

Finally, the choice of the hardening bath seemed to influence the microgel particle, as previously reported [28]. Of all formulations, ethanol allowed higher sphericity, smaller microgels, and reduced particle size distribution. The toroidal shape formed by DEGEE-based hardening baths, instead, was maintained and enhanced by the presence of HNT in the microgel. This further confirmed the influence of HNT presence on microgel morphology during prilling.

3.2.5.3 Protein stability

The protein stability was evaluated after the prilling process and following enzymatic digestion. This stability study was important to preliminarily assess the delivery system's protection from GI enzymes. Moreover, it allowed to differentiate the individual effects of nanotubes, microgels, and NiMOS using an *in vitro* enzymatic digestion test. One of the key findings of this work is that NiMOS indeed showed superior protection from trypsin digestion. Compared to the positive control, blank microgels were not able to offer significant protection from the enzymatic digestion. Treated and non-treated HNT alone provided limited benefit to protein stability. Instead, NiMOS showed a significant increase in BSA protection from digestion. Furthermore, the treated bHNT exhibited an advantage in terms of protection both when used alone and when it was present in microgels. The mechanistic explanation for this protection is both challenging and interesting. The release kinetics could be contributors to the results obtained by NiMOS, but this may not be the only relevant mechanism. In fact, BSA was released from HNT in a shorter time than from blank microgels, whereas the enzymatic protection was higher. Electrostatic interactions between anionic MCC polymer and trypsin could have influenced the result. Bovine trypsin has an isoelectric point of ~10.3 [448] which was likely resulting in a positive charge on the enzyme surface at the buffered pH 6.8 [449]. Trypsin may have interacted with the negatively-charged external wall of the nanotubes to a higher extent than BSA. Both compounds, in fact, have been shown to interact with and adhere on silicate surfaces [450,451]. The mechanistic explanation of the enzymatic degradation reduction may be a balance and combination of the aforementioned effects, as well as due to prolonged release. In light of these findings, there is a strong biopharmaceutical rationale in favour of NiMOS compared to HNT alone. NiMOS could be further loaded as dry powder into hard or soft capsules. The capsules can be provided with enteric coating to enhance the protection from enzymatic degradation.

An important finding was that the manufacture of NiMOS via prilling appeared to be harmless to the protein structure in case of the model drug. The BSA loading on HNT did not alter the protein three-dimensional structure. Also, the chemical activation was correctly achieved without leaving residues potentially harmful for the protein. While prilling in non-aqueous media has been earlier described as feasible for proteins [28], some lipid-based formulations have shown to be potentially detrimental [426]. An example of a known protein denaturant is ethanol [415].Potential conformational changes in the protein, which may be caused by ethanol denaturation, should be detected in either circular dichroism or Trp-212 emitted fluorescence spectra [407,421,422]. Despite the influence of HNT on the microgel structure, ethanol was apparently not able to cause harm to the loaded protein, as shown by α-helix fractions and the fluorescence emission spectra.

3.2.6 Conclusion

The present work demonstrated the successful feasibility of Nanotubes-in-Microgel Oral System (NiMOS) prepared by prilling for delivery of macromolecules. The manufacture of these nanocomposite microgels appeared to be not harmful for the model protein BSA. Halloysite (HNT), a natural, cheap, and non-toxic clay, proved suitable for protein loading due to its favourable nanotubular hollow structure. The chemical etching of the nanotube lumen was leading to improved loading efficiency. The prilling approach allowed formulation of a nanocomposite hydrogel, which showed interesting properties in terms of enzymatic protection and modified release. Especially, the preliminary *in vitro* assessment of protection from enzymatic degradation showed promising results for the NiMOS for local oral protein delivery. The combination of nanotubes and microgels had a synergic effect that prevented our model protein's digestion. NiMOS provide a versatile DDS, either dispersed with lipid-based system [28,426] or directly filled in capsules as a dry powder as suggested in the present paper.

An adequate fine-tuning of the polymer type and properties may allow modification of the release profiles of the system, thus adapting the NiMOS to the therapeutic needs of the loaded macromolecule. The multi-compartment system could be further used to create fixed-dose combination dosage forms, with tailored release profiles and optimal enzymatic protection from the gastrointestinal environment. Prilling also bears the potential to provide a two compartment system, *i.e.*, a microcapsule with a core and a shell, thus forming a highly versatile and adaptable system. Further research on the proposed NiMOS may explore the advantages of such structured systems, as well as address in-depth *in vitro* modelling and preliminary *in vivo* biopharmaceutical studies of therapeutically active proteins.

Chapter 4

Manufacturing and formulation quality aspects of LB pharmaceutical dispersions as drug delivery systems

4.1 A systematic study on manufacturing of prilled microgels into lipids for oral protein delivery §

4.1.1 Summary

The development of novel systems with oral protein delivery as ultimate goal represents an important field of pharmaceutics. Prilling of protein-loaded polymeric solutions into lipid-based hardening baths could provide here an attractive formulating technology. Since the obtained microgel dispersion can be directly capsule-filled, no drying step is required and thermal drug degradation is avoided. This study aims to find excipient combinations for the novel prilling process and investigate systematically diverse material and process factors. Bovine serum albumin and mono-N-carboxymethyl chitosan were selected as model protein and prilling polymer, respectively. The prilling suitability of 880 formulations was screened with 60 ternary phase diagrams comprising two co-solvents, ten different glycerides and three so-called complementary excipients. Preliminary capsule compatibility was tested for one month on 245 formulations in hard and soft capsules with different shell materials. Ternary phase diagrams' centre points were used to evaluate morphology, encapsulation efficiency, and protein stability of the prilled microgels. As result, several formulations proved suitable for prilling and compatible for capsule filling. Statistical analysis using partial least square regression revealed significant factors regarding different quality attributes of microgel dispersions. Therefore, an improved understanding was obtained for this promising drug delivery approach.

4.1.2 Introduction

Oral delivery of protein drugs is a challenging field of modern pharmaceutical sciences, and there is a rising interest in this type of drug delivery [18,185,383,423]. However, the gastrointestinal tract (GI) represents a major hurdle in terms of bioavailability for proteins and peptides administered orally. Macromolecules like proteins and peptides generally require protection from gastric degradation and enzymatic digestion. Additionally, they

§ de Kruif JK *et al*. A systematic study on manufacturing of prilled microgels into lipids for oral protein delivery. *Journal of Pharmaceutical Sciences*, **2015**, 104:3351-3365.

must cross the mucus and mucosal layer if absorption is needed to achieve a therapeutic effect [183]. Depending on the pharmacological target, it is possible that only luminal activity or additional mucus penetration is sufficient to ensure the macromolecule's efficacy. Many approaches have been proposed over the years to overcome the GI tract biopharmaceutical barriers. Microencapsulation was found to be very promising for oral protein delivery especially in terms of protection from enzymatic degradation [21,22,389]. Furthermore, some polymers used for microencapsulation, like chitosan derivatives, are known to have mucoadhesive properties and even permeation enhancing characteristics [192,278,396]. Such properties have been reported for the non-toxic and water-soluble mono-N-carboxymethyl chitosan (MCC), which may thus qualify as a polyfunctional polymer [169,394,395]. Hydrogels formed from similar polymers are further able to create a suitable environment for a macromolecule, *e.g.*, in terms of pH and ionic strength, to ensure drug integrity [21,389,397,452]. Moreover, the microencapsulation may allow protection from the GI milieu [20]. A combination of microgels and lipid-based drug delivery was targeted in this work by means of a prilling process. This approach holds a biopharmaceutical promise, but its primary formulation rationale is of technical nature to enable a manufacturing in capsules as oral dosage form. Prilling is a mild microencapsulation technique that is suitable for protein loading [22]. This technique allows the entrapment of an API into a hydrogel by dropping a drug-containing polymeric solution into a hardening bath [245,250]. During prilling (Figure 4.1), a liquid stream of the polymer and API solution is extruded from a nozzle. The stream is disrupted into droplets of the same size by applying a vibration at high frequency. The droplets can be visualised mid-air through a set of vertically aligned stroboscopic lights. The droplets can be charged by falling through a ring electrode, to prevent mid-air coalescence [238]. Finally, they are collected into the hardening bath, where gelling can occur, for example, by ionic cross-linking or by changes in temperature. The conventional hardening baths are water-based [245,250,453], but this leads to further manufacturing steps, such as drying, that may harm a loaded macromolecule. A notable exception to aqueous hardening baths was presented by Buthe *et al.*, who proposed n-butanol as a calcium-containing non-aqueous medium to harden alginate beads [247]. However, this reference study neither reported the loading of API into the beads, nor employed an orally acceptable excipient. De Kruif *et al.* recently introduced a non-aqueous lipid-based hardening bath to obtain protein-loaded hydrophilic microgels formed by ionic cross-linking [28]. This new approach provides a lipid-based fill mass ready to be directly loaded into hard or soft shell capsules without any intermediate drying step. Nevertheless, there are multiple formulation and process factors that can influence the

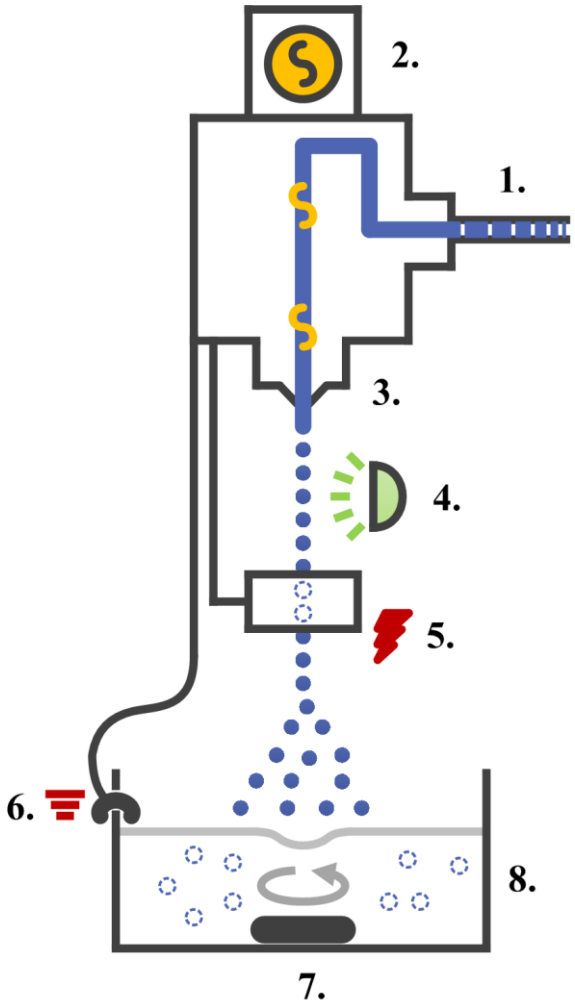

FIGURE 4.1 – Scheme of vibrating nozzle system. 1 polymeric solution feed; 2 vibrating unit; 3 nozzle; 4 stroboscopic light; 5 electrode ring; 6 grounding; 7 magnetic stirrer; 8 hardening bath. Not to scale.

microgel dispersion quality. Therefore, our aim was to systematically study the influence of different excipient factors on various formulations attributes. The final purpose was to explore a potential design space for the formulation principle.

4.1.3 Materials and methods

4.1.3.1 Materials

Transcutol® HP (diethylene glycol monoethyl ether; DEGEE), Maisine™ 35-1 (glyceryl monolinoleate), and Labrafil® M2125CS (linoleoyl macrogol-6 glycerides) were

kindly offered by Gattefossé SAS (Saint Priest, France). Absolute ethanol was obtained from Brenntag Schweizerhall AG (Basel, Switzerland). Capmul® MCM EP (glyceryl monocaprylocaprate), Capmul® MCM-C10 EP (glyceryl monocaprate), Capmul® MCM-C8 EP (glyceryl monocaprylate), Captex® 8000 (glyceryl tricaprylate), Captex® 1000 (glyceryl tricaprate), and Acconon® CC-6 (caprylocaprate macrogol-6 glycerides) were purchased from ABITEC Co. (Janesville, WI). Miglyol® 812 (glyceryl tricaprylocaprate), Imwitor® 742 (glyceryl caprylocaprate), and peppermint oil were bought from Hänseler AG (Herisau, Switzerland). Polyethylene glycol (PEG) 600 was obtained from AppliChem GmbH (Darmstadt, Germany). Mono-N-carboxymethyl chitosan (deacetylation degree 96.1%, carboxymethylation degree 82.1%, loss on drying 20.5%, molecular weight 9000-13 000 g mol^{-1}) was supplied by Shanghai Boyle Chemical Co. Ltd (Shanghai, China). Beta-mercaptoethanol, bovine serum albumin 96% (BSA), calcium chloride anhydrous, propylene carbonate, potassium dihydrogen phosphate, sodium dihydrogen phosphate dihydrate, sodium hydroxide and dipotassium hydrogen phosphate were purchased from Sigma-Aldrich (Saint-Louis, MO). The Low Molecular Weight Reagent Kit was purchased from Perkin Elmer (Schwerzenbach, Switzerland) and the Micro BCA™ Protein Assay Kit was obtained from Thermo Fisher Scientific AG (Rockford, IL).

4.1.3.2 Polymeric solution preparation

The polymeric solution was prepared by modifying a previously reported method [28]. Briefly, a 4.5% (dry substance; w/v) solution of MCC was prepared by dissolving the polymer in demineralised water. The complete hydration of the polymer solution was allowed by mixing thoroughly overnight. The polymeric solution was then vacuum-filtered through glass microfiber filters Whatman™ GF/D and BSA was added to the solution to obtain a 2.5% (w/v) concentration. This solution was subsequently stored in a brown glass bottle at +4°C, and it was allowed to reach room temperature before each use. The solutions were discarded after one week from preparation, to avoid possible microbial contamination. Placebo solutions were prepared in the same way without adding any BSA to the solution.

4.1.3.3 Ternary phase diagrams

The ternary phase diagrams were prepared by mixing three components at different ratios, namely one co-solvent (DEGEE or ethanol), one glyceride (Acconon® CC-6, Capmul® MCM, Capmul® MCM-C8, Capmul® MCM-C10, Captex® 8000, Captex® 1000, Imwitor® 742, Labrafil® M2125CS, Maisine™ 35-1, or Miglyol® 812), and one complementary excipient (PEG 600, propylene carbonate, or peppermint oil). The glycerides were chosen according to their high diversity in chemical composition. In fact, the glycerides' composition varied in terms of fatty acid chain length (caprylates, caprates, and linoleates), predominance of unsubstituted glyceride hydroxyl groups ("free hydroxyl groups"), as well as presence of a PEG group. The predominance of unsubstituted glyceride hydroxyl groups was categorised according to the hydroxyl value of the glycerides in low (less than 150 mg_{KOH} g^{-1}), medium (between 150 and 300 mg_{KOH} g^{-1}) and high (more than 300 mg_{KOH} g^{-1}). The hydroxyl values were obtained from the glycerides' certificate of analyses. Table 4.1 summarises the properties of all the components employed in the ternary phase diagrams. Each ternary phase diagram comprised 25 mixtures. While all the mixtures were prepared at room temperature, the single components were heated or melted before use, according to the excipient manufacturers' instructions. The components were weighed into a glass vial to the appropriate ratio and subsequently mixed at room temperature for one hour with a magnetic stirrer. After one-hour equilibration, the miscibility of the components was visually assessed and a score was assigned to each formulation. The score was labelled as 2 for a homogeneous system, 1 for signs of incomplete miscibility or turbidity, or 0 for an immediate phase separation. An aliquot of calcium chloride anhydrous (4.5% w/w) was added to the mixture and the turbidity was evaluated after thorough mixing for 24 hours. In this case, the score assigned was 2 for a clear solution, 1 for opalescence or slight turbidity, or 0 in any other case. Finally, the MCC polymeric solution was dripped from a syringe mounted with a blunt needle (gauge size 18) into each hardening bath formulation. The suspended droplets were immediately mixed at maximum speed using an Ika® Vortex Genius 3 (Hüber & Co. AG, Reinach, Switzerland) to verify their gelling. The assigned score was 2 for spherical hydrogels, 1 for irregular or partially coalesced droplets, and 0 if gelling did not occur. After overlaying the ternary phase diagrams of the different mixture characteristics, an overall score was assigned by multiplying each partial score according to Equation 4.1.

$$Overall\ score = miscibility\ score \times solubility\ score \times gelling\ score \quad (4.1)$$

Therefore, possible values of this overall score were 0, 1, 2, 4, or 8.

4.1.3.4 Capsule compatibility with hardening bath excipients

Four types of commercially available capsules were filled with the hardening baths and stored for 4 weeks at 25°C

TABLE 4.1 – Hardening bath component list and properties of the selected glycerides.

Excipient list	**Glyceride properties**		
	Free hydroxyl group content [j]	***Chain length***	***PEGylation***
Co-solvents			
Ethanol			
DEGEE [k]			
Glycerides			
Acconon® CC-6	medium	8-10	yes
Imwitor® 742	medium	8-10	no
Captex® 8000	low	8	no
Captex® 1000	low	10	no
Capmul® MCM-C8	high	8	no
Capmul® MCM-C10	high	10	no
Miglyol® 812	low	8-10	no
Capmul® MCM	high	8-10	no
Labrafil® M2125CS	low	18	yes
Maisine™ 35-1	medium	18	no
Complementary excipients			
PEG 600			
Propylene carbonate			
Peppermint oil			

[j] *categorised according to the hydroxyl value; further explanation in the text*
[k] *diethylene glycol monoethyl ether*

and 45% relative humidity. The two-piece hard capsules were gelatine Licaps® (Capsugel France SAS, Colmar, France) and hypromellose Quali-V® (Qualicaps® Europe SAU, Alcobendas, Spain). Both capsule types were opaque white and of size 0. The soft capsules were oval and of size 10, and their shell material was gelatine (SGC) or starch (VegaGels®), both supplied by Aenova GmbH (Kirchberg, Switzerland). All capsules were kindly provided by their respective manufacturer. Only formulations with an overall score higher than 1 and a co-solvent fraction lower than 0.35 were selected for capsule filling. The two-piece hard capsules were loaded with 500 µL of the hardening baths. The same quantity of hardening bath formulation was injected in the soft capsules with a 20 gauge needle. The opening thereby formed was sealed on a hot plate. All capsules were kept in the darkness in upright position for four weeks. After each week, the capsules were inspected for signs of incompatibility, *e.g.* deformations or leaking. Capsules which showed signs of incompatibility already after the first week were classified as "immediately" incompatible. If the capsules showed signs of incompatibility after the second or third week, then they were described by "short-term" incompatibility. Finally, capsules without any sign of capsule deformation, crack formation, or leaking were assigned to the "absent" incompatibility category.

4.1.3.5 Prilling of the polymeric solution

The hydrophilic microgels were prepared with the vibrating nozzle technique using the Encapsulator Biotech (EncapBioSystems Inc., Greifensee, Switzerland; currently, this instrument is manufactured and distributed by Büchi Labortechnik AG, Flawil, Switzerland). The polymeric solution containing BSA was loaded into 60 mL Omnifix® plastic syringes (B. Braun Melsungen AG, Melsungen, Germany). This solution was then extruded through a 300 µm stainless steel nozzle at a rate of 12.1 mL min^{-1}, using a vibration frequency of 1060 Hz and an amplitude set to 9. The droplets flowed through the electrode ring charged at 2460 V and fell from ~15 cm into 100 mL of the hardening bath containing dissolved calcium chloride, which was stirred at ~600 rpm. These conditions were found to be optimal for the prilling process. A total of 5 g of polymeric solution was used for each batch and the produced microgels were left in their respective hardening bath for one hour before further analysis.

4.1.3.6 Morphological characterisation of the microgels

The microgels were analysed in term of particle size and shape by dynamic image analysis using an XPT-C

flow-through cell particle analyser (PS-Prozesstechnik GmbH, Basel, Switzerland). The microgels (n = 200) were suspended in their hardening bath and then pumped into the flow-through cell of the instrument. The particle size was described in terms of Waddle disk diameter, which is the diameter of a disk with the same area as that projected by a given particle.

The particle shape was expressed as the elongation factor, which is the maximum Feret diameter (the linear segment connecting the two perimeter points that are the furthest apart) divided by the Feret equivalent rectangular short side (the shortest side of the rectangle with the same area as the particle and the longest side equal in length to the maximum Feret diameter). For a perfectly spherical particle, the elongation factor is $4/\pi$ (≈1.27). The XPT-C equipment also allowed the imaging of each analysed particle to visually assess the morphology of the microgels.

4.1.3.7 BSA encapsulation efficiency in microgels

Each 5 g batch of hardened microgels was filtered over a 125 µm opening stainless steel sieve. The particles were washed with absolute ethanol to remove traces of hardening bath, which could interfere with the protein assay. The samples were first dissolved in phosphate buffer saline pH 6.8 overnight at room temperature to release BSA completely, and then stored at +4°C before further analysis. The required amount of solution was centrifuged at 10 000 rpm for 10 minutes in a 5415C centrifuge (Eppendorf GmbH, Leipzig, Germany), and the supernatant was subsequently filtered through Titan 3 nylon filters 0.45 µm (SMI-LabHut Ltd, Maisemore, UK). The protein content of the sample was determined using the Micro BCA™ Protein Assay Kit, which is based on the bicinchoninic acid assay [401–404]. After treating the sample according to the protocol supplied by the manufacturer, the protein content was measured spectrophotometrically in a SpectraMax M2^e plate reader (Molecular Devices LLC, Sunnydale, CA) at 750 nm after being loaded in 96-well clear BRANDplates® pureGrade™ (Brand GmbH + CO KG, Wertheim, Germany). The encapsulation efficiency (EE) is expressed as shown in Equation 3.3.

4.1.3.8 Protein stability

4.1.3.8.1 Circular dichroism of BSA

The modification of BSA's secondary structure was evaluated by comparing the protein circular dichroism spectra after release from the microgels. The spectra were recorded on a Jasco J-810 spectropolarimeter (Jasco Inc., Easton, MD). The sample was loaded in a 1 cm optical path quartz cuvette and analysed in the far-UV range (200-260 nm). For a visual and qualitative analysis, the profiles were normalised by their intensity to remove the influence of protein concentration on the evaluation. The data are expressed as mean residue ellipticity (mdeg cm^2 g^{-1}), which is calculated according to Equation 3.4.

For quantitative assessment, the profiles were deconvoluted with the software CDNN v2.1 [441]. The software calculates the fraction of the protein's secondary structures, namely α-helices, β-coil, antiparallel β-sheet, parallel β-sheet, and random coils. The modification of BSA's secondary structure was assessed from the change in α-helix fraction. Our reference BSA sample's α-helix content was 54.7%, which was in good agreement with the literature [454].

4.1.3.8.2 Microfluidic capillary electrophoresis

The microfluidic capillary electrophoresis was conducted to detect potential protein aggregation or degradation. The analysis was carried out on a LabChip® GXII high throughput chip microfluidic capillary electrophoresis (Caliper Life Sciences, Hopkinton, MA) by using the Low Molecular Weight Reagent Kit. The samples were prepared both in reducing and non-reducing conditions. In the former case, beta-mercaptoethanol was used as a reducing agent. The samples were measured according to the protocol supplied by the manufacturer. The software used to evaluate the acquired data was LabChip® GX (Caliper Life Sciences). The output of the instrument is analogous to a chromatographic curve, with the retention time substituted by the molecular weight. The aggregates and impurities are defined as any signal other than the BSA peak at 66.5 kDa, and are expressed as a fraction of the whole sample.

4.1.3.9 Data handling and partial least square (PLS) regression analyses

The data generated in the different steps of this work were analysed by partial least square (PLS) regression. When several experimental factors and response variables have been measured, PLS allows fitting a model to the data that can represent the variation of the responses to the variation of the factors. The statistical software used for the PLS regression analyses was MODDE v10.1 (Umetrics AB, Umeå, Sweden). Three separate PLS regressions were used to evaluate the ternary phase diagrams, the capsule compatibility, and the microgel properties. The data were arranged according to a user-specified d-optimal design. The number of components was chosen according to significance by cross-validation. The models obtained were evaluated in terms of goodness of fit (R^2) and cross-validation value (Q^2). Specifically, R^2 is the percent of the response variation that could be explained by the model. Q^2 is the percent of the response predicted by the model

according to cross-validation. The cross-validation of each regression was carried out by removing one element at a time. The Q^2 is calculated by the statistical software according to Equation 4.2.

$$Q^2 = \left(1 - \frac{PRESS}{SS}\right) \cdot 100 \qquad 4.2$$

Where PRESS is the prediction residual sum of squares (Equation 2.22), and SS is the total sum of squares of the response variables corrected for the mean (Equation 2.24). R^2 and Q^2 are expressed as a percentage, and the analysed models are considered to have statistical relevance if higher than 50%.

The experimental factors used for the ternary phase diagram evaluation were the co-solvent fraction, the glyceride fraction, the glyceride chain length, the glyceride hydroxyl value, and the glyceride PEGylation. For the purpose of statistical evaluation, the chain lengths were classified in medium chain (caprylates and caprates) and long chain glycerides (linoleates). The hydroxyl values were grouped in low (< 150 $mg_{KOH}\ g^{-1}$), medium (between 150 and 300 $mg_{KOH}\ g^{-1}$), and high (> 300 $mg_{KOH}\ g^{-1}$). The response variable chosen for the evaluation was the overall score. The initial sample set (n = 880) was divided according to the type of co-solvent employed, thus providing two separate subsets. After the first screening, some outliers with high standardised residuals were removed. Thus, the models applied for the ethanol subset and the DEGEE subset had n = 497 and n = 534, respectively.

The statistical analysis of the capsule compatibility was carried out on 245 samples. The experimental factors chosen were the same as listed for the ternary phase diagram evaluation. The response variables were the compatibility of the prepared receiving bath mixtures in each of the four capsule types, namely Licaps®, Quali-V®, SGC, and VegaGels®. The levels for these variables were "immediate incompatibility", "short-term compatibility", and "absent incompatibility".

Further properties of the prilled microgels, such as their morphology, the EE, and the protein stability, were also evaluated in a PLS analysis. The centre points of the 60 phase diagrams were used as data set. The chosen experimental factors and the response variables are listed in Table 4.2.

4.1.4 Results

4.1.4.1 Ternary phase diagrams

Based on initial experiments, mixtures of glycerides with a co-solvent were found to be of interest regarding a suitable hardening bath for prilling microgels into lipids. While ethanol and DEGEE were main candidates for suitable co-

TABLE 4.2 – List of response variables and experimental factors for partial least square regression analysis of the microgel properties.

Experimental factors		**Response variables**	
Name (*type*)	**Level**	**Name (*unit*)**	**Objective (*target*)**
Glyceride chain length (*continuous, multi-level*)	Medium chain, long chain	Microgel size (*μm*)	Minimise (*min. 300 μm*)
Hydroxyl value (*continuous, multi-level*)	Low, mid, high	Microgel shape	Minimise (*min. 1.27*)
PEGylation (*categorical*)	Yes, no	Encapsulation efficiency (*%*)	Maximise (*max. 100%*)
Complementary excipient type (*categorical*)	PEG 600, propylene carbonate, peppermint oil	α-helix content [l] (*%*)	Hit target (*54.7%*)
Co-solvent type (*categorical*)	Ethanol, DEGEE	Electrophoresis impurities (*%*)	Minimise (*min. 0%*)

[l] *percentage of α-helix structure after deconvolution*

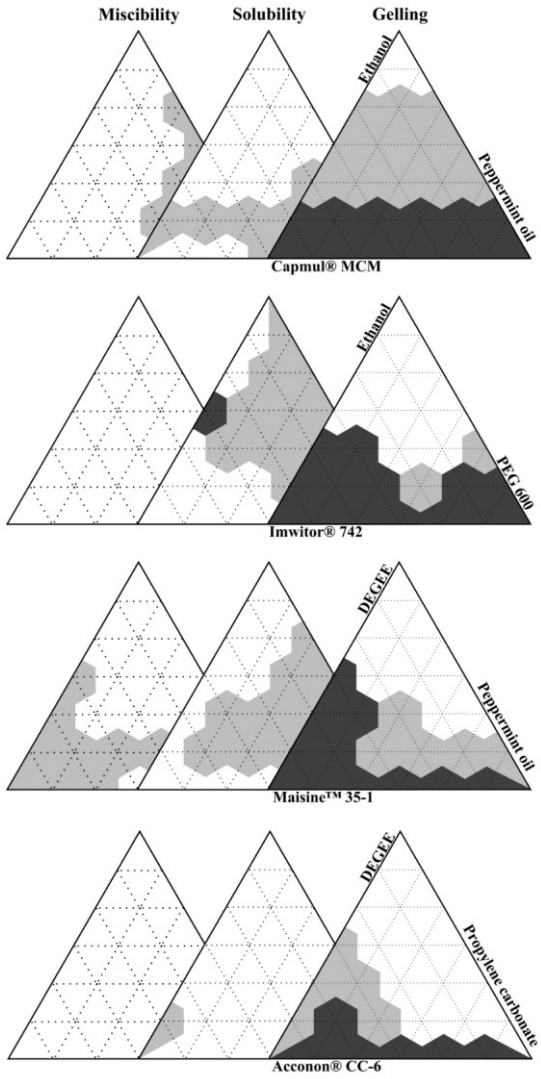

FIGURE 4.2 – Four examples of the overlaid ternary phase diagrams. Each corner represents 100% of the component indicated. The white, light grey, and dark grey areas correspond to scores of 2, 1, and 0, respectively.

solvents, there was also the possibility to include additional excipients to the mixtures. The additional or "complementary" excipient constituted a third component in diverse phase diagrams that used the excipients as listed in Table 4.3. A total of 60 ternary phase diagrams provided an overview of the interactions occurring between the three components in terms of excipient miscibility, calcium chloride solubility, and MCC gelling. Once these mixture characteristics were assessed, the ternary phase diagrams were overlaid to calculate an overall score of the formulations, as shown in Figure 4.2. The findings of the mixture characteristics are discussed in the following paragraphs and are summarised in Table 4.3, together with a report of the statistical factor significance.

4.1.4.1.1 Excipient miscibility

It was evident that the fraction of both co-solvents increased the overall score of the formulations. There was a trend showing that miscibility of the excipients was even more favoured in the presence of ethanol compared with DEGEE as co-solvent. In the case of glycerides, mono- and diglycerides were miscible in most formulations and at various ratios. Triglycerides could also be mixed with the other components preferentially with ethanol as a co-solvent. However, longer chain glycerides tended to have less favourable miscibility profiles. There was a net positive effect of PEGylation noted for miscibility (Table 4.3). Moreover, the three different types of complementary excipients seemed to alter the miscibility in the ternary phase diagrams according to their polarity. As expected, the least polar complementary excipient, *i.e.* peppermint oil, was found to be better miscible with triglycerides than propylene carbonate or PEG 600.

4.1.4.1.2 Calcium chloride solubility

Sufficient calcium chloride dissolution to achieve a suitable hardening bath for prilling was targeted in the lipid-based mixtures. It was expected that the salt solubility would be strongly dependent on the overall polarity of the mixtures. It was found in all systems that a minimum amount of co-solvent was required to dissolve calcium chloride. Only in few cases, the binary mixtures alone of glyceride and complementary excipient could solubilise the calcium chloride completely. Ethanol was especially effective in dissolving this excipient salt. Furthermore, free hydroxyl groups of glycerol in mono- and diglycerides increased the formulation polarity, and thereby contributed to the calcium chloride solubility. After the salt addition, some formulations containing medium chain triglycerides exhibited a precipitation which appeared to be a salting out of an initially liquid component. This phenomenon occurred especially at comparatively lower co-solvent concentrations. Long fatty acid chains appeared to reduce the solubility of calcium chloride at least in the DEGEE data subset. In addition, glyceride PEGylation led generally to a slight increase in solubility of the calcium ions. Among the complementary excipients, especially peppermint oil hindered salt solubilisation, which typically resulted in opalescent solutions or turbid suspensions. The other complementary excipients were able to dissolve the calcium chloride at the given concentration.

TABLE 4.3 – Summary of the factors' effects on the scores in the ternary phase diagrams. Significant increase (++), non-significant increase (+), significant decrease (--), and non-significant decrease (-) $p \leq 0.05$ from PLS regression analysis.

Factor	Miscibility	Solubility	Gelling	Overall
		ethanol subset / DEGEE subset		
Co-solvent fraction	++ / ++	++ / ++	++ / ++	++ / ++
Glyceride fraction	+ / +	-- / ++	-- / --	-- / --
Chain length	-- / --	- / --	- / --	- / --
Hydroxyl value	++ / ++	++ / ++	-- / -	++ / ++
Glyceride PEGylation	++ / ++	++ / ++	++ / +	++ / ++

4.1.4.1.3 Mono-N-carboxymethyl chitosan (MCC) gelling

Adding a co-solvent was found to be of critical importance for MCC gelling, regardless of the type used. A comparatively higher co-solvent concentration allowed the formation of well-defined spherical microgels without signs of particle interpenetration or coalescence. Conversely, a higher content of either glycerides or complementary excipients led to rather poor gelling characteristics, likely due to a lower extent of cross-linking. In these cases, the systems formed rather irregular particle shapes, had increased coalescence, or exhibited poor mechanical resistance to vortexing. In specific mixtures, even the absence of gelling was noted. The increase in chain length had a rather negative effect on the gelling properties of MCC. Similarly, increased hydroxyl values of the glycerides resulted in a relatively negative effect on MCC gelling. PEGylation had a positive effect on the polymer gelling for both subsets (Table 4.3), although it appeared to be significant only with ethanol as a co-solvent.

4.1.4.1.4 Overall score

According to the initial PLS analysis of the ternary phase diagrams (Table 4.3), both co-solvents had a positive effect on overall score. Conversely, the fraction increase of glycerides and complementary excipient led to poorer suitability of the hardening bath for prilling. The most advantageous glyceride characteristics for this process were a high hydroxyl value and PEGylation. Instead, the increase in fatty acid chain length was shown to reduce the suitability of the lipid-based hardening bath for prilling. In terms of interactions, the DEGEE subset revealed several statistically significant interactions between co-solvent fraction and different glyceride properties. Higher DEGEE fractions combined with increased glyceride chain length appeared to reduce the overall suitability of the formulation for prilling. However, the presence of PEGylated residues on the glycerides appeared to positively influence the hardening baths' properties at high co-solvent concentrations. As expected, an opposite interaction was seen with the increase of glyceride fraction. As for the ethanol-containing subset, only a positive interaction between PEGylation and glyceride fraction proved to be statistically significant. This effect was opposite to the one found for DEGEE. This result indicates that overall effects had to be carefully analysed regarding factor interactions to obtain a more refined view on the data, as it was here meaningful to differentiate the ethanol and the DEGEE data sets. A common interaction for both datasets was between the co-solvent and glyceride fractions. Thus, a simultaneous increase of both excipient fractions meant a lower complementary excipient content in the formulation. The negative influence of this factor interaction on the overall score entailed that the complementary excipient played a critical role for obtaining a suitable hardening bath. Overall, the PLS regression analysis yielded models with high goodness of fit and cross-validation predictivity for both the ethanol subset (R^2 = 85.3%, Q^2 = 83.9%) and the DEGEE subset (R^2 = 86.0%, Q^2 = 84.4%).

4.1.4.1.5 Capsule compatibility

Not all hardening bath compositions were further evaluated regarding capsule shell compatibility. Only formulations with an overall score higher than unity and with a co-solvent fraction lower that 0.35 were evaluated. As a result, two-piece hard gelatine capsules appeared to have higher compatibility with the different hardening baths and 87.5% of these capsules were visually compatible over the 4-week stability period. However, the SGC did not perform as well because in several cases (> 55.6%), the liquid filling showed signs of immediate incompatibility and started to leak out before the end of the first week. The two-piece hypromellose capsules and the starch-based soft capsules

TABLE 4.4 – Capsule compatibility characteristics of the centre point (phase diagrams) formulations. Details of score assignment and compatibility testing are given in the text.

Centre point composition	**Overall score**	**Incompatibility according to capsule type**			
		Licaps®	***Quali-V®***	***SGC***	***VegaGels®***
Ethanol Miglyol® 812 Peppermint oil	4	absent	absent	absent	absent
Ethanol Captex® 1000 Peppermint oil	8	absent	absent	immediate	absent
Ethanol Imwitor® 742 Peppermint oil	4	absent	absent	immediate	absent
DEGEE Imwitor® 742 Peppermint oil	8	absent	absent	immediate	absent

also exhibited comparatively lower compatibility from the beginning, with 52.3% and 45.8% capsules that were deformed or clearly harmed after the first week of stability testing, respectively. In line with the expectation that hydrophilic excipients can cause shell incompatibility, it was found that a higher fraction of co-solvent was critical regarding capsule compatibility [81,455]. An increased amount of glycerides appeared to generally increase capsule compatibility. When comparing the different types of glycerides, there was no remarkable effect of PEGylation or of fatty acid chain length.

In Table 4.4 we listed the formulations with the best compatibility characteristics among the ternary phase diagrams centre points. However, although the sample size was rather large, no overriding effect could be found because the PLS regression analysis did not result in a significant model.

TABLE 4.5 – Goodness of fit (R^2) and cross-validation predictivity (Q^2) values from the partial least square analysis using the centre points of the phase diagrams.

Response variable	**Goodness of fit, R^2**	**Cross-validation predictivity, Q^2**
Waddle disk diameter	89.1	77.2
Elongation factor	91.8	64.4
Encapsulation efficiency	96.9	87.8
α-helix content [m]	82.2	57.0
Electrophoresis impurities	76.5	62.8

[m] *percentage of α-helix structure after deconvolution*

4.1.4.2 Prilling of the microgels

The 60 hardening baths from the centre points of the different phase diagrams were selected for prilling trials using the vibrating nozzle equipment. While all the data are provided in the complementary data of this article, Figure 4.3 summarises the effect plots of the experimental factors on the individual response variables. The Q^2 and the R^2 of the PLS regression model are specified in Table 4.5.

4.1.4.2.1 Morphological characterisation of the microgels

According to the manufacturer, the prilled polymer droplets are roughly twice the size of the nozzle from which they were extruded. Consequently, the microgels' median Waddle disk diameter ranged overall between 424.57 µm and 600.69 µm. Since the employed nozzle diameter of this study was 300 µm, the measured particle sizes were in good agreement with the expected size range. Ethanol and DEGEE were not significantly different in altering the particle size. Instead, the complementary excipients appeared to have a stronger influence on the size.

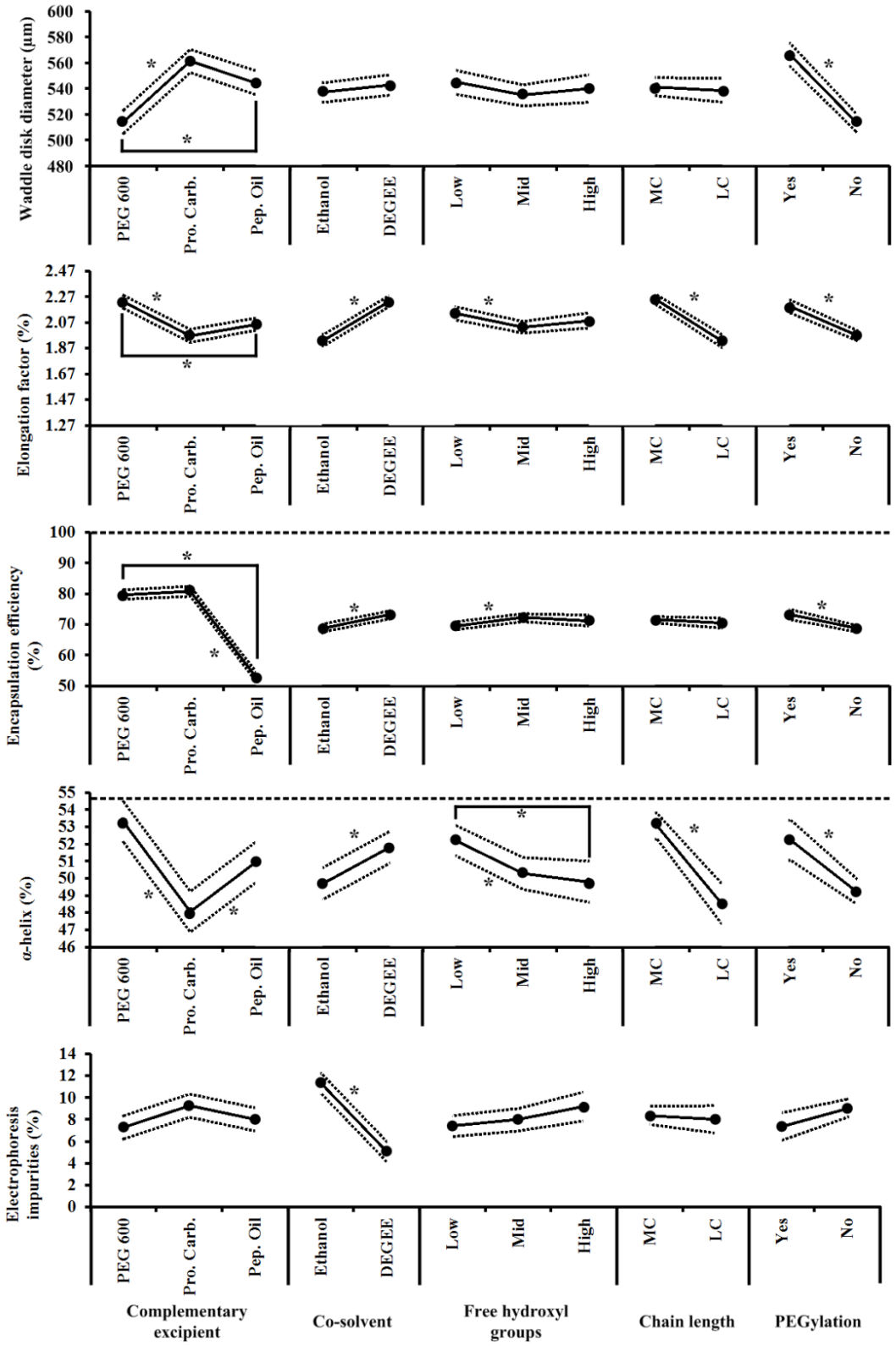

FIGURE 4.3 – Effect plots of the factors used in the PLS regression for the microgel characteristics. Among the complementary excipients, "Pro. Carb." stands for propylene carbonate, and "Pep. Oil" for peppermint oil. MC is medium chain length, whereas LC is long chain. A significant difference is represented by an asterisk ($p \leq 0.05$).

Formulations containing PEG 600 led to smaller microgels, compared to propylene carbonate and peppermint oil. Among the glyceride properties, PEGylation appeared to increase the volume of the microgels. Interestingly, the interaction of PEGylated glycerides and PEG 600 increased significantly the median particle size. These results indicate that there was no simple explanation of overall polarity that improved or hindered microgel swelling. Depending on the individual composition, there was a specific arrangement of the hardening bath microstructure that eventually determined the final swelling (or de-swelling) of the microgels in the mixtures.

The particular swelling characteristics were also determining the shape of the particles. This particle shape varied greatly among the different hardening bath formulations, from 1.44 to 2.52. Ethanol allowed the formation of more regular microgels when compared to DEGEE. The type of complementary excipient also appeared to influence the microgel shape. PEG 600, especially, increased the overall ellipticity of the prilled droplets. This effect was not as remarkable when using propylene carbonate or peppermint oil. The glyceride characteristics which affected mostly the particle shape appeared to be the fatty acid chain length and the PEG-substitution of the glycerol. A most notable and significant interaction was found between propylene carbonate and long chain glycerides that led to smaller elongation factors.

Figure 4.4 shows different morphological characteristics of the microgels. Spherical microgels could be obtained (Figure 4.4a), although different morphologies within the same batch could be found (Figure 4.4b). The latter case occurred especially in presence of DEGEE. A particular

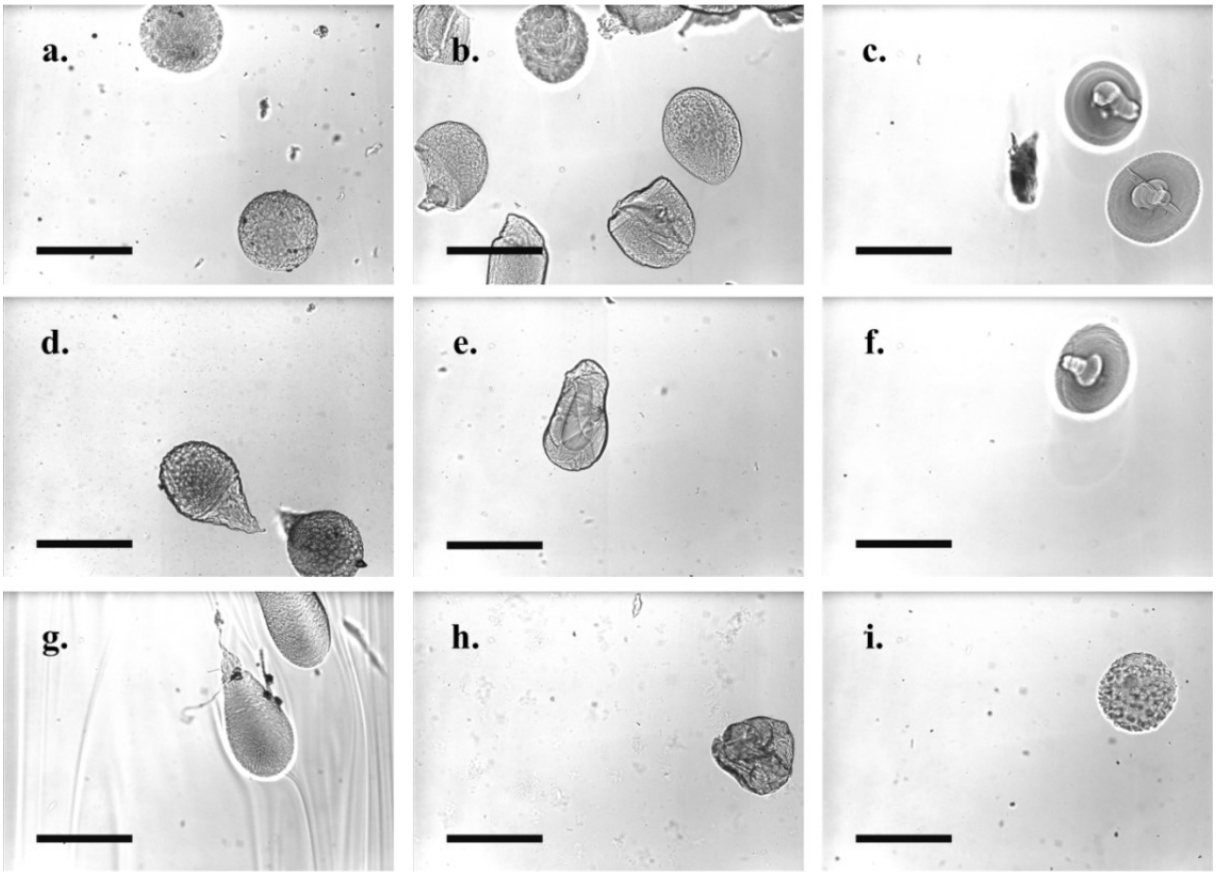

FIGURE 4.4 – Microgel pictures taken by the XPT-C during dynamic image analysis. The microgels shown were formed in DEGEE, Captex®, and peppermint oil (a), DEGEE, Capmul® MCM, and propylene carbonate (b), ethanol, Capmul® MCM-C10, and propylene carbonate (c, f), DEGEE, Maisine™ 35-1, and peppermint oil (d), ethanol, Imwitor® 742, and PEG 600 (e), ethanol, Capmul® MCM-CM8, and peppermint oil (g), ethanol, Acconon® CC-6, and PEG 600 (h), and DEGEE, Labrafil® M2125CS, and peppermint oil (i). All hardening baths' components were in a ratio of 1:1:1. Scale bar is 500 μm.

shape commonly found in prilling is represented in Figure 4.4d. Here, the droplets are slightly elongated and retain a small "tail" on their surface. A similarly elongated shape can be seen in Figure 4.4g, but here the characteristic "tail" is strongly combined to the elongated shape of the microgel. Other irregular shapes can be seen in Figure 4.4e and 4.4h, where the microgels appeared to be mechanically deformed (which may have resulted from the impact on the hardening bath surface) and in Figures 4.4c and 4.4f, where the microgels have a concave geometry. Interestingly, some microgels were macroscopically spherical, while a complex rough surface was obtained as seen from the example in Figure 4.4i.

4.1.4.2.2 BSA encapsulation efficiency in microgels

The overall EE of all the formulations varied between 44.2% and 89.3%. Such difference among the hardening baths was mostly due to the different complementary excipients. PEG 600 and propylene carbonate allowed higher EE values compared to formulations containing peppermint oil. Microgels formed with peppermint oil could not retain more that 63.0% of the BSA. Figure 4.3 shows further effects that are statistically significant but changed the EE on the average only slightly. Among the significant interactions, mixtures of ethanol and medium chain glycerides showed lower EE than mixtures with DEGEE. Similarly, when compared to DEGEE, ethanol mixed with peppermint oil had lower EE.

4.1.4.3 Protein stability

4.1.4.3.1 Circular dichroism

From a qualitative point of view, most profiles did not differ from those which were recorded with BSA standard, as shown in Figure 4.5b. However, some formulations modified the secondary structure of the encapsulated BSA. In Figure 4.5a we present the three worst-case profiles which were recorded. The α-helix profile, which is typical for this far-UV region, was completely lost or its intensity was reduced [219]. This showed a modification of the protein's secondary structure, which may correspond to denaturation. From the analysis of the deconvoluted circular dichroism spectra, our BSA reference had an α-helix fraction of 54.7%. Ethanol appeared to have a stronger influence than DEGEE on protein denaturation. Among the complementary excipients, PEG 600 and peppermint oil resulted as the least harmful for BSA.

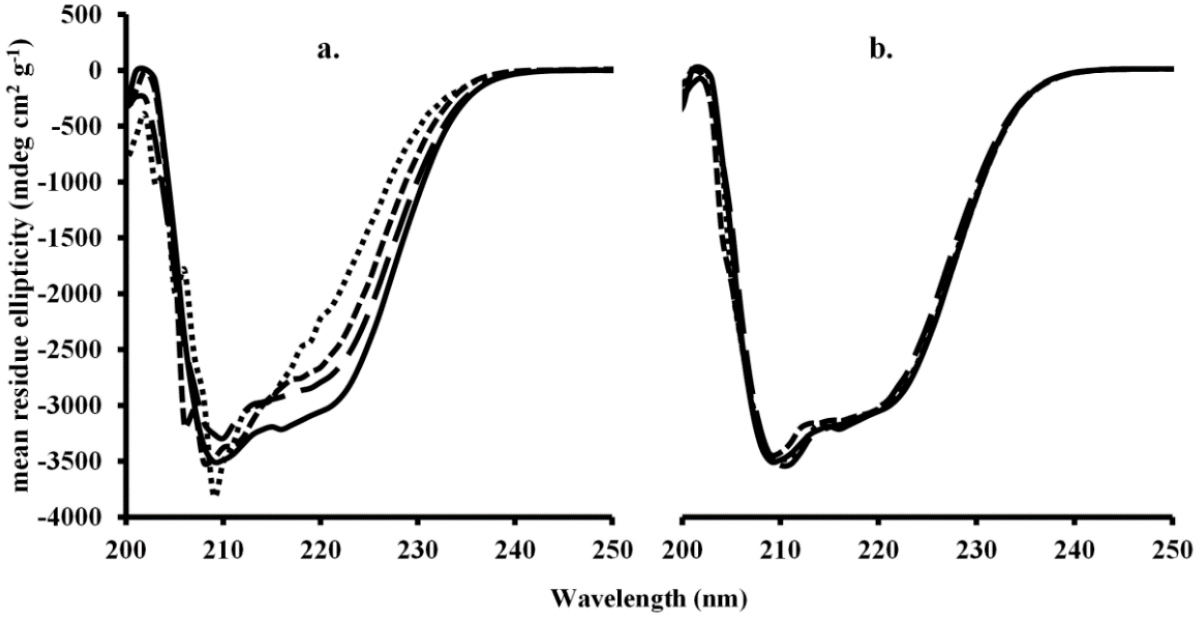

FIGURE 4.5 – Circular dichroism profiles of BSA. In a.: BSA reference (solid line), ethanol, propylene carbonate, and Maisine™ 35-1 (dotted line), ethanol, propylene carbonate, and Imwitor® 742 (short dashes), and ethanol, PEG 600, and Acconon® CC-6 (long dashes). In b.: BSA reference (solid line), ethanol, PEG 600, and Acconon® CC-6 (dotted line), DEGEE, PEG 600, and Miglyol® 812 (short dashes), and ethanol, peppermint oil, and Imwitor® 742 (long dashes). All hardening baths' components were in a ratio of 1:1:1.

Consequently, propylene carbonate showed the strongest denaturing effect. The composition of the glycerides also influenced the protein's secondary structure. Low hydroxyl values appeared to have minimal influence on the protein structure. Long fatty acid chains contributed to a negative modification of the secondary structure, whereas PEGylation helped to retain the three-dimensional arrangement of the protein. The altering effect of the chain length in combination with ethanol was markedly higher.

4.1.4.3.2 Microfluidic capillary electrophoresis

The microfluidic capillary electrophoresis was conducted both in reducing and non-reducing conditions to detect protein aggregation or protein fragments, respectively. All the samples which were prepared in reducing conditions did not show any trace of impurity. On the other hand, the samples prepared in non-reducing conditions revealed the presence of impurities up to concentrations of 19.0%. The only impurity found in all analysed samples was a compound with molecular weight between 105 and 110 kDa, which would represent a BSA dimer (Figure 4.6). As a co-solvent, DEGEE appeared to prevent protein aggregation better than ethanol. While propylene carbonate had a negative influence on protein stability, no significant difference could be determined when compared to the other complementary excipients. None of the glycerides' properties was found to be significantly related to a variation in protein aggregation. However, the interaction between co-solvents and complementary excipients with PEGylated glycerides appeared to reduce the possible denaturing effects of hardening baths.

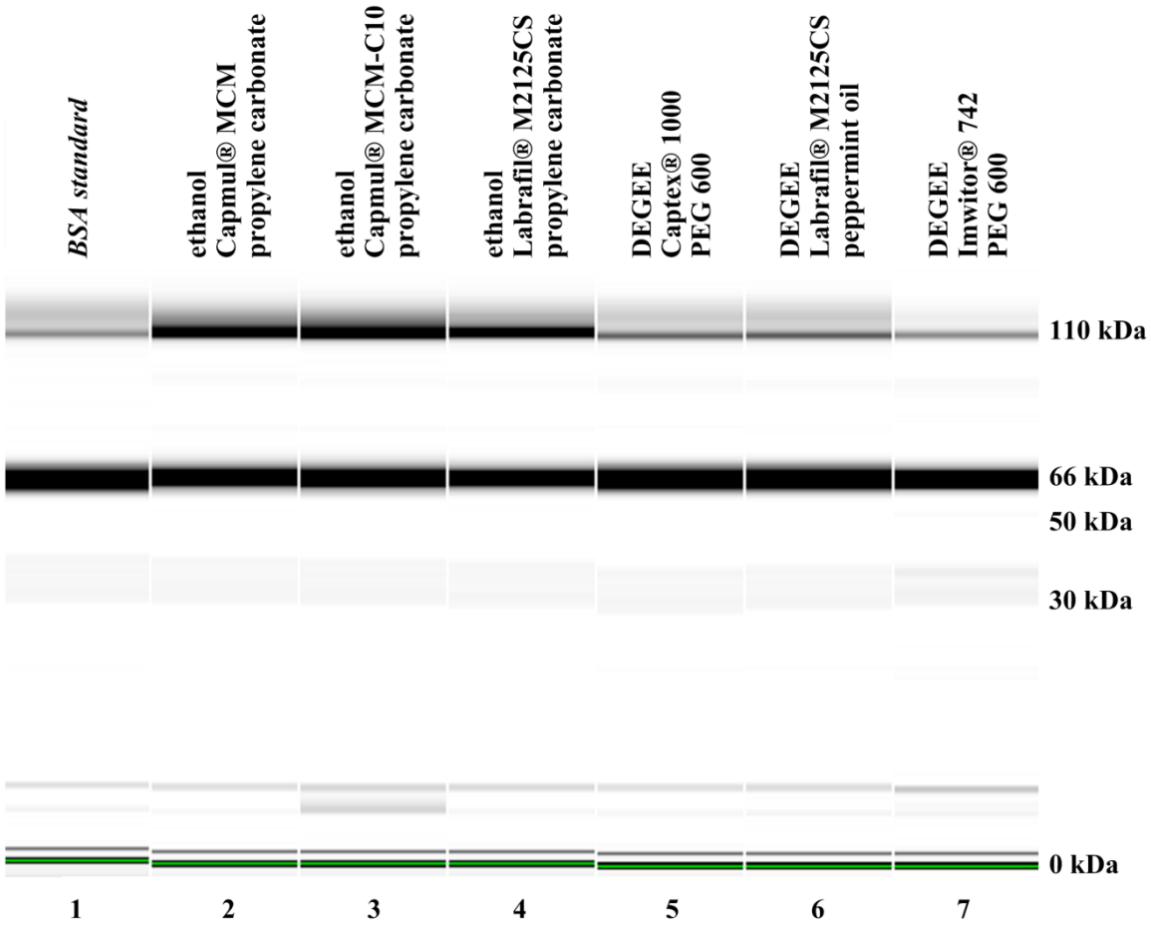

FIGURE 4.6 – Data evaluation of microfluidic capillary electrophoresis profiles. BSA standard band is at 66 kDa, as shown in lane 1. Lanes 2, 3, and 4 had the highest fraction of BSA dimer impurity (~110 kDa). Lanes 4, 5, and 6 had the lowest fraction. From left to right, the impurity content was 1.8, 19.0, 17.2, 15.6, 3.1, 3.0, and 2.2%. All hardening baths' components were in a ratio of 1:1:1.

4.1.5. Discussion

Formulating proteins without harmful manufacturing processes is an important task of modern pharmaceutical technology. An interesting recent finding was manufacturing protein-loaded microgels into lipid-based formulations by means of prilling [28]. This delivery system is appealing given that the components bear the potential to increase oral protein bioavailability. Since the formulation requirements depend on the therapeutic target, the current formulation approach may only aim for luminal protection or mucus penetration, or even additional uptake of the active macromolecule by the enterocytes. We evaluated systematically the influence of the hardening baths' composition on the prilling process. Subsequently, the suitability of these systems was determined for capsule filling. A last step employed the centre point formulations of the different ternary phase diagrams as receiving baths to study prilling. The model protein BSA was microencapsulated by prilling using a vibrating nozzle equipment. The responses of particle morphology, encapsulation efficiency, BSA loading, and protein stability were analysed. Partial least square analysis was used to gain a correlative understanding from the large dataset.

4.1.5.1 Ternary phase diagrams and capsule compatibility

Commonly, the prilling technique is used to encapsulate APIs or living cells into polymeric microgels hardened in aqueous hardening baths. To represent a suitable alternative, compatible with pharmaceutical capsule shells, non-aqueous hardening baths must possess adequate characteristics. Miscibility of the different non-aqueous excipients is a first requirement for the microgel dispersion. Thus, a phase separation would certainly not lead to a viable pharmaceutical formulation. The chemical similarity among the glycerides explained the miscibility of several combinations. However, mixtures of triglycerides and PEG 600 or propylene carbonate could not be mixed, except with high fractions of co-solvent added, namely above 70%. Mono- and diglycerides were particularly suited to achieve a good miscibility because of their higher polarity compared to triglycerides. The hardening bath polarity was important to dissolve salts that are necessary in ionotropic gelling. Yet, especially at low co-solvent fractions, the addition of calcium chloride led to phase separation (*e.g.* in formulations containing glyceryl tricaprate, PEG 600, and ethanol) and solidification (*e.g.* in formulations containing glyceryl tricaprylocaprate, propylene carbonate, and DEGEE). Dissolved salt was expected to interact with the polar moieties of the excipients, and such microstructural change was obviously critical for phase separation with some systems. While the co-solvent fraction increase seemed beneficial for miscibility and salt solubility, it also led to a higher risk of capsule incompatibility. Moreover, the negative interaction between the co-solvent and glyceride fraction indicated that the presence of the third complementary excipient was valuable regarding system suitability for prilling. While all properties contribute to the overall success of prilling and to the quality of the hydrogel dispersion, the polymeric gelling is particularly crucial to allow an efficient encapsulation. Many of the tested mixtures exhibited adequate excipient miscibility and ion solubility, whereas the finding of suitable polymer swelling was more rarely encountered. For example, formulations containing glyceryl monolinoleate were easily miscible with both co-solvents and all complementary excipients. However, most of these formulations were unable to effectively form hydrogels after the polymeric solution was dripped in. Concerning prilling suitability, the results clearly showed that the specific combination of mixture properties was required. This combination was difficult to predict theoretically so that extensive experimentation was pursued.

To get an overview from the large dataset (n = 880), the PLS regression analysis proved to be a powerful tool. It was possible, for example, to statistically assess the overriding effect of the co-solvent component on the different mixture properties. Furthermore, this approach allowed to identify subtle effects given by the type of glyceride component. Since many different glycerides (and mixtures thereof) are available for pharmaceutical purposes, the study of different glyceride grades may aid the formulation screening for prilling. However, in this work, the glyceride choice was narrowed by the melting point. An increase in fatty acid chain length of a glyceride raises the melting point. In the case of triglycerides, the melting point of glyceryl tricaprylate, tricaprate, trilaurate, and tristearate, is 8.3°C, 31.5°C, 46.4°C, and 73.5°C, respectively [456]. Such increase in melting points occurs similarly in mono- and diglycerides series. Still, for use in hardening baths, glycerides must remain in the liquid phase at room temperature. Any elevated temperature required to maintain this single phase could harm a macromolecule loaded in the microgels [457]. Therefore, the long chain glycerides employed in this work contained linoleic acid as fatty acid, whose triglyceride has a melting point of -12.7°C [458]. Such unsaturated fatty acids are certainly chemically less stable than saturated fatty acids. Although no evidence of oxidation was found in the present work, the addition of antioxidants in lipid-filled capsules would have to be considered for a later stage of formulation development [459]. Our study focused on short-term capsule compatibility over four weeks. Harmful effects of the formulation on the shell material were expected especially at high co-solvent levels based on earlier reports in the literature [81,111,460]. The obtained compatibility data showed that formulations with a high hardening bath score were also promising regarding shell compatibility using different capsule types. The differences among the capsule

types, however, should not be over interpreted. Soft capsules may exhibit improved capsule compatibility when hydrophilic excipients are pre-added to the shell composition [88]. Such a modification of the shell composition would be a typical part of the drug-specific formulation development. Still, this was certainly beyond the scope of the present compatibility study, which is intended as a first assessment only.

4.1.5.2 Microgel characteristics

The presence of ethanol had been already described in the literature as relevant to reduce particle size [28]. However, an even stronger effect of PEG 600 on this reduction was an interesting finding in the present study. This excipient influence was opposite regarding the elongation factor. For example, PEG 600 appeared to increase the ellipticity of the microgels, whereas ethanol promoted sphericity. A mechanistic explanation of such empirical findings regarding particle morphology is challenging. It is likely that several material characteristics as well as process variables heavily influence the overall particle shape. While the relevant process factors and polymer solution characteristics have been studied to some extent, little effort has been directed to understand which of the hardening bath's properties could influence the prilled particle morphology [27,453,461]. To the best of our knowledge, only the work by Buthe *et al.* addressed the use of non-aqueous hardening baths [247]. The most critical aspect when using non-aqueous hardening baths is the gelling process. The polymeric gel surface properties are affected by those of the surrounding medium [462]. To retain suitable swelling without excessive shrinking of the polymeric chains, the physicochemical affinity between the medium and the polymer has to be high [463]. When the affinity remains low, the surface chains undergo local coiling [55]. Such conformational polymer change may occur in a microgel zone close to the surface. Moreover, hydrophilic components of the hardening bath can partition into the microgels thereby affecting polymer swelling. These effects can reduce the overall size of the microgel, as well as alter its shape.

The physicochemical interaction between the hardening bath and the polymer appeared to influence also the encapsulation efficiency. Different types of solvents and co-solvents are known to affect the gel structure and stability [411,464]. In the present work, the EE varied widely depending on the given excipients. In our previous study [28], a mechanism explaining such high EE was proposed. Briefly, the formed MCC gel is generally in a "swollen" state, where the polymer is well expanding and network points include the interactions of calcium ions with MCC's carboxylic groups. On the surface (or in an interfacial zone), there is a different environment because of the dissimilar polarity of the surrounding media. Thus, some polymer coiling on the microgel surface may contribute to maintaining the BSA within the gel boundaries. The "swollen" nature of the microgel network has previously shown a rather fast protein release during dissolution testing that entails the need for additional enteric coating after capsule filling [28]. In the present work, the EE for most formulations was above 70%. However, a significant EE reduction occurred in presence of peppermint oil. From the dynamic imaging results (Figure 4.4a, 4.4d, 4.4g, and 4.4i), we noticed that the surface of microgels formed in peppermint oil was comparatively rough. A rougher surface is the likely result of a different arrangement of the polymeric chains close to the surface. Moreover, a direct consequence of roughness is an increase in contact surface between microgel and surrounding medium. Altered surface characteristics may explain an initial higher leakage of BSA from the MCC polymer network, and consequently a lower EE.

4.1.5.3 Protein stability

The formulation of proteins using potential denaturants appeared to be a challenging endeavour. Ethanol is a well-known protein denaturant, which alters the α-helices and other tertiary structures [405,413,415]. Furthermore, propylene carbonate is known in literature to denature proteins [416], although the mechanism has not been investigated. The data gathered in terms of structural modification and protein aggregation showed that propylene carbonate affected BSA, especially when combined with ethanol. These excipients caused both a loss in the α-helix fraction, as well as an increase in the amount of dimers formed. Interestingly, the lowest α-helix fraction was found in the formulation composed of ethanol, propylene carbonate, and glyceryl monolinoleate. The latter excipient contains polyunsaturated fatty acid chains, which are prone to peroxidation [465]. This reaction is known to damage proteins [466], especially on its thiol-containing groups and lysine amino acids [418,419,467]. BSA possesses a free surface cysteine group (Cys-34), which may form disulphide-mediated BSA dimers [406]. Lysine has a very high α-helix propensity [420], and any modification may lead to an altered secondary protein structure. As for DEGEE, recent non-clinical trials showed its lack of toxicity in food, cosmetic, and pharmaceutical applications [468]. Moreover, there has not been a report on protein denaturation using DEGEE, as far as we know. Our data confirmed the absence of denaturing activity in the microgels containing DEGEE. Similarly, PEG 600 did not alter the protein structure. PEGs have been used to precipitate proteins, but they are known not to cause a protein denaturation due to steric exclusion from the protein structure [469]. Another notable finding of the present study is that PEGylated lipids positively influenced the overall BSA stability even in presence of potential

denaturing agents such as ethanol and propylene carbonate.

Many therapeutically active proteins are formulated with lipids, for example as solid lipid nanoparticles, emulsions, or liposomes [470,471]. To the best of our knowledge, no denaturation effect has been related to the fatty chain length. However, in our work, it appeared that longer chain glycerides hindered the BSA α-helix structure. In this case, the denaturing effect may be associated with the polyunsaturated fatty chains of the chosen glycerides. As mentioned previously, glycerides with saturated long chain fatty acids are solid at room temperature, and the heat required to compound them with the other components of the hardening bath would have probably harmed the BSA. This indicates that even gentle heating during compounding of long fatty chain glycerides may harm the protein. Thus, the importance of having a manufacturing process that avoids heating as much as possible is further stressed. Finally, the free hydroxyl groups appeared to have a slight influence on lowering the protein stability. A possible explanation is here the presence of impurities in the mono- and diglyceride mixtures, namely glycerol, which is known to cause protein precipitation [472].

4.1.6 Conclusions

Formulating proteins as microgels in a lipid system by prilling is a novel approach to avoid potentially harmful processing during manufacturing. The current study provided an extensive data set to evaluate the influence of several excipients on the quality of the final dispersions using bovine serum albumin as model protein.

A partial least square regression analysis proved to be a viable tool to find overriding effects and to guide formulation development. The tested formulations included two different non-aqueous and non-toxic additives (ethanol and DEGEE) that were proposed as potentially suitable co-solvents. Both were found to improve the outcome of the prilling process, although some protein stability and capsule compatibility issues may still occur with ethanol especially at rather high concentrations. Three complementary excipients with different chemical and physical properties were added to the formulation. Polarity played a dominating role in terms of formulation stability. A major focus was put on the glyceride selection. These compounds' chemical properties were studied, namely glyceride chain length, free hydroxyl groups, and PEGylation. The statistical analysis showed significant effects of all glyceride components on different aspects of prilling. Notably, PEGylation appeared to positively influence the formulation suitability for prilling, the EE, and the protein stability, although it led to larger microparticles with less spherical morphology. The choice of the optimal hardening bath must consider the critical formulation and drug characteristics. Different suspension media compositions may be considered as optimal depending on whether protein structure is especially instable (DEGEE, PEGylated medium chain glyceride, and PEG 600) or particle morphology is paramount (ethanol, unmodified long chain glyceride, and propylene carbonate). This work should guide formulations scientists in finding suitable compositions when using non-aqueous hardening baths for subsequent capsule filling.

The present study provided a first systematic approach to study microgels formed through prilling into lipid-based hardening baths. Much knowledge has been generated on a correlative level together with some mechanistic hypotheses. Future research should on the one hand follow-up on such mechanistic aspects, as well as to further study this type of delivery system using more biopharmaceutical tests. Moreover, the protein integrity should be further investigated in the microgel lipid-based suspensions by ICH stability testing. Some preliminary stability and dissolution data exist for selected formulations of the model protein BSA, and results are promising. Future biopharmaceutical studies should include an *in vitro* as well as an *in vivo* assessment to better clarify the pharmaceutical potential of this oral delivery approach. Such potential is depending on the therapeutic target, and aims may range from luminal drug protection to the quite ambitious goal of macromolecule absorption.

4.2 Novel Quality-by-Design tools for concentrated drug suspensions: surface energy profiling and the fractal concept of flocculation [**]

4.2.1 Summary

Quality-by-design is an important concept, but only limited research has been invested in concentrated pharmaceutical suspensions. A need exists for novel analytical tools to thoroughly characterise the drug as well as its aggregated particle structure in suspension. This work focuses on a lipid-based pharmaceutical suspension for filling of capsules. A rheological approach, namely the fractal concept of flocculation, is introduced to the pharmaceutical

[**] de Kruif JK *et al*. Novel Quality by Design Tools for Concentrated Drug Suspensions: Surface Energy Profiling and the Fractal Concept of Flocculation. *Journal of Pharmaceutical Sciences*, **2013**, 102, 993-1007.

field. The model drug mebeverine hydrochloride was first physicochemically analysed. A special aim was to study the surface energy profiles using inverse gas chromatography as a critical characteristic for the suspension's rheological behaviour. Lipid-based suspensions were manufactured in laboratory process equipment while applying different homogenisation speeds. Flow curves of the final suspensions were measured using a cone-and-plate rheometer. As a result, surface energy profiles revealed differences from one mebeverine lot to another. Different homogenisation intensities greatly affected the viscosity and the Mooney model was able to predict experimental values as a function of the drug volume fraction. The fractal concept of flocculation characterised mebeverine in suspension and a slight increase of fractal dimension was noted when homogenisation speed was increased. It was concluded that the introduced concepts have large potential for designing quality into concentrated pharmaceutical suspensions.

4.2.2 Introduction

Rather concentrated drug suspensions are widely used in pharmaceutics. They can be found as final dosage forms as well as intermediate bulk products; a special interest is their filling into capsules for oral drug delivery [105]. These formulations are generally lipid-based to assure adequate capsule compatibility. The dispersed drug is often rather concentrated to provide required dose strength. However, the suspension would have to exhibit adequate rheological properties for the filling of hard or soft capsules. Especially for the two-piece hard capsules the filling process critically depends on the rheology of the fill mass. Kattige *et al.* [473] showed that highly viscous suspensions can form a string at the dosing nozzle. A bridging from one capsule to another can occur depending on the process speed. A direct consequence is increased variability of the capsule weight, which is a critical quality attribute of the dosage form. An increased or variable viscosity can therefore be a severe manufacturing issue in liquid-filling of capsules. Such effects on critical quality attributes are important to understand when attempting to implement Quality by Design (QbD) in pharmaceutical suspensions [32].

The rheological influence of a suspension on the final capsule attributes is one important aspect, while another is to learn about how rheological properties are determined by the raw materials. Due to the complexity of particle interactions and structure, the science of concentrated suspensions is not fully understood and is still subject to basic research [50,474,475]. However, some important aspects can already be inferred from the early models of the mid-20th century [60,62]. The viscosity has been assumed to increase non-linearly with the volume fraction of the solid (Φ), *i.e.* the drug. Herein there is not a constant exponent in a power or exponential law assumed, but the exponent is characteristic for the given drug. In the case of the Mooney law [62], it is the crowding factor (k) that dictates the curve shape. Equation 4.3 displays the relative viscosity η_r (viscosity divided by the viscosity of the drug-free formulation) according to the Mooney law:

$$\eta_r = exp\left(\frac{2.5 \cdot \Phi}{1 - k \cdot \Phi}\right) \qquad 4.3$$

The equation was developed partially in a heuristic way, and the factor 2.5 was in accordance to Einstein's first rheology studies of dilute dispersions [58]. The crowding factor was previously interpreted as reciprocal of a maximal packing fraction Φ_{max} so that Equation 4.4, modified from 2.9, can be obtained [61,476]:

$$\eta = \eta_0 exp\left(\frac{2.5 \cdot \Phi}{1 - \frac{\Phi}{\Phi_{max}}}\right) \qquad 4.4$$

Where η holds for the suspension's apparent (measured) viscosity and η_0 represents the viscosity of the drug-free vehicle. The non-linearity of the equation as well as the non-universal character of the exponent can be problematic from a practical consideration. Given that the model describes adequately a pharmaceutical suspension, it is possible that even a small effect of the solid fraction may greatly affect the viscosity. Rheology of a concentrated pharmaceutical suspension may be influenced significantly by rather subtle batch-to-batch differences of an active pharmaceutical ingredient (API) (*e.g.*, due to impurities, enantiomeric excess, or particle characteristics). Thus, some questions arise from a QbD viewpoint. Are there sufficient experimental tools available to detect such subtle variances among different batches of a drug? What is the effect of a given process factor or small formulation change on viscosity? Is it possible to assess the evolving particle structure in a concentrated suspension?

Concerning tools to analyse an API for suspensions, a review by Rawle *et al.* emphasised that powder characterisation proved to be critical [477]. The authors highlighted several methods to measure particle size distribution, including dynamic image analysis, which provides the means to additionally determine the shape of particles. However, the influence of surface energies was not taken in consideration. Especially the profiling of surface energies would be of interest. The standard technique to assess the surface energy is the contact angle measurement; its use, however, is problematic for samples in powder form [478]. For this surface energy analysis (SEA), a novel technique based on inverse gas

chromatography (iGC) has become recently available. Such iGC technique has been used to profile surface energy of powders in solid dosage forms [479–485]. However, energy profiling based on iGC has, to the best of our knowledge, never been applied to study drugs that were intended for pharmaceutical suspensions. A first aim of this study is to profile the surface energies of mebeverine hydrochloride using the iGC, and to correlate them with the rheological parameters of different batches in lipid-based suspensions.

Another aim of this study addresses the question, whether or not it is possible to study the aggregation structure of a drug in suspension. The fractal concept of flocculation is therefore to be introduced to pharmaceutical suspension analysis [50]. This approach describes the structure of particle aggregation in terms of a fractal dimension [486]. As model drug we selected mebeverine hydrochloride, which is commonly used in the treatment of lower-bowel inflammations and diseases [487].

4.2.3 Materials and methods

4.2.3.1 Materials

Mebeverine hydrochloride ((RS)-4-(ethyl[1-(4-methoxyphenyl)propan-2-yl]amino)butyl-3,4-dimethoxybenzoate hydrochloride) was supplied by Tillotts Pharma AG (Rheinfelden, Switzerland) from two different batches (A and B). Lipoid PPL-600 was from Lipoid GmbH (Ludwigshafen, Germany). Refined peanut oil and fumed silica was purchased from Hänseler AG (Herisau, Switzerland). Isopropyl alcohol, n-hexane, and methanol (all branded J.T. Baker®) were purchased from Avantor performance materials BV (Deventer, Netherlands). Triethylamine, sodium chloride, and silver nitrate 0.1 M solution were supplied by Fluka GmbH (Buchs, Germany). For the surface energy measurements, high purity helium and methane were both supplied by BOC gases Ltd (Guildford, UK), whereas n-heptane, n-octane, n-nonane, n-decane, ethanol, ethyl acetate, dichloromethane, acetone, and acetonitrile (all HPLC/GC grade solvents) were purchased from Sigma-Aldrich Ltd (Gillingham, UK). All raw materials were used as received.

4.2.3.2 Methods

4.2.3.2.1 Active pharmaceutical ingredient (API) characterisation

Radwan *et al.* suggested a method to determine the racemic ratio of mebeverine hydrochloride by means of enantio-selective high performance liquid chromatography (HPLC) [488]. We applied this method on an Agilent 1200 Series HPLC (Agilent Technologies AG, Switzerland) using the same column, conditions, and detector as described in the original article. Briefly, a mixture of n-hexane, isopropyl alcohol, and triethylamine (90.0:9.9:0.1, v/v/v) was used as a mobile phase. The calibration curve was prepared by dissolving the API powder directly in methanol at a concentration of 1 mg mL^{-1} and consequently diluting it to a concentration range from 0.5 to 20 µg mL^{-1} with mobile phase. The samples were prepared in the same way, but the final concentration was 10 µg mL^{-1}.

To assay impurities, we chemically studied the batches in addition to the initial release analysis that was documented by the certificate of analysis. We modified the aforementioned HPLC assay by increasing ten-fold the quantity of sample tested; the samples for calibration were treated in the same way. This procedure was intended to increase the signal-to-noise ratio with respect to impurity detection. The release analysis employed thin layer chromatography to analyse impurities according to the local Pharmacopoeia [489], and both batches were within the specification limits.

Following the enantio-selective analysis, the ratio between free base of mebeverine and chloride salt was studied. A potentiometric titration was conducted using an 809 Titrando system (Metrohm AG, Switzerland), which was connected to an 801 Stirrer and 800 Dosino dosing pump. Before analysing the sample, we plotted a calibration curve (R^2 = 100.0%) by titrating a range from 25 to 75 mg of sodium chloride. The titration was carried out by diluting 250 mg of mebeverine hydrochloride in 200 mL of water, and measuring the volume of silver nitrate 0.1 M solution used. The quantified chloride content was then converted to the corresponding salt concentration of mebeverine.

Mebeverine hydrochloride batches were studied using differential scanning calorimetry (DSC) on a DSC 30 (Mettler Toledo AG, Switzerland). Samples of 5 mg were weighed for each measurement using the XS105DualRange balance (Mettler Toledo AG, Switzerland) and the samples were subsequently sealed in individual 40 µl aluminium pan. A heating rate of 10°C min^{-1} was selected in a range from 10°C to 360°C using inert argon environment (100 mL min^{-1}). We then determined the melting temperature (T_m) and the heat of fusion (ΔH_f) of mebeverine hydrochloride from the peak maximum and the area under the peak, respectively.

The X-ray powder diffraction analysis was carried out on a D2 Phaser diffractometer (Bruker AXS Inc., Germany) equipped with a LYNXEYE™ detector and DIFFRAC^{plus} EVA software. The sample was put on a holder, which was set to rotate at 15 rpm. The radiation source was Co Kα at 30 kV and 10 mA, and the measurement range was 2 theta from 5° to 80°.

We investigated the true density (ρ_t) of the mebeverine hydrochloride batches with a helium Multipycnometer

MVP-1 (Quantachrome Instruments Inc., USA) on an average of 20.0 g of sample, which was weighed on a PB3002DeltaRange balance (Mettler Toledo, Switzerland).

The particle size and shape were measured by dynamic image analysis using an XPT-C particle analyser (Prozesstechnik GmbH, Switzerland). Each sample was dispersed in refined peanut oil to a suitable dilution, and sonicated for 10 minutes in a UR1 ultrasound bath (Retsch GmbH, Germany). A constant magnetic stirring was employed during the image analysis.

The image analysis was based on ~10 000 particles, and for a size measure we calculated the Waddle disk diameter, which is the diameter of a disk having the same area as the projected image of the given particle. This diameter was analysed as median as well as 5th and 95th percentile of the size distribution. To describe the particle shape, we selected the elongation factor. This form factor is defined as the ratio between the maximal intercept (length of the longest segment in the convex hull of the particle) and mean intercept perpendicular (the mean length of the chords in the particle perpendicular to its maximal intercept).

The particle morphology of the powder was evaluated by scanning electron microscopy (SEM) with an M-SEM Supra (Carl Zeiss AG, Switzerland). The electron high tension was set to 5 kV. The samples were prepared by depositing the mebeverine hydrochloride powder on an adhesive carbon plate and removing the excess material with compressed air.

4.2.3.2.2 Surface energy profiling

Gemini V BET analyser (Micromeritics Instrument Inc., USA) was used to determine the BET (Brunauer Emett Teller) specific surface area of each sample. Sample tubes were initially dried for 3 hours at 105°C along with the mebeverine hydrochloride. Then, 1 g of the sample was weighed and heated in the tube to 105°C under nitrogen overnight. The instrument ran the analysis at -196°C.

Surface energy profiles were obtained directly from inverse gas chromatography Surface Energy Analyser (iGC-SEA, Surface Measurement Systems Ltd, Alperton, Middlesex, UK). Approximately 300 mg were packed into individual iGC silanised columns (300 mm length, 3 mm internal diameter) plugged at both ends by silanised glass wool. The specific surface area of the sample was first determined by measuring the octane adsorption isotherms at 30°C and 0% relative humidity using the iGC-SEA. As for the surface energy measurement, each sample column was conditioned in-situ for 2 hours at 30°C and 0% relative humidity in a 10 cm^3 min^{-1} flow of helium carrier gas. The column dead volume corrections were determined by using methane as an inert probe at an injection time of 5 seconds and an injection volume of 30 cm^3.

This instrument determined the total surface energy (γ_s^T) of the sample, which is the sum of its polar (the specific surface energy, γ_s^{AB}) and apolar (dispersive surface energy, γ_s^D) components. The specific interactions mostly take place between polar groups and can be Lewis acid-base interactions, whereas the apolar component of surface energy is mainly based on Lifshitz-van der Waals interactions. Another thermodynamic parameter, the work of cohesion (W_{coh}), was also considered in this work. This normalised work equals to twice the value of the total surface energy $2\gamma_s^T$; it represents the tendency of particles to adhere to each other.

The iGC measurement principle is based on packing a column with the sample and allowing different probe vapours to flow through it; thus, the retention time of the probe can be measured and then the net retention volume (V_N) is calculated (Equation 4.5) [490].

$$V_N = \frac{j}{M} \cdot F(t_R - t_0) \cdot \frac{T_s}{T_{Ref}} \qquad 4.5$$

Where j is the James-Martin correction; M is the sample mass; F is the flow rate; t_R is the probe retention time; t_0 is the retention time of a non-interacting probe, in our case methane; T_s is the column temperature; T_{Ref} is the reference temperature for the flow rate determination.

The obtained retention volume V_N in Equation 4.5 allows determining the aforementioned surface energies. Hence, the γ_s^D and γ_s^{AB} can be determined; for the former, a set of alkane eluents with different carbon number (n-heptane, n-octane, n-nonane, and n-decane) were used, whereas for the latter probes with different polarities were employed (acetone, acetonitrile, ethanol, ethyl acetate, dichloromethane). Using the first set of experimental alkane eluents, the γ_s^D was determined according to the Dorris-Gray method by plotting $R\,T\,ln(V_N)$ against the carbon number of the alkanes [491], and then by using Equation 4.6.

$$R \cdot T \cdot \ln V_N = 2N_A \cdot \sqrt{\gamma_{CH_2} \cdot \gamma_s^D} \cdot a_{CH_2} \qquad 4.6$$

Where N_A is Avogadro's number; γ_{CH_2} is the methylene surface energy; a_{CH_2} is the molecular area of a methylene group; R is the universal gas constant (8.314 J mol^{-1} K^{-1}); T the temperature in Kelvin.

In a second step, γ_s^{AB} was obtained by the polarisation method of Donnet *et al.* where $R\,T\,ln(V_N)$ is plotted against the molar deformation polarisation of the probes [492]. The difference between the measured $R\,T\,ln(V_N)$ and the ones

obtained with the alkane series is the free energy of desorption ΔG_{SP}. By applying the van Oss concept of acid-base surface chemistry [493], ΔG_{SP} can be related to the acid and base components of γ_s^{AB} (Equations 4.7 and 4.8).

$$\Delta G_{SP} = N_A \cdot a_P \cdot \left(\sqrt{\gamma_P^+ \cdot \gamma_s^-} + \sqrt{\gamma_P^- \cdot \gamma_s^+} \right) \qquad 4.7$$

$$\gamma_s^{AB} = 2 \cdot \sqrt{\gamma_s^+ \cdot \gamma_s^-} \qquad 4.8$$

Where a_P is the cross sectional area of the probe; γ_s^+ and γ_s^- are the acid and base components of sample's surface, respectively; γ_P^+ and γ_P^- are the acid and base component of the probe, respectively (*e.g.*, dichloromethane and ethyl acetate).

Part of the energy profiling was the study of surface heterogeneity by injecting different amounts of probe vapour, thereby creating different surface coverages as expressed by the ratio n_i/n_m. Herein, n_i is the moles of probe injected, where n_m refers to the monolayer capacity of the probe molecule. This monolayer capacity of the probe molecule is determined by the sample's specific surface area and by the area occupied by each probe molecule.

4.2.3.2.3 Suspension manufacture

Suspensions were manufactured on a small-scale of 1000 g using laboratory process equipment MI-MOLTO (Krieger, Switzerland). The instrument uses two couples of counter-rotating stirring blades to mix the loaded ingredients; the blades are also equipped with a set of vertical and horizontal baffles in order to prevent material from sticking to the sides of the manufacturing vessel. The central rotor/stator element homogenises the particles of the suspension by disrupting particle agglomerates and reducing the particle size. Temperature was controlled with a double jacketed vessel connected to a Julabo HC5/8 water bath (Julabo Labortechnik GmbH, Germany). and vacuum was obtained with a Vacfox VGD 15 rotary vacuum pump (Rietschle Thomas GmbH + Co. KG, Germany). Before mixing the ingredients, mebeverine hydrochloride was sieved (1 mm opening). All needed quantities were weighed on a PB5001-L balance (Mettler Toledo AG, Switzerland). Ingredients were added directly in the following order: Aerosil 200 1.82% (w/w), Lipoid PPL-600 13.64% (w/w), and then refined peanut oil 84.55% (w/w). Aerosil 200 was chosen to provide an adequate stability to the manufactured suspension; Lipoid PPL-600, a liquid formulation of soybean phospholipids enriched in phosphatidylcholine (40%), was added to increase the wettability of the particles; refined peanut oil served as the lipid continuous phase. The drug-free formulation (placebo) was then placed in the homogenising vessel under vacuum at 40°C for 5 min, 30 rpm stirrer speed, and manufactured at the selected homogenisation speeds (0, 3000, 6000, and 9000 rpm). Different drug concentrations were then incorporated in the placebo: 0, 15, 30, 35, 39, 43, 45, 47, and 51% (w/w) (Table 4.6).

For each concentration, level n = 3 individual batches were manufactured and the effect of homogenisation intensity was studied by employing a cascade of increasing homogenisation steps. Thus, mebeverine hydrochloride was first incorporated at 40°C in the placebo and premixed at 30 rpm; then, the dispersion was mixed thoroughly maintaining the same temperature at 100 rpm for 30 minutes under vacuum. The suspension was further mixed for 20 minutes without homogenisation at 20 rpm mixing for degassing and a first sample of 50 mL sample was drawn. The remaining suspension was subsequently mixed at 100 rpm for 10 minutes and homogenised at 3000 rpm for 2 minutes. We degassed again as previously described and drew another sample. The remaining suspension followed the same procedure of mixing, homogenising, degassing, and sampling twice: the first time at 6000 rpm and the second at 9000 rpm. All manufactured suspension samples were further stored for 3 hours in a Salvis KVTS 11 vacuum chamber (SalvisLab AG, Switzerland) at 45°C.

TABLE 4.6 – Ingredients' list of the lipid-based suspension at different drug fractions. Values are expressed as w/w %. Please note that the relative ratio between the excipients (*i.e.*, refined peanut oil, Lipoid PPl-600, and Aerosil) remains constant.

Mebeverine hydrochloride	**Refined peanut oil**	**Lipoid PPL-600**	**Aerosil 200**
0	84.55	13.64	1.82
15	71.86	11.59	1.55
30	59.18	9.55	1.27
35	54.95	8.86	1.18
39	51.57	8.32	1.11
43	48.19	7.77	1.04
45	46.50	7.50	1.00
47	44.81	7.23	0.96
51	41.43	6.68	0.89

4.2.3.2.4 Suspension analysis

The rheology of the suspensions was studied using a Bohlin Gemini rheometer (Malvern Instruments Ltd, UK). The system was equipped with a Bohlin Peltier drive and a PNEUDRI MiDAS DAS-2 air bearing (Parker Domnick Hunter Ltd, UK). A cone-plate sensor was employed. The cone was truncated with a diameter of 40 mm diameter and 4° inclination. The apparent viscosity (η) of the formulations was obtained at 25°C by recording a flow curve from 0 to 100 s^{-1} and using the value obtained at a reference shear rate (γ) of 30 s^{-1}. This upper value was for all suspensions clearly below a critical shear rate for which a loss of homogenous force transmission limits the flow curve.

We selected the Casson model [494] to describe shear stress (σ) as a function of applied shear and the yield stress (σ_0) was extrapolated from the up-curve in a range of 0 to 30 s^{-1} (Equation 4.9):

$$\sqrt{\sigma} = \sqrt{\sigma_0} + \sqrt{\eta \cdot \gamma} \qquad 4.9$$

The viscosity of the drug-free formulation provided the vehicle for the different suspensions and provided the value η_0. The ratio between η and η_0 is called relative viscosity (η_r). The placebo density (ρ_0) was measured using a DA-100M densitometer (Mettler Toledo AG, Switzerland) at 25°C.

To convert the mass fraction of API (w_{API}) to the volume fraction (Φ) Equation 4.10 was used.

$$\Phi = \frac{w_{API}/\rho_t}{w_{API}/\rho_t + (1 - w_{API})/\rho_0} \qquad 4.10$$

To measure the fractal dimension (D_f) of the particle structure in suspension, we employed the fractal concept of flocculation [50]. Thus, yield stress was plotted as logarithm against the logarithmic volume fraction of the drug. A linear range using the four highest concentrations (43%, 45%, 47%, 51% w/w) was selected for regression analysis and determination of the slope (m). The fractal dimension D_f was then calculated from the embedding Euclidean dimension d (d = 3) using the following Equation (4.11):

$$D_f = d - \frac{2}{m} \qquad 4.11$$

4.2.3.2.5 Data analysis

For statistical analyses and model fitting of the Mooney equation (Equation 4.4), the software STATGRAPHICS Centurion XVI version 16.1.15 from StatPoint Technologies Inc. (Warrenton, USA) was used. All other calculations were based on Microsoft Office Excel 2010 (Microsoft Inc., Redmond, USA). Statistical significance was assumed with a p-value lower than 0.05. Results were expressed as means ± standard deviations (from n = 3 experiments), except where differently specified. A Student's t-test was conducted after having assured that variances were homogenous (by an F-test) when comparing the means from two groups; when more than two groups were analysed, an analysis of the variance (ANOVA) was used.

4.2.4 Results

4.2.4.1 Initial API characterisation

Two mebeverine hydrochloride batches were used in this study, which were both of high purity and showed no difference based on their chemical certificate of analysis. However, since drug batch release analysis did not include enantiomeric purity, we studied the batches using an enantio-selective HPLC method. Table 4.7 displays the enantiomeric excess for the two batches studied. As expected for a racemic mixture, the enantiomeric excess yielded low values close to zero. There was no difference revealed between the batches based on a statistical comparison of the enantiomeric excess.

In accordance with the certificate of analysis, our assay of mebeverine hydrochloride showed that both batch A and batch B were within specification limits as for the total of unknown impurities (less than or equal to 0.5% [489]). The method detected two peaks that did not appear in the blank runs, with a retention time lower than that of mebeverine hydrochloride's enantiomers. The two unknown impurities were found at a retention time of 8.444 ± 0.089 minutes and 9.774 ± 0.085 minutes, while the relative retention time (RRT) to the first API peak at 10.743 ± 0.095 minutes were 0.785 and 0.897, respectively. The impurity amounts are shown in Table 4.7 and they are lower in batch A than in batch B. The differences were found to be significant and thus could theoretically contribute to technical batch-to-batch differences at later stages of manufacturing.

Another kind of chemical purity analysis for mebeverine hydrochloride is the molar ratio of the drug truly present as hydrochloride salt compared to the total amount of API. The results of the titration analysis demonstrated for both batches a hydrochloride salt fraction close to unity (Table 4.7). No significant difference was found between the batches in terms of the hydrochloride salt fraction and the high purity indicated that free base was barely present.

TABLE 4.7 – Enantiomeric excess, hydrochloride salt fraction, and impurity content of the mebeverine hydrochloride batches (mean values ± standard deviations; n = 3 experiments).

Property	**Batch A**	**Batch B**	**Student's t-test (*p*-value)**
Enantiomeric excess (%)	0.0495 ± 0.0342	0.0727 ± 0.0160	0.347
Hydrochloride salt fraction	0.9892 ± 0.0127	0.9990 ± 0.0009	0.311
Impurity content by relative retention time (%)			
RRT = 0.785	0.0281 ± 0.0063	0.0581 ± 0.0049	0.003
RRT = 0.897	0.0058 ± 0.0052	0.0397 ± 0.0006	< 0.001

Figure 4.7 shows the overlaid DSC profiles of the two batches. The fusion temperature was the same and also in terms of the fusion enthalpy, Student's t-test could not show a significant difference between the two batches. To complement the solid state analysis from thermal methods, we further conducted X-ray powder diffraction. Figure 4.8 demonstrates that the two diffractograms reflected the same crystallinity of the batches. The intensity, shape, and position of the peaks were practically the same so that complete overlaying of the diffractograms was possible. It appeared from the distinct peaks and absence of a pronounced halo that both batches were highly crystalline. In line with this solid state analysis, it was expected that also the true densities of the materials would also be nearly the same. The results from gas pycnometry indeed confirmed the true densities of both batches could not be distinguished statistically (Table 4.8).

A next batch comparison emphasised the size distribution and shape of the particles. For size distribution, the 5th, the 50th, and the 95th percentile (or d5, d50, and d95, respectively) were selected and determined by means of dynamic image analysis. Some skewness was noted in the size distributions. Table 4.8 exhibits the comparison of the batches, and interestingly a significant difference was found for the d5 values. The effect was rather subtle and no significance was obtained when comparing the d50 or d95 values. Image analysis could not reveal further batch-to-batch differences. For quantitative shape analysis, the mean

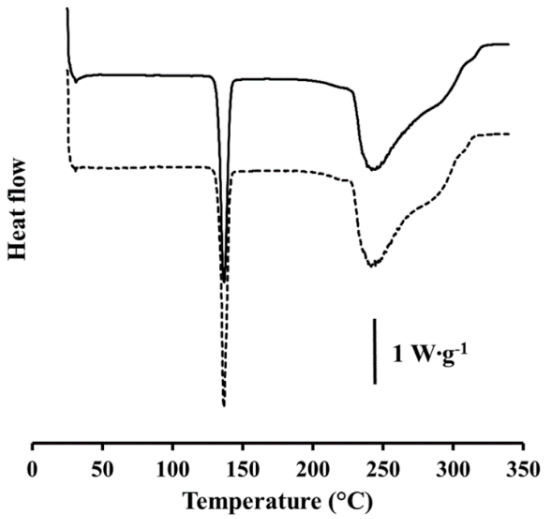

FIGURE 4.7 – Overlaid DSC profiles of batch A (dotted line) and B (continuous line).

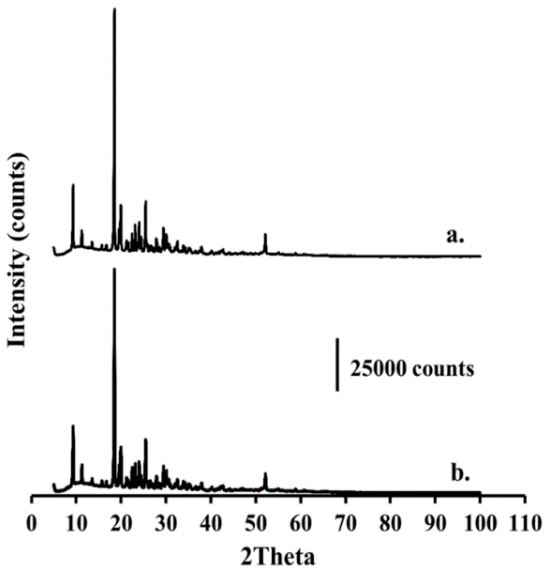

FIGURE 4.8 – Overlaid X-ray diffractogram profiles of batch A (a) and B (b).

TABLE 4.8 – Comparison of physical properties between the mebeverine hydrochloride batches (mean values ± standard deviations; n = 3 experiments).

Property	Batch A	Batch B	Student's t-test (*p*-value)
Fusion enthalpy (J g^{-1})	104.85 ± 0.58	104.09 ± 0.47	0.151
Fusion temperature (°C)	136.56 ± 0.56	136.85 ± 0.38	0.499
True density (g cm^{-3})	1.213 ± 0.005	1.212 ± 0.004	0.886
Particle size distribution as Waddle disk diameter			
d5 (μm)	10.34 ± 0.15	9.38 ± 0.20	0.003
d50 (μm)	25.72 ± 0.85	26.19 ± 0.87	0.541
d95 (μm)	64.50 ± 7.71	62.71 ± 17.36	0.878
Particle shape			
elongation factor	2.59 ± 0.03	2.63 ± 0.06	0.337

elongation factor was determined but both batches resulted in similar values (Table 4.8). The obtained shape parameter indicated a rather elongated habitus of mebeverine hydrochloride particles. Such elongated particle shape was also observed in the scanning electron microscopy (SEM) images (Figure 4.9). Moreover, a cohesive tendency was noted for both batches since smaller particles were adhering to the larger ones.

4.2.4.2 Specific surface area measurement

The specific surface areas assessed by BET-nitrogen adsorption were 0.2385 ± 0.0229 m^2 g^{-1} for batch A and 0.7227 ± 0.0058 m^2 g^{-1} for batch B ($p < 0.001$). The difference was statistically significant and it was in line with the finding that batch B had a slightly lower d5 value of the fine particle fraction. This effect certainly contributed to higher surface area, but it may not fully explain the observed difference. There might have been an additional difference in surface roughness or in intra-particulate pores, although it was difficult to detect clear differences in the SEM images.

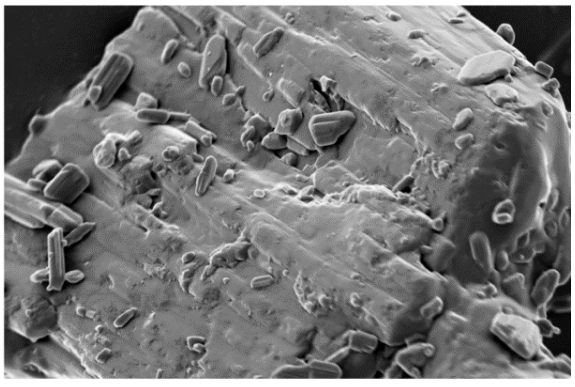

FIGURE 4.9 – Example of a scanning electron microscopy image of mebeverine hydrochloride (batch A at 4960 x magnification).

4.2.4.3 Surface energy profiling

Analysis of the dispersive surface energy γ_s^D (Figure 4.10a) revealed another subtle difference between the batches. Batch B exhibited higher γ_s^D compared to batch A at rather low surface coverage. Once the surface was more extensively covered, the two curves of γ_s^D gradually converged to similar values. There was even a tendency that γ_s^D of batch A levelled off at a slightly higher plateau. However, the energy change with increasing surface coverage was more pronounced with batch B. The extent of this decline in surface energy is a marker of energetic inhomogeneity and it shows that batch B exhibited more energy heterogeneity with respect to the various surface sites. Such a distinction of surface heterogeneity was previously observed for energies on the surface of an excipient by Ho *et al*. In the present study, γ_s^D results pointed to another physical difference of the solid state using the mebeverine hydrochloride batches [482].

Figure 4.10b shows the specific surface energy γ_s^{AB} of the two batches. This polar contribution to total surface energy γ_s^T was evidently much smaller than the dispersive surface energy γ_s^D. Given the small specific energy contribution, the difference between the batches was also minor. However, batch B demonstrated significantly higher values of γ_s^{AB} primarily at low surface coverage.

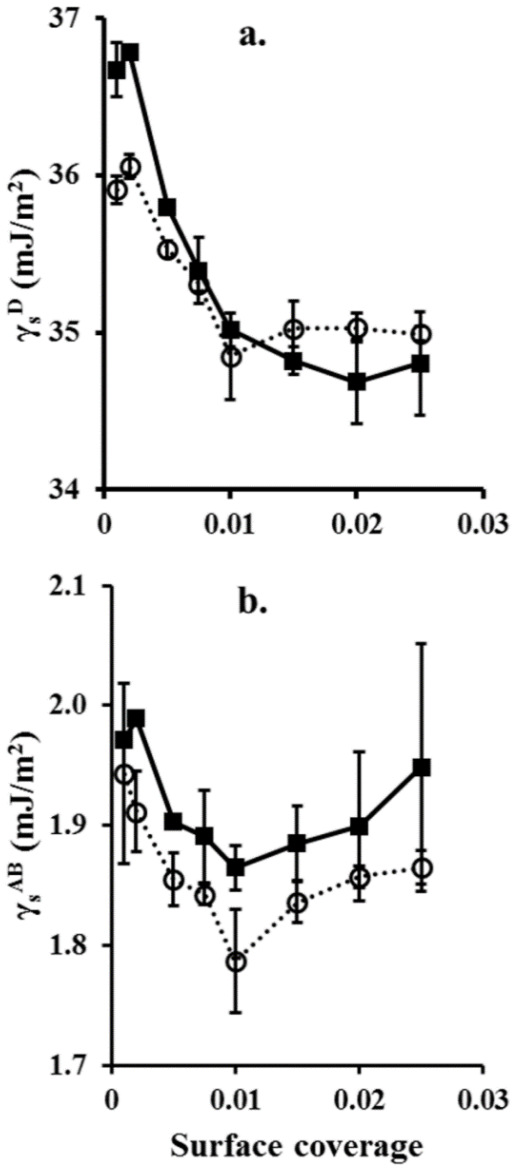

FIGURE 4.10 – The dispersive surface energy γ_s^D (a) and specific γ_s^{AB} surface energy (b) vs. surface coverage of batch A (open circles) and batch B (black squares). Error bars show standard deviations (n = 3).

In line with the previous findings, the batch B revealed a higher work of cohesion W_{coh} than batch A at a low surface coverage (Figure 4.11). The profiles were similar to those of the dispersive energy. Since W_{coh} equals to $2\gamma_s^T$, the results confirmed the view that most of the total surface energy was attributed to the dispersive contribution.

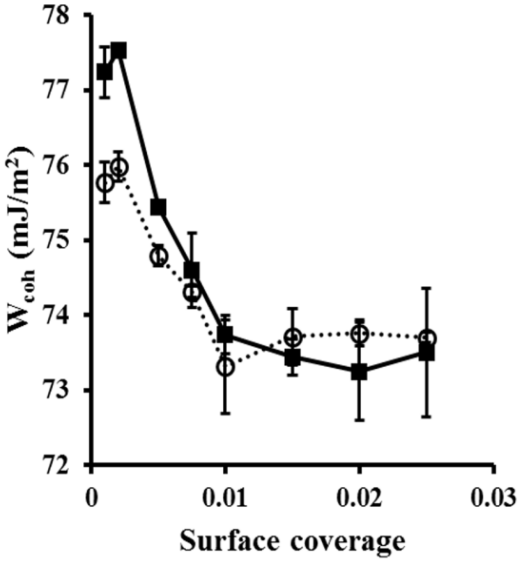

FIGURE 4.11 – The work of cohesion W_{coh} vs. surface coverage of batches A (open circles) and B (black squares). Error bars show standard deviation (n = 3).

4.2.4.4 Rheological suspension analysis

The formulation viscosity against API volume fraction (for batches A and B) was plotted in Figure 4.12. The viscosity increase at low volume fractions appeared to be nearly linear, whereas at higher solid concentrations the change in viscosity became highly nonlinear. While there was hardly a difference in viscosity observed for suspensions at low volume fractions, the concentrated systems revealed a batch-to-batch difference. Batch A showed lower viscosity compared to batch B, but this difference was statistically significant ($p < 0.001$) only at a drug concentration $w_{API} > 30\%$.

The range of concentrated suspensions further revealed different viscosities for varying homogenisation intensities. Figure 4.13 exhibits the effect of homogenisation intensity for two selected volume fractions of the suspensions. It can be inferred from Figure 4.13 that homogenisation speed barely made a difference for the viscosity of the 30% (w_{API}) suspension, whereas a significant trend was observed at w_{API} of 51%. A rising homogenisation intensity decreased viscosity in the concentrated suspensions. This range of higher drug concentrations obviously not only demonstrated a rheological difference from batch-to-batch, but provided also a clear differentiation among the process conditions.

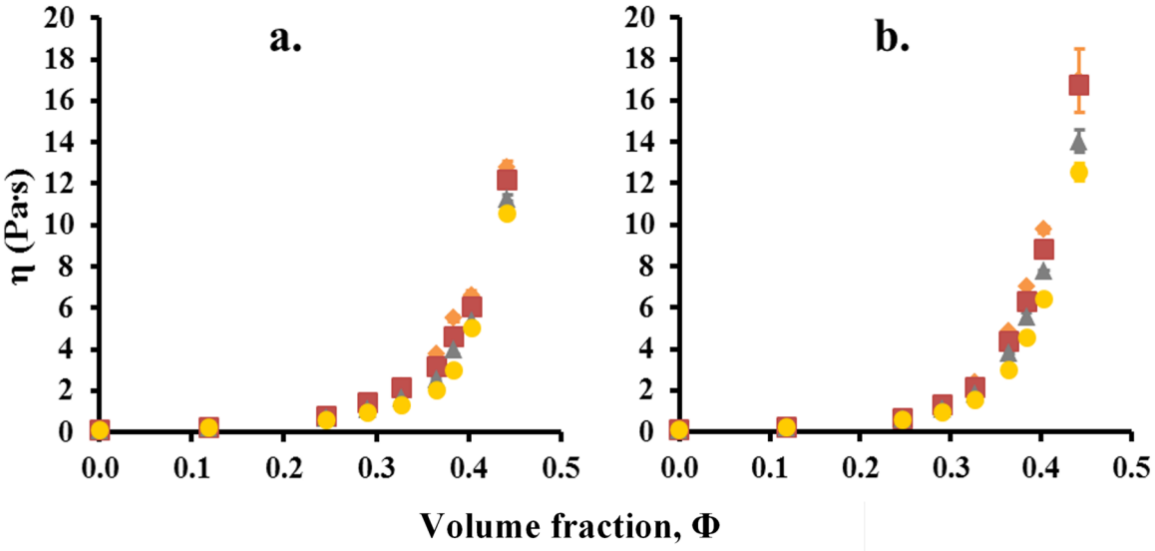

FIGURE 4.12 – Viscosity values η of batches A (a) and B (b) at different API volume fractions (Φ). The values are sorted by homogenisation intensity during manufacturing: no homogenisation (orange diamonds), 3000 rpm (red squares), 6000 rpm (grey triangles), 9000 rpm (yellow circles).

The yield values σ_0 of the suspensions were studied in a second step. Extrapolation according to Casson (Equation 4.9) provided estimates that are depicted in Figure 4.14. The double- logarithmic plot of yield value (log σ_0) against the volume fraction (log Φ) displayed two linear ranges, as it was expected from the rheological literature on concentrated dispersions [50,495]. The range of higher concentrations provided excellent linear regression models with R^2 values in a range of 97.44% to 98.66%. Slopes of the regression lines appeared to be only slightly different but the effect was still found to be significant ($p < 0.001$). The different slopes were used to calculate fractal dimensions D_f of the flocculated particles according to Equation 4.11. Figure 4.15 indicates that higher homogenisation speed increased the fractal dimension. Like in other physical applications of fractal geometry, the values differed only slightly. However, the trend was observed with both batches and the slopes for calculation of D_f generally differed from batch to batch ($p < 0.001$).

Finally, the flow curves were further studied by fitting the Mooney model in the form of Equation 4.4. The obtained parameters from the non-linear regression are listed in Table 4.9. Excellent model fits were found, with adjusted-R^2 values generally higher than 98.00%. Figure 4.16 shows that the models adequately described the increase in viscosity as a function of the drug volume fraction. Curves at different homogenisation level were equally well described by the Mooney model indicating that higher homogenisation intensity generally lowered the viscosity. Homogenisation intensity further affected both of the fitted parameters, *i.e.* the vehicle viscosity η_0 as well as the maximal packing fraction Φ_{max}.

4.2.5 Discussion

4.2.5.1 Surface energy profiling

A better understanding of critical material properties for drug product performance can be deemed a cornerstone of QbD [32]. It has been reported that drug surface energy can be critical for its solid bulk properties such as particle flow or wetting behaviour

of powders [496]. The present study focused on drug suspensions. Herein, the surface energy of a powder is expected to play a role in how the particles immerse in the formulation liquid and how a surfactant can adhere to the available surface sites. Surface energetics can theoretically make a difference in the process of dispersion as well as in the properties of the evolving drug suspension.

We employed surface energy profiling by means of iGC with pharmaceutical suspensions. A broad spectrum of surface

analytical information was provided by this method and enabled a differentiation of the model batches using mebeverine hydrochloride. The analysis at a series of surface coverages was especially useful to delineate the surface energy heterogeneity. Most of the surface energy was shown to arise from dispersive interactions. At lower surface coverages, there were higher energy sites at the drug surface interacting with the different eluent gases. Batch B possessed significantly higher dispersive surface energy and thus higher work of cohesion than batch A. This increase in work of cohesion can correspond to an increase in inter-particle friction forces and in interaction between the particles and the vehicle of the suspension. In addition, batch B showed a broader distribution of energy levels at various surface sites.

There are several potential sources which can lead to the energetic differences in the surface sites. These sources mainly comprise of the differences in physicochemical characteristics between the particle surface and the powder bulk. The presence on the surface of differences in terms of amorphous drug content, enantiomeric excess, free base concentration, and presence of impurities can vary the final product's properties [497,498]. However, the bulk techniques employed for the characterisation of the aforementioned properties, namely XRPD, DSC, enantio-selective HPLC, and volumetric titration, couldn't discriminate between the batch-to-batch differences captured by inverse gas chromatography.

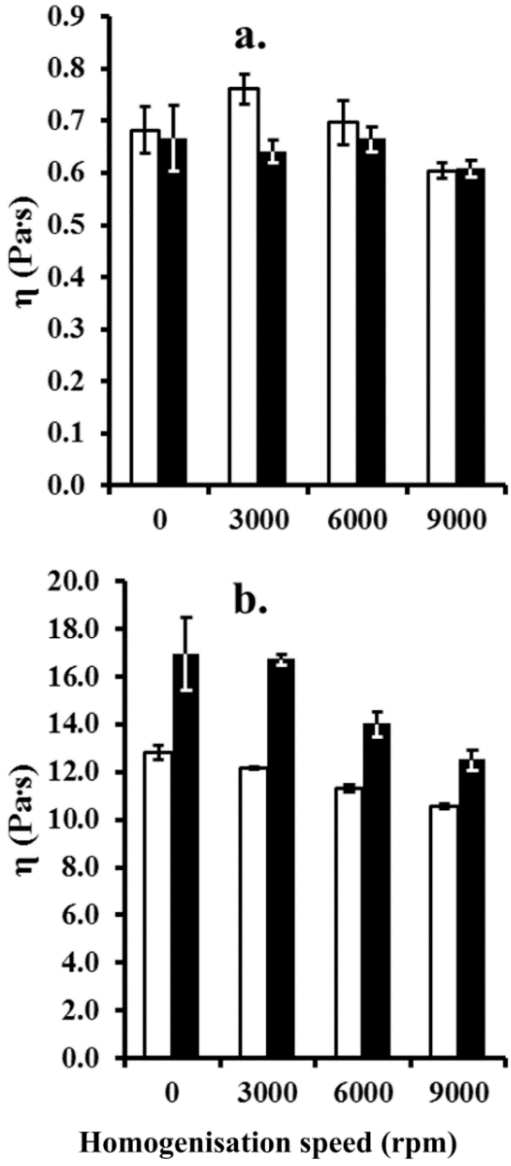

FIGURE 4.13 – Interactions at w_{API} 0.30 (a) and 0.51 (b) of batches A (white) and B (black). Error bars show standard deviation (n = 3).

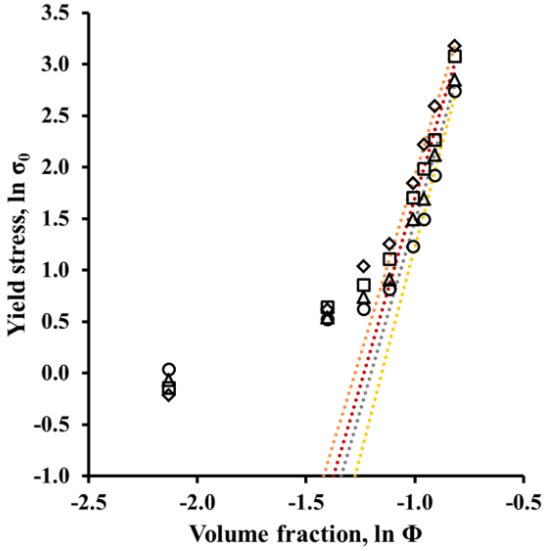

FIGURE 4.14 – Linear extrapolations of the yield stress ($ln\ \sigma_0$) at higher API concentrations ($ln\ \Phi$) for batch A. The measured values are the open markers (diamonds = no homogenisation, squares = 3000 rpm, triangles = 6000 rpm, circles = 9000 rpm) and fitted/estimated values are the dotted lines (orange = no homogenisation, red = 3000 rpm, grey = 6000 rpm, yellow = 9000 rpm). The values are fitted using the four higher points ($\Phi > 0.35$, $w_{API} \geq 0.43$) and linear extrapolation provides a theoretical maximum packing fraction.

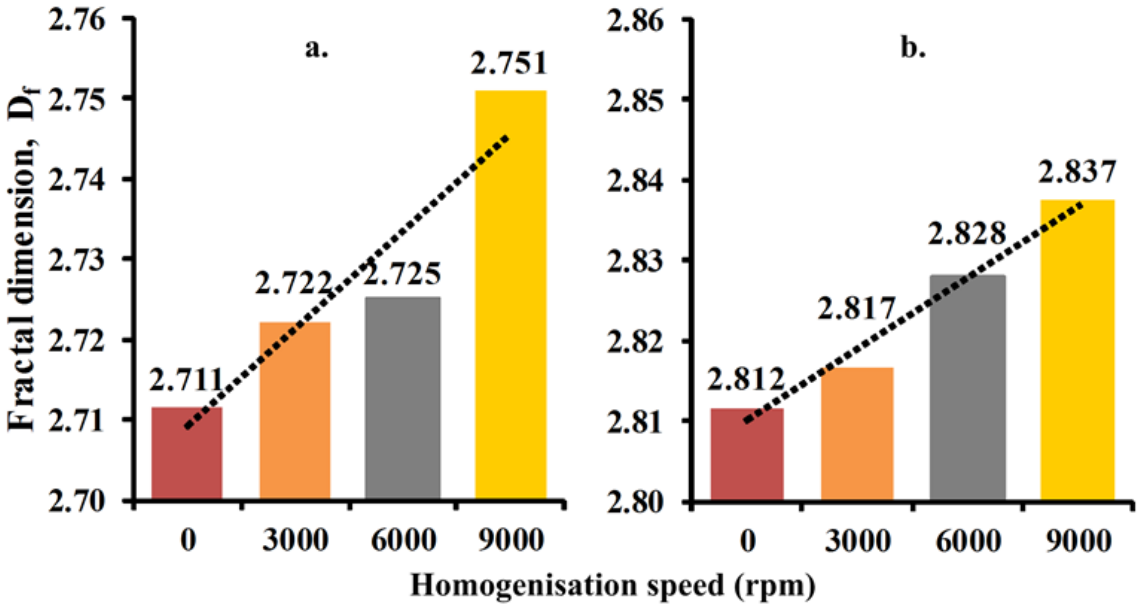

FIGURE 4.15 – Homogenisation level-specific fractal dimension D_f for batches A (a) and B (b); the black dotted line indicates the trend according to homogenisation level.

It is a common observation in pharmaceutics that, albeit release analysis of the API points to the same quality within specifications, the manufacturing process and the final product still exhibit a relevant batch-to-batch variability. From a QbD perspective, it is thus vital to learn in which pharmaceutical systems even small API differences can translate into batch-related differences, as we have observed with the concentrated suspensions of mebeverine hydrochloride. The availability of novel sensitive analytical tools is equally important. Based on our findings, the surface energy profiling proved to be highly promising for drug characterisation with respect to concentrated suspensions.

4.2.5.2 Rheology and the fractal concept of flocculation

The flow curves exhibited a different viscosity for batch A and B but the effect was mainly observed in the concentrated suspensions. For suspensions with

TABLE 4.9 – Fitted constants (*i.e.*, viscosity of the drug-free vehicle η_0 and maximal packing fraction Φ_{max}) of the Mooney model according to Equation 4.4 together with standard errors of the estimates.

Homogenisation level	Estimated η_0 (Pa s)	Estimated Φ_{max}	Adjusted-R^2 (%)
Batch A			
no homogenisation	0.553 ± 0.032	0.696 ± 0.009	98.28
3000 rpm	0.453 ± 0.022	0.681 ± 0.007	98.89
6000 rpm	0.390 ± 0.020	0.678 ± 0.007	98.72
9000 rpm	0.309 ± 0.014	0.663 ± 0.006	99.14
Batch B			
no homogenisation	0.643 ± 0.059	0.665 ± 0.012	96.61
3000 rpm	0.560 ± 0.039	0.654 ± 0.008	98.24
6000 rpm	0.508 ± 0.038	0.661 ± 0.009	97.79
9000 rpm	0.393 ± 0.025	0.649 ± 0.007	98.51

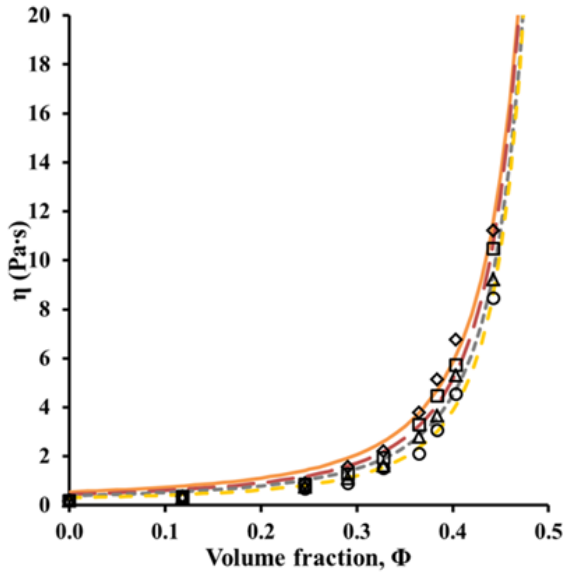

FIGURE 4.16 – Mooney model fitted to the viscosity values η of batch A vs. volume fraction Φ, sorted by homogenisation intensity. The measured values are the open points (diamonds = no homogenisation, squares = 3000 rpm, triangles = 6000 rpm, circles = 9000 rpm) and fitted values are the lines (orange continuous = no homogenisation, red long dash = 3000 rpm, grey short dash = 6000 rpm, yellow medium dash = 9000 rpm).

$w_{API} > 0.30$, the average viscosity difference increased sharply to about 30%. This was a remarkable difference in the drug product thinking of the only subtle physicochemical differences that were found between the API batches. The small differences in surface energy profiles and particle characteristics were evidently amplified in the dispersion process to result in notable rheological differences of the lipid-based suspensions.

Another factor on suspension viscosity was the intensity of homogenisation. Higher homogenisation intensity can have several effects on a suspension depending on the type of particle systems and the given energy input. A recent study of nanoparticulate pharmaceutical vehicles demonstrated a similar rheological effect caused by homogenisation as in case of the mebeverine suspensions [499]. Thus, rising homogenisation intensity was generally lowering the viscosity under shear, as well as decreasing the yield point σ_0. Apart from the homogenisation effects, the observed shear thinning in the flow curves of the lipid-based suspension is likely due to orientation effects of anisometric particles or their flocs [500,501].

The concentrated suspensions of mebeverine hydrochloride displayed in the image analysis diverse aggregates that can be named alternatively as flocs. Such flocs were earlier described by means of fractal geometry [502,503]. We employed the fractal concept of flocculation and determined the fractal dimension D_f from the different yield points as a function of the solid volume fraction (Figure 4.15) [50]. Two ranges were clearly distinguished that represented different structures. It was expected that in a high concentration range, the flocs would increasingly inter-penetrate to form dense structures. These structures were characterised by the fractal dimensions in this study.

We found different fractal dimensions for the various homogenisation levels. The differences were small but based on slopes that were statistically different (Equation 4.11). Homogenisation intensity appeared to define the dimension of the inter-penetrating floc structure. This is interesting to compare with the findings of Maggi [504], who studied concentrated suspensions of kaolinite and showed variable fractal dimensions depending on shear and flocculation kinematics. Different systems are certainly not always directly comparable as they differ in primary particle size, floc structure and on how strongly the particles were aggregated. However, the changes in the fractal structure depending on API batch and process conditions were an important finding. It was shown that small differences in the raw materials, for example surface energy profiles of the drug, were generating different structures in the concentrated suspensions, which in turn resulted in quite different viscosity values.

Since the fractal dimensions were extrapolated from yield points, they primarily characterised the particle structure at rest. To learn more about the particle packing under flow, we fitted the Mooney model (Equation 4.4) to the flow curves. As already suggested by Krieger [61], this version of the Mooney model (*i.e.*, including the maximal packing fraction) was particularly suited to describe concentrated suspensions. The obtained maximal packing fractions were in a reasonable range of 0.66 to 0.70 (Table 4.9) [50]. However, some care is needed with detailed interpretation of these fitted values. It was interestingly observed that values of Φ_{max} slightly decreased with rising homogenisation speed. Since higher homogenisation was leading to an increased fractal dimension, it was notable that the effective maximal packing under flow conditions was supposed to be comparatively smaller than from suspensions where less homogenisation was applied. This consideration is in agreement with the experimental finding that higher homogenisation speed produced suspensions with comparatively higher yield point and lower viscosity under shear. It seems that in complex flocculated systems Φ_{max} can be viewed as an apparent value for the packing of floc structures that evolve in a shear field.

An apparent fitting constant was also η_0. Some care is needed when interpreting this value as a constant viscosity of the vehicle. In case of simple oil, η_0 would indeed be constant. However, in the complex pharmaceutical model suspensions, the drug-free vehicle contained a small amount of colloidal silicon dioxide. The volume fraction of these particles was almost negligible compared to the amount of drug in suspension (average Φ of colloidal silicon dioxide less than 1.8%), but it may explain why obtained values of η_0 were not constant.

In summary, the fractal concept of flocculation was found to be a useful tool to study the particle structures in the concentrated mebeverine hydrochloride suspensions. In this respect, the effects of the API batch as well as of the homogenisation conditions were described in a range of comparatively high drug loads. This concentrated range exhibited a substantial non-linearity of the rheological properties, which was also supported by the analysis of the viscosity values with the Mooney model. The fractal concept of flocculation as well as the viscosity fitting according to Mooney can be termed as semi-empirical models. Such a model is different from a purely correlative model as it is obtained from any statistical design. Even though statistical designs are useful and widely employed in pharmaceutics these days, they can *a priori* only correlate data. We should not forget that a main idea of QbD is to target an improved process and product understanding. To this end, the applied semi-empirical models provided advanced tools to analyse the mebeverine hydrochloride suspensions.

4.2.6 Conclusion

The rheological properties of a suspension are generally critical to pharmaceutical quality. However, it seems to be difficult to design robust drug suspensions, when formulating at comparatively high concentrations. Especially at such drug concentrations, smallest differences in raw materials can greatly affect the suspension rheology. Moreover, the effect of homogenisation intensities was highly relevant for the resulting dispersion viscosity.

The fractal concept of flocculation was introduced to this field of pharmaceutics and it demonstrated a change of aggregated particle structure depending on process conditions as well as on the batch used. This was particularly remarkable, since the model batches hardly revealed differences in a first physicochemical testing. However, differences were observed using a novel method of iGC that allowed a surface energy profiling. Some inter-batch variability was demonstrated regarding the extent and heterogeneity of surface energies. Thus, iGC-SEA proved to be a useful QbD technique for characterisation of mebeverine hydrochloride in concentrated suspensions. More research is needed to optimally apply the novel tools in the future development and manufacture of concentrated drug suspensions. For example, the Mooney law could be used to simulate the viscosity of a suspension in formulation development. An early anticipation of the realistic variability is crucial for rational specification setting and hence for avoidance of manufacturing failures.

Chapter 5

Final remarks and outlook

Oral protein delivery represents a major challenge of modern pharmaceutics. While systemic exposure is a particularly ambitious goal, the local delivery of a therapeutic macromolecule to the GI tract as site of action is a more realistic target. Lipid-based (LB) systems have shown much promise in this regard [3]. Still, many formulation and manufacturing aspects, apart from the biopharmaceutical performance, must be considered to achieve a stable drug product and, eventually, successful delivery. The present thesis focused on the manufacturing and Quality-by-Design (QbD) aspects of LB dispersions. A particular aim was to introduce novel lipid-based drug delivery architectures and to adapt the production thereof for oral (local) protein administration by encapsulation while ensuring adequate pharmaceutical quality.

Manufacturing of protein-loaded microgels was successfully achieved by means of prilling directly into lipid-based hardening baths. These lipid-based dispersions exhibited potential for direct capsule filling. The model protein remained stable throughout the entire process, thus showing great promise to be formulated through this microencapsulation technology. The proposed polymer, mono-N-carboxymethyl chitosan, did

not interact with the protein structure, and its polyfunctional characteristics, namely bioadhesion and permeation enhancement, may prove useful at later stages of pharmaceutical development. Ionotropic gelling, a non-toxic method of polymeric cross-linking, was achieved even in non-aqueous media. This technique allowed high protein encapsulation efficiency, yet did not hinder protein release during *in vitro* testing. Moreover, by avoiding the standard aqueous hardening bath, a water removal process that could otherwise harm a therapeutic protein was avoided. The further advancement of this system by adding an extra nanotubular compartment in the microgel was technically demonstrated. This hierarchical multi-compartmental drug delivery system (DDS) took the advantages of the previously introduced protein-loaded microgels, but in addition it modified protein release and limited enzymatic digestion *in vitro*. The nanotubular clay used, halloysite (HNT), is a non-toxic, natural, and cost-effective material, which has already been successfully suggested as drug carrier. While this Nanotubes-in-Microgel Oral System was intended primarily for local administration to the gastrointestinal tract, this DDS theoretically even holds potential for systemic action. The microgel polymer has previously shown mucoadhesiveness, the HNT therein contained has a suitable particle size to penetrate the mucus layer, and the lipids from dispersing media have been reported to possess permeation enhancing properties.

LB dispersions have shown their potential as DDS and they display an especially high flexibility in terms of formulation. LB dispersions can be loaded both with small active pharmaceutical ingredients (API) as well as with macromolecular drugs. A thorough experimental design allowed identifying the significant factors of lipid composition that influence the microgel LB dispersion. Lipid's chemical properties such as glyceride chain length or PEG-modification were found to have statistical influence on process parameters, microgel morphological properties, encapsulated protein stability and quantity, and overall dispersion characteristics. These systematic evaluations are typical of the Quality-by-Design (QbD) initiative, which aims to increase understanding of pharmaceutical development steps to embed quality directly in the dosage form design. The application of this approach is not only challenging with the novel microgel dispersions in lipids, but is also a current topic for concentrated dispersions of drugs with low molecular weight. The latter model systems were employed to demonstrate the suitability of novel QbD tools and it was possible to more mechanistically interpret the behaviour of these systems. Specific surface energy profiling was employed to analyse batch-to-batch differences, which represent a common pitfall in formulation and process control. Mathematical model fitting allowed preliminary

prediction of LB suspension's viscosity at high concentrations. Finally, the introduction of a fractal analysis based on rheological data was found valuable in the dispersion characterisation and with regard to its stability

The present thesis introduced novel possibilities in terms of design, production, characterisation, and control of LB formulations. While this work embraces different aspects of pharmaceutical development, it also leads to further research opportunities and options. The protein-loaded microgel LB dispersion and the Nanotubes-in-Microgel Oral System can be further studied in terms of *in vivo* characterisation, since both systems have been thoroughly characterised *in vitro*. For instance, *in vivo* performance can be assessed according to the intended site of action, *i.e.*, local or systemic. Furthermore, the proposed model protein, bovine serum albumin, can be substituted with more therapeutically relevant macromolecules, such as enzymes or antibodies. Technical improvements may be implemented, for instance enteric coating of the final dosage form after capsule filling. This coating can ensure additional protection from enzymatic degradation and it may lead to increased oral exposure where this is targeted. For local delivery, the protection should ensure suitable local drug availability. The latter application may limit or prevent systemic exposure that could otherwise lead to undesired drug effects.

In terms of quality, an experimental design can be carried out on the multi-compartmental DDS to find optimal process settings and define critical aspects of formulation. Further research can also address formulation optimisation of the hereby introduced DDS based on prilling. A more mechanistic understanding of the complex prilling process could integrate the preliminary DoE findings to provide additional control over the prilling process. Additionally, a systematic study could complement the proposed QbD tools for highly concentrated LB suspensions, with the ultimate goal of creating robust formulation from these systems.

This work proposed significant advances in terms of novel architectures applied to LB dispersion design, as well as formulation of proteins for oral administration with these DDS. This thesis addresses aspects of formulation development within a QbD framework, thus implementing technically innovative approaches with emphasis on feasibility and final drug product quality. The findings indicated the potential of LB systems and microencapsulation for oral (local) delivery of therapeutically active proteins. A technical and quality oriented advancement has been obtained in the field of pharmaceutical lipid-based dispersions.

Bibliography

[1] Mu H, Holm R, Mu ̈llertz A. Lipid-based formulations for oral administration of poorly water-soluble drugs. *International Journal of Pharmaceutics*. 2013;453(1):215–24.

[2] Nash RA. Pharmaceutical suspensions. In: Lieberman H, Rieger MM, editors. Pharmaceutical dosage forms, Volume 1. New York: Marcel Dekker; 1988. p. 151.

[3] Li P, Nielsen HM, Müllertz A. Oral delivery of peptides and proteins using lipid-based drug delivery systems. *Expert Opinion on Drug Delivery*. 2012;9(10):1289–304.

[4] Costantinides PP, Scalart JP, Lancaster C, Marcello J, Marks G, Ellens H, Smith PL. Formulation and intestinal absorption enhancement evaluation of water-in-oil microemulsions incorporating medium-chain glycerides. *Pharmaceutical Research*. 1994;11(10):1382–90.

[5] Chao AC, Nguyen J V, Broughall M, Griffin A, Fix JA, Daddona PE. In vitro and in vivo evaluation of effects of sodium caprate on enteral peptide absorption and on mucosal morphology. *International Journal of Pharmaceutics*. 1999;191(1):15–24.

[6] Brown LR. Commercial challenges of protein drug delivery. *Expert Opinion on Drug Delivery*. 2005;2(1):29–42.

[7] Albericio F, Kruger HG. Therapeutic peptides. *Future Medicinal Chemistry*. 2012;4(12):1527–31.

[8] Dimitrov DS. Therapeutic proteins. In: Voynov V, Caravella JA, editors. Therapeutic proteins, Methods and protocols. 2nd ed. New York: Humana Press; 2012. p. 1–26.

[9] Vellard M. The enzyme as drug: Application of enzymes as pharmaceuticals. *Current Opinion in Biotechnology*. 2003;14(4):444–50.

[10] Lee VHL. Changing needs in drug delivery in the era of peptide and protein drugs. In: Lee VHL, editor. Peptide and protein drug delivery. New York: Marcel Dekker; 1990. p. 1–56.

[11] Manning M, Pater K, Borchardt RT. Stability of protein pharmaceuticals. *Pharmacological Research*. 1989;6(11):903–18.

[12] Oliva A, Santoveña A, Fariña J, Llabrés M. Effect of high shear rate on stability of proteins: kinetic study. *Journal of Pharmaceutical and Biomedical Analysis*. 2003;33(2):145–55.

[13] Jorgensen L, Nielsen HM, Frokjaer S. Biotechnology-based pharmaceuticals. In: Florence AT, Siepmann J, editors. Modern pharmaceutics, Volume 2, Applications and advances. New York: Informa Healthcare; 2009. p. 259–92.

[14] Smart AL, Gaisford S, Basit AW. Oral peptide and protein delivery: intestinal obstacles and commercial prospects. *Expert Opinion on Drug Delivery*. 2014;11(8):1323–35.

[15] Woodley J. Enzymatic barriers. In: Bernkop-Schnürch A, editor. Oral delivery of macromolecular drugs, Barriers, strategies and future trends. New York: Springer; 2009. p. 1–20.

[16] Sinha VR, Kumria R. Colonic drug delivery: Prodrug approach. *Pharmaceutical Research*. 2001;18(5):557–64.

[17] Perez-Vilar J. Gastrointestinal mucus gel barrier. In: Bernkop-Schnürch A, editor. Oral delivery of

macromolecular drugs, Barriers, strategies and future trends. New York: Springer; 2009. p. 21–48.

[18] Pinto-Reis C, Silva C, Martinho N, Rosado C. Drug carriers for oral delivery of peptides and proteins: accomplishments and future perspectives. *Therapeutic Delivery*. 2013;4(2):251–65.

[19] Li X, Yu M, Fan W, Gan Y, Hovgaard L, Yang M. Orally active-targeted drug delivery systems for proteins and peptides. *Expert Opinion on Drug Delivery*. 2014;11(9):1435–47.

[20] Ma G. Microencapsulation of protein drugs for drug delivery: Strategy, preparation, and applications. *Journal of Controlled Release*. 2014;193:324–40.

[21] Yeo Y, Baek N, Park K. Microencapsulation methods for delivery of protein drugs. *Biotechnology and Bioprocess Engineering*. 2001;6:213–30.

[22] Tran VT, Benoît JP, Venier-Julienne MC. Why and how to prepare biodegradable, monodispersed, polymeric microparticles in the field of pharmacy? *International Journal of Pharmaceutics*. 2011;407(1-2):1–11.

[23] Whelehan M, Marison IW. Microencapsulation using vibrating technology. *Journal of Microencapsulation*. 2011;28(8):669–88.

[24] Homar M, Suligoj D, Gašperlin M. Preparation of microcapsules with self-microemulsifying core by a vibrating nozzle method. *Journal of Microencapsulation*. 2007;24(1):72–81.

[25] Finotelli PV, Da Silva D, Sola-Penna M, Rossi AM, Farina M, Andrade LR, Takeuchi AY, Rocha-Leão MH. Microcapsules of alginate/chitosan containing magnetic nanoparticles for controlled release of insulin. *Colloids and Surfaces B: Biointerfaces*. 2010;81(1):206–11.

[26] Zhang Y, Rochefort D. Comparison of emulsion and vibration nozzle methods for microencapsulation of laccase and glucose oxidase by interfacial reticulation of poly(ethyleneimine). *Journal of Microencapsulation*. 2010;27(8):703–13.

[27] Del Gaudio P, Colombo P, Colombo G, Russo P, Sonvico F. Mechanisms of formation and disintegration of alginate beads obtained by prilling. *International Journal of Pharmaceutics*. 2005;302(1-2):1–9.

[28] De Kruif JK, Fasler-Kan E, Varum F, Bravo R, Kuentz M. On Prilling of Hydrophilic Microgels in Lipid Dispersions Using Mono-N-Carboxymethyl Chitosan for Oral Biologicals Delivery. *Journal of Pharmaceutical Sciences*. 2014;103:3675–87.

[29] Kriegel C, Amiji M. Oral TNF-alpha gene silencing using a polymeric microsphere-based delivery system for the treatment of inflammatory bowel disease. *Journal of Controlled Release*. 2011;150(1):77–86.

[30] Tran LTC, Lesieur S, Faivre V. Janus nanoparticles: materials, preparation and recent advances in drug delivery. *Expert Opinion on Drug Delivery*. 2014;11(7):1061–74.

[31] Forbes DC, Peppas NA. Oral delivery of small RNA and DNA. *Journal of Controlled Release*. 2012;162(2):438–45.

[32] Yu LX. Pharmaceutical quality by design: product and process development, understanding, and control. *Pharmaceutical Research*. 2008;25(4):781–91.

[33] Food and Drug Administration. Pharmaceutical cGMP for the 21st century - a risk-based approach. Final report. 2004.

[34] Food and Drug Administration. Guidance for industry. Q8(R2) pharmaceutical development. 2009.

[35] Singh B, Kumar R, Ahuja N. Optimizing drug delivery systems using systematic "design of experiments". Part I: fundamental aspects. *Critical Reviews in Therapeutic Drug Carrier Systems*. 2005;22(3):27–105.

[36] Scrimgeour CM, Harwood JL. Fatty acid and lipid structure. In: Gunstone FD, Harwood JL, Dijkstra AJ, editors. The lipid handbook. Boca Raton: CRC Press; 2007. p. 1–36.

[37] Hauss DJ. Oral lipid-based formulations, Enhancing the bioavailability of poorly water-soluble drugs. New York: Informa Healthcare; 2007. vii-viii p.

[38] Amidon GL, Lennermäs H, Shah VP, Crison JR. A theoretical basis for a biopharmaceutic drug classification: the correlation of in vitro drug product dissolution and in vivo bioavailability. *Pharmaceutical Research*. 1995;12(3):413–20.

[39] O'Driscoll CM, Griffin A. Biopharmaceutical challenges associated with drugs with low aqueous solubility – the potential impact of lipid-based formulations. *Advanced Drug Delivery Reviews*. 2008;60:617–24.

[40] Kuentz M. Lipid-based formulations for oral delivery of lipophilic drugs. *Drug Discovery Today: Technologies*. 2012;9(2):e71–174.

[41] Gonzáles-Caballero F, de Dios García López-Durán J. Suspension formulation. In: Nielloud F, Marti-

Mestres G, editors. Pharmaceutical emulsions and suspensions. 1st ed. New York: Marcel Dekker; 2000. p. 1–190.

[42] Strickley RG. Currently marketed oral lipid-based dosage forms: drug products and excipients. In: Hauss DJ, editor. Oral lipid based formulations, Enhancing the bioavailability of poorly water-soluble drugs. New York: Informa Healthcare; 2007. p. 1–32.

[43] Gibson L. Lipid-based excipients for oral drug delivery. In: Hauss DJ, editor. Oral lipid based formulations, Enhancing the bioavailability of poorly water-soluble drugs. New York: Informa Healthcare; 2007. p. 33–62.

[44] Serajuddln ATM. Solid dispersion of poorly water-soluble drugs: Early promises, subsequent problems, and recent breakthroughs. *Journal of Pharmaceutical Sciences*. 1999;88(10):1058–66.

[45] Müller RH, Mehnert W, Lucks JS, Schwarz C, zur Mühlen A, Weyhers H, Freitas C, Rühl D. Solid lipid nanoparticles (SLN) - an alternative colloidal carrier system for controlled drug delivery. *European Journal of Pharmaceutics and Biopharmaceutics*. 1995;41:62–9.

[46] Müller RH, Shegokar R, Keck CM. Years of Lipid Nanoparticles (SLN & NLC): Present State of Development & Industrial Applications. *Current Drug Discovery Technologies*. 2011;8(3):207–27.

[47] Saupe A, Wissing SA, Lenk A, Schmidt C, Müller RH. Solid Lipid Nanoparticles (SLN) and Nanostructured Lipid Carriers (NLC) - Structural investigations on two different carrier systems. *Bio-Medical Materials and Engineering*. 2005;15(5):393–402.

[48] Kuentz M. Oral self-emulsifying drug delivery systems , from biopharmaceutical to technical formulation aspects. 2011;21(1):1–10.

[49] Martin AN. Coarse dispersions. In: Sinko PJ, editor. Martin's physical pharmacy and pharmaceutical sciences. 5th ed. Philadelphia: Lippincott, Williams & Wilkins; 2006. p. 499–530.

[50] Tadros T. Interparticle interactions in concentrated suspensions and their bulk (rheological) properties. *Advances in Colloid and Interface Science*. 2011;168(1-2):263–77.

[51] Derjaguin B V, Landau L. Theory of the stability of strongly charged lyophobic sols and of the adhesion of strongly charged particles in solutions of electrolytes. *Acta Physicochimica URSS*. 1941;14:633.

[52] Verwey EJ, Overbeek JTG. Theory of the stability of lyophobic colloids. Amsterdam: Elsevier; 1948.

[53] Babchin AJ, Schramm LL. Osmotic repulsion force due to adsorbed surfactants. *Colloids and Surfaces B: Biointerfaces*. 2012;91:137–43.

[54] Hesselink FT, Vrij A, Overbeek JTG. Theory of the stabilization of dispersions by adsorbed macromolecules. II. Interaction between two flat particles. *The Journal of Physical Chemistry*. 1971;75(5):2094–103.

[55] Flory PJ. The configuration of real polymer chains. *Journal of Chemical Physics*. 1949;17(3):303–10.

[56] Flory PJ, Krigbaum WR. Statistical mechanics of dilute polymer solutions. II. *Journal of Chemical Physics*. 1950;18:1086–93.

[57] Fritz G, Schdler V, Willenbacher N, Wagner NJ, Scha V. Electrosteric Stabilization of Colloidal Dispersions Electrosteric Stabilization of Colloidal Dispersions. *Macromolecules*. 2002;18(16):6381–90.

[58] Einstein A. A new determination of the molecular dimensions. *Annalen der Physik*. 1906;19(2):289–306.

[59] Batchelor GK. Brownian diffusion of particles with hydrodynamic interaction. *Journal of Fluid Mechanics*. 1976;74(1):1–29.

[60] Krieger IM, Dougherty TJ. A mechanism for non-newtonian flow in suspensions of rigid spheres. *Transactions of the Society of Rheology*. 1959;3(1):137–52.

[61] Krieger IM. Rheology of monodisperse latices. *Advances in Colloid and Interface Science*. 1972;3(2):111–36.

[62] Mooney M. The viscosity of a concentrated suspension of spherical particles. *Journal of Colloid Science*. 1951;6(2):162–70.

[63] Brady JF, Aditya S. Khair, Swaroop M. On the bulk viscosity of suspensions. *Journal of Fluid Mechanics*. 2006;554:109–23.

[64] Vaithiyalingam S, Nutan M, Reddy I, Khan M. Preparation and characterization of a customized cellulose acetate butyrate dispersion for controlled drug delivery. *Journal of Pharmaceutical Sciences*. 2002;91(6):1512–22.

[65] Allahham A, Stewart P, Marriott J, Mainwaring D. Factors affecting shear thickening behavior of a concentrated injectable suspension of levodopa. *Journal of Pharmaceutical Sciences*. 2005;94(11):2393–402.

[66] Tadros TF. Rheology of dispersions: principles and applications. New York: Wiley; 2010.

[67] Nutan THM, Reddy IK. General principles of suspensions. In: Kulshreshtha AK, Singh ON, Wall GM, editors. Pharmaceutical suspensions From formulation development to manufacturing. New York: Springer; 2010. p. 39–65.

[68] Van Mil PJJM, Crommelin DJ a., De Blaey CJ. Characterization of flocs in coarse suspensions in a non-polar medium. *Colloids and Surfaces*. 1984;12:99–111.

[69] Van Mil PJJM, Crommelin DJA, Wiersema PH. Stability of coarse suspensions in nonpolar media: effect of gravity on the interaction between particles. *Journal of Colloid and Interface Science*. 1984;98(1):61–71.

[70] Van Mil PJJM, Nutan M, Reddy I, Khan M. Flocculation in a coarse suspension of sodium chloride in triglycerides. *Colloids and Surfaces*. 1985;14:47–58.

[71] Lyklema J. Principles of the stability of lyophobica colloidal dispersions in nonaqueous media. *Advances in Colloid and Interface Science*. 1968;2(2):65–114.

[72] Briceño MI. Rheology of suspensions and emulsions. In: Nielloud F, Marti-Mestres G, editors. Pharmaceutical emulsions and suspensions. 1st ed. New York: Marcel Dekker; 2000. p. 557–607.

[73] Illing A, Unruh T. Investigation on the flow behavior of dispersions of solid triglyceride nanoparticles. *International Journal of Pharmaceutics*. 2004;284:123–31.

[74] Clarke B. Rheology of coarse settling suspensions. *Transactions of the Institution of Chemical Engineers*. 1967;45:T251–6.

[75] Chen-Quay SC, Eiting KT, Li AWA, Lamharzi N, Quay SC. Identification of tight junction modulating lipids. *Journal of Pharmaceutical Sciences*. 2008;98(2):606–19.

[76] Sugano K, Kataoka M, da Costa Mathews C, Yamashita S. Prediction of food effect by bile micelles on oral drug absorption considering free fraction in intestinal fluid. *European Journal of Pharmaceutical Sciences*. 2010;40(2):118–24.

[77] Brasitus TA, Schachter D. Lipid composition and fluidity of rat enterocyte basolateral membranes. *Biochimica et Biophysica Acta*. 1984;774(1):138–46.

[78] Kaukonen AM, Boyd BJ, Charman WN, Porter CJH. Drug Solubilization Behavior during in Vitro Digestion of Suspension Formulations of Poorly Water-Soluble Drugs in Triglyceride Lipids. *Pharmaceutical Research*. 2004;21(2):254–60.

[79] Augsburger LL. Hard- and soft-shell capsules. In: Florence AT, Siepmann J, editors. Modern pharmaceutics, Volume 1, Basic principles and systems. New York: Informa Healthcare; 2009. p. 499–564.

[80] Overgaard AB, Højsted J, Hansen R, Møller-Sonnergaard J, Christrup LL. Patients' evaluation of shape, size and colour of solid dosage forms. *Pharmacy World and Science*. 2001;23(5):185–8.

[81] Kuentz M, Röthlisberger D. Determination of the optimal amount of water in liquid-fill masses for hard gelatin capsules by means of texture analysis and experimental design. *International Journal of Pharmaceutics*. 2002;236:145–52.

[82] The European Pharmacopoeia Commission. European Pharmacopoeia. 6th ed. Strasbourg: European Directorate for the Quality of Medicines and Healthcare; 2007.

[83] Edwards D. Applications of capsule dosing techniques for use in dry powder inhalers. *Therapeutic Delivery*. 2010;1(1):195–201.

[84] Hickey AJ, Mansour HM. Delivery of drugs by the pulmonary route. In: Florence AT, Siepmann J, editors. Modern pharmaceutics, Volume 2, Applications and advances. New York: Informa Healthcare; 2009. p. 191–120.

[85] Mothes FAB. No title. France; 9690, 1834.

[86] Lehuby JC. No Title. France; 4435, 1846.

[87] Jones BE. Gelatine alternatives and additives. In: Podczeck F, editor. Pharmaceutical Capsules. 2nd ed. London: Pharmaceutical Press; 2004. p. 61–78.

[88] Reich G. Formulation and physical properties of soft capsules. In: Podczeck F, editor. Pharmaceutical Capsules. 2nd ed. London: Pharmaceutical Press; 2004. p. 201–12.

[89] Chiwele I, Jones BE, Podczeck F. The shell dissolution of various empty hard capsules. *Chemical and Pharmaceutical Bulletin*. 2000;48(7):951–6.

[90] Sherry Ku M, Li W, Dulin W, Donahue F, Cadé D, Benameur H, Hutchison K. Performance qualification of a new hypromellose capsule: Part I. Comparative evaluation of physical, mechanical and processability quality attributes of Vcaps Plus,

Quali-V and gelatin capsules. *International Journal of Pharmaceutics*. 2010;386:30–41.

[91] Sherry Ku M, Lu Q, Li W, Chen Y. Performance qualification of a new hypromellose capsule: Part II. Disintegration and dissolution comparison between two types of hypromellose capsules. *International Journal of Pharmaceutics*. 2011;416(1):16–24.

[92] Tuleu C. A scintigraphic investigation of the disintegration behaviour of capsules in fasting subjects: a comparison of hypromellose capsules containing carrageenan as a gelling agent and standard gelatin capsules. *European Journal of Pharmaceutical Sciences*. 2007;30(3-4):251–5.

[93] Cole ET, Scott RA, Cadé D, Connor AL, Wilding IR. In vitro and in vivo pharmacoscintigraphic evaluation of ibuprofen hypromellose and gelatin capsules. *Pharmaceutical Research*. 2004;21(5):793–8.

[94] Podczeck F, Jones BE. The in vitro dissolution of theophylline from different types of hard shell capsules. *Drug Development and Industrial Pharmacy*. 2002;28(9):1163–9.

[95] Jones BE, Podczeck F. On the performance qualification of hypromellose capsules. *International Journal of Pharmaceutics*. 2012;434:503–6.

[96] Jones BE, Basit AW, Tuleu C. The disintegration behaviour of capsules in fed subjects: A comparison of hypromellose (carrageenan) capsules and standard gelatin capsules. *International Journal of Pharmaceutics*. 2012;424(1-2):40–3.

[97] Vilivalam VD, Illum L, Iqbal K. Starch capsules: An alternative system for oral drug delivery. *Pharmaceutical Science and Technology Today*. 2000;3(2):64–9.

[98] Burns SJ, Corness D, Hay G, Higginbottom S, Whelan I, Attwood D, Barnwell SG. An in vitro assessment of liquid-filled Capill potato starch capsules with biphasic release characteristics. *International Journal of Pharmaceutics*. 1996;134:223–30.

[99] Scott R, D C, He X, Cole ET. Pullulan capsules. United States; 20050249676 A1, 2005.

[100] Zema L, Loreti G, Macchi E, Foppoli A, Maroni A, Gazzaniga A. Injection-molded capsular device for oral pulsatile release: development of a novel mold. *Journal of Pharmaceutical Sciences*. 2013;102(2):489–99.

[101] Bae HJ, Cha DS, Whiteside WS, Park HJ. Film and pharmaceutical hard capsule formation properties of mungbean, waterchestnut, and sweet potato starches. *Food Chemistry*. 2008;106:96–105.

[102] Misic Z, Muffler K, Sydow G, Kuentz M. Novel Starch-Based PVA Thermoplastic Capsules for Hydrophilic Lipid-Based Formulations. *Journal of Pharmaceutical Sciences*. 2012;101(12):4516–28.

[103] Scherer RP. Method of and machine for making capsules. United States; 1970396 A, 1931.

[104] Podczeck F. Technology to manufacture soft capsules. In: Podczeck F, Jones BE, editors. Pharmaceutical Capsules. 2nd ed. London: Pharmaceutical Press; 2004. p. 195–200.

[105] Cole ET, Cadé D, Benameur H. Challenges and opportunities in the encapsulation of liquid and semi-solid formulations into capsules for oral administration. *Advanced Drug Delivery Reviews*. 2008;60(6):747–56.

[106] Niederquell A, Kuentz M. Introduction of a theoretical splashing degree to assess the performance of low-viscosity oils in filling of capsules. *AAPS PharmSciTech*. 2011;12(1):323–30.

[107] Strickrodt J. Fully automatic process for filling high viscosity pastes into hard gelatin capsules. *Pharmaceutical Industry*. 1990;52:1276–9.

[108] Rowley G. Filling of liquids and semi-solids into hard two-piece capsules. In: Podczeck F, Jones BE, editors. Pharmaceutical Capsules. 2nd ed. London: Pharmaceutical Press; 2004. p. 169–94.

[109] Wittwer F, Tanka I. Apparatus and method of sealing capsules. United States; 4539060, 1985.

[110] Cadé D, Cole ET, Mayer JP, Wittwer F. Liquid filled and sealed hard gelatin capsules. *Acta Pharmaceutica Technologica*. 1987;33(2):97–100.

[111] Cole ET. Liquid filled and sealed hard gelatin capsules. *Bulletin Technique Gattefossé*. 1999;92:67–77.

[112] Klotz U, Schwab M. Topical delivery of therapeutic agents in the treatment of inflammatory bowel disease. *Advanced Drug Delivery Reviews*. 2005;57:267–79.

[113] Mutlu EA, Farhadi A, Kshavarzian A. New developments in the treatment of inflammaotry bowel disease. *Expert Opinion on Investigational Drugs*. 2002;11(3):365–85.

[114] Gupta S, Jain A, Chakraborty M, Sahni JK, Ali J, Dang S. Oral delivery of therapeutic proteins and peptides: a review on recent developments. *Drug Delivery*. 2013;20(6):237–46.

[115] Carroll IM, Ringel-Kulka T, Ferrier L, Wu MC, Siddle JP, Bueno L, Ringel Y. Fecal Protease Activity Is Associated with Compositional Alterations in the Intestinal Microbiota. *PLoS ONE*. 2013;8(10):1–10.

[116] Macfarlane GT, Cummings JH, Allison C. Protein degradation by human intestinal bacteria. *Journal of general Microbiology*. 1986;132(6):1647–56.

[117] Saffran M, Bedra C, Kumar GS, Neckers DC. Vasopressin: a model for the study of effects of additives on the oral and rectal administration of peptide drugs. *Journal of Pharmaceutical Sciences*. 1988;77(1):33–8.

[118] Yamamoto A, Taniguchi T, Rikyun K, Tsuji T, Fujita T, Murakami M, Muranishi S. Effects of various protease inhibitors on the intestinal absorption and degradation of insulin in rats. *Pharmaceutical Research*. 1994;11(10):1496–500.

[119] McClellan GBJ, Gardner CW. Purification and properties of human intestine alanine aminopeptidas. *Biochimica et Biophysica Acta*. 1980;613(1):160–7.

[120] Fujii S, Yokohama TE, Ikegaya K, Salo F, Yakoo N. Promoting effect of the new chymotrypsin inhibitor FK-448 on the intestinal absorption of insulin in rats and dogs. *Journal of Pharmacy and Pharmacology*. 1985;37(8):545–9.

[121] Reseland JE, Holm H, Jacobsen MB, Jenssen TG, Hanssen LE. Proteinase inhibitors induce selective stimulation of human trypsin and chymotrypsin secretion. *Journal of Nutrition*. 1996;126(3):634–42.

[122] Kimura TE, Sato K, Sugimoto K, Tao R, Murakami T, Kurosaki Y, Nakayama T. Oral administration of insulin as poly(vinyl alcohol)-gel spheres in diabetic rats. *Biological and Pharmaceutical Bulletin*. 1996;19(6):897–900.

[123] Otsuki M, Ohki A, Okabayahi Y, Suehiro I, Baba S. Effect of synthetic protease inhibitor camostate on pancreatic exocrine function in rats. *Pancreas*. 1987;2(2):164–9.

[124] Dasgupta P, Singh A, Mukherjee R. N-terminal acylation of somatostatin analog with long chain fatty acids enhances its stability and anti-proliferative activity in human breast adenocarcinoma cells. *Biological and Pharmaceutical Bulletin*. 2002;25(1):29–36.

[125] Ramon J, Saez V, Baez R, Aldana R, Hardy E. PEGylated interferon-alpha2b: a branched 40K polyethylene glycol derivate. *Pharmaceutical Research*. 2005;22(8):1375–87.

[126] Werle M, Schmitz T, Huang H, Wentzel A, Kolmar H, Bernkop-Schnürch A. The potential of cystine-knot microproteins as novel pharmacophoric scaffolds in oral peptide drug delivery. *Journal of Drug Targeting*. 2006;14(3):137–46.

[127] Calceti P, Salmaso S, Walker G, Bernkop-Schnürch a. Development and in vivo evaluation of an oral insulin-PEG delivery system. *European Journal of Pharmaceutical Sciences*. 2004;22:315–23.

[128] Khafagy ES, Morishita M. Oral biodrug delivery using cell-penetrating peptide. *Advanced Drug Delivery Reviews*. 2012;64(6):531–9.

[129] Petrus AK, Fairchild TJ, Doyle RP. Traveling the vitamin B12 pathway: Oral delivery of protein and peptide drugs. *Angewandte Chemie - International Edition*. 2009;48:1022–8.

[130] Asada H, Douen T, Waki M, Adachi S, Fujita T, Yamamoto A, Muranishi S. Absorption characteristics of chemically modified-insulin derivatives with various fatty acids in the small and large intestine. *Journal of Pharmaceutical Sciences*. 1995;84(6):682–7.

[131] Kidron M, Dinh S, Menachem Y, Abbast R, Variano B, Goldberg M, Arbit E, Bar-On H. A novel per-oral insulin formulation: Proof of concept study in non-diabetic subjects. *Diabetic Medicine*. 2004;21:354–7.

[132] Varum FJO, Mcconnell EL, Sousa JJS. Mucoadhesion and the. 2008;25(3):207–58.

[133] Ponchel G, Irache JM. Specific and non-specific bioadhesive particulate systems for oral delivery to the gastrointestinal tract. *Advanced Drug Delivery Reviews*. 1998;34(2-3):191–219.

[134] Smart JD. The basics and underlying mechanisms of mucoadhesion. *Advanced Drug Delivery Reviews*. 2005;57:1556–68.

[135] Khutoryanskiy V V. Advances in Mucoadhesion and Mucoadhesive Polymers. *Macromolecular Bioscience*. 2011;11:748–64.

[136] Derjaguin B V, Toporov YP, Muller VM, Aleinikova IN. On the relationship between the electrostatic and the molecular component of the adhesion of elastic particles to a solid surface. *Journal of Colloid and Interface Science*. 1977;58(3):528–33.

[137] Kinloch AJ. The science of adhesion. *Journal of Material Science*. 1980;15(9):2141–66.

[138] Peppas NA. Surface, interfacial and molecular aspects of polymer bioadhesion. *Journal of Controlled Release*. 1985;2:257–75.

[139] Lafitte G. Structure of the gastrointestinal mucus layer and implications for controlled release and delivery of functional food ingredients. In: Garti N, editor. Delivery and controlled release of bioactives in foods and nutraceuticals. Cambridge: Woodhead Publishing; 2008. p. 26–52.

[140] Ponchel G, Touchard F, Duchêne D, Peppas NA. Bioadhesive analysis of controlled-release systems. I. Fracture and interpenetration analysis in poly(acrylic acid)-containing systems. *Journal of Controlled Release*. 1987;5(2):129–41.

[141] Yang X, Robinson JR. Bioadhesion in mucosal drug delivery. In: Okano T, editor. Biorelated polymers and gels: controlled release and applications in biomedical engineering. San Diego: Academic Press; 1998. p. 135–92.

[142] Lamprecht A, Schäfer U, Lehr CM. Size-dependent bioadhesion of micro- and nanoparticulate carriers to the inflamed colonic mucosa. *Pharmaceutical Research*. 2001;18(6):788–93.

[143] Des Rieux A, Pourcelle V, Cani PD, Marchand-Brynaert J, Préat V. Targeted nanoparticles with novel non-peptidic ligands for oral delivery. *Advanced Drug Delivery Reviews*. 2013;65(6):833–44.

[144] Leo E, Brina B, Forni F, Vandelli MA. In vitro evaluation of PLA nanoparticles containing a lipophilic drug in water-soluble or insoluble form. *International Journal of Pharmaceutics*. 2004;278:133–41.

[145] Fonseca C, Simões S, Gaspar R. Paclitaxel-loaded PLGA nanoparticles: Preparation, physicochemical characterization and in vitro anti-tumoral activity. *Journal of Controlled Release*. 2002;83:273–86.

[146] Galindo-Rodriguez SA, Allemann E, Fessi H, Doelker E. Polymeric nanoparticles for oral delivery of drugs and vaccines: a critical evaluation of in vivo studies. *Critical Reviews in Therapeutic Drug Carrier Systems*. 2005;22(5):419–64.

[147] Johnson FA, Craig DQ, Mercer AD. Characterization of the block structure and molecular weight of sodium alginates. *Journal of Pharmacy and Pharmacology*. 1997;49(1986):639–43.

[148] Eiamtrakarn S, Itoh Y, Kishimoto J, Yoshikawa Y, Shibata N, Murakami M, Takada K. Gastrointestinal mucoadhesive patch system (GI-MAPS) for oral administration of G-CSF, a model protein. *Biomaterials*. 2002;23:145–52.

[149] Varum FJO, Merchant HA, Basit AW. Oral modified-release formulations in motion: The relationship between gastrointestinal transit and drug absorption. *International Journal of Pharmaceutics*. 2010;395(1-2):26–36.

[150] Borchard G. The absorption barrier. In: Bernkop-Schnürch A, editor. Oral delivery of macromolecular drugs, Barriers, strategies and future trends. New York: Springer; 2009. p. 49–64.

[151] Sugano K, Kansy M, Artursson P, Avdeef A, Bendels S, Di L, Ecker GF, Faller B, Fischer H, Gerebtzoff G, Lennernaes H, Senner F. Coexistence of passive and carrier-mediated processes in drug transport. *Nature Reviews Drug Discovery*. 2010;9:597–614.

[152] Huang W, Lee SL, Yu LX. Mechanistic approaches to predicting oral drug absorption. *AAPS Journal*. 2009;11(2):217–24.

[153] Di L, Artursson P, Avdeef A, Ecker GF, Faller B, Fischer H, Houston JB, Kansy M, Kerns EH, Krämer SD, Lennernäs H, Sugano K. Evidence-based approach to assess passive diffusion and carrier-mediated drug transport. *Drug Discovery Today*. 2012;17(15-16):905–12.

[154] Kell DB, Dobson PD, Oliver SG. Pharmaceutical drug transport: The issues and the implications that it is essentially carrier-mediated only. *Drug Discovery Today*. 2011;16(15-16):704–14.

[155] Bergström CAS, Holm R, Jørgensen SA, Andersson SBE, Artursson P, Beato S, Borde A, Box K, Brewster M, Dressman J, Feng KI, Halbert G, Kostewicz E, McAllister M, Muenster U, Thinnes J, Taylor R, Mullertz A. Early pharmaceutical profiling to predict oral drug absorption: Current status and unmet needs. *European Journal of Pharmaceutical Sciences*. 2014;57(1):173–99.

[156] Lipka E, Crison J, Amidon GL. Transmembrane transport of peptide type compounds: Prospects for oral delivery. *Journal of Controlled Release*. 1996;39(2-3):121–9.

[157] Antunes F, Andrade F, Ferreira D, Nielsen HM, Sarmento B. Models to predict intestinal absorption of therapeutic peptides and proteins. *Current Drug Metabolism*. 2013;14(1):4–20.

[158] Youdim KA, Avdeef A, Abbott NJ. In vitro trans-monolayer permeability calculations: Often forgotten assumptions. *Drug Discovery Today*. 2003;8(21):997–1003.

[159] Balimane P V., Chong S. Cell culture-based models for intestinal permeability: A critique. *Drug Discovery Today*. 2005;10(5):335–43.

[160] Bowe CL, Mokhtarzadeh L, Venkatesan P, Babu S, Axelrod HR, Sofia MJ, Kakarla R, Chan TY, Kim JS,

Lee HJ, Amidon GL, Choe SY, Walker S, Kahne D. Design of compounds that increase the absorption of polar molecules. *Proceedings of the National Academy of Sciences of the United States of America*. 1997;94(22):12218–23.

[161] Tsuji A. Transporter-mediated Drug Interactions. *Drug metabolism and pharmacokinetics*. 2002;17(4):253–74.

[162] Kuppens IE, Bosch TM, Van Maanen MJ, Rosing H, Fitzpatrick A, Beijnen JH, Schnellens JH. Oral bioavailability of docetaxel in combination with OC144-093 (ONT-093). *Cancer Chemotherapy and Pharmacology*. 2005;55(1):72–8.

[163] Lin Y, Shen Q, Katsumi H, Okada N, Fujita T, Jiang X, Yamamoto A. Effects of Labrasol and other pharmaceutical excipients on the intestinal transport and absorption of rhodamine123, a P-glycoprotein substrate, in rats. *Biological and Pharmaceutical Bulletin*. 2007;30(7):1301–7.

[164] Föger F, Schmitz T, Bernkop-Schnürch A. In vivo evaluation of an oral delivery system for P-gp substrates based on thiolated chitosan. *Biomaterials*. 2006;27(23):4250–5.

[165] Carreno-Gomez B, Duncan R. Composition with enhanced oral bioavailability. World; 2001052896 A3, 2001.

[166] Aungst BJ, Saitoh H, Burcham DL, Huang S, Mousa A, Hussain MA. controlled release Enhancement of the intestinal absorption of peptides and non-peptides. 1996;41:19–31.

[167] Yamamoto A, Tatsumi H, Maruyama M, Uchiyama T, Okada N, Fujita T. Modulation of intestinal permeability by nitric oxide donors: implications in intestinal delivery of poorly absorbable drugs. *Journal of Pharmacology and Experimental Therapeutics*. 2001;296:84–90.

[168] Artursson P, Lindmark T, Davis SS, Illum L. Effect of chitosan on the permeability of monolayers of intestinal epithelial cells (Caco-2). *Pharmaceutical Research*. 1994;11(9):1358–61.

[169] Thanou M, Verhoef JC, Junginger HE. Oral drug absorption enhancement by chitosan and its derivatives. *Advanced Drug Delivery Reviews*. 2001;52:117–26.

[170] Aungst BJ. Absorption Enhancers: Applications and Advances. *AAPS Journal*. 2012;14(1):10–8.

[171] Choonara BF, Choonara YE, Kumar P, Bijukumar D, du Toit LC, Pillay V. A review of advanced oral drug delivery technologies facilitating the protection and absorption of protein and peptide molecules. *Biotechnology Advances*. 2014;32:1269–82.

[172] Renukuntla J, Vadlapudi AD, Patel A, Boddu SHS, Mitra AK. Approaches for enhancing oral bioavailability of peptides and proteins. *International Journal of Pharmaceutics*. 2013;447(1-2):75–93.

[173] Wang W. Instability, stabilization, and formulation of liquid protein pharmaceuticals. *International Journal of Pharmaceutics*. 1999;185:129–88.

[174] Tanford C. Oral drug absorption enhancement by chitosan and its derivatives. *Advances in Protein Chemistry*. 1968;23:121–282.

[175] Roy I, Gupta MN. Freeze-drying of proteins: some emerging concerns. *Biotechnology and Applied Biochemistry*. 2004;39(Pt 2):165–77.

[176] Krishnamurthy R, Manning MC. The stability factor: importance in formulation development. *Current Pharmaceutical Biotechnology*. 2002;3:361–71.

[177] Cleland JL, Powell MF, Shire SJ. The development of stable protein formulations: a close look at protein aggregation, deamidation, and oxidation. *Critical Reviews in Therapeutic Drug Carrier Systems*. 1993;10(4):307–77.

[178] Kauzmann W. Some factors in the interpretation of protein denaturation. *Advances in Protein Chemistry*. 1959;14:1–63.

[179] Carpenter JF, Pikal MJ, Chang BS, Randolph TW. Rational design of stable lyophilized protein formulations: Some practical advice. *Pharmaceutical Research*. 1997;14:969–75.

[180] Akersand MJ, DeFelippis MR. Peptides and proteins as parenteral solutions. In: Hovgaard L, Frokjaer S, Van de Weert M, editors. Pharmaceutical formulation development of peptides and proteins. 2nd ed. Boca Raton: CRC Press; 2012. p. 149–292.

[181] Hwang SR, Byun Y. Advances in oral macromolecular drug delivery. *Expert Opinion on Drug Delivery*. 2014;11(12):1955–67.

[182] Chin J, Foyez Mahmud KA, Kim SE, Park K, Byun Y. Insight of current technologies for oral delivery of proteins and peptides. *Drug Discovery Today: Technologies*. 2012;9(2):e105–12.

[183] Park K, Kwon IC, Park K. Oral protein delivery: Current status and future prospect. *Reactive and Functional Polymers*. 2011;71(3):280–7.

[184] Morishita M, Peppas NA. Is the oral route possible for peptide and protein drug delivery? *Drug Discovery Today*. 2006;11(19-20):905–10.

[185] Bruno BJ, Miller GD, Lim CS. Basics and recent advances in peptide and protein drug delivery. *Therapeutic Delivery*. 2013;4(11):1443–67.

[186] Singh MN, Hemant KSY, Ram M, Shivakumar HG. Microencapsulation: A promising techniques for controlled drug delivery. *Research in Pharmaceutical Science*. 2010;5(2):65–77.

[187] Bysell H, Månsson R, Hansson P, Malmsten M. Microgels and microcapsules in peptide and protein drug delivery. *Advanced Drug Delivery Reviews*. 2011;63(13):1172–85.

[188] George M, Abraham TE. Polyionic hydrocolloids for the intestinal delivery of protein drugs: Alginate and chitosan - a review. *Journal of Controlled Release*. 2006;114:1–14.

[189] Illum L. Chitosan and its use as a pharmaceutical excipient. *Pharmaceutical Research*. 1998;15(9):1326–31.

[190] Lehr CM. Bioadhesion technologies for the delivery of peptide and protein drugs to the gastrointestinal tract. *Critical Reviews in Therapeutic Drug Carrier Systems*. 1994;11(2-3):119–60.

[191] Amidi M, Mastrobattista E, Jiskoot W, Hennink WE. Chitosan-based delivery systems for protein therapeutics and antigens. *Advanced Drug Delivery Reviews*. 2010;62(1):59–82.

[192] Werle M, Takeuchi H, Bernkop-Schnürch A. Modified chitosans for oral drug delivery. *Journal of Pharmaceutical Sciences*. 2009;98(5):1643–56.

[193] Prego C, Torres D, Alonso MJ. The potential of chitosan for the oral administration of peptides. *Expert Opinion on Drug Delivery*. 2005;2(5):843–54.

[194] Chen MC, Mi FL, Liao ZX, Hsiao CW, Sonaje K, Chung MF, Hsu LW, Sung HW. Recent advances in chitosan-based nanoparticles for oral delivery of macromolecules. *Advanced Drug Delivery Reviews*. 2013;65(6):865–79.

[195] Agnihotri SA, Mallikarjuna NN, Aminabhavi TM. Recent advances on chitosan-based micro- and nanoparticles in drug delivery. *Journal of Controlled Release*. 2004;100:5–28.

[196] Sonia TA, Sharma CP. Chitosan and its derivatives for drug delivery perspective. *Advances in Polymer Science*. 2011;243:23–54.

[197] Scholes PD, Coombes AGA, Illum L, Daviz SS, Vert M, Davies MC. The preparation of sub-200 nm poly(lactide-co-glycolide) microspheres for site-specific drug delivery. *Journal of Controlled Release*. 1993;25(1-2):145–53.

[198] Niwa T, Takeuchi H, Hino T, Kunou N, Kawashima Y. Preparations of biodegradable nanospheres of water-soluble and insoluble drugs with D,L-lactide/gylcolide copolymer by a novel spontaneous emulsification solvent diffusion method, and the drug release behavior. *Journal of Controlled Release*. 1993;25(1-2):89–98.

[199] Tom JW, Debenedetti PG. Particle formation with supercritical fluids - a review. *Journal of Aerosol Science*. 1991;22(5):555–84.

[200] Soppimath KS, Aminabhavi TM, Kulkarni AR, Rudzinski WE. Biodegradable polymeric nanoparticles as drug delivery devices. *Journal of Controlled Release*. 2001;70:1–20.

[201] Bansode SS, Banarjee SK, Gaikwad DD, Jadhav SL, Thorat RM. Microencapsulation: a review. *International Journal of Pharmaceutical Sciences Review and Research*. 2010;1(2):38–43.

[202] Jyothi NVN, Prasann PM, Sakarkar SN, Prabha KS, Ramaiah PS, Srawan GY. Microencapsulation techniques, factors influencing encapsulation efficiency. *Journal of Microencapsulation*. 2010;27(3):187–97.

[203] Sarmento B, Ribeiro A, Veiga F, Sampaio P, Neufeld R, Ferreira D. Alginate/chitosan nanoparticles are effective for oral insulin delivery. *Pharmaceutical Research*. 2007;24(12):2198–206.

[204] Rekha MR, Sharma CP. Synthesis and evaluation of lauryl succinyl chitosan particles towards oral insulin delivery and absorption. *Journal of Controlled Release*. 2009;135(2):144–51.

[205] Hong P, Koza S, Bouvier ESP. Size-Exclusion Chromatography for the Analysis of Protein Biotherapeutics and their Aggregates. *Journal of liquid chromatography & related technologies*. 2012;35:2923–50.

[206] Karlsson E, Hirsh I. Ion exchange chromatography. In: Janson JC, editor. Protein purification: principles, high resolution methods, and applications. 3rd ed. Hoboken: Wiley; 2011. p. 93–134.

[207] Weber K, Osborn M. The Reliability of Molecular Weight Determinations Sulf ate-Polyacrylamide Gel Electrophoresis. *The Journal of Biological Chemistry*. 1969;244(16):4406–12.

[208] Shapiro AL, Viñuela E, Maizel JVJ. Molecular weight estimation of polypeptide chains by electrophoresis in SDS-polyacrylamide gels.

Biochemical and Biophysical Research Communications. 1967;28(5):815–20.

[209] Wiktorowicz JE, Colburn JC. Protein analysis by capillary electrophoresis. In: Grossman PD, Colburn JC, editors. Capillary electrophoresis: theory and practice. London: Academic Press; 1992. p. 273–300.

[210] Righetti PG. Isoelectric focusing in gels. *Journal of Chromatography A*. 1974;98(2):271–321.

[211] Righetti PG, Gianazza E. New developments in isoelectric focusing. *Journal of Chromatography A*. 1980;184(4):415–56.

[212] Biemann K, Martin SA. Mass spectrometric determination of the amino acid sequence of peptides and proteins. *Mass Spectrometry Review*. 1987;6(1):1–75.

[213] Pelton JT, McLean LR. Spectroscopic methods for analysis of protein secondary structure. *Analytical Biochemistry*. 2000;277:167–76.

[214] Jackson M, Mantsch HH. The use and misuse of FTIR spectroscopy in the determination of protein structure. *Critical Reviews in Biochemistry and Molecular Biology*. 1995;30(2):95–120.

[215] Bunaciu AA, Aboul-Enein HY, Hoang VD. Raman spectroscopy for protein analysis. *Applied Spectroscopy Reviews*. 2015;(ahead of publication).

[216] Nemecek D, Stepanek J, Thomas GJJ. Raman spectroscopy of proteins and nucleoproteins. *Current Protocols in Protein Science*. 2013;71(17.8):1–52.

[217] Kueltzo LA. Ultraviolet absorption spectroscopy. In: Jiskoot W, Crommelin DJA, editors. Methods for structural analysis of protein pharmaceuticals. Arlington: AAPS; 2005. p. 1–26.

[218] Eftink MR. Fluorescence techniques for studying protein structure. In: Suelter CH, editor. Methods of biochemical analysis: protein structure determination, Volume 35. Hoboken: Wiley; 1991. p. 127–205.

[219] Kelly SM, Price NC. The use of circular dichroism in the investigation of protein structure and function. *Current protein & peptide science*. 2000;1(4):349–84.

[220] Chiu MH, Prenner EJ. Differential scanning calorimetry: An invaluable tool for a detailed thermodynamic characterization of macromolecules and their interactions. *Journal of Pharmacy and Bioallied Sciences*. 2011;3(1):39–59.

[221] Chen T, Oakley DM. Thermal analysis of proteins of pharmaceutical interest. *Thermochimica Acta*. 1995;248:229–44.

[222] Murphy R. Static and dynamic light scattering of biological macromolecules: what can we learn? *Current Opinion in Biotechnology*. 1997;8:25–30.

[223] Svergun DI, Koch MHJ. Advances in structure analysis using small-angle scattering in solution. *Current Opinion in Structural Biology*. 2002;12:654–60.

[224] Wlodawer A, Minor W, Dauter Z, Jaskolski M. Protein crystallography for non-crystallographers, or how to get the best (but not more) from published macromolecular structures. *FEBS Journal*. 2008;275:1–21.

[225] Bax A. Twoi-Dimensional Nmr and. *Annual Review of Biochemistry*. 1989;58:223–56.

[226] O'Kennedy R, Byrne M, O'Fafain C, Berns G. A review of enzyme-immunoassay and a description of a competitive enzyme-linked immunosorbent assay for the detection of immunoglobulin concentrations. *Biochemical Education*. 1990;18(3):136–40.

[227] Li M, Rouaud O, Poncelet D. Microencapsulation by solvent evaporation: state of the art for process engineering approaches. *International Journal of Pharmaceutics*. 2008;363(1-2):26–39.

[228] Verfahren zur Überführung von Kalksalpeter oder ähnlichen Stoffen in fein zerkleinerte Form ohne Stauabbildung. Germany; 287307 C, 1913.

[229] Heinzen C, Berger A, Marision I. Use of vibration technology for jet break-up for encapsulation of cells microbes and liquids in monodisperse microcapsules. *Fundamentals of cell immobilisation biotechnology*. 2004;8A:257–75.

[230] Strutt JW. On the stability of liquid jets. *Proceedings of the London Mathematical Scociety*. 1878;10(4).

[231] Weber C. Zum Zerfall eines Flüssigkeitstrahles. *Zeitschrift für angewandte Mathematik und Mechanik*. 1931;11:136–55.

[232] Serp D, Cantana E, Heinzen C, Von Stockar U, Marison IW. Characterization of an encapsulation device for the production of monodisperse alginate beads for cell immobilization. *Biotechnology and bioengineering*. 2000;70:41–53.

[233] Brandenberger H, Widmer F. A new multinozzle encapsulation/immobilisation system to produce uniform beads of alginate. *Journal of Biotechnology*. 1998;63(1):73–80.

[234] Vervaeck A, Saerens L, De Geest BG, De Beer T, Carleer R, Adriaensens P, Remon JP, Vervaet C. Prilling of fatty acids as a continuous process for the development of controlled release multiparticulate dosage forms. *European Journal of Pharmaceutics and Biopharmaceutics*. 2013;85(3 part A):587–96.

[235] Pivette P, Faivre V, Daste G, Ollivon M, Lesieur S. Rapid cooling of lipid in a prilling tower. *Journal of Thermal Analysis and Calorimetry*. 2009;98(1):47–55.

[236] Oh CM, Guo Q, Wan P, Heng S, Chan LW. Spray-congealed microparticles for drug delivery - an overview of factors influencing their production and characteristics. *Expert Opinion on Drug Delivery*. 2014;11(7):1047–60.

[237] Oxley JD. Spray cooling and spray chilling for food ingredients and nutraceutical encapsulation. In: Garti N, McClements DJ, editors. Encapsulation technologies and delivery systems for food ingredients and nutraceuticals. Cambridge: Woodhead Publishing; 2012. p. 110–30.

[238] Brandenberger H, Nüssli D, Piëch V, Widmer F. Monodisperse particle production: A method to prevent drop coalescence using electrostatic forces. *Journal of Electrostatics*. 1999;45(3):227–38.

[239] Rodríguez-Rivero C, Del Valle EMM, Galán MA. Development of a new technique to generate microcapsules from the breakup of non-Newtonian highly viscous fluid jets. *AIChE Journal*. 2011;57(12):3436–47.

[240] Vilesov AD, Zhuravsky EP, Vilessova MS, Netchaeva EA, Ayzenshtadt NI, Stankevich RP, Isidorov R V. New-types of apparatus for producing microcapsules and microgranules. *International Journal of Pharmaceutics*. 2002;242:101–6.

[241] Brandau E. Process and plant for the production of spherical alginate pellets. United States; 5472648 A, 1995.

[242] Brandau T. Preparation of monodisperse controlled release microcapsules. *International Journal of Pharmaceutics*. 2002;242:179–84.

[243] Chandramouli V, Kailasapathy K, Peiris P, Jones M. An improved method of microencapsulation and its evaluation to protect Lactobacillus spp. in simulated gastric conditions. *Journal of Microbiological Methods*. 2004;56(1):27–35.

[244] Freitas S, Merkle HP, Gander B. Microencapsulation by solvent extraction/evaporation: Reviewing the state of the art of microsphere preparation process technology. *Journal of Controlled Release*. 2005;102:313–32.

[245] Auriemma G, Mencherini T, Russo P, Stigliani M, Aquino RP, Del Gaudio P. Prilling for the development of multi-particulate colon drug delivery systems: pectin vs. pectin-alginate beads. *Carbohydrate polymers*. 2013;92(1):367–73.

[246] Dorati R, Genta I, Modena T, Conti B. Microencapsulation of a hydrophilic model molecule through vibration nozzle and emulsion phase inversion technologies. *Journal of Microencapsulation*. 2013;30(6):559–70.

[247] Buthe A, Hartmeier W, Ansorge-Schumacher MB. Novel solvent-based method for preparation of alginate beads with improved roundness and predictable size. *Journal of Microencapsulation*. 2004;21(8):865–76.

[248] Zhou Y, Kajiyama S, Masuhara H, Hosokawa Y, Kaji T, Fukui K. A new size and shape controlling method for producing calcium alginate beads with immobilized proteins. *Journal of Biomedical Science and Engineering*. 2009;2:287–93.

[249] Séquier F, Faivre V, Daste G, Renouard M, Lesieur S. Critical parameters involved in producing microspheres by prilling of molten lipids: From theoretical prediction of particle size to practice. *European Journal of Pharmaceutics and Biopharmaceutics*. 2014;87(3):530–40.

[250] Zvonar A, Kristl J, Kerc J, Grabnar PA. High celecoxib-loaded nanoparticles prepared by a vibrating nozzle device. *Journal of Microencapsulation*. 2009;26(8):748–59.

[251] Sharpe LA, Daily AM, Horava SD, Peppas NA. Therapeutic applications of hydrogels in oral drug delivery. *Expert Opinion on Drug Delivery*. 2014;11(6):901–15.

[252] Peppas NA, Bures P, Leobandung W, Ichikawa H. Hydrogels in pharmaceutical formulations. *European Journal of Pharmaceutics and Biopharmaceutics*. 2000;50:27–46.

[253] Hoffman AS. Hydrogels for biomedical applications. *Advanced Drug Delivery Reviews*. 2012;64:18–23.

[254] Soppimath KS, Aminabhavi TM, Dave AM, Kumbar SG, Rudzinski WE. Stimulus-responsive "smart" hydrogels as novel drug delivery systems. *Drug Development and Industrial Pharmacy*. 2002;28(8):957–74.

[255] Hennink WE, van Nostrum CF. Novel crosslinking methods to design hydrogels. *Advanced Drug Delivery Reviews*. 2002;54(1):13–36.

[256] De Prisco A, Maresca D, Ongeng D, Mauriello G. Microencapsulation by vibrating technology of the probiotic strain Lactobacillus reuteri DSM 17938 to enhance its survival in foods and in gastrointestinal environment. *LWT - Food Science and Technology*. 2015;61(2):452–62.

[257] Del Gaudio P, Auriemma G, Russo P, Mencherini T, Campiglia P, Stigliani M, Aquino RP. Novel co-axial prilling technique for the development of core-shell particles as delayed drug delivery systems. *European Journal of Pharmaceutics and Biopharmaceutics*. 2014;87(3):541–7.

[258] Chan LW, Jin Y, Heng PWS. Cross-linking mechanisms of calcium and zinc in production of alginate microspheres. *International Journal of Pharmaceutics*. 2002;242:255–8.

[259] Aslani P, Kennedy RA. Studies on diffusion in alginate gels. I. Effect of cross-linking with calcium or zinc ions on diffusion of acetaminophen. *Journal of Controlled Release*. 1996;42(1996):75–82.

[260] Blandino A, Macías M, Cantero D. Formation of calcium alginate gel capsules: Influence of sodium alginate and CaCl2 concentration on gelation kinetics. *Journal of Bioscience and Bioengineering*. 1999;88(6):686–9.

[261] Lee KY, Mooney DJ. Alginate: Properties and biomedical applications. *Progress in Polymer Science*. 2012;37(1):106–26.

[262] Gombotz WR, Wee SF. Protein release from alginate matrices. *Advanced Drug Delivery Reviews*. 2012;64:194–205.

[263] Liu P, Krishnan TR. Alginate-pectin-poly-L-lysine particulate as a potential controlled release formulation. *Journal of Pharmacy and Pharmacology*. 1999;51:141–9.

[264] Rasmussen MR, Snabe T, Pedersen LH. Numerical modelling of insulin and amyloglucosidase release from swelling Ca-alginate beads. *Journal of Controlled Release*. 2003;91:395–405.

[265] Yang JS, Xie YJ, He W. Research progress on chemical modification of alginate: A review. *Carbohydrate Polymers*. 2011;84(1):33–9.

[266] Pawar SN, Edgar KJ. Alginate derivatization: A review of chemistry, properties and applications. *Biomaterials*. 2012;33(11):3279–305.

[267] Martinez L, Agnely F, Bettini R, Besnard M, Colombo P, Couarraze G. Preparation and characterization of chitosan based micro networks: Transposition to a prilling process. *Journal of Applied Polymer Science*. 2004;93(6):2550–8.

[268] Sinha VR, Singla AK, Wadhawan S, Kaushik R, Kumria R, Bansal K, Dhawan S. Chitosan microspheres as a potential carrier for drugs. *International Journal of Pharmaceutics*. 2004;274(1-2):1–33.

[269] Varshosaz J. The promise of chitosan microspheres in drug delivery systems. *Expert Opinion on Drug Delivery*. 2007;4(3):263–73.

[270] Fan W, Yan W, Xu Z, Ni H. Formation mechanism of monodisperse, low molecular weight chitosan nanoparticles by ionic gelation technique. *Colloids and Surfaces B: Biointerfaces*. 2012;90:21–7.

[271] Calvo P, Remuñán-López C, Vila-Jato JL, Alonso MJ. Novel Hydrophilic Chitosan – Polyethylene Oxide Nanoparticles as Protein Carriers. *Journal of Applied Polymer Science*. 1997;63:125–32.

[272] Takeuchi H, Yamamoto H, Kawashima Y. Mucoadhesive nanoparticulate systems for peptide drug delivery. *Advanced Drug Delivery Reviews*. 2001;47(1):39–54.

[273] He P, Davis SS, Illum L. In vitro evaluation of the mucoadhesive properties of chitosan microspheres. *International Journal of Pharmaceutics*. 1998;166(1):75–88.

[274] Riva R, Ragelle H, Des Rieux A, Duhem N, Jérôme C, Préat V. Chitosan and chitosan derivatives in drug delivery and tissue engineering. *Advances in Polymer Science*. 2011;244(1):19–44.

[275] Bansal V, Sharma PK, Sharma N, Pal OP, Malviya R. Applications of Chitosan and Chitosan Derivatives in Drug Delivery. *Biological Research*. 2011;5(1):28–37.

[276] Bernkop-Schnürch A. Chitosan and its derivatives: Potential excipients for peroral peptide delivery systems. *International Journal of Pharmaceutics*. 2000;194:1–13.

[277] Mourya VK, Inamdar NN, Tiwari A. Carboxymethyl chitosan and its applications. *Advanced Materials Letters*. 2010;1(1):11–33.

[278] Mourya VK, Inamdar NN. Trimethyl chitosan and its applications in drug delivery. *Journal of Materials Science Materials in Medicine*. 2009;20(5):1057–79.

[279] Upadhyaya L, Singh J, Agarwal V, Tewari RP. The implications of recent advances in carboxymethyl chitosan based targeted drug delivery and tissue engineering applications. *Journal of Controlled Release*. 2014;186:54–87.

[280] Chen F, Zhang ZR, Yuan F, Qin X, Wang M, Huang Y. In vitro and in vivo study of N-trimethyl chitosan nanoparticles for oral protein delivery. *International Journal of Pharmaceutics*. 2008;349:226–33.

[281] El-Sherbiny IM. Synthesis, characterization and metal uptake capacity of a new carboxymethyl chitosan derivative. *European Polymer Journal*. 2009;45(1):199–210.

[282] Patil RT, Speaker TJ. Water-based microsphere delivery system for proteins. *Journal of Pharmaceutical Sciences*. 2000;89(1):9–15.

[283] Morris ER, Nishinari K, Rinaudo M. Gelation of gellan - A review. *Food Hydrocolloids*. 2012;28(2):373–411.

[284] Saigal N, Baboota S, Ahuja A, Ali J. Multiple-pulse drug delivery systems: setting a new paradigm for infectious disease therapy. *Expert Opinion on Drug Delivery*. 2009;6(4):441–52.

[285] Del Curto MD, Maroni A, Palugan L, Zema L, Gazzaniga A, Sangalli ME. Oral Delivery System for Two-pulse Colonic Release of Protein Drugs and Protease Inhibitor/Absorption Enhancer Compounds. *Journal of Pharmaceutical Sciences*. 2011;100(8):3251–9.

[286] Costa RR, Castro E, Arias FJ, Rodríguez-Cabello JC, Mano JF. Multifunctional compartmentalized capsules with a hierarchical organization from the nano to the macro scales. *Biomacromolecules*. 2013;14:2403–10.

[287] Gazzaniga A, Sangalli ME, Giordano F. Oral Chronotopic® drug delivery systems: achievement of time and/or site specificity. *European Journal of Pharmaceutics and Biopharmaceutics*. 1994;40(4):246–50.

[288] Amidon GL, Leesman GD, Sherman LB. Plug releasable upon application of pressure from inner chamber. United States; 5387421 A, 1995.

[289] Crison JR, Amidon GL. Method for making a multi-stage drug delivery system. United States; 5976571 A, 1995.

[290] Rathbone MJ, Hadgraft J, Roberts MS, Lane ME, editors. Modified-release drug delivery technology, Volume 1. 2nd ed. London: Informa Healthcare; 2008.

[291] Rathbone MJ, Hadgraft J, Roberts ME, Lane ME, editors. Modified-release drug delivery technology, Volume 2. 2nd ed. London: Informa Healthcare; 2008.

[292] Wilson CG, Crowley PJ, editors. Controlled release in oral drug delivery. New York: Springer; 2011.

[293] Iannuccelli V, Coppi G, Bernabei MT, Cameroni R. Air compartment multiple-unit system for prolonged gastric residence. Part I. Formulation study. *International Journal of Pharmaceutics*. 1998;174:47–54.

[294] Iannuccelli V, Coppi G, Sansone R, Ferolla G. Air compartment multiple-unit system for prolonged gastric residence. Part II. In vivo evaluation. *International Journal of Pharmaceutics*. 1998;174:55–62.

[295] Xie H, She ZG, Wang S, Sharma G, Smith JW. One-step fabrication of polymeric Janus nanoparticles for drug delivery. *Langmuir*. 2012;28:4459–63.

[296] Lahann J. Recent progress in nano-biotechnology: Compartmentalized micro- and nanoparticles via electrohydrodynamic co-jetting. *Small*. 2011;7:1149–56.

[297] Hwang S, Lahann J. Differentially degradable Janus particles for controlled release applications. *Macromolecular Rapid Communications*. 2012;33(14):1178–83.

[298] Rahmani S, Park TH, Dishman AF, Lahann J. Multimodal delivery of irinotecan from microparticles with two distinct compartments. *Journal of Controlled Release*. 2013;172(1):239–45.

[299] Pan J, Wen M, Yin D, Jiang B, He D, Guo L. Design and synthesis of novel amphiphilic Janus dendrimers for bone-targeted drug delivery. *Tetrahedron*. 2012;68(14):2943–9.

[300] Li X, Zhou L, Wei Y, El-toni AM, Zhang F, Zhao D. Anisotropic Growth-Induced Synthesis of Dual-Compartment Janus Mesoporous Silica Nanoparticles for Bimodal Triggered Drugs Delivery. *Journal of American Chemical Society*. 2014;136(42):15086–92.

[301] Misra AC, Bhaskar S, Clay N, Lahann J. Multicompartmental particles for combined imaging and siRNA delivery. *Advanced Materials*. 2012;24(28):3850–6.

[302] Yoon J, Lee KJ, Lahann J. Multifunctional polymer particles with distinct compartments. *Journal of Materials Chemistry*. 2011;21:8502.

[303] Kisak ET, Coldren B, Evans CA, Boyer C, Zasadzinski JA. The vesosome - a multicompartment drug delivery vehicle. *Current Medicinal Chemistry*. 2004;11:199–219.

[304] Paleos CM, Tsiourvas D, Sideratou Z, Pantos A. Formation of artificial multicompartment vesosome and dendrosome as prospected drug and gene delivery carriers. *Journal of Controlled Release*. 2013;170(1):141–52.

[305] Boyer C, Zasadzinski JA. Multiple lipid compartments slow vesicle contents release in lipases and serum. *ACS Nano*. 2007;1(3):176–82.

[306] Balasubramanian V, Onaca O, Enea R, Hughes DW, Palivan CG. Protein delivery: from conventional drug delivery carriers to polymeric nanoreactors. *Expert Opinion on Drug Delivery*. 2010;7(1):63–78.

[307] De Hoog H-PM, Nallani M, Tomczak N. Self-assembled architectures with multiple aqueous compartments. *Soft Matter*. 2012;8(17):4552–61.

[308] Marguet M, Bonduelle C, Lecommandoux S. Multicompartmentalized polymeric systems: towards biomimetic cellular structure and function. *Chemical Society Reviews*. 2013;42(2):512–29.

[309] Attarwala H, Amiji M. Multi-compartmental nanoparticles-in-emulsion formulation for macrophage-specific anti-inflammatory gene delivery. *Pharmaceutical Research*. 2012;29:1637–49.

[310] Shahiwala A, Amiji MM. Enhanced mucosal and systemic immune response with squalane oil-containing multiple emulsions upon intranasal and oral administration in mice. *Journal of Drug Targeting*. 2008;16(4):302–10.

[311] Bhavsar MD, Tiwari SB, Amiji MM. Formulation optimization for the nanoparticles-in-microsphere hybrid oral delivery system using factorial design. *Journal of Controlled Release*. 2006;110:422–30.

[312] Bhavsar MD, Amiji MM. Gastrointestinal distribution and in vivo gene transfection studies with nanoparticles-in-microsphere oral system (NiMOS). *Journal of Controlled Release*. 2007;119:339–48.

[313] Bhavsar MD, Amiji MM. Development of novel biodegradable polymeric nanoparticles-in-microsphere formulation for local plasmid DNA delivery in the gastrointestinal tract. *AAPS PharmSciTech*. 2008;9(1):288–94.

[314] Kriegel C, Attarwala H, Amiji M. Multi-compartmental oral delivery systems for nucleic acid therapy in the gastrointestinal tract. *Advanced Drug Delivery Reviews*. 2013;65(6):891–901.

[315] Kaye SR, Purewal TS, Alpar HO. Simultaneously manufactured nano-in-micro (SIMANIM) particles for dry-powder modified-release delivery of antibodies. *Journal of Pharmaceutical Sciences*. 2009;98(11):4055–68.

[316] Jabr-Milane L, van Vlerken L, Devalapally H, Shenoy D, Komareddy S, Bhavsar M, Amiji M. Multi-functional nanocarriers for targeted delivery of drugs and genes. *Journal of Controlled Release*. 2008;130(2):121–8.

[317] Plapied L, Duhem N, des Rieux A, Préat V. Fate of polymeric nanocarriers for oral drug delivery. *Current Opinion in Colloid and Interface Science*. 2011;16(3):228–37.

[318] Bakhru SH, Furtado S, Morello AP, Mathiowitz E. Oral delivery of proteins by biodegradable nanoparticles. *Advanced Drug Delivery Reviews*. 2013;65(6):811–21.

[319] Coco R, Plapied L, Pourcelle V, Jérôme C, Brayden DJ, Schneider YJ, Préat V. Drug delivery to inflamed colon by nanoparticles: Comparison of different strategies. *International Journal of Pharmaceutics*. 2013;440(1):3–12.

[320] Smart SK, Cassady AI, Lu GQ, Martin DJ. The biocompatibility of carbon nanotubes. *Carbon*. 2006;44:1034–47.

[321] Lvov Y, Abdullayev E. Functional polymer-clay nanotube composites with sustained release of chemical agents. *Progress in Polymer Science*. 2013;38(10-11):1690–719.

[322] Liu M, Jia Z, Jia D, Zhou C. Recent advance in research on halloysite nanotubes-polymer nanocomposite. *Progress in Polymer Science*. 2014;39(8):1498–525.

[323] Abdullayev E, Lvov Y. Halloysite clay nanotubes as a ceramic "skeleton" for functional biopolymer composites with sustained drug release. *Journal of Materials Chemistry B*. 2013;1(23):2894–903.

[324] Anthony JW, Bideaux RA, Bladh KW, Nichols MC. Handbook of mineralogy, Silica, Silicates, Volume 2. Tucson: Mineral Data Publishing; 1995. 904 p.

[325] White RD, Bavykin D V., Walsh FC. The stability of halloysite nanotubes in acidic and alkaline aqueous suspensions. *Nanotechnology*. 2012;23(6):065705.

[326] Joussein E, Petit S, Churchman J, Theng B, Righi D, Delvaux B. Halloysite clay minerals – a review. *Clay Minerals*. 2005;40(4):383–426.

[327] Pasbakhsh P, Churchman GJ, Keeling JL. Characterisation of properties of various halloysites relevant to their use as nanotubes and microfibre fillers. *Applied Clay Science*. 2013;74:47–57.

[328] Price RR, Gaber BP, Lvov Y. In-vitro release characteristics of tetracycline HCl, khellin and nicotinamide adenine dineculeotide from halloysite; a cylindrical mineral. *Journal of Microencapsulation*. 2001;18(6):713–22.

[329] Kelly HM, Deasy PB, Ziaka E, Claffey N. Formulation and preliminary in vivo dog studies of a novel drug delivery system for the treatment of periodontitis. *International Journal of Pharmaceutics*. 2004;274(1-2):167–83.

[330] Levis SR, Deasy PB. Characterisation of halloysite for use as a microtubular drug delivery system. *International Journal of Pharmaceutics*. 2002;243(1-2):125–34.

[331] Veerabadran NG, Price RR, Lvov YM. Clay Nanotubes for Encapsulation and Sustained Release of Drugs. *Nano*. 2007;02(02):115–20.

[332] Levis SR, Deasy PB. Use of coated microtubular halloysite for the sustained release of diltiazem hydrochloride and propranolol hydrochloride. *International Journal of Pharmaceutics*. 2003;253(1-2):145–57.

[333] Yuan P, Southon PD, Liu Z, Kepert CJ. Organosilane functionalization of halloysite nanotubes for enhanced loading and controlled release. *Nanotechnology*. 2012;23(37):375705.

[334] Fan L, Zhang J, Wang A. In situ generation of sodium alginate/hydroxyapatite/halloysite nanotubes nanocomposite hydrogel beads as drug-controlled release matrices. *Journal of Materials Chemistry B*. 2013;1(45):6261.

[335] Cornejo-Garrido H, Nieto-Camacho A, Gómez-Vidales V, Ramírez-Apan MT, del Angel P, Montoya JA, Domínguez-López M, Kibanova D, Cervini-Silva J. The anti-inflammatory properties of halloysite. *Applied Clay Science*. 2012;57:10–6.

[336] Liu M, Zhang Y, Wu C, Xiong S, Zhou C. Chitosan/halloysite nanotubes bionanocomposites: structure, mechanical properties and biocompatibility. *International journal of biological macromolecules*. 2012;51(4):566–75.

[337] Chiew CSC, Poh PE, Pasbakhsh P, Tey BT, Yeoh HK, Chan ES. Physicochemical characterization of halloysite / alginate bionanocomposite hydrogel. *Applied Clay Science*. 2014;101:444–54.

[338] Chao C, Zhang B, Zhai R, Xiang X, Liu J, Chen R. Natural nanotube-based biomimetic porous microspheres for significantly enhanced biomolecule immobilization. *ACS Sustainable Chemistry and Engineering*. 2014;2:396–403.

[339] Abdullayev E, Joshi A, Wei W, Zhao Y, Lvov Y. Enlargement of halloysite clay nanotube lumen by selective etching of aluminum oxide. *ACS Nano*. 2012;6(8):7216–26.

[340] Wang Q, Zhang J, Wang A. Alkali activation of halloysite for adsorption and release of ofloxacin. *Applied Surface Science*. 2013;287:54–61.

[341] Guo M, Wang A, Muhammad F, Qi W, Ren H, Guo Y, Zhu G. Halloysite Nanotubes, a Multifunctional Nanovehicle for Anticancer Drug Delivery. *Chinese Journal of Chemistry*. 2012;30(9):2115–20.

[342] Zhai R, Zhang B, Wan Y, Li C, Wang J, Liu J. Chitosan–halloysite hybrid-nanotubes: Horseradish peroxidase immobilization and applications in phenol removal. *Chemical Engineering Journal*. 2013;214:304–9.

[343] Shamsi MH, Geckeler KE. The first biopolymer-wrapped non-carbon nanotubes. *Nanotechnology*. 2008;19(7):075604.

[344] Gustafsson JP. The surface chemistry of imogolite. *Clays and Clay Minerals*. 2001;49(1):73–80.

[345] Woodcock J. The concept of pharmaceutical quality. *American Pharmaceutical Review*. 2004;(November-December):1–3.

[346] Yu LX, Amidon G, Khan M a, Hoag SW, Polli J, Raju GK, Woodcock J. Understanding pharmaceutical quality by design. *AAPS Journal*. 2014;16(4):771–83.

[347] Juran JM. Juran on quality by design, The new steps for planning quality into goods and service. New York: Simon and Schuster; 1992.

[348] Singh B, Kapil R, Nandi M, Ahuja N. Developing oral drug delivery systems using formulation by design: vital precepts, retrospect and prospects. *Expert Opinion on Drug Delivery*. 2011;8(10):1341–60.

[349] Huang J, Kaul G, Cai C, Chatlapalli R, Hernandez-Abad P, Ghosh K, Nagi A. Quality by design case study: An integrated multivariate approach to drug product and process development. *International Journal of Pharmaceutics*. 2009;382:23–32.

[350] Huang J, Goolcharran C, Ghosh K. A Quality by Design approach to investigate tablet dissolution

shift upon accelerated stability by multivariate methods. *European Journal of Pharmaceutics and Biopharmaceutics*. 2011;78(1):141–50.

[351] Charoo NA, Shamsher AAA, Zidan AS, Rahman Z. Quality by design approach for formulation development: A case study of dispersible tablets. *International Journal of Pharmaceutics*. 2012;423(2):167–78.

[352] Verma S, Lan Y, Gokhale R, Burgess DJ. Quality by design approach to understand the process of nanosuspension preparation. *International Journal of Pharmaceutics*. 2009;377:185–98.

[353] Wu H, White M, Khan MA. Quality-by-Design (QbD): An integrated process analytical technology (PAT) approach for a dynamic pharmaceutical co-precipitation process characterization and process design space development. *International Journal of Pharmaceutics*. 2011;405(1-2):63–78.

[354] Rathore AS. Roadmap for implementation of quality by design (QbD) for biotechnology products. *Trends in Biotechnology*. 2009;27:546–53.

[355] Dhawan S, Kapil R, Singh B. Formulation development and systematic optimization of solid lipid nanoparticles of quercetin for improved brain delivery. *Journal of Pharmacy and Pharmacology*. 2011;63:342–51.

[356] Xu X, Khan MA, Burgess DJ. A quality by design (QbD) case study on liposomes containing hydrophilic API: I. Formulation, processing design and risk assessment. *International Journal of Pharmaceutics*. 2011;419(1-2):52–9.

[357] Xu X, Khan MA, Burgess DJ. A quality by design (QbD) case study on liposomes containing hydrophilic API: II. Screening of critical variables, and establishment of design space at laboratory scale. *International Journal of Pharmaceutics*. 2012;423(2):543–53.

[358] Xu X, Costa AP, Khan MA, Burgess DJ. Application of quality by design to formulation and processing of protein liposomes. *International Journal of Pharmaceutics*. 2012;434(1-2):349–59.

[359] Pund S, Shete Y, Jagadale S. Multivariate analysis of physicochemical characteristics of lipid based nanoemulsifying cilostazol-Quality by design. *Colloids and Surfaces B: Biointerfaces*. 2014;115:29–36.

[360] Pawar YB, Purohit H, Valicherla GR, Munjal B, Lale S V., Patel SB, Bansal AK. Novel lipid based oral formulation of curcumin: Development and optimization by design of experiments approach. *International Journal of Pharmaceutics*. 2012;436(1-2):617–23.

[361] Patil H, Feng X, Ye X, Majumdar S, Repka MA. Continuous production of fenofibrate solid lipid nanoparticles by hot-melt extrusion technology: a systematic study based on a quality by design approach. *AAPS Journal*. 2015;17(1):194–205.

[362] Beg S, Sandhu PS, Batra RS, Khurana RK, Singh B. QbD-based systematic development of novel optimized solid self-nanoemulsifying drug delivery systems (SNEDDS) of lovastatin with enhanced biopharmaceutical performance. *Drug Delivery*. 2014;7544:1–20.

[363] Singh B, Singh R, Bandyopadhyay S, Kapil R, Garg B. Optimized nanoemulsifying systems with enhanced bioavailability of carvedilol. *Colloids and Surfaces B: Biointerfaces*. 2013;101:465–74.

[364] Singh B, Dahiya M, Saharan V, Ahuja N. Optimizing drug delivery systems using systematic "design of experiments". Part II: retrospect and prospects. *Critical Reviews in Therapeutic Drug Carrier Systems*. 2005;22(3):215–94.

[365] Lewis GA, Mathieu D, Phan-Tan-Luu R. Pharmaceutical Experimental Design. 1st ed. New York: Marcel Dekker; 1999.

[366] Shek E, Ghani M, Jones RE. Simplex search in optimisation of capsule formulation. *Journal of Pharmaceutical Sciences*. 1980;69(10):1135–42.

[367] Fonner DEJ, Buck JR, Banker GS. Mathematical optimization techniques in drug product design and process analysis. *Journal of Pharmaceutical Sciences*. 1970;59(11):1587–96.

[368] Doornbos DA. Optimisation in pharmaceutical sciences. *Pharmaceutisch Weekblad, Scientific Edition*. 1981;3:33–61.

[369] Haaland PD. Experimental design in biotechnology. Boca Raton: CRC Press; 1989.

[370] Fisher RA. Statistical methods for research workers. Edinbourgh: Oliver and Boyd; 1925.

[371] Bolton S, Bon C. Factorial designs. Pharmaceutical Statistics: Practical and Clinical Applications. 4th ed. New York: Marcel Dekker; 2004. p. 265–88.

[372] Plackett RL, Burman JP. The design of optimum multifactorial experiments. *Biometrica*. 1946;33:305–25.

[373] Box GEP, Wilson KB. On the experimental attainment of optimum conditions. *Journal of the Royal Statistical Society: Series B*. 1951;13:1–45.

[374] Box GEP, Behnken DW. Some new three-level designs for the study of quantitative variables. *Technometrics*. 1960;2:455–75.

[375] Lewis GA, Chariot M. Non-classical experimental designs in pharmaceutical formulations. *Drug Development and Industrial Pharmacy*. 1991;17:1551–70.

[376] Smith WF. Experimental design for formulation. Philadelphia: SIAM; 2005.

[377] Bolton S, Bon C. Linear regression and correlation. Pharmaceutical Statistics: Practical and Clinical Applications. 4th ed. New York: Marcel Dekker; 2004. p. 173–214.

[378] Myers RH. Classical and modern regression with applications. Boston: PWS-KENT Publishing; 1990.

[379] Jolliffe IT. Principal components analysis. 2nd ed. New York: Springer; 2002. 167-198 p.

[380] Wold S, Sjöström M, Eriksson L. PLS-regression: A basic tool of chemometrics. *Chemometrics and Intelligent Laboratory Systems*. 2001;58:109–30.

[381] Sun Y, Peng Y, Chen Y, Shukla AJ. Application of artificial neural networks in the design of controlled release drug delivery systems. *Advanced Drug Delivery Reviews*. 2003;55:1201–15.

[382] Takayama K, Fujikawa M, Obata Y, Morishita M. Neural network based optimization of drug formulations. *Advanced Drug Delivery Reviews*. 2003;55:1217–31.

[383] Boh R, Kardos D. Microcapsule patents and products: innovation and trend analysis. In: Arshady R, Boh B, editors. The MML Series Volume 6: Microcapsule patents and products. London: Citus Books; 2003. p. 47–83.

[384] Dai C, Wang B, Zhao H. Microencapsulation peptide and protein drugs delivery system. *Colloids and Surfaces B: Biointerfaces*. 2005;41(2-3):117–20.

[385] Yang S, Yuan W, Jin T. Formulating protein therapeutics into particulate forms. *Expert Opinion on Drug Delivery*. 2009;6(10):1123–33.

[386] Jain RA. The manufacturing techniques of various drug loaded biodegradable poly(lactide-co-glycolide) (PLGA). *Biomaterials*. 2000;21(23):2475–90.

[387] Vehring R. Pharmaceutical particle engineering via spray drying. *Pharmaceutical Research*. 2008;25(5):999–1022.

[388] Amsden B. The production of uniformly sized polymer microspheres. *Pharmaceutical Research*. 1999;16(7):1140–3.

[389] Lima AC, Sher P, Mano JF. Production methodologies of polymeric and hydrogel particles for drug delivery applications. *Expert Opinion on Drug Delivery*. 2012;9(2):231–48.

[390] Hulst AC, Tramper J, van't Riet J, Wasterbeek MM. A new technique for the production of immobilized biocatalyst in large quantities. *Biotechnology and Bioengineering*. 1985;27(6):870–6.

[391] Auriemma G, Del Gaudio P, Barba AA, D'Amore M, Aquino RP. A combined technique based on prilling and microwave assisted treatments for the production of ketoprofen controlled release dosage forms. *International Journal of Pharmaceutics*. 2011;415(1-2):196–205.

[392] Zvonar A, Bolko K, Gašperlin M. Microencapsulation of self-microemulsifying systems: Optimization of shell-formation phase and hardening process. *International Journal of Pharmaceutics*. 2012;437(1-2):294–302.

[393] Dash M, Chiellini F, Ottenbrite RM, Chiellini E. Chitosan—A versatile semi-synthetic polymer in biomedical applications. *Progress in Polymer Science*. 2011;36(8):981–1014.

[394] Sayin B, Somavarapu S, Li XW, Sesardic D, Senel S, Alpar OH. TMC-MCC (N-trimethyl chitosan-mono-N-carboxymethyl chitosan) nanocomplexes for mucosal delivery of vaccines. *European Journal of Pharmaceutical Sciences*. 2009;38(4):362–9.

[395] Alamelu S, Rao KP. Studies on the carboxymethyl chitosan-containing liposomes for their stability and controlled release of dapsone. *Journal of Microencapsulation*. 1991;8(4):505–19.

[396] Di Colo G, Zambito Y, Zaino C. Polymeric Enhancers of Mucosal Epithelia Permeability: Synthesis, Transepithelial Penetration-Enhancing Properties, Mechanism of Action, Safety Issues. *Journal of Pharmaceutical Sciences*. 2008;97(5):1652–80.

[397] Liu Z, Jiao Y, Zhang Z. Calcium-carboxymethyl chitosan hydrogel beads for protein drug delivery system. *Journal of Applied Polymer Science*. 2007;103(5):3164–8.

[398] Bravo R, Varum F, de Kruif JK, Kuentz M. Multiparticulate drug delivery system. Europe; 13192657.8-1455, 2013.

[399] Lowry OH, Rosebrough NJ, Farr AL, Randall RJ. Protein measurement with the Folin phenol

reagent. *Journal of Biological Chemistry*. 1951;193:265–75.

[400] Peterson GL. Review of the Folin phenol protein quantitation method of Lowry, Rosebrough, Farr, and Randall. *Analytical Biochemistry*. 1979;100(2):201–20.

[401] Brown RE, Jarvis KL, Hyland KJ. Protein measurement using bicinchoninic acid: elimination of interfering substances. *Analytical Biochemistry*. 1989;180(1):136–9.

[402] Kessler RJ, Fanestil DD. Interference by lipids in the determination of protein using bicinchoninic acid. *Analytical Biochemistry*. 1986;159(1):138–42.

[403] Smith PK, Krohn RI, Hermanson GT, Mallia AK, Gartner FH, Provenzano MD, Fujimoto EK, Goeke NM, Olson BJ, Klenk DC. Measurement of protein using bicinchoninic acid. *Analytical Biochemistry*. 1985;150(1):76–85.

[404] Wiechelman KJ, Braun RD, Fitzpatrick JD. Investigation of the bicinchoninic acid protein assay: identification of the groups responsible for color formation. *Analytical Biochemistry*. 1988;175(1):231–7.

[405] Liu R, Qin P, Wang L, Zhao X, Liu Y, Hao X. Toxic effects of ethanol on bovine serum albumin. *J Biochem Mol Toxicol*. 2010;24(1):66–71.

[406] Peters TJ. Serum albumin. *Advances in Protein Chemistry*. 1985;37:161–245.

[407] Togashi DM, Ryder AG, O'Shaughnessy D. Monitoring local unfolding of bovine serum albumin during denaturation using steady-state and time-resolved fluorescence spectroscopy. *Journal of Fluorescence*. 2010;20(2):441–52.

[408] Lee H-H, Park O-J, Park JM, Yang J-W. Continuous Production of Uniform Calcium Alginate Beads by Sound Wave Induced Vibration. *Journal of Chemical Technology & Biotechnology*. 1996;67(3):255–9.

[409] Mouritsen OG. Life is a matter of fat, The emerging science of lipidomics. Heidelberg: Springer; 2005. 66-71 p.

[410] Guvendiren M, Burdick JA, Yang S. Solvent induced transition from wrinkles to creases in thin film gels with depth-wise crosslinking gradients. *Soft Matter*. 2010;6(22):5795–801.

[411] Sano M, Hosoya O, Taoka S, Kawaguchi T, Sugibayashi K, Juni K, Morimoto Y. Relationship between solubility of chitosan in alcoholic solution and its gelation. *Chemical and Pharmaceutical Bulletin*. 1999;47(7):1044–6.

[412] Ge S, Kojio K, Takahara A, Kajiyama T. Bovine serum albumin adsorption onto immobilized organotrichlorosilane surface: Influence of the phase separation on protein adsorption patterns. *Journal of Biomaterials Science, Polymer Edition*. 1998;9(2):131–50.

[413] Pace CN, Treviño S, Prabhakaran E, Scholtz JM. Protein structure, stability and solubility in water and other solvents. *Philosophical Transactions of the Royal Society of London Series B, Biological Sciences*. 2004;359(1448):1225–34; discussion 1234–5.

[414] Tanaka S, Oda Y, Ataka M, Onuma K, Fujiwara S, Yonezawa Y. Denaturation and aggregation of hen egg lysozyme in aqueous ethanol solution studied by dynamic light scattering. *Biopolymers*. 2001;59(5):370–9.

[415] Thomas PD, Dill KA. Local and nonlocal interactions in globular proteins and mechanisms of alcohol denaturation. *Protein Science: a publication of the Protein Society*. 1993;2(12):2050–65.

[416] Pace CN, Marshall HFJ. A comparison of the effectiveness of protein denaturants for beta-lactoglobulin and ribonuclease. *Archives of Biochemistry and Biophysics*. 1980;

[417] Ubaidulla U, Khar RK, Ahmad FJ, Sultana Y, Panda AK. Development and characterization of chitosan succinate microspheres for the improved oral bioavailability of insulin. *Journal of Pharmaceutical Sciences*. 2007;96(11):3010–23.

[418] Refsgaard HH, Tsai L, Stadtman ER. Modifications of proteins by polyunsaturated fatty acid peroxidation products. *Proceedings of the National Academy of Sciences of the United States of America*. 2000;97(2):611–6.

[419] Uchida K, Sakai K, Itakura K, Osawa T, Toyokuni S. Protein modification by lipid peroxidation products: formation of malondialdehyde-derived N(epsilon)-(2-propenol)lysine in proteins. *Archives of Biochemistry and Biophysics*. 1997;346(1):45–52.

[420] Pace CN, Scholtz JM. A helix propensity scale based on experimental studies of peptides and proteins. *Biophysical Journal*. 1998;75(1):422–7.

[421] Pajot P. Fluorescence of Proteins in 6 M Guanidine Hydrochloride, A method for the quantitative determination of tryptophan. *European Journal of Biochemistry*. 1976;63(1):263–9.

[422] Quiming NS, Vergel B, Nicolas G, Villanueva JA. Interaction of bovine serum albumin and

metallothionein. *Journal of Health Sciences*. 2005;51(1):8–15.

[423] Kumar TR, Soppimath K, Nachaegari SK. Novel delivery technologies for protein and peptide therapeutics. *Current Pharmaceutical Biotechnology*. 2006;7:261–76.

[424] Singh R, Singh S, Lilliard JW. Past, present, and future technologies for oral delivery of therapeutic proteins. *Journal of Pharmaceutical Sciences*. 2008;97:2497–523.

[425] Anal AK, Tuladhar A. Biopolymeric micro- and nanoparticles: preparation, characterization and industrial applications. *Advances in Polymer Science*. 2013;254:269–96.

[426] De Kruif JK, Varum FJO, Bravo R, Kuentz M. A systematic study on manufacturing of prilled microgels into lipids for oral protein delivery. *Journal of Pharmaceutical Sciences*. 2015;

[427] Machado AHE, Lundberg D, Ribeiro A, Veiga JB, Miguel MG, Lindman B, Olsson U. Encapsulation of DNA in Macroscopic and Nanosized Calcium Alginate Gel Particles Encapsulation of DNA in Macroscopic and Nanosized Calcium Alginate Gel Particles. *Langmuir*. 2013;29(51):15926–35.

[428] Laroui H, Theiss AL, Yan Y, Dalmasso G, Nguyen HTT, Sitaraman S V., Merlin D. Functional TNF-alpha gene silencing mediated by polyethyleneimine/TNF-alpha siRNA nanocomplexes in inflamed colon. *Biomaterials*. 2011;32(4):1218–28.

[429] Bianco A, Kostarelos K, Prato M. Applications of carbon nanotubes in drug delivery. *Current Opinion in Chemical Biology*. 2005;9:674–9.

[430] Lai X, Agarwal M, Lvov YM, Pachpande C, Varahramyan K, Witzmann FA. Proteomic profiling of halloysite clay nanotube exposure in intestinal cell co-culture. *Journal of Applied Toxicology*. 2013;33(11):1316–29.

[431] Vergaro V, Abdullayev E, Lvov YM, Zeitoun A, Cingolani R, Rinaldi R, Leporatti S. Cytocompatibility and uptake of halloysite clay nanotubes. *Biomacromolecules*. 2010;11(3):820–6.

[432] Byrne RS, Deasy PB. Use of porous aluminosilicate pellets for drug delivery. *Journal of Microencapsulation*. 2005;22(4):423–37.

[433] Engqvist KAN, Strømme M, Bredenberg S, Forsgren J, Ja E. A Ceramic Drug Delivery Vehicle for Oral Administration of Highly Potent Opioids. 2010;99(1):219–26.

[434] Ghebaur A, Garea SA, Iovu H. New polymer-halloysite hybrid materials - potential controlled drug release system. *International Journal of Pharmaceutics*. 2012;436(1-2):568–73.

[435] Abdullayev E, Lvov Y. Clay nanotubes for corrosion inhibitor encapsulation: release control with end stoppers. *Journal of Materials Chemistry*. 2010;20:6681.

[436] Wang Q, Zhang J, Mu B, Fan L, Wang A. Facile preparation of magnetic 2-hydroxypropyltrimethyl ammonium chloride chitosan/Fe3O4/halloysite nanotubes microspheres for the controlled release of ofloxacin. *Carbohydrate Polymers*. 2014;102:877–83.

[437] Moore JW, Flanner HH. Mathematical comparison of dissolution profiles. *Pharmaceutical Technology*. 1996;20:60–74.

[438] Shah VP, Tsong Y, Sathe P, Liu JP. In vitro dissolution profile comparison- Statistics and analysis of the similarity factor, f2. *Pharmaceutical Research*. 1998;15:889–96.

[439] Costa P, Sousa Lobo JM. Modeling and comparison of dissolution profiles. *European Journal of Pharmaceutical Sciences*. 2001;13:123–33.

[440] Zhang Y, Huo M, Zhou J, Zou A, Li W, Yao C, Xie S. DDSolver: an add-in program for modeling and comparison of drug dissolution profiles. *AAPS Journal*. 2010;12(3):263–71.

[441] Böhm G, Muhr R, Jaenicke R. Quantitative analysis of protein far UV circular dichroism spectra by neural networks. *Protein engineering*. 1992;5(3):191–5.

[442] Schägger H, von Jagow G. Tricine-sodium dodecyl sulfate-polyacrylamide gel electrophoresis for the separation of proteins in the range from 1 to 100 kDa. *Analytical Biochemistry*. 1987;166:368–79.

[443] Halfman CJ, Nishida T. Influence of pH and electrolyte on the fluorescence of bovine serum albumin. *Biochimica et Biophysica Acta*. 1971;243:284–93.

[444] Squire PG, Moser P, O'Konski CT. The hydrodynamic properties of bovine serum albumin monomer and dimer. *Biochemistry*. 1968;7:4261–72.

[445] Wright AK, Thompson MR. Hydrodynamic structure of bovine serum albumin determined by transient electric birefringence. *Biophysical Journal*. 1975;15(3):137–41.

[446] De Kruif JK, Khoo J, Bravo R, Kuentz M. Novel Quality by Design Tools for Concentrated Drug Suspensions: Surface Energy Profiling and the Fractal Concept of Flocculation. *Journal of Pharmaceutical Sciences*. 2012;102(3):994–1007.

[447] Cavallaro G, Gianguzza A, Lazzara G, Milioto S, Piazzese D. Applied Clay Science Alginate gel beads fi lled with halloysite nanotubes. *Applied Clay Science*. 2012;72:132–7.

[448] Walsh KA. Trypsinogens and trypsins of various species. *Methods in Enzymology*. 1970;19:41–63.

[449] Weiner PK, Langridge R, Blaney JM, Schaefer R, Kollman PA. Electrostatic potential molecular surfaces. *Proceedings of the National Academy of Sciences of the United States of America*. 1982;79:3754–8.

[450] Rivera JG, Messersmith PB. Polydopamine-assisted immobilization of trypsin onto monolithic structures for protein digestion. *Journal of Separation Science*. 2012;35:1514–20.

[451] Vanea E, Simon V. XPS study of protein adsorption onto nanocrystalline aluminosilicate microparticles. *Applied Surface Science*. 2011;257(6):2346–52.

[452] Van der Lubben IM, Verhoef JC, Borchard G, Junginger HE. Chitosan and its derivatives in mucosal drug and vaccine delivery. *European Journal of Pharmaceutical Sciences*. 2001;14:201–7.

[453] Del Gaudio P, Russo P, Rosaria Lauro M, Colombo P, Aquino RP. Encapsulation of ketoprofen and ketoprofen lysinate by prilling for controlled drug release. *AAPS PharmSciTech*. 2009;10(4):1178–85.

[454] Foster JF. Some aspects of the structure and conformational properties of serum albumin. In: Rosenoer VM, Oratz M, Rothschild MA, editors. Albumin: Structure, Function and Uses. Oxford: Pergamon Press; 1977. p. 53–84.

[455] Mei X, Etzler FM, Wang Z. Use of texture analysis to study hydrophilic solvent effects on the mechanical properties of hard gelatin capsules. *International Journal of Pharmaceutics*. 2006;324(2):103–200.

[456] Timms RE. Heats of fusion of glycerides. *Chemistry and Physics of Lipids*. 1978;21(12):113–29.

[457] Moriyama Y, Watanabe E, Kobayashi K, Harano H, Inui E, Takeda K. Secondary structural change of bovine serum albumin in thermal denaturation up to 130 degrees C and protective effect of sodium dodecyl sulfate on the change. *The journal of physical chemistry B*. 2008;112:16585–9.

[458] Knothe G, Dunn RO. A comprehensive evaluation of the melting points of fatty acids and esters determined by differential scanning calorimetry. *Journal of the American Oil Chemists's Society*. 2009;112(51):16585–9.

[459] Sirois P. Feasibility assessment and considerations for scaling initial prototype lipid-based formulations to phase I/II clinical trial batches. In: Hauss DJ, editor. Oral lipid based formulations, Enhancing the bioavailability of poorly water-soluble drugs. New York: Informa Healthcare; 2007. p. 63–78.

[460] Moreton RC, Armstrong NA. The effect of film composition on the diffusion of ethanol through soft gelatin films. *International Journal of Pharmaceutics*. 1998;161:123–31.

[461] Chan ES, Lee BB, Ravindra P, Poncelet D. Prediction models for shape and size of ca-alginate macrobeads produced through extrusion-dripping method. *Journal of Colloid and Interface Science*. 2009;338(1):63–72.

[462] Chen J, Zhuang H, Zhao J, Gardella JA. Solvent effects on polymer surface structure. *Surface and Interface Analysis*. 2001;31:713–20.

[463] Miller-Chou BA, Koenig JL. A review of polymer dissolution. *Progress in Polymer Science*. 2003;28:1223–70.

[464] Dang QF, Zou SH, Chen XG, Liu CS, Li JJ, Zhou X, Liu Y, Cheng XJ. Characterization of chitosan-based highly porous hydrogel - the effects of the solvent. *Journal of Applied Polymer Science*. 2012;125:E88–98.

[465] Porter NA. Mechanisms for the Autoxidation of Polyunsaturated Lipids. *Accounts of Chemical Research*. 1986;19(12):262–8.

[466] Roubal WT, Tappel AL. Damage to proteins, enzymes, and amino acids by peroxidizing lipids. *Archives of Biochemistry and Biophysics*. 1966;113(1):58.

[467] Little C, O'Brien PJ. The effectiveness of a lipid peroxide in oxidizing protein and non-protein thiols. *The Biochemical Journal*. 1968;106:419–23.

[468] Sullivan DW, Gad SC, Julien M. A review of the nonclinical safety of Transcutol®, a highly purified form of diethylene glycol monoethyl ether (DEGEE) used as a pharmaceutical excipient. *Food and Chemical Toxicology*. 2014;72:40–50.

[469] Rothstein F. Differential precipitation of proteins: science and technology. In: Harrison R, editor.

Protein purification process engineering. New York: CRC Press; 1993. p. 115–208.

[470] Almeida AJ, Souto E. Solid lipid nanoparticles as a drug delivery system for peptides and proteins. *Advanced Drug Delivery Reviews*. 2007;59:478–90.

[471] Du AW, Stenzel MH. Drug carriers for the delivery of therapeutic peptides. *Biomacromolecules*. 2014;15:1097–114.

[472] Baier SK, Decker EA, McClements DJ. Impact of glycerol on thermostability and heat-induced gelation of bovine serum albumin. *Food Hydrocolloids*. 2004;18:91–100.

[473] Kattige A, Rowley G. Influence of rheological behaviour of particulate/polymer dispersions on liquid-filling characteristics for hard gelatin capsules. *International Journal of Pharmaceutics*. 2006;316(1-2):74–85.

[474] Starov V, Zhdanov V, Meireles M, Molle C. Viscosity of concentrated suspensions: influence of cluster formation. *Advances in Colloid and Interface Science*. 2002;96(1-3):279–93.

[475] Santamaría-Holek I, Mendoza CI. The rheology of concentrated suspensions of arbitrarily-shaped particles. *Journal of Colloid and Interface Science*. 2010;346(1):118–26.

[476] Guyot A, Chu F, Schneider M, Graillat C, McKenna TF. High solid content latexes. *Progress in Polymer Science*. 2002;27(8):1573–615.

[477] Rawle AF. Analytical tools for suspension characterization. In: Kulushreshtha AK, Singh ON, Wall GM, editors. Pharmaceutical suspensions From formulation development to manufacturing. 1st ed. New York: Springer; 2010. p. 177–230.

[478] Buckton G, Gill H. The importance of surface energetics of powders for drug delivery and the establishment of inverse gas chromatography. *Advanced Drug Delivery Reviews*. 2007;59(14):1474–9.

[479] Jallo L, Chen Y, Bowen J, Etzler F, Dave R. Prediction of inter-particle adhesion force from surface energy and surface roughness. *Journal of Adhesion Science and Technology*. 2011;25(4-5):367–84.

[480] Grimsey IM, Feeley JC, York P. Analysis of the surface energy of pharmaceutical powders by inverse gas chromatography. *Journal of Pharmaceutical Sciences*. 2002;91(2):571–83.

[481] Brum J, Burnett D. Quantification of surface amorphous content using dispersive surface energy: the concept of effective amorphous surface area. *AAPS PharmSciTech*. 2011;12(3):887–92.

[482] Ho R, Muresan AS, Hebbink G a, Heng JYY. Influence of fines on the surface energy heterogeneity of lactose for pulmonary drug delivery. *International Journal of Pharmaceutics*. 2010;388(1-2):88–94.

[483] Gamble JF, Leane M, Olusanmi D, Tobyn M, Supuk E, Khoo J, Naderi M. Surface energy analysis as a tool to probe the surface energy characteristics of micronized materials - a comparison with inverse gas chromatography. *International Journal of Pharmaceutics*. 2012;422(1-2):238–44.

[484] Jefferson AE, Williams DR, Heng JYY. Computing the Surface Energy Distributions of Heterogeneous Crystalline Powders. *Journal of Adhesion Science and Technology*. 2012;25(4-5):339–55.

[485] Chen Y, Jallo L, Quintanilla MAS, Dave R. Characterization of particle and bulk level cohesion reduction of surface modified fine aluminium powders. *Colloids and Surfaces A*. 2010;361(1-3):66–80.

[486] Mandelbrot BB. Snowflakes and other Koch curves. In: Mandelbrot BB, editor. The fractal geometry of nature. 2nd ed. New York: WH Freeman and Company; 1983. p. 34–57.

[487] Gilbody JS, Fletcher CP, Hughes IW, Kidman SP. Comparison of two different formulations of mebeverine hydrochloride in irritable bowel syndrome. *International Journal of Clinical Practice*. 2000;54(7):461–4.

[488] Radwan MA, Abdine HH, Aboul-Enein HY. A validated chiral HPLC method for the determination of mebeverine HCl enantiomers in pharmaceutical dosage forms and spiked rat plasma. *Biomedical chromatography : BMC*. 2006;20(2):211–6.

[489] The British Pharmacopoeia Commission. British Pharmacopoeia. London: British Pharmacopoeia Commission; 2012.

[490] Thielmann F. Introduction into the characterisation of porous materials by inverse gas chromatography. *Journal of Chromatography A*. 2004;1037(1-2):115–23.

[491] Dorris GM, Gray DG. Adsorption of n-alkanes at zero surface coverage on cellulose paper and wood fibers. *Journal of Colloid and Interface Science*. 1980;77(2):353–62.

[492] Donnet JB, Park SJ, Balard H. Evaluation of specific interactions of solid surfaces by inverse gas chromatography. A new approach based on

polarizability of the probes.pdf. *Chromatographia*. 1991;31(9-10):434–40.

[493] Van Oss CJ, Chaudhury MK, Good RJ. Monopolar surfaces. *Advances in Colloid and Interface Science*. 1987;28(1):35–64.

[494] Casson N. A flow equation for pigment-oil dispersions of the printing-ink type. In: Mill CC, editor. Rheology of disperse systems, Proceedings of the Conference of University College of Swansea. London: Pergamon Press; 1957. p. 84–104.

[495] Goodwin JW, Hughes RW. Nonlinear responses. In: Goodwin JW, Hughes RW, editors. Rheology for chemists: An introduction. 2nd ed. Cambridge: Royal Society of Chemistry; 2008. p. 194–257.

[496] Hlinak AJ, Kuriyan K, Morris KR, Reklaitis G V, Basu PK. Understanding critical material properties for solid dosage form design. *Journal of Pharmaceutical Innovation*. 2006;1(1):12–7.

[497] Tung HH, Paul EL, Midler M, McCauley JA. Adsorption, hygroscopicity, and deliquescence. In: Tung HH, Paul EL, Midler M, McCauley JA, editors. Crystallization of organic compounds: An industrial perspective. 1st ed. Hoboken: Wiley; 2009. p. 39–44.

[498] Ho R, Wilson DA, Heng JYY. Crystal habits and the variation in surface energy heterogeneity. *Crystal Growth & Design*. 2009;9(11):4907–11.

[499] Cavegn M, Douglas R, Akkermans G, Kuentz M. Study of an ultrasound-based process analytical tool for homogenization of nanoparticulate pharmaceutical vehicles. *Journal of Pharmaceutical Sciences*. 2011;100(8):3374–85.

[500] Sato ACK, Cunha RL. Influence of dispersing media and particle characteristics on rheological behavior of noncolloidal suspensions. *Journal of Dispersion Science and Technology*. 2012;33(3):437–46.

[501] Gunes DZ, Scirocco R, Mewis J, Vermant J. Flow-induced orientation of non-spherical particles: Effect of aspect ratio and medium rheology. *Journal of Non-Newtonian Fluid Mechanics*. 2008;155(1-2):39–50.

[502] Goodwin JW, Hughes RW. The dynamics and phase of concentrated dispersions. *Advances in Colloid and Interface Science*. 1992;42:303–51.

[503] Mills PDA, Goodwin JW, Grover BW. Shear field modification of strongly flocculated suspensions - aggregate morphology. *Colloid and Polymer Science*. 1991;269(9):949–63.

[504] Maggi F. Variable fractal dimension: A major control for floc structure and flocculation kinematics of suspended cohesive sediment. *Journal of Geophysical Research*. 2007;112(C7):C07012.

List of abbreviations

ANOVA	analysis of variance
API	active pharmaceutical ingredient
APS	ammonium persulphate
APTES	γ-aminopropyltriethoxysilane
BCA	bicinchoninic acid
BCS	biopharmaceutics classification system
BET	Brunauer, Emett, Teller
BSA	bovine serum albumin
CD	circular dichroism
CFA	critical formulation attributes
CMA	critical material attributes
COST	changing one single variable at a time
CPP	Critical Process Parameter
CQA	Critical Quality Attribute
DDS	drug delivery system
DEGEE	diethylene glycol monoethyl ether (or ethoxydiglycol)
DLS	dynamic light scattering
DLVO	Derjaguin, Landau, Verwey, Overbeek
DoE	Design of Experiments
DSC	differential scanning calorimetry
DTT	dithiothreitol
EE	encapsulation efficiency
ELISA	enzyme-linked immunosorbent assay
EtOH	ethanol-based hardening bath
FbD	Formulation-by-Design
FDA	Food and Drug Administration
FFA	free fatty acid
FMEA	failure mode and effect analysis
FTIR	Fourier transform infrared spectroscopy
GI	gastrointestinal
HBA	lipid-based hardening bath containing ethoxydiglycol

HBB	lipid-based hardening bath containing ethoxydiglycol, glyceryl caprylocaprate, and propylene carbonate
HBC	lipid-based hardening bath containing ethoxydiglycol, glyceryl monocaprylate, and propylene carbonate
HBD	lipid-based hardening bath containing ethoxydiglycol, glyceryl monocaprylocaprate, and PEG 600
HBE	lipid-based hardening bath containing ethoxydiglycol, macrogol-6 glycerides, and peppermint oil
HBW	water-based hardening bath
HGC	hard gelatine capsule
HNT	halloysite nanotubes
HPMC	hydroxypropyl methylcellulose
HRP	horseradish peroxidase
HVO	Hesselink, Vrij, Overbeek
IEC	ion exchange chromatography
IEF	isoelectric focussing
iGC	inverse gas chromatography
LB	lipid-based
MCC	mono-N-carboxymethyl chitosan
MLR	multiple linear regression
MOPS	3-(N-morpholino)propanesulphonic acid
MS	mass spectrometry
NBE	new biological entity
NCE	new chemical entity
NiE	nanoparticles-in-emulsions
NiMOS	nanoparticles-in-microsphere oral system
NLC	nanostructured lipid carriers
NMR	nuclear magnetic resonance
OFAT	one factor at a time
OLS	ordinary least square
OVAT	one variable at a time
PCA	principal component analysis
PCL	poly(ε-caprolactone)
PCR	principal component regression
PEG	polyethylene glycol
PLGA	poly(lactic-*co*-glycolic acid)
PLS	partial least squares
PLS-DA	partial least squares discriminant analysis
PRESS	predicted residual sum of squares
PVA	polyvinyl alcohol
QbD	Quality-by-Design
QbT	Quality-by-Testing
QTPP	Quality Target Product Profile
SANS	small angle neutron scattering
SAXS	small angle X-ray scattering
SDS-PAGE	sodium dodecyl sulphate polyacrylamide gel electrophoresis
SEA	surface energy analysis
SEC	size exclusion chromatography

SGC	soft gelatine capsule
SEM	scanning electron microscopy
siRNA	small interfering RNA
SLN	solid lipid nanoparticles
SLS	static light scattering
SMES	self-microemulsifying system
SNEDDS	self-nanoemulsifying drug delivery system
S-PVA	starch-polyvinyl alcohol
TEMED	tetramethylethylenediamine
TGA	thermogravimetric analysis
TMC	N,N,N-trimethyl chitosan
TRIS	tris(hydroxymethyl)aminomethane
UV	ultraviolet
XRPD	X-ray powder diffraction

List of symbols

a_P	cross-sectional area of the probe
c	sample concentration
d_{10}	10th percentile
d_{50}	median value
d_{90}	*90th percentile*
d	Euclidean dimension
d_d	drop diameter
d_j	jet diameter
d_n	nozzle diameter
d_p	particle diameter
f	frequency
f_i	predicted data point
$f_{i,-i}$	predicted values
g	gravitational acceleration
h	shortest distance between two particles
j	James-Martin correction
k	crowding factor
k_B	Boltzmann constant
l	optical path length
m	regression slope
n	number of amino acids
n_2	number of polymer or surfactant chains per unit area
n_i	probe moles injected
n_m	monolayer capacity of the probe molecule
r	particle radius
t_0	non-interacting probe retention time
t_R	retention time
v_j	jet velocity
v_s	settling velocity
w_{API}	API mass fraction
$\bar{y}$	mean of observed data

y_i	measured datapoint
A	Hamaker constant
D_f	fractal dimension
F	volumetric flow
G_a	van der Waals attraction energy
G_{con}	elastic repulsion energy (loss of conformational entropy)
G_{mix}	polymer free mixing energy
G_r	electrostatic repulsion energy
G_t	sum of interaction energies
M	sample mass
N_A	Avogadro's number
Q^2	cross-validation predictivity of a model
R	gas constant
R^2	goodness of fit of a model
$SS_{residual}$	residual sum of squares
SS_{total}	total sum of squares
T	temperature
T_m	melting temperature
T_{Ref}	reference temperature
T_s	column temperature
$V_{m,1}$	molar volume of the dispersing medium
$V_{m,2}$	molar volume of the polymer or surfactant chain
V_N	net retention time
W_{coh}	work of cohesion
X	independent variable
Y	dependent variable
β	regression coefficient
γ	shear rate
γ_{CH2}	methylene surface energy
γ_p^+	acid component of the probe surface
γ_p^-	basic component of the probe surface
γ_s^+	acid component of the sample surface
γ_s^-	basic component of the sample surface
γ_s^{AB}	specific surface energy
γ_s^D	disperse surface energy
γ_s^T	total surface energy
δ	surfactant or polymer layer thickness
ΔG_{SP}	free energy of desorption
ΔH_f	fusion enthalpy
ε_0	permittivity in vacuum
ε_r	relative permittivity
η	fluid viscosity

$[\eta]$	intrinsic viscosity
η_0	dispersion medium viscosity
η_r	relative viscosity
ϑ	high order interactions
θ	circular dichroism measured ellipticity
$[\theta m]$	mean residue ellipticity
κ	reciprocal Debye length
λ	wavelength
λ_{em}	emission wavelength
λ_{ex}	excitation wavelength
λ_{max}	maximum wavelength
λ_{opt}	optimal wavelength
ρ_0	placebo density
ρ_f	fluid density
ρ_p	particle density
ρ_t	true density
σ	shear stress
σ_0	yield stress
ς	surface tension
Φ	volume fraction
Φ_{eff}	effective volume fraction
Φ_{max}	maximum packing fraction
χ	Flory-Huggins interaction parameter
ψ_0	surface potential
Ω_∞	configuration number for freely rotating surfactant or polymeric chain
Ω_h	configuration number for sterically hindered surfactant or polymeric chain

List of equations

2.1	Stokes equation for particle sedimentation	6
2.2	Electrostatic repulsion energy	6
2.3	Van der Waals attraction energy	6
2.4	Free mixing energy	7
2.5	Elastic repulsion energy	7
2.6	Einstein equation for viscosity of very diluted suspensions	7
2.7	Batchelor equation for viscosity of diluted suspensions	7
2.8	Krieger-Dougherty equation for viscosity of concentrated suspensions	7
2.9	Mooney equation for viscosity of highly concentrated suspensions	7
2.10	Effective volume fraction	7
2.11	Frequency	17
2.12	Optimal wavelength during prilling	17
2.13	Weber equation for optimal wavelength during prilling	17
2.14	Droplet diameter in prilling	17
2.15	Flow during prilling	17
2.16	Droplet diameter in relation to wavelength during prilling	18
2.17	Linear correlation in ordinary least square regression	25
2.18	2nd order correlation in ordinary least square regression	25
2.19	Correlation in multiple linear regression	25
2.20	Goodness of fit	26
2.21	Residual sum of squares	26
2.22	Total sum of squares	26
2.23	Cross-validation predictivity of model	27
2.24	Predicted residual sum of squares	27
3.1	Span (particle size distribution)	45
3.2	Loading efficiency	47
3.3	Encapsulation efficiency	47

3.4	Mean residue ellipticity	47
3.5	Protection from enzymatic digestion	48
4.1	Overall score of ternary phase diagrams	60
4.2	Cross-validation predictivity of model in percentage	63
4.3	Mooney equation for viscosity with crowding factor	74
4.4	Mooney equation for apparent (measured) viscosity	74
4.5	Retention volume during inverse gas chromatography	76
4.6	Disperse surface energy according to Dorris-Grey	76
4.7	Free energy of desorption	77
4.8	Acid and basic components (according to van Oss) of specific surface energy	77
4.9	Casson model for yield stress extrapolation	78
4.10	Conversion of mass fraction to volume fraction	78
4.11	Fractal dimension	78

List of figures

2.1	Schematics of the rotary die method and bubble method for liquid capsule filling process, and of the capsule sealing techniques using banding and LEMS™	10
2.2	Gastrointestinal barriers to drug action and absorption.	11
2.3	Microparticle types.	15
2.4	Different types of prilling.	17
2.5	Development Plateau-Rayleigh instability on a liquid stream.	17
2.6	Chemical structures of natural and semi-synthetic polymers for prilling.	19
2.7	Schematics of multi-compartmental drug delivery systems.	20
2.8	Chemical structure of halloysite nanotube.	22
2.9	Graphical explanation of principal component analysis (PCA) and principal component regression (PCR).	26
2.10	Graphical explanation of partial least square (PLS) regression.	26
3.1	Schematics of vibrating nozzle apparatus.	29
3.2	Ternary phase diagrams of different mixtures.	30
3.3	Microscope pictures of BSA-loaded microgels from different hardening baths.	35
3.4	Morphology and size of microgels formed in DEGEE.	36
3.5	Overlaid circular dichroism spectra of BSA-loaded microgels over 4-week stability.	37
3.6	SDS-PAGE of BSA loaded in microgels after 4-week stability.	38
3.7	Overlaid fluorescence spectra of BSA-loaded microgels at time zero and after 4-week stability.	39
3.8	BSA release profiles of microgels in PBS pH 6.8, 50 rpm, and 37°C.	40
3.9	Schematic approach of Nanotubes-in-Microgels (as a Nanoparticle in Microparticle Oral System, NiMOS) manufacturing by means of prilling.	44
3.10	TEM and SEM pictures of HNT.	49
3.11	Optical microscope images of prilled microgels with and without HNT.	50
3.12	BSA release profiles over four hours in PBS pH 6.8 of microgels, HNT, and NiMOS.	52
3.13	Overlaid circular dichroism profiles of BSA from microgels, HNT, and NiMOS.	53
3.14	Overlaid emitted fluorescence profiles of BSA from microgels, HNT, and NiMOS.	54
3.15	SDS-PAGE of BSA loaded into microgels, HNTs, and NiMOS after trypsin digestion.	55

4.1	Schematics of vibrating nozzle system (2).	59
4.2	Examples of overlaid ternary phase diagrams.	64
4.3	Effect plots of the factors affecting microgel characteristics after PLS regression.	67
4.4	Microgel pictures from dynamic image analysis.	68
4.5	Overlaid circular dichroism profiles of BSA: worst cases and best cases.	69
4.6	Data evaluation of microfluidic capillary electrophoresis profiles of BSA.	70
4.7	Overlaid DSC profiles of mebeverine batches.	79
4.8	Overlaid X-ray diffractograms of mebeverine batches.	79
4.9	SEM picture of mebeverine powder.	80
4.10	Dispersive and specific surface energy vs. coverage of mebeverine batches.	81
4.11	Work of cohesion vs. surface coverage of mebeverine batches.	81
4.12	Viscosity of mebeverine suspension at different volume fractions and homogenisation conditions.	82
4.13	Effect of homogenisation on viscosity at different solid volume fractions.	83
4.14	Linear extrapolation of yield stress at high API concentrations.	83
4.15	Homogenisation level-specific fractal dimensions for mebeverine batches.	84
4.16	Mooney model fitted to the viscosity values of mebeverine batch A vs. volume fraction, sorted by homogenisation intensity.	85

List of tables

2.1	Lipids commonly employed in oral pharmaceutical formulations.	5
2.2	Interparticle interactions.	6
2.3	Relevant enzymes of the gastrointestinal tract (GI) tract.	12
2.4	Mucoadhesion theory.	13
2.5	Structures of proteins.	14
2.6	Protein characterisation techniques.	16
2.7	Brief glossary of Quality by Design terms.	24
3.1	Hardening bath composition.	31
3.2	Hardening bath characterisation.	34
3.3	List of capsule compatible with the proposed hardening baths.	34
3.4	Microgel shape and size characterisation.	36
3.5	Encapsulation efficiency (EE) and leakage of the microgels after 4 weeks.	37
3.6	Comparison of non-treated and treated nanotubes (nHNT and bHNT, respectively).	49
3.7	Particle size and shape of nNiMOS formed in different hardening baths.	51
3.8	Encapsulation efficiency of NiMOS and blank microgels formed in different hardening baths.	51
3.9	f_2 similarity factors calculated from the release profiles.	52
3.10	Comparison of protein stability after manufacturing and enzymatic digestion.	53
4.1	Hardening bath component list and properties of the selected glycerides.	61
4.2	List of response variables and experimental factors for partial least square regression analysis of the microgel properties.	63
4.3	Summary of the factors' effects on the scores in the ternary phase diagrams.	65
4.4	Capsule compatibility characteristics of the centre point (phase diagrams) formulations.	66
4.5	Goodness of fit (R^2) and cross-validation predictivity (Q^2) values from the partial least square analysis using the centre points of the phase diagrams.	66
4.6	Ingredients' list of the lipid-based suspension at different drug fractions.	77
4.7	Enantiomeric excess, hydrochloride salt fraction, and impurity content of the mebeverine hydrochloride batches (mean values ± standard deviations; n = 3 experiments).	79

4.8	Comparison of physical properties between the mebeverine hydrochloride batches.	80
4.9	Fitted constants (*i.e.*, viscosity of the drug-free vehicle η_0 and maximal packing fraction Φ_{max}) of the Mooney model.	84